Modulation of Inflammatory Pain in Intervertebral Disc Degeneration: A Therapeutic Biomaterials Approach

A thesis submitted to the National University of Ireland for the degree of Doctor of Philosophy

Isma Liza Mohd Isa

June 2017

Centre for Research in Medical Devices, Anatomy and School of Medicine, National University of Ireland, Galway

Research Supervisors: Prof. Abhay Pandit and Prof. Peter Dockery

Table of Contents

Table of Figures

Chapter 1

Chapter 3

Chapter 4

Appendices

Table of Tables

Chapter 1

Chapter 2

Chapter 3

Chapter 4

Chapter 5

Appendices and Future Directions

I certify that the thesis is all my own work and I have not obtained a degree in this University, or elsewhere, on the basis of this work

Acknowledgements

‘Great minds discuss the ideas…’ by Eleanor Roosevel, a social activist during the nineteenth century. Such a mentorship approach is the one I experienced over the past four years. Therefore, I would like to express special appreciation to my brilliant supervisor, Prof. Abhay Pandit who has been a tremendous mentor to me during my PhD journey. From the guidance he provided, I can explore new ideas in the study of pain in degenerative disc disease. I am extremely grateful to have been supervised by him, a world-renowned biomaterials expert from whom I learned so much in this field. I also make special mention of my co-supervisor in anatomy, Prof. Peter Dockery. He guided me in histology, imaging and stereology analysis. My special thanks to a very important person in my study, Prof. David P. Finn, Centre for Pain Research, who taught and trained me in the study of pain from behaviour tests and dissection to post-mortem analysis. To Dr Michelle Kilcoyne, ‘thank you’ for your guidance in glycobiology study which was one of the key elements in this thesis. And not forgetting Mr Aiden Devitt, an orthopedic consultant who contributed to the clinical input in this thesis. To my GRC committee, Dr Una Fitzgerald, Dr Dimitrios Zeugolis and Dr Manus Biggs who provided me the great comments and advice throughout the years of my PhD. Most importantly, I would like to acknowledge my funding body, Majlis Amanah Rakyat (MARA), a Malaysian government agency that supported me for my entire study (ROG1112). Also, the support from the Mass Spectrometry Resource, Conway Institute of Biomolecular and Biomedical Research, University College Dublin, and Centre for Molecular Biology Facility, Bioresources Unit of Pre-clinical Facility and Centre for Microscopy and Imaging, NUI Galway.

For me a PhD is not only the focus in study; it is a story of how I can survive on this challenging path. To my eternal soulmate, best friend, labmate and husband, Asrizal Abdul Rahman; a million thanks for being at my side through both the ups and downs. No words can describe how grateful I am for your support at every step. Being a mum with two daughters, demands commitment beyond that of normal life. I started my PhD when my younger daughter, Adni Khayla Batrisyia, was three months-old, and her sister, Auji Adni Umairah was two years-old. While I didn’t know if I could handle this, I am certain kids are the most precious gift ever. My

adorable Auji is a very smart kid and well behaved. Khayla is a clever and helpful girl. And together, these girls are my greatest motivation and source of strength.

I would like to thank my colleagues in the Network of Excellent for Functional Biomaterials and CÚRAM. My first lesson was PCR with Dr Eugene See who introduced me to disc research. I really appreciate the skills and knowledge I got from him. I am grateful as well to have worked with Dr Akshay Srivastava in developing a hydrogel system for disc tissue engineering. Another important person in my study was Dr Oliver Carroll who manages the lab and pre-clinical documentation. The lab could not run without him. Thanks also to my best buddy Mr David Tiernan, an orthopedic surgeon who trained me in the rat tail model and other surgical techniques. To Dr Sunny Abbah, I really appreciate your guidance and assistance over the entire animal studies. Not to forget, Dr Natasha Solovyova for taking care of my animals during the study. Dr Kieran Wyne (UCD) who helped me in proteomic study. Also, the help from Dr Peter Owens who always knows how to trouble shoot the confocal microscope. Not to forget, Mr Mark Canney who helped in the histology and Dr Siobhan McMahon for lending me the instruments for pain behaviour tests. Thanks to Dr Peadar Rooney who helped me in the biology part of phase I study. Thanks to all.

Special dedication to my mom, Aznah Md Noh who always worried about me especially when I was sick. Many thanks for those encouraging words and guidance which make me even stronger! I hope you will always be in good health. To my late father, Mohd Isa Hashim; today, I owe it all to you. I miss you, abah.. I am grateful to have my siblings; Issham, Ismaaizan, Isnirah, Ismadziah, Ismadziha and Izdihar and their in-law families who have boosted my morale and given motivational support to me. Special mention to mother-in-law, Hasnah Hassan and my family-in-law: thanks for being there for me. Thanks also to my grandmother and family members back in Malaysia. Not to forget my very best friend and motivator, Hasbah Juwaini, for always being supportive with every move I have made.

I was so thankful for the friendship developed over the years. To my close friend, Dr Siti Ismail - thanks for your help and motivational words. To Mangesh Morey and Catalina Vallejo; thanks for your kindness and being great friends of mine. My good friends, Rachel Ronan and Ana Lucia Rebelo, who were willing to share their beautiful xenopus images and good moments with me. Aitor Larranaga and Juhi Samal, hope we can always have lunch together and share our life stories!

My best Italian friends, Paolo Contessotto and Grazia Marsico who have always been so nice to me. To Dilip Thomas, I always like to hear your excellent thoughts. Special mention to Azim Patar (Anatomy), the first person I knew in Galway and who has always been helpful to me and family. My best Malaysian friend, Atiqah and her husband Nasarudin (Ryan Institute) - thanks for your help and taking care of the kids. To Dr Marlini and Dr Hisyam (Physiology) who always gave me the positive vibes to succeed! Also, my good friend Nurhayati Akhir, who helped me in difficult situations.

The most helpful person during my thesis writing was Anthony Sloan. I learned a lot from him about English writing. To Tara Cosgrave and Fidelma Gallen - thank you for sorting all the management processes regarding my study. Not to forget, Maciej Doczyk who designed the schematics in this thesis. Sorry, if I was a bit fussy! I am grateful to know Claire Riordan who guided me in engaging with the public community. A great industry experience with help from Carmel McGroarty-Mitchell and Neil Ferguson. Thanks to you all.

I would like to thank all lab members for sharing the lab space and giving the great comments during the lab meetings. Friends since NFB times (Sahana Ganesh, Diana Pereira, Afeedah Salehudin, Eleni Tsekoura and Shane Brown). CÚRAM members (Christos Tapeinos, Eugenia Pugliese, Vaibhav Patil, Marc Fernandez, Aniket Kshirsagar, Niranja Kotla, Secil Demir, Busra Gunay, Gillian Murphy, Adriona Kelly, Renza Spelat, Valeria Graceffa, Alexandre Trotier, Enrico Bagnoli, James Britton and Vijaya Kanala). Not to forget, members from David Finn lab; Elaine Jennings, Manish Madasu, Jessica Gaspar, Orlaith Mannion, Emer Power, Sarah Jarrin, Mehnaz Ferdausi and Álvaro Lorente – 'thanks guys'.

Last but not least, thanks to all staff; Keith Feerick, Vidoja Kovacevic, Derek Welan, Mairead Ui Fhatharta, Dr Elke Rink, Dr Sarah Gundy, Dr Stefania Spada, Dr Brendan Harhen, Andrea Fitzpatrick and Dr Ruth Dooley. Not to forget, my close friends in UK (Aminatul) and Malaysia (Norazurashima, Maizatul, Norazlina, Salma, Hasniza, Fathy, Darina, Rodziah, Farina and Izzah), my ex-students in Ministry of Health, Malaysia and Malaysian-Indonessian community in Galway, who have supported me along the way. Thank you all very much!

List of Abbreviations

LBP	Low Back Pain
IVD	Intervertbral Disc
NP	Nucleus Pulposus
AF	Annulus Fibrosus
CEP	Cartilaginous Endplate
ECM	Extracellular Matrix
TNF	Tumor Necrosis Factor
IL	Interleukin
ADAMTS	A Disintegrin and Metalloprotease with Thrombospondin Motifs
MMP	Matrix Metalloproteinase
MAPK	Mitogen-activated Protein Kinase
NF-κB	Nuclear Factor-kappa B
IFN	Interferon
BDNF	Brain-derived Neurotrophic Factor
NGF	Nerve Growth Factor
GAP43	Growth-associated Protein 43
NSAID	Non Steroidal Anti-inflammatory Drug
HA	Hyaluronic Acid
CS	Chondroitin Sulfate
KS	Keratan Sulfate
DRG	Dorsal Root Ganglion
Asn	Asparagine
Ser	Serine
Thr	Threonine
Gly	Glycine
GalNAc	*N*-acetylgalactosamine
GlcNAc	*N*-acetylglucosamine
Fuc	Fucose
Glc	Glucose
Gal	Galactose
PG	Proteoglycan

TGF	Transforming Growth Factor
RANTES	Regulated and Normal T Cell Expressed and Secreted
TIMP	Tissue Inhibitor of Metalloproteinase
SOX-9	SRY (sex determining region Y)-box 9
JNK	Jun N-terminal Kinase
MRI	Magnetic Resonance Imaging
VEGF	Vascular Endothelial Growth Factor
CGRP	Calcitonin Gene-Related Peptide
PGP 9.5	Protein Gene Product 9.5
Trk	Tyrosine Kinase Receptor
ASIC	Acid Sensing Ion Channel
p75NTR	Low-affinity Neurotrophin Receptor
AMPA	α-amino-3-hydroxy-5-methyl-4-isoxazolepropionic Acid
NMDA	N-methyl-D-aspartate
GAG	Gycosaminoglycan
DMMB	Dimethylmethylene Blue
CXCL1	C-X-C Motif Chemokine Ligand 1
eNOS	Endothelial Nitric Oxide Synthase
ILK	Integrin-linked Kinase
RHAMM	Receptor for Hyaluronan Mediated Motility
TRPV1	Transient Receptor Potential Vanilloid 1
COL	Collagen
ACAN	Aggrecan
HMW	High Molecular Weight
LMW	Low Molecular Weight
ODI	Oswestry Disability Index
GABA	Gamma-aminobutyric Acid
NHS	N-hydroxysuccinimide
DMEM	Dulbecco’s Modified Eagle’s Medium
FDR	False Discovery Rate
S.E.M	Standard Error of Mean
s.c	Subcutaneous
TBAB	Tetrabutyl Ammonium Bisulfate
rpm	Revolutions Per Minute

PBS	Phosphate Buffer Saline
GFAP	Glial Fibrillary Acidic Protein
Iba1	Ionized Calcium Binding Adaptor Molecule 1
5HT	Serotonin
H&E	Hematoxylin and Eosin
IHC	Immunohistochemistry
CD	Cluster of Differentiation
RT	Reverse Transcription
qPCR	Quantitative Polymerase Chain Reaction
ELISA	Enzyme Linked Immunosorbent Assay
IB-4	Isolectin B4
MSC	Mesenchymal Stem Cell
SMAD3/Smad3	Mothers Against Decapentaplegic Homolog 3
FN	Fibronectin
IRAK	IL-1R-associated Kinase
JAK	Janus Kinase
FBS	Fetal Bovine Serum
P/S	Penicillin/Streptomycin
BSA	Bovine Serum Albumin
mTOR	The Mechanistic Target of Rapamycin
IPA	Ingenuity Pathway Analysis
EIF2	Eukaryotic Initiation Factor 2
O.C.T	Optimal Cutting Temperature Compound
TBS	Tris-buffered Saline
MAA	*Maackia amurensis* Agglutinin
WGA	Wheat Germ Agglutinin
IL-1R1	Interleukin-1 Receptor 1
MyD88	Myeloid Differentiation Primary Response Gene 88
PEG	Polyethylene Glycol
GTA	Glutaraldehyde
HBSS	Hanks' Balanced Salt Solution
FITC	Fluorescein Isothiocyanate
TRITC	Tetramethylrhodamine Isothiocyanate

ANOVA	Analysis of Variance
Con A	Concanavalin A
DAPI	4,6-diamidino-2-phenylindole
HAS	Hyaluronan Synthases
ADSC	Adipose-derived Stem Cell
SNA-I	*Sambucus nigra* Agglutinin I
GPCR	G-Protein Coupled Receptors
dNTP	Deoxynucleotide
D.P.X	Distyrene. Plasticiser. Xylene
PFA	Paraformaldehyde
GAPDH/*Gapdh*	Glyceraldehyde 3-phosphate Dehydrogenase
DNIC	Diffuse Noxious Inhibitory Control
UEA-I	*Ulex europaeus* Agglutinin I
PNA	Peanut Agglutinin
GS-IB4	*Griffonia simplicifolia* Isolectin
WFA	*Wisteria floribunda* Agglutinin
TNBSA	2,4,6-trinitrobenzene Sulfonic Acid
FTIR	Fourier Transform Infra Red
MPC	Mesenchymal Progenitor Cell
EDTA	Ethylenediaminetetraacetic Acid
EthD-1	Ethidium Homodimer
CT	Threshold Cycle
HIF-1	Hypoxia Inducing Factor-1
IFIT3	Interferon-induced Protein with Tetratricopeptide Repeats 3
STAT	Signal Transducer and Activator of Transcription
VAS	Visual Analog Scale
EDC	1-ethyl-3-(3-dimethylaminopropyl)carbodiimide
LFQ	Label Free Quantification
MS	Mass Spectrometry
QST	Quantitative Sensory Testing
ChABC	Chondroitinase ABC

Abstract

Discogenic low back pain (LBP) is a very common health problem that imposes a socio-economic burden on society. Primarily, intervertebral disc degeneration is one of the causative factors of LBP. It is mediated by an inflammation and an imbalance of extracelullar matrix homeostasis that can induce hyper-innervation and sensory sensitization in the disc and results in discogenic pain. The use of hyaluronic acid (HA) as a therapeutic agents offers promising results in tissue regeneration as it can reduce inflammation and pain, but the effects of HA therapy on glycosylation and pain associated with disc degeneration have not previously been determined. The overall aim of this study was to develop an optimally cross-linked high molecular weight of HA hydrogel, and further informed as to its therapeutic efficacy in alleviating inflammatory pain in degenerative disc disease.

In phase I, the hydrogel was optimally crosslinked at 75 mM PEG, exerted hydrolytic stability and resistance to enzymatic degradation. No cytotoxic effect of NP cells was marked after treatment with HA hydrogels for one, three and seven days. IL-1β signalling molecules of IL-1R1 and MyD88 were significantly suppressed in the presence of HA hydrogel. Additionally, NGF and BDNF mRNA were down-regulated after treatment with cross-linked HA hydrogel. A possible protective mechanism of HA is shown by the binding of the CD44 receptor of NP cells to HA and which prevents NP cells from undergoing further inflammation. These findings indicate that optimally stabilized cross-linked HA hydrogel has a therapeutic effect in response to neurogenic inflammatory insult and becomes an ideal matrices hydrogel for NP repair.

Nonetheless, the efficacy of HA hydrogel in alleviating pain in degenerative disc disease is still unknown. Therefore, a novel pre-clinical model of pain was established in phase II of the study as an intervention platform. The surgically puncture-induced disc injury was adopted in the rat tail. Here, for the first time, surgically puncture-induced disc injury evoked robust pain phenotype by exhibiting thermal hyperalgesia and mechanical allodynia close to the site of injury and up-regulation of spinal nociception marker, *c-Fos* mRNA. Conversely, the tail flick test revealed hypoalgesia at a lower level of the rat tail, suggesting a phenomenon of persistent pain as seen in clinical chronic pain. Moreover, disc injury induced

structural disc degeneration and differently regulated glycosignature in both AF and NP tissues. Thus, the inhibition of nociceptive behaviour by low dose morphine, a current reversible analgesic that validates this pain model. Conclusively, the results indicate the first demonstration of nociception in the rat tail, anatomical disc degeneration and distinct glycosylation in AF and NP, thereby provide a platform to study pathogenesis of disc degeneration and testing of potential therapeutic target for disc repair in treating discogenic pain.

Using this model, the potential efficacy of HA hydrogel in alleviating inflammatory pain in disc degeneration was evaluated in phase III of the study. HA hydrogel has been seen to alleviate nociceptive behaviour by reducing thermal hyperalgesia and mechanical allodynia close to the site of injury in the rat tail. Using the tail flick test, HA hydrogel demonstrated an inhibition of hypoalgesia at a lower level of the rat tail. These results indicate an anti-nociceptive effect of HA hydrogel that is comparable to low dose morphine treatment. The HA hydrogel also down-regulated spinal nociception markers, *c-Fos* and *Tac1* (precusor for substance P), and pro-nociceptor of TRPV1 and Trk-A in AF and NP. An inhibition of sensory hyper-innervation was indicated by GAP43 and CGRP protein. Furthermore, HA altered glycosylation pattern than in injured AF and NP tissues. The mechanism of action of HA was determined by modulating key inflammatory pathways of IL-6 and IL-1β, and regulatory signalling pathways of Smad3 via TGF-β1 to respectively attenuate inflammation and regulate matrix components. Therefore, these results represent inflammatory pain modulation by HA hydrogel through alteration in glycomic and protein regulatory pathways, and thus suggesting that HA hydrogel as a promising clinical candidate for treatment of back pain caused by degenerated discs.

Introduction

Sections of this chapter have been published and are in preparation:

Graceffa, V., Wu, Z., Gaspar, D., Spanoudes, K., **Isa, I. L. M.**, Biggs, M., Mullen, A.M., Pandit, A. and Zeugolis, D.I. 'Xenogenic Tissues and Biomaterials for the Skeletal System.' *Reference Module in Materials Science and Materials Engineering*, 2017

Isa I. L. M., Devitt A., Abbah S. A. and Pandit A. Therapeutic biomaterials for intervertebral disc regeneration in the treatment of discogenic pain, submitted to

1.1 Introduction

The lifetime prevalence of low back pain (LBP) is estimated at 54–80% of the population [1-5]. In the year 2005 alone, the incidence of self-reported back pain increased to 24.7% from 20.7% in the previous year in the US population [6]. The World Health Organisation estimated that LBP accounts for the highest number of disability-adjusted life years worldwide [7-9]. In the US, the economic costs of spine-related issues were estimated at $85.9 billion, which is higher expenditure than that on other medical conditions including arthritis and cancer [6]. This compares with an estimated economic burden of £12.3 billion in the UK and €16.5–€ 50 billion in Germany annually [8][10].

The cause of LBP is multifactorial but disc degeneration is considered the primary aetiological factor accounting for between 26% and 42% of patients with low back pain [11-13]. The intervertebral disc (IVD) is a fibrocartilaginous structure connecting adjacent vertebral bodies. It provides mechanical stability to the spine by transmitting the load, and allows the movements such as flexion, extension, side bending and rotation at the level of the motion segment [14]. It also maintains proper spatial orientation of the vertebral bodies and facet joints. The complex anatomical features of the IVD comprises a central core proteoglycan-rich gelatinous nucleus pulposus (NP), that is surrounded peripherally by the collagen-rich fibrous annulus fibrosus (AF). The cartilaginous endplate (CEP) superiorly and inferiorly connects the adjacent vertebral bodies together forming the functional spinal unit (motion segment) [15]. The proteoglycan in the NP absorbs large amounts of water which contributes to high osmotic pressure. However, this is resisted by the fibre orientation of the AF which allows the disc to absorb compressive forces under healthy conditions [16].

Degeneration of the IVD is associated with a loss of capacity for adequate intrinsic self-repair due to the avascular nature of the disc. A decrease in NP progenitor cells characterised by $Tie2^{+}$ marker has been identified in the human disc as an indication of the aging and degeneration progress, suggesting that the disc loses its ability to regenerate [17]. The imbalance of extracellular matrix (ECM) homeostasis is caused by a decrease of anabolic (ECM synthesis) and an increase in catabolic activities (ECM degradation). Aging has been associated with an increase

of cellular senescence which changes the cellular phenotype modulating ECM activities [18]. What also influences disc degeneration are mechanical load and injury, deficient IVD nutrition supply [19], genetic predisposition [20] and risks such as smoking [21] and obesity [22].

During degeneration, the NP tissue becomes more fibrous, and the outer annulus fibrosus (AF) has to bear heavy loads and this leads to tears, bulging, rupture, and herniation [23]. Cellular and biochemical changes can result in abnormal ECM deposition and eventually leads to an imbalance in homeostasis between anabolic and catabolic processes in the disc [24]. These changes appear to be initiated by mediators such as pro-inflammatory cytokines (TNF-α and IL-1β) that induce matrix degradative enzymes (ADAMTS-4, ADAMTS-5, MMP-1, MMP-2, MMP-3, MMP-13 and MMP-14) resulting in degradation of ECM components [25-26]. It has been suggested that major intracellular signalling pathways such as mitogen-activated protein kinase (MAPK), nuclear factor-kappa B (NF-κB) and Wnt/b-catenin are involved in the molecular event of disc degeneration [18][27]. Interferon (IFN-γ) signalling and IGFBP3 are other important molecules that have been involved in mediating degeneration in AF tissue [28].

Apart from these, inflammatory mediators and neurotrophins produced by disc cells and infiltrating immune cells regulate nerve ingrowth and sensory sensitization in the degenerated disc [29]. For example, IL-1β and TNF-α induce expression of neurotrophins such as nerve growth factor (NGF) and brain-derived neurotrophic factor (BDNF) in NP cells of degenerated human disc [30]. Hence, these neurotrophic factors play an important role in promoting the growth of sensory fibers in the aneural disc [31]. Clinical onset of discogenic pain is associated with ingrowth of sensory nerve fibres (usually accompanied by a blood vessel) into the normally aneural disc. The sensory nerves are projected into the inner third of the AF and into the NP to initiate the development of nociception [32]. In addition, Freemont *et. al.* demonstrated that human degenerated discs associated with chronic low back pain abundantly show nerve marker of nociceptive neurotransmitter (substance P) and a protein expressed during axonogenesis such as growth-associated protein 43 (GAP43) [32].

Current treatment modalities are based either on conservative treatment or surgical intervention. Rehabilitation includes physical exercise, and back

manipulation which are commonly employed to alleviate pain and improve flexibility [33]. Pharmacologic treatment includes the use of non-steroidal anti-inflammatory drugs (NSAIDs), systemic and epidural corticosteroids, opioid analgesics and muscle relaxants [34-35]. An increasing number of percutaneous minimally invasive modifications have been advocated to alleviate discogenic back pain in patients. Surgery such as spinal fusion or disc arthroplasty is widely available especially at later stages of degeneration [36]. These existing treatments focus primarily on the relief of pain, and critically they are not regenerative in nature as they do not address the underlying degeneration caused by the disease. Furthermore, surgical interventions are destructive to the normal disc anatomy and none of the approved therapeutic strategies restore the native structure and function of the disc.

Tissue engineering strategies which use biomaterials as therapeutic agents offer promising outcomes in IVD degeneration for the treatment of back pain by restoring the anatomical and mechanical functions of the disc [37]. Biomaterial approaches can modulate the disc ECM by providing an optimal micro-environment for cell adhesion and proliferation, and the synthesis of protein and macromolecules. These influence multiple signaling pathways and offer protection from hostile local injection/implantation environments and thus enhance the efficacy of the therapeutic strategy [37]. The success of a tissue engineering strategy will be determined by the ability of the biomaterials system to compensate local tissue responses, maintain disc phenotype, attain tissue biochemical homeostasis and promote anatomical tissue repair to provide functional mechanical support. Fine tuning of the macromolecular architecture includes viscoelasticity, injectability/implantability and physical/functional mechanical stability, all of which are key elements in developing biomaterials scaffolds for IVD repair. One particular treatment that has shown much promise in pre-clinical models is that of hyaluronic acid (HA). HA shows significant potential to promote IVD regeneration by maintaining the IVD phenotype, compensating for the imbalance of ECM and cellular function. HA also facilitates disc biomechanics, promoting disc tissue remodelling and targeting multiple signalling pathways underlying the disease by attenuating the inflammatory response from further degeneration and pain. It thus represents a promising therapeutic strategy to regenerate the degenerative disc and relieve discogenic pain.

1.2 Spine

The spine is an axial skeleton which consists of mechanical structures including vertebrae as levers, facets and discs function as pivots, ligaments and muscles act as passive restraints and actuators respectively [38]. The vertebral column comprises the axial load-bearing structures of the vertebral bodies and the intervertebral discs. The pedicles of the vertebral body tie the anterior column to the posterior column at each spinal segment. The laminae act as a roof to the spinal canal for spinal nerve/root passage and attach to the ligamentum flavum. The facet joints provide rotation, flexion, extension, lateral bending and translation motion. The muscles and ligaments also limit torso movement while contributing to the axial load-bearing capacity [38].

1.3 Intervertebral Disc

A fundamental knowledge of normal IVD homeostasis is required to understand the rationale for any therapy in degenerative disc. Anatomically (Figure 1.1), the intervertebral disc (IVD) is located between adjacent vertebrae and consists of one third of the total height of vertebral column with a total of 23 discs. Although IVDs lie between the cervical, thoracic, and lumbar vertebrae, they do not lie between the first two cervical vertebrae, sacrum and coccyx. The thickness and surface area of the discs are greater at the lumbar and thinnest at the cervical levels [14][39]. Macroscopically, a normal IVD is approximately 8-10 mm in height, 4 cm in diameter and consists of two distinct regions which are the gel-like structures of the nucleus pulposus (NP) and the fibrocartilage of the annulus fibrosus (AF). NP and AF are confined superiorly and inferiorly by cartilage end plates (CEP) [39]. The IVD mainly provides a mechanical cushion with support and flexibility to distribute loads arising from body weight and muscle activity through the spine and to allow multi-axial motions such as bending, flexion and torsion [40]. It also maintains proper spatial orientation of vertebral bodies and facet joints.

1.3.1 Annulus Fibrosus

The AF is a type of fibrocartilagenous tissue which is composed of 15-25 lamellae of collagen fibres. Each lamella lies parallel with an orientation of 60° and each adjacent lamella alternates to the left and right in relation to its direction from the vertical axis [41]. Between the lamellae are elastin fibers that extend radially to bind

the lamellae together and allow the disc to return to its original position following flexion or extension [39]. The AF region can be subdivided into outer and inner AF [40]. The outer AF is highly organised with a collagenous structure with more type I collagen in the inner AF than in the outer AF [42]. A thin, fibrous band of tissue, referred to as the transitional zone between AF and NP with the unique morphology of thin extensive cytoplasmic projections (some more than 30 mm), can be found in cells of both the AF and NP [39]. The average cellularity of AF is 9 x 10^3/mm^3 with cells that are aligned parallel to the collagen fibres and with a morphology that changes from being elongated or fibroblast-like shaped cells in the outer AF to rounded cells in the inner AF [43-44].

1.3.2 Nucleus Pulposus

The NP is a central region of IVD that contains loosely organized type II collagen, and irregularly shaped elastin fibres. These fibres hold a gel-like structure composed of proteoglycan molecules, namely aggrecan, that have hydrophilic chondroitin sulfate (CS) and keratin sulfate (KS) aggregated to them. This allows them to bind water molecules and produce osmotic pressure, and subsequently maintain tissue hydration [39]. NP cellularity is considered as low cell density at an average of 4 x 10^3/mm^3 [43] with more cells irregularly distributed in the central region than in the periphery. In human immature and young intervertebral discs, NP cells are notochordal cells which originate from mesodermal cells. Notochordal cells have a larger morphology and vacuolated features (physoliferous), containing prominent cellular processes and intracellular glycogen deposits. With maturation and ageing, the cells become smaller and rounded resembling chondrocytes [45].

1.3.3 Cartilaginous Endplate

The CEP is characterised by a thin horizontal layer of hyaline cartilage, approximately 1 mm thick [46], defining a morphological and functionally distinct interface between the AF and the vertebral body. It adheres to the IVD superiorly and inferiorly to the growing trabecular structure of adjacent vertebral bodies [15]. The primary collagen fibres lie horizontal and parallel to the vertebral body [47]. The CEP is formed by chondrocytes similar to those in articular cartilage, which secrete a type II collagen and proteoglycan in the ECM [48]. In immature tissue, it has a high degree of vascularisation, but this decreases as aging continues and

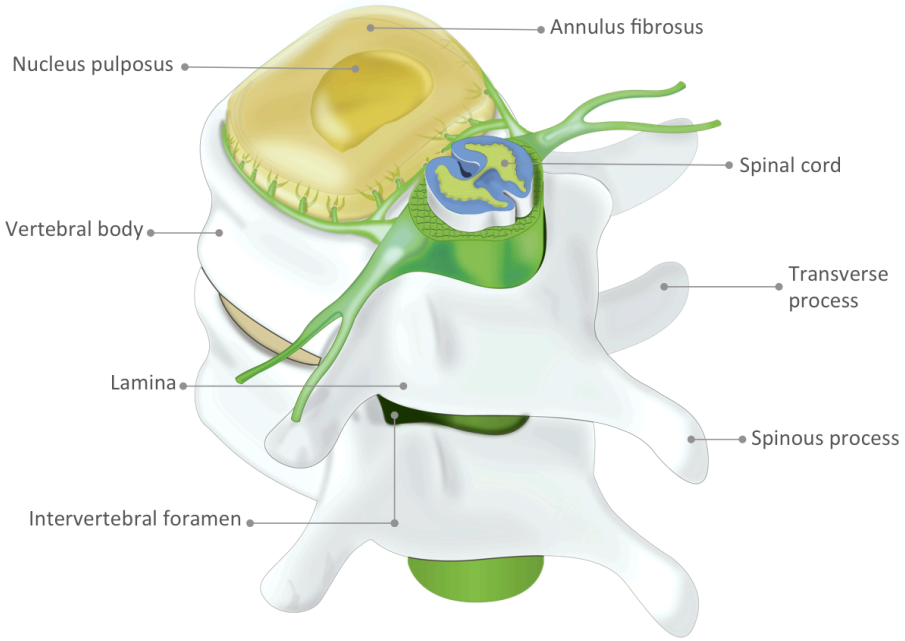

Figure 1.1 Anatomical representation of left posterolateral view of articulated vertebrae in the spine. The IVD is located between the vertebral body, which consists of inner core nucleus puposus and concentric ring annulus fibrosus. Pedicels tie the anterior to the posterior vertebrae. Laminae act as a dome for the intervertebral foramen for spinal nerve route. The spinal cord passes through the spinal column [14].

eventually turns into an avascular zone after the third decade [14].

1.3.4 Extracellular Matrix

The biomechanical and physiological functions of the disc are related to the composition and interactions between the major ECM components of collagen, proteoglycan and elastin. In the AF, ECM is made up by 70% water, 5% proteoglycan and 15% collagen fibres. NP comprises of 77% water, 14% proteoglycan and 4% collagen. Proteoglycan monomers in the disc are smaller and more polydispersed than these in cartilage tissue. Aggrecan is a major proteoglycan in AF and NP that maintains tissue hydration through the osmotic pressure provided by its constituent chondroitin and keratan sulfate chains. It forms macromolecule aggregates with hyaluronic acid (HA); however, these are less aggregated (30%) and more heterogeneous in the disc than in articular cartilage (80% aggregated). Collagens are more abundant in the AF than in the NP, where the fibrillar matrix is made up of collagen type I in the outer AF which functions to provide maximal tensile strength to the disc. Type II collagen is found predominantly in the NP, inner AF and end-plate, which function to resist the compression loads [49]. Elastic fibres are composed of centrally located amorphous hydrophobic elastin surrounded by hydrophilic microfibrils and comprise about 2% of the dry weight of the disc. In the NP, elastins are organised radially and vertically, penetrating the end-plate; the fibers, however, lie both parallel and orthogonal to the collagen fibres in the AF. Physiologically, elastin fibres contribute to the rapid recovery of disc size and shape prior to load applications [50]. These ECM macromolecules are degraded by proteiniases such as the matrix metalloproteinase (MMPs) and aggrecanases (ADAMTs) which are secreted by AF/NP cells. The equilibrium between synthesis and accumulation (anabolism), and degradation (catabolism) maintains the ECM homeostasis and provides further mechanical integrity in the disc [14].

1.3.5 Nutrition Exchange

The IVD requires nutrients for optimal function. Adequate amounts of nutrients e.g. oxygen and glucose, and substrates for ECM production such as amino acids and sulfate are furnished in the disc by the blood supply at the disc's periphery. These nutrients are exchanged from the surrounding capillaries through the disc ECM to the cells via diffusion under gradients produced by cellular metabolism [51-52]. A

sufficient amount of glucose is important to maintain viability and cellular functions. Cellular death occurs if glucose deficiency <0.5 mmol/L occurs after only a few days. The avascular environment permits disc cells to encounter anaerobic metabolism e.g. glycolysis instead of oxidative metabolism, by consuming glucose and producing lactic acid to generate energy, and also to synthesize collagen and proteoglycans. The production of lactic acid results in a mild acidic pH range between 6.9 and 7.2 [53]. Additionally, the collagen network embedded in the polyanionic proteoglycan in ECM exhibits selective permeability of molecules into the disc. Low concentrations of large molecules such as growth factors and protease inhibitors, can enter the disc. Increased transport of small cations such as sodium is in proportion to the proteoglycan concentration; however, anions such as sulfate and chloride are moderately restricted. The higher concentration of proteoglycan in the NP than in the AF allows large solutes and negatively charged molecules to enter into the AF more freely than into the NP. Overall, oxygen consumption and lactate production are influenced by both oxygen concentration and pH under acidic and hypoxia conditions [52].

1.3.6 Vascular Supply

The IVD is known as the largest avascular tissue, with approximately 8 mm of distance between disc cells and the nearest blood vessels [54]. Blood vessels branch from the spinal artery present in the CEP before one year of age; however, the vessels only remain in the longitudinal ligaments adjacent to the disc [39]. The CEP is totally avascular in the healthy adult [14]. In the disc, only a few arterioles and capillaries that are restricted to between 1 and 2 mm lie in the outer AF and are distributed equally around the disc's margin. The vessels that are smaller run horizontally around the disc. Blood vessels branch from the segmental artery supply to the vertebral body and the CEP. Approximately 7-10% of vascular beds are occupied at the interface between the vertebra and cartilage, with a tendency to be smaller in the peripheral than in central region. A larger blood supply of 20-30% is in the interface between vertebra and cartilage, and have direct contact to marrow space [43].

1.3.7 Innervation

The unique avascularity of the disc and metabolic restriction result in the disc being poorly innervated. Discs are innervated posteriorly by nerves that normally accompany the blood vessels arise from sinuvertebral nerves, forming ascending and descending branches after branching off from dorsal root ganglion (DRG) [39]. For example, the lumbar discs from L1–L2 to L4–L5 are multisegmentally innervated by the T11 through L5 of DRG [55]. Sinuvertebral nerves relay sensory information to the spinal cord segmentally through the dorsal horn or extrasegmentally through the paravertebral sympathetic chain [39] and reach the DRG via ramus communicans at L2 [55]. The anterior portion of the disc, e.g. L5-L6, is innervated by sensory nerves that arise from DRG at level L1-L2 [56]. Laterally, discs are innervated by branches of the ventral rami and grey rami communication. In contrast, the posterior longitudinal ligament is innervated by sinuvertebral nerves, and the anterior longitudinal ligament by branches from grey rami communicantes [57-58]. In the disc, small unmyelinated and encapsulated nerve endings terminate in the surface of the outer AF, and small free nerve endings project approximately 3 mm into the outermost layers of the AF. These nerve fibres express a nociceptive neurotransmitter such as substance P, and a protein expressed during the axonogenesis e.g. growth-associated protein 43 (GAP43) [32]. The nerve fibres terminate frequently as free nerve endings, or mechanoreceptors such as Ruffini and Golgi type receptors [59]. There is no nerve supply in the inner AF or NP region [53][60].

1.3.8 Biomechanics

The main biomechanical functions of IVDs are to transmit loads arising from body weight and muscle activity through the spinal column, and allow movements such as bending, flexion, and torsion [14]. IVDs are routinely exposed to heavy loads during activities especially at lumbar level [45], including tension, compression, torsion, and bending with stresses ranging between 0.1 and 2.3 MPa [61-62]. Thus, the biomechanics of IVDs must be capable to distribute multi-directional loads by acting as a pressurized vessel due to viscoelasticity of the NP in response to compressive or eccentric loading of the motion segment. The internal fluid pressurization of the NP converts to tensile hoop stresses that are radial to the anisotropic non-linear of AF fibres [63]. This electrochemical force is produced by negatively charged

proteoglycan-induced binding of water so as to enhance the compressive strength of the NP [39]. In AF, the alternating collagen fiber network permits resistance to bending and torsion while undergoing direct compression, plus radial and circumferential stress from the NP bulging under physiological loading. In addition, the 30° angled orientation of AF fibres with respect to the end plate makes it effective in resisting rotation, but not in resisting compression [45].

1.4 Glycans

The IVD is characterised by a large carbohydrate complex which is considered an inert material, to become hydrated and contribute to the structural scaffold. However, its composition and function depend on a topographical-specific factor whether it is in AF or NP tissue [64]. Specifically, glycans are the basic units of cellular components other than DNAs, proteins and lipids [65]. They are found abundantly in the cell extracellular interface, which is an environment with higher protein compositions such as growth factors, cytokines, immune receptors and enzymes [66]. Therefore, they are normally in the front lines to communicate between the cells by facilitating numerous interactions that can be both *in cis* (on the same cell) and *in trans* (on different cells) [67], and thereby play a key role in mediating cell-cell and cell-ECM interaction [68-70] from cell migration, and immune response to disease progression [71]. In future, the ability to remodel glycan conformation will offer a potential approach to target a specific cellular phenotype.

1.4.1 Glycan Structure and Synthesis

Generally, glycans are called carbohydrates, which consist of saccharides varying from monosaccharide to oligosaccharides. These glycans are more diverse in regard their chemical structure [65]. Each monosaccharide includes glucose, galactose, *N*-acetylglucosamine, fucose, sialic acid, mannose, *N*-acetylgalactosamine, glucuronic acid and xylose which can accommodate to a various conformations [72]. The saccharides can be linked to each other by different types of glycosidic bonds at different hydroxyl groups [72]. Encoding the enzymes by over 500 genes, glycan biosynthesis *syn* glycosylation starts in the endoplasmic reticulum and then follows in the Golgi apparatus where most of the structural variations occur [65][73-74]. The glycosylation is not template driven and involves coordinated expression of multiple glycosyltransferases, and some of these have additional tissue-specific isoforms [66].

The glycosylation is a common post-translational modification in the secretory pathway and membrane-anchored proteins, glycolipids and proteoglycans [75]. These glycoproteins and proteoglycans carry glycans via a covalent bond to protein backbones in various linkages.

1.4.2 Glycan Motifs

Based on the linkage to the protein backbone, glycans are categorised as linear and branched sugars. Branched glycans are present as *N*-linked and *O*-linked glycosylation on glycoproteins or on glycolipids [65]. Examples of glycan classification are as below (Figure 1.2):

1. *N*-glycans are synthesized continously in a step-wise manner by glycosyltransferases and glycosidases [65]. *N*-glycans, the branched sugars with a minimal amino acid sequence, begin with asparagine followed by any amino acid except proline and ends with serine or threonine (Asn-X-Ser/Thr) [76].
2. *O*-glycans, the branched polymeric structure with an initial glycan an *N*-acetylgalactosamine (GalNAc) or *N*-acetylglucosamine (GlcNAc) or mannose (Man) or fucose (Fuc) or glucose (Glc) residue linked to a Ser/Thr residue [77].
3. Glycosaminoglycans (GAGs), the linear polymer structures linked to a Ser residue by an initial xylose (Xyl). These oligosaccharide polymers comprise repeated units of sulfated disaccharide that are *O*-linked to a core protein, the latter forming a proteoglycan aggregate. This GAG family includes heparan sulfate (HS), chondroitin sulfate (CS) and dermatan sulfate (DS) [78][65].
4. Hyaluronic acid, a linear polymeric structure of the non-sulfated high molecular weight of GAGs family that is composed of the repeating disaccharide glucuronic acid β1,3-*N*-acetylglucosamine β1–4 and is not linked to any lipid or protein core [65].
5. Glycolipids, diverse, linear and branched sugars that are attached on ceramides with an initial motif galactose (Gal) or Glc- β-(1,4)-Gal residues [65].

1.4.3 Glycan Modifications

Modifications to terminal glycan linkages may be different from core linkages due to the preference for the most distal positions in the glycosylation. Thus, these linkages are usually expressed in a lineage-specific manner. This is in contrast with core linkages, which are expressed in many cell lineages and tissue types. The unique

modifications on one glycan biosynthesis site may alter the function or recognition within a specific cellular contex, but may also cause other knockout effects, and thereby contribute to the glycan diversity [74]. Examples of modification of fucosylation, sialylation and sulfation occur in many *N*- and *O*-linked glycans as well as GAGs are:

1. Glycan sialylation is represented by sialic acid in α-(2,3), α-(2,6), or α-(2,8)-linkage to a variety of underlying glycan precursors in mammals. It is known that 20 isoforms of sialyltransferases are responsible for glycan sialylation.
2. Fucosylation of glycans is characterised by α-(1,2)-, α-(1,3)-, and α-(1,4)-linked fucose to linkages terminal and subterminal substitutents of N-, O-, and lipid-linked glycans.
3. Glycan sulfation is a characteristic of the glycosaminoglycans, however, it is also found among other classes of glycans. At least 30 sulfotransferases are responsible for glycan sulfation by utilising 3'phosphoadenosine 5'-phosphosulfate as a sulfate donor from the environment. This will give a substantial diversity in glycan sulfation.

1.4.4 Glycosaminoglycans

GAGs are anionic linear heteropolysaccharide chains of repeating disaccharide units. At present, four different families of GAGs are identified. These are: CS, DS, HS and HA. DS, HS and CS and are covalently linked to proteins forming proteoglycans (PGs) aggregates [65]. HA, however, is a free chain non sulfated GAG and cell-surface-associated polysaccharide. HA is important not only for ECM composition, but also for regulation of various biological functions [79].

The CS comprises repeating disaccharide units of glucuronic acid (GlcA) and *N*-acetylgalactosamine (GalNAc) [(GlcA-β-(1,3)-GalNAc-β-(1,4))n]. The synthesis of these *O*-linked glycans is initiated via a conserved tetrasaccharide Xyl-Gal-Gal-GlcA, where Xyl and Gal indicate xylose and galactose respectively [74]. The initial step consists of the transfer of a xylose molecule on the serine/threonine residues [80] by catalysis activity of two enzymes, the xylosyltransferases I and II (XT-I and XT-II) within the endoplasmic reticulum. It is then transferred within the golgi apparatus, where the GlcA and GalNAc residues are assembled by the activity of glycosyltransferases (GalNAc transferases, GlcA transferase, chondroitin synthases,

CS *N*-acetylgalactosaminyltransferases I and II, CS glucuronyltransferases and CS polymerising factors) [81]. The CS chain is modified by epimerization and sulfation at different degrees of the glycan chain, giving high specificity and multiple biological activities. In mammals, CS is usually sulfated at the C-4 and/or C-6 positions of GalNAc. Nevertheless, the structure of CS depends on the species, normal or pathologic conditions, and the biological sources [82]. CS sulfation can occur on the carbons position at C-2 and C-3 of the GlcA and on the carbons position C-4 and C-6 of the GalNAc. The terminologies of CS-A, CS-C, CS-D and CS-E have been used to describe CS rich in [GlcA-GalNAc(4S)], [GlcA-GalNAc(6S)], [GlcA(2S)-GalNAc(6S)] and [GlcA–GalNAc(4S,6S)] respectively [82]. In the disc, the Ser-Gly dipeptide repeats in the aggrecan are covalently-linked to CS chains. These are negatively-charged within aggrecan which allows them to absorb a large amount of water to become hydrated [83]. Thus a higher CS in aggrecan composition exerts a nerve inhibitory effect in the disc [84]. The regulation of CS has been associated with the presence of growth factors such as TGF-β which regulates the production of CS in many tissues [85]. Thus, a growth factor such as semaphorin 3A is bound to CS and further exerts a repulsive effect on cortical interneurons [86]. In the spine, notochordal NP tissue with semaphorin 3A and CS is capable of inhibiting axonal growth and increasing proteoglycan content [87].

KS is a linear sugar comprising of N-acetylactosamine [→3Gal-β-(1→4)GlcNAc-β-(1→]*n* [88]. A structurally unique GAG, KS chain contains D-galactose but not hexuronic acid . The GAG sulfation occurs on the 6-carbon of both sugar moieties [88]. The structure and composition of KS differ from these of the various tissues in which KS chain is linked to protein results in KS I and II. KS I is linked to Asn in core proteins via a complex-type *N*-linked branched oligosaccharide, which is predominantly found in corneal tissue. While in cartilage, KS I is also attached to *N*-linked to modify the proteins fibromodulin [89] and osteoadherin, and small leucine-rich proteoglycans [83]. The KS II is *O*-linked via GalNAc and mucin core-2 to Ser and Thr respectively. Most of the KS II consists of highly sulfated chain sugars linked to protein aggrecan [90]. In contrast to CS, the relative proportion of KS to CS in aggrecan increases with age and in the degenerated disc [84]. HA is the only GAG which is synthesized at the cell membrane and not at the Golgi apparatus and is present in protein-free chains. The

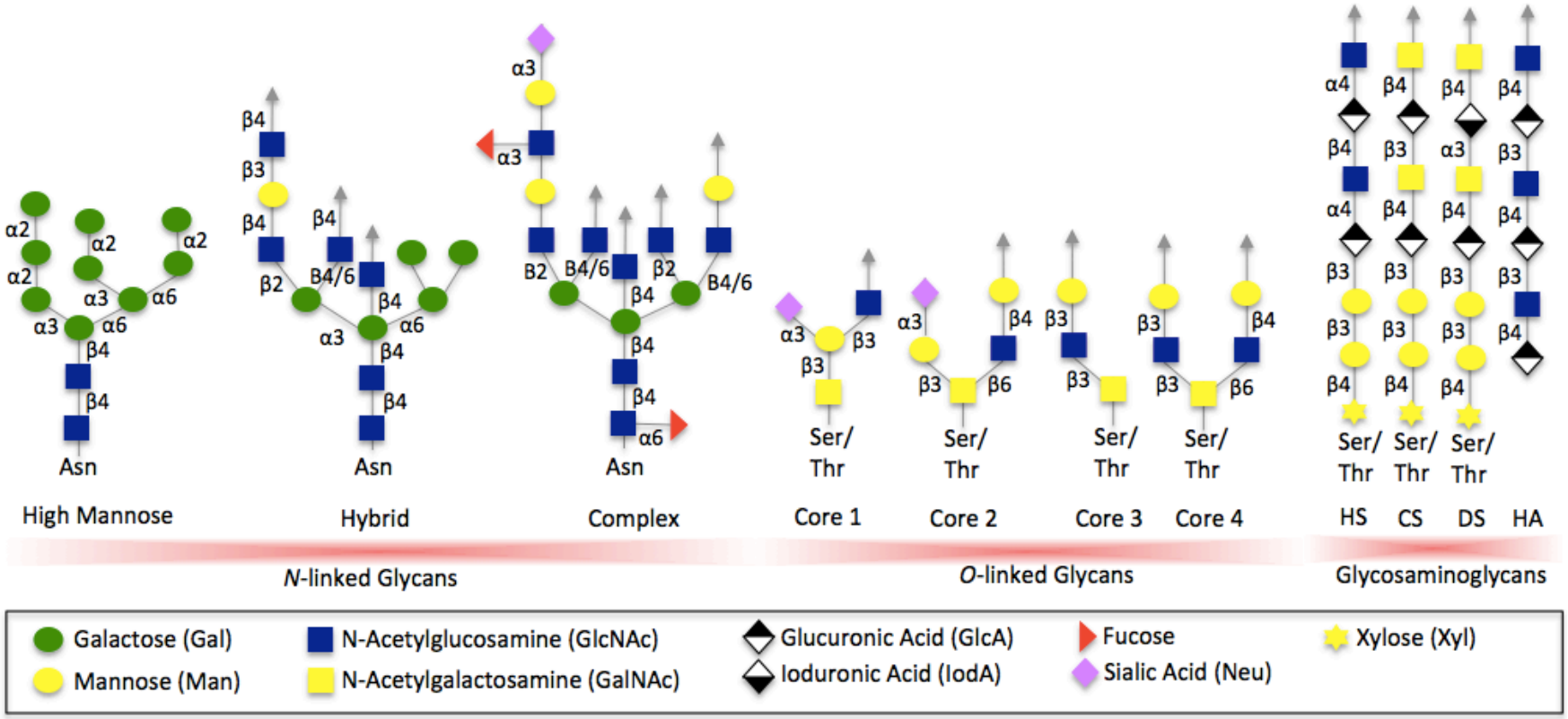

Figure 1.2 Chemical variety of glycans. Different classes of glycans are in relation to their symbol nomenclature. Linkages between monosaccharides comprise of alfa or beta glycosidic bond. Abbreviations: HS, heparan sulfate; CS, chondroitin sulfate; DS, dermatan sulfate; HA, hyaluronic acid [65].

HA molecule is a microenvironmental cue that co-regulates cell behaviour during embryonic development, healing processes, inflammation and tumour development. A comprehensive understanding of HA is presented in **section 1.10.**

1.5 Pathophysiology of Intervertebral Disc Degeneration

The onset of IVD degeneration starts in the young adult and progresses with aging and on-going degenerative events [91-92]. Disc degeneration is initiated by an imbalance of catabolic and anabolic processes in the ECM and is also mediated by an inflammatory milieu [18]. The pathogenesis of disc degeneration is summarised in Figure 1.3.

1.5.1 Phase I

The early stage of degeneration is manifested as asymptomatic with an alteration of biochemical content in the ECM due to dysregulation of ECM homeostasis whereby ECM anabolism is decreased and ECM catabolism is increased in the NP [45]. A decrease of proteoglycan and type II collagen as well as water content occurs in the NP, resulting in poor hydrodynamic transfer of axial stresses to the AF [93-95]. Additionally, aging is associated with increased cellular senescence and a decrease in cellular density and changes in cellular phenotype. These result in a loss of the cell's capacity to synthesise ECM content which perturbs ECM homeostasis. Moreover, enzymes mediating ECM degradation, including matrix metalloproteinases and aggrecanases are also increased during degeneration and aging [18][96]. The most significant dysregulation of biochemical content due to ECM degradation is the loss of proteoglycan that initiates the degradation of aggrecan, shifting the glycosaminoglycan (GAG) proportion from chondroitin sulphate (CS) to keratan sulphate (KS), and increasing other ECM compositions such as fibronectin, versican, biglycan and decorin [97]. As degeneration progresses, the lamellae of the AF become disorganised with type II collagen shifting to the outer AF and type I forming stronger collagen fibrils predominantly found within the NP and the inner AF. Also, the loss of water content decreases the osmotic pressure which makes the disc less hydrated and this leads to a loss of weight-bearing capacity and disc height [98-99]. The pathologic features, including prolonged depletion of ECM proteoglycan, cause the movement of large uncharged molecules such as cytokines, serum proteins and neurotrophins into the disc which influences

cellular phenotypes, mediates the inflammatory insult and the progression of degeneration [100].

1.5.2 Phase II

The severity of disc degeneration is represented by the levels of inflammatory mediators in the disc. Over-production of pro-inflammatory mediators is secreted by both NP and AF cells, macrophages, T cells and neutrophils during disc degeneration [101-102]. These mediators include TNF-α, IL-1α, IL-1β, IL-6, IL-17, IL-8, IL-2, IL-4, IL-10, interferon-γ (IFN-γ), regulated and normal T cells expressed and secreted (RANTES), various chemokines and prostaglandin E2 (PGE2) [25][103-106]. Pro-inflammatory cytokines such as TNF-α and IL-1β have been implicated in regulating catabolic phenotype by increasing the expression of matrix-degrading enzymes including MMPs (matrix metalloproteinases- 3, 13) and the aggrecanases, ADAMTS (a disintegrin and metalloprotease with thrombospondin motifs- 1, 4, 5, 9 and 15), over their natural inhibitors TIMP (tissue inhibitor of metalloproteinases- 1, 2 and 3) and down-regulating the anabolic of aggrecan, collagen II, collagen I, and SOX6 in native disc cells [99][25-26][107-109]. TNF-α and IL-1β has been reported to increase ADAMTS-4, an important enzyme for aggrecan degradation via the MAPK and NF-kB signaling pathways in the human NP [110]. Additionally, TNF-α and IL-1β promote the expression of MMP-3 through cooperative pathways of syndecan 4, MAPK and NF-kB [111]. Also, IL-17 has been shown to mediate the inflammatory response via p38/*c-Fos* and JNK/*c-Jun* activation in an AP-1-dependent manner in the human NP [112].

1.5.3 Phase III

At a later stage, structural changes cause the disc to lose its biomechanical function throughout the spine [45]. Fissures start to develop in the AF, allowing extrusion of the NP, providing a source for nerves and blood vessels to grow into the disc resulting in a painful spine which is symptomatic [113]. Disc cells and the infiltrating immune cells continue to release cytokines and neurogenic factors including nerve growth factor (NGF) and brain-derived neurotrophic factor (BDNF). The role of cytokines such as IL-6 at the systemic level in disc disease has been demonstrated where back pain patients diagnosed with degenerative disc disease have higher serum cytokine levels. This suggests that such patients have low-grade

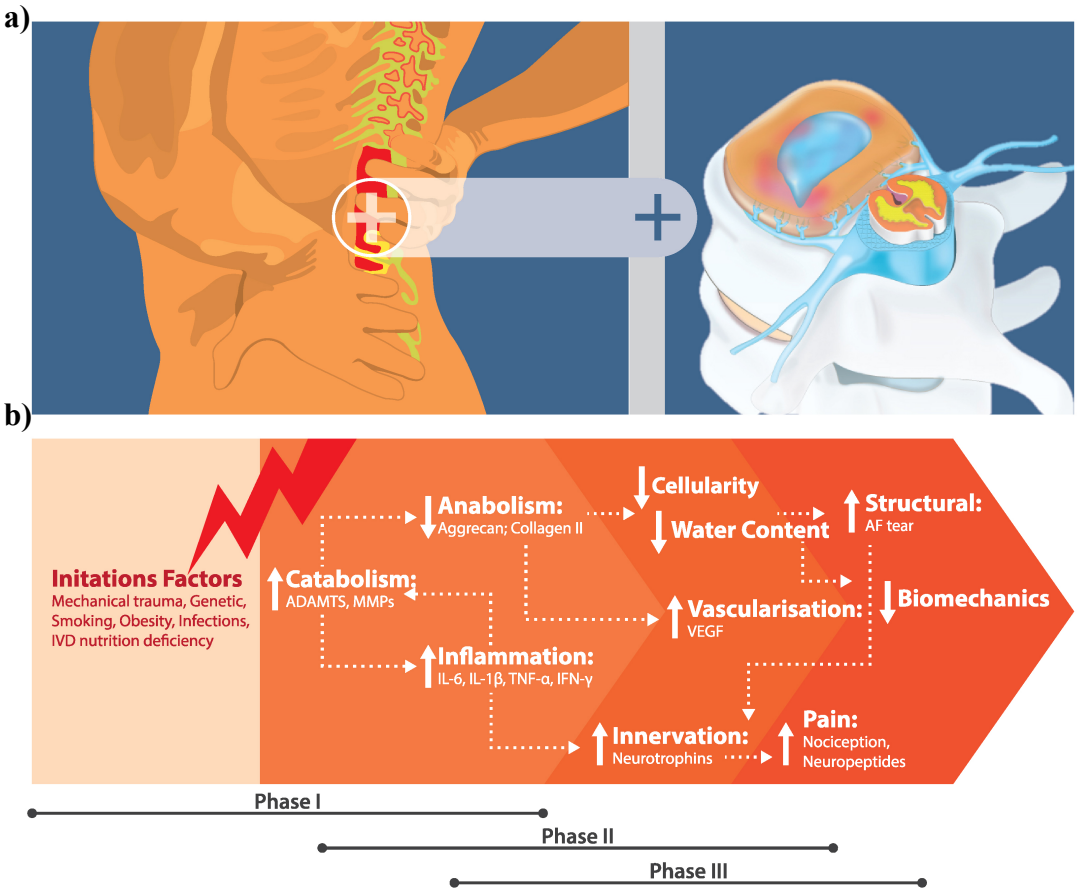

Figure 1.3 Schematic of discogenic pain caused by disc degeneration (a) and overlay phases summarise the degenerative events (b). A multifactorial condition causes an imbalance of ECM metabolism in the early phase of degeneration by increasing degradative enzymes such as ADAMTS and MMPs to promote ECM degradation that includes aggrecan and collagen. Alteration of ECM biochemical compositions induce IVD cells to produce pro-inflammatory cytokines including TNF, IL-1β and IL-6 and IFN. In phase II, inflammatory insult results in further ECM degradation and loss of cell density. Further, pro-inflammatory cytokines stimulate AF and NP cells, as well as infiltration of immune cells to release growth factor such as VEGF and neurotrophins such as NGF, BDNF to respectively promote neovascularisation and nerve ingrowth in the IVD. Phase III is characterised with continuous neurogenic insults to induce pro-nociceptive molecules such as neuropeptides to be released in IVD and spinal level, and activation of pro-nociceptor to sensitize and develop pain. Advanced structural breakdown results in annular tears and mechanical instability, and in some instances contributes to disc herniation [101].

Inflammation [114]. In a painful degenerated disc, IL-1β and TNF-α have been demonstrated to up regulate NGF and BDNF expression in human NP/AF cells to promote innervation of peptidergic small nociceptive neurons into the aneural IVD [115][30][116], and vascularisation induced by vascular endothelial growth factor (VEGF) [30]. The close relationship between the inflammatory milieu in the degenerative disc, the sensitization of nociceptors and pain processing neurons provide one explanation for the development of discogenic pain caused by degenerative disc disease.

1.6 Pain Pathway

Pain or nociception is defined as an unpleasant sensory and emotional experience associated with actual or potential tissue damage, or described in terms of such damage. This painful or noxious input is transduced by the receptors into an electrical signal and transmitted from the peripheral tissue to the central nervous system via ascending and descending tracts [117]. There are two type of nociceptors which are high-threshold mechanoreceptor and polymodal nociceptors that repond to mechanical stimulus and tissue damage mediators respectively. The inflammatory mediators (such as hydrogen ions (protons) 5-hydoxytryptamine (5-HT), cytokines, bradykinin, histamine, prostaglandins and leucotrienes) activate and sensitize these nociceptors so as to transmit nociceptive input [117].

To transmit nociception, afferent neurons via sympathetic chains [118] project to distinct areas of laminae (called Rexed laminae) in the dorsal horn of the spinal cord depending on the stratification of afferent subtypes. The afferent Aδ and C fibers project to lamina I and much of lamina II, which responds to noxious stimulation that is nociceptive specific [119]. Medium diameter myelinated Aδ afferents convey acute, well-localized “first” or fast pain, while small diameter unmyelinated C fibers mediate poorly localized, “second” or slow pain [120]. Neurons in laminae III and IV are primarily responsive to innocuous stimulation such as mechanical stimulation via Aβ fibres, while neurons in the lamina V receive a convergent non-noxious and noxious input via direct (monosynaptic) Aδ and Aβ inputs and indirect (polysynaptic) C fiber inputs [120][117].

During inflammation, an increase in the sensitisation of Aδ and C fibers occurs in the peripheral terminals at the site of inflammation as well as an increase in the excitability of afferent neurons in the dorsal horn by amplifying all sensory

inputs. Aβ fibers phenotype shift into a subpopulation such as C fibers and further increases post-synaptic transmission and exaggerates the central response to innocuous stimuli [121]. An increase of pre-synaptic neurotransmitters sufficiently depolarizes post-synaptic neurons. This includes neurotransmitters exitatory amino acids (EAAs) including glutamate and aspartate which act at both matabotropic (mGlu) receptors and ionotropic receptors including α-amino-3-hydroxy-5-methyl-4-isoxazolepropionic acid receptor (AMPA), N-methyl-D-aspartate (NMDA); pro-nociceptive tachykinins including substance P and neurokinin (NK) which acts at NK_1 and NK_2; and pronociceptive neuropeptides including CGRP action via receptor $CGRP_1$ and $CGRP_2$, to generate receptors excitatory post-synaptic currents (EPSCs) in post-synaptic neurons of the dorsal horn [122-123]. The primary activation of AMPA receptors mediates a rapid depolarisation and excitatory transmission, followed by slower and sustained EPSCs by NMDA, mGlu, NK and CGRP receptors [122]. In addition, neurotrophins such as BDNF also potentiate glutamatergic transmission, which localise in the lamina I and the lamina II of the dorsal horn. BDNF binds to its high affinity receptor of Trk B at pre-synaptic neurons to modulate glutamate and neuropeptide release. At the post-synaptic membrane, BDNF activates Trk B by autophosphorylation, leading to activation of MEK/ERK and PLC/PKC cascades. The second messengers of these pathways phosphorylate NMDA and AMPA receptors modulate their activity. NMDA receptors are implicated in BDNF-induced AMPA receptor potentiation by regulating receptor phosphorylation and trafficking [124]. In addition, synaptic transmission induces the expression of an immediate early gene *c-Fos* messenger system in post-synaptic neurons to convey nociceptive input to higher centres in the brain [125].

To convey nociceptive signals to the brain (Figure 1.4), afferent neurons cross over to the opposite site (contra-lateral) and relay pain signals along the spinothalamic tract to the thalamus and terminate in the somatosensory cortices, insula, anterior cingulate cortex, prefrontal cortex and periaqueductal grey matter (PAG) for pain localisation. Pain signals are also conducted via the spinoreticulothalamic tract to the reticular formation of the brainstem, before projecting to the thalamus and hypothalamus for emotional pain processing [117]. Furthermore, ascending pain pathway can be modulated by the activity of the second order neurons of the descending pain pathway that release neurotransmitters

resulting in facilitation (potentiate) or inhibition (supress). Descending tracts originate from the hypothalamus, limbic areas or cortex and then project to the PAG and brainstem to terminate in the dorsal horn of the spinal cord [126].

1.7 Discogenic Pain

While disc pathology is considered to be one of the causative factors that contribute to low back pain, the pathogenesis of discogenic low back pain is not well established [127]. The chances of suffering from back pain in patients with degenerated discs is 2-3 fold higher than in those individuals without a degenerated disc [128]. Back pain is mostly localized to the lower back often with corresponding changes in the low lumbar discs on MRI (Figure 1.5). Individuals with continuous multi-level disc degeneration are predisposed to a higher presence and greater severity of low back pain than in those patients with skipped level disc degeneration [129]. Mechanistically, nerve damage and sensory neuronal sensitization are hypothesized to play a key role in chronic back pain associated with degenerative disc disease [127]. Radicular pain in the distribution of one or more nerve roots may result from irritation or compression of the corresponding nerve root due to stenosis resulting from a loss of disc height or an unstable motion segment [130-133].

1.7.1 Sensory Innervation

One direct underlying mechanism of discogenic low back pain is the nerve ingrowth of sensory fibres into the aneural degenerative disc precipitated by inflammatory insults [130][134]. Early studies reported that sensory nerve fibres expressed calcitonin gene-related peptide (CGRP) [135] and nociceptive neurotransmitter including substance P. The GAP43 protein was also identified in the inner third of the AF and in the deep NP tissue in patients with chronic back pain and a degenerated disc [32]. It has been reported that the interaction of neurogenic mediators such as pro-inflammatory cytokines and neurotrophins with their receptors triggers this process [115]. Conversely, the first study reported that semaphorin 3A (sema3A), an axonal guidance molecule that highly expressed in the healthy discs than in the degenerated discs, might therefore give a repulsive effect in suppressing neural ingrowth into the healthy discs [136]. This is in line with a study demonstrated that notochordal-rich NP tissue contains higher sema3A and

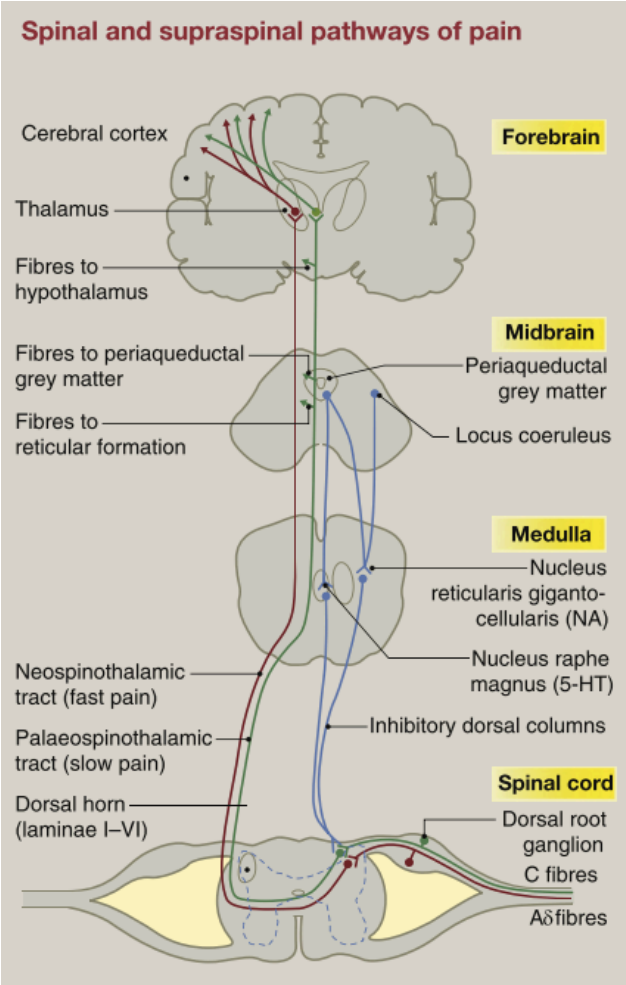

Figure 1.4 Ascending and descending pain pathways. Primary afferent neurons transmit the fast (red) and slow (green) nociceptive input to the dorsal horn of the spinal cord. The nociceptive input is then relayed to thalamus and terminated in post-central gyrus of the cortex. Descending inhibitory tracts is indicated in blue. Figure adapted from Steeds, 2016.

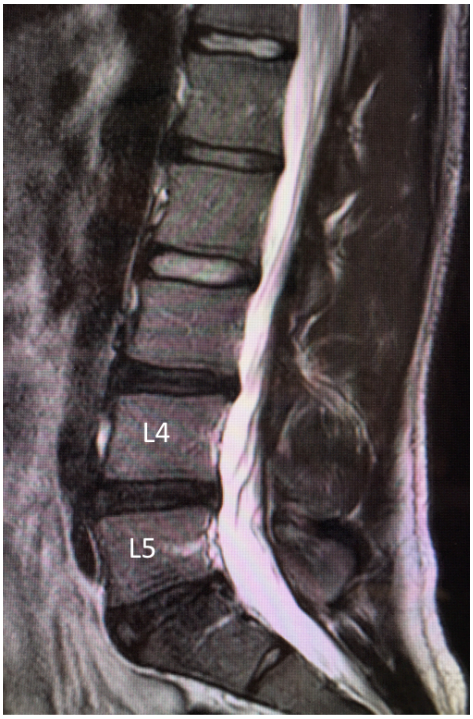

Figure 1.5 Sagittal T2-weighted MRI image demonstrates multi-level lumbar degenerative disc (indicated in black discs) from patient suffered with LBP.

chondroitin sulfate inhibited axonal growth and also promoted proteoglycan deposition, thereby it may suppress the development of discogenic pain [137].

1.7.2 Neurogenic Inflammation

Pro-inflammatory cytokines such as IL-1β have been demonstrated to stimulate neurotrophins such as NGF and BDNF with an expression of neuronal markers of the protein gene product 9.5 (PGP9.5), resulting in innervation and painful degenerated discs [30]. Interestingly, increased local production of NGF and its receptor Trk A occurs simultaneously with ingrowth of the nociceptive nerves into the degenerated disc [31]. These indicate a peptidergic population of sensory fibers present in the disc, which releases the neuropeptides, substance P, and CGRP and also expresses the Trk A neurotrophin receptor, which responds to the nerve growth factor (NGF) [120]. These nociceptive nerve fibres contain neuropeptides which originate from the DRG and are categorized as small diameter NGF-sensitive neurons [138] which play a critical role in hyperalgesic responses induced by inflammation [139-141].

The neurotrophin NGF is not only required for survival and ingrowth of the sensory nerve fibers into the degenerated disc, but also for the processes of nociception [31][142]. The binding of NGF to its high affinity receptor, Trk A, sensitizes nerve action potential by amplifying the membrane current potential that is carried by the non-selective ion channel TRPV1 [143] via activation of the p38 MAPK pathway [144] for nociceptive processing. Also, NGF increases the synthesis of nociceptive neuropeptides including substance P and CGRP [145] and central pain neuromodulators including BDNF [146] in the afferent nociceptive neurons. These neurotrophins and neuropeptides are anterogradely are transported to the peripheral terminals, and thereby induce significant neurogenic inflammation in human degenerated disc cells [147-148][115]. They are also retrogradely transported to the central terminals in the dorsal horn to enhance central sensitization for nociceptive processing [121][149-150]. As with TRPV1, NGF also maintains the basal expression of the acid sensing ion channel (ASIC) 3 through the low-affinity neurotrophin receptor (p75NTR) and extracellular matrix regulated kinase (ERK) signaling in disc cells [151]. An acidic microenvironment, and the production of lactic acid and protons via anaerobic metabolism activates nociceptor ASIC to generate musculoskeletal pain [120]. Other receptors including calcium and

potassium voltage-gated ion channels, P2X3 and G-protein-coupled receptors, are also regulated by NGF [152]. Depolarization of these nociceptor ion channels in the peripheral region of the disc may play a key role in sensitizing nociception to promote discogenic pain and enhance neurogenic inflammation mediated disc degeneration.

1.7.3 Sympathetic Afferents

From peripheral terminals, the main afferent pathways of pain are from the low intervertebral discs through the L2 spinal nerve root, via sympathetic afferents from the sinuvertebral nerves that innervates the discs [56]. This explains why many patients with disc herniation complain of sciatica without low back pain. The spinal nerve roots are being compressed proximal to the branching site of the sinuvertebral nerves, in contrast to the afferent pathways for discogenic low back pain which are not at the same level in the spinal nerves [56].

1.8 Pre-clinical Models of Disc Degeneration and Pain

An appropriate animal model of discogenic low back pain is essential to provide insights into the pathophysiology of symptomatic or painful intervertebral disc degeneration and also to determine a screening platform for testing potential therapeutic interventions. To date, pre-clinical studies in the degenerative disc have used a wide range of animal models (Table 1.1). However, pain-related behaviour and markers associated with intervertebral disc degeneration and/or herniation have thus far only been established in rodents. This is because the reliable signs of pain, such as nociceptive behavioural responses, are well established in rodents and the neurophysiological process underlying pain in rodents closely mimics human physiology [153]. Surgically induced annular injury has been extensively adopted to induce structural disc degeneration because damage to the AF plays a critical role in humans. To study regeneration, the surgically induced annular injury may serve as a superior model as complete annular injury induces NP avulsion resulting in disc degeneration relatively quickly [154]. Indeed, most animal studies focusing on radicular pain have investigated the pathophysiology of painful disc herniation after an induced annular puncture with leaking of the NP [155-157]. For example autologous NP tissues, either from lumbar or caudal disc, was grafted to the spinal nerve, DRG or nerve root to induce neuropathic or radicular pain in rats [158-162].

To date, only four studies have investigated mechanical low back pain that is pain-related behaviour following annular puncture-induced disc degeneration. An annular puncture with TNF-α intradiscal injection evoked mechanical hyperalgesia and an increase of substance P in DRG neurons with evidence of structural disc degeneration [163]. Thus, the injection of PBS into the punctured lumbar discs elicited mechanical and thermal hyperalgesia, altered gait stability and mediated structural changes in the disc [164]. Annular puncture in the lumbar disc resulted in impaired gait function, including longer stance phases and shorter strides, and an increase in sensory neuropeptides in DRG neurons [165]. Additionally, removal of the NP after puncturing the disc induced vocalisation and mechanical allodynia and decreased the disc height in rats [166]. Apart from the behaviour phenotype, pain markers at the tissue, cellular and molecular level are important indicators in determining discogenic low back pain in disc degeneration. Neuropeptides such as CGRP have been demonstrated to increase nerve innervation into the disc after disc injury in rodents [167-168]. A remarkable increase of GAP43 and PGP9.5 proteins indicates an increase in nerve ingrowth into the injured disc in rat and sheep models [169-170]. Analysis of the disc height by plane radiography, disc hydration using MRI, and ECM content such as proteoglycan and collagens by histology are the main characteristics used to determine structural degeneration in animal models such as rats [171-172] and rabbits [173-175].

In addition to complete annular injury, a superficial annular stab incision and the removal of the NP has been demonstrated to induce structural degeneration in rabbits [176-177]. Static or cyclic compressions have also been imposed commonly in the tail disc to alter the mechanical environment, thus influencing the biological behaviour of the disc [178-181]. Animal models of spontaneous disc degeneration such as sand rat [182-183], pintail mouse [184], monkey [185], and chondrodystrophic dogs [186] also have been used to study disc degeneration. Monkey models, chondrodystrophic dog models present structural degeneration such as loss of notochordal cells and glycosaminoglycan content, and promote metalloproteinase activity similar to that observed in human patients suffering low back pain due to disc degeneration [187]. Moreover, the clinical manifestation, macroscopic and microscopic appearance, diagnostics, and clinical interventions in these models are similar to those in humans [188-189].

Table 1.1 Degenerative disc disease *in vivo* models.

Species Characteristic	Model	Location	Treatment	Description of Markers	Analysis and Results	Ref
Neuropathic/Radicular Pain Model						
Rat Sprague Dawley Female	Annular puncture using a 0.4 mm diameter of needle and injected small air into the center of the disc to induced leakage of NP	IVD L4–L5	Doxycycline or infliximab locally and systemically	General discomfort	Pain behaviour: Treatment reduced wet-dog shakes and grooming	[155]
Rat Sprague Dawley Female	Annular puncture using a 0.4-mm diameter injection needle. Injected a small amount of air into the center of the disc to induced leakage of NP	IVD L4–L5	-	General discomfort	Pain behaviour: Injury increased wet-dog shakes and grooming, immobilization, minor motion, locomotion, lifting of leg on operated side Rearing and ipsilateral bending, contralateral bending	[156]
Rat Sprague Dawley	Autologous lumbar NP grafted on the left DRG	DRG L5	-	Pain – Mechanical hyperalgesia Pain – Thermal hyperalgesia Nerve transmission	Pain behaviour: Injury decreased von Frey in hindpaw Injury decreased Hargreaves in hindpaw Injury decreased peak on electromyography	[158]

Table 1.1 (Continued)

Species characteristic	Model	Location	Treatment	Description of markers	Analysis and Results	Ref
				Nerve damage	Histology: L5 spinal nerves and of sciatic nerves assessed for toluidine blue staining - swelling of myelin sheaths, demyelination, and degeneration of axoplasms	
Rat Sprague Dawley Male	Autologous caudal NP grafted on the right DRG	DRG L5	-	Pain – Mechanical allodynia Gait function Weight distribution Astrocyte and microglial activation	Pain Behaviour: Model increased hypersensitivity on von Frey test in hindpaw Rat ambulation – imbalance, gait asymmetry and stance time Incapacitance meter for weight-bearing in left and right limb DRG immunostaining: Immuno-positive of GFAP, ionized calcium binding adaptor molecule 1 (Iba1)	[159]

Table 1.1 (Continued)

Species characteristic	Model	Location	Treatment	Description of markers	Analysis and Results	Ref
				Pain – Neurotransmitter Receptors Cerebrospinal fluid biomarker	Midbrain IHC: Immuno-positive metabotropic glutamate (mGluR4 and 5), μ-opoid receptors, serotonin 2b receptor (5HT2b) ELISA for monocyte-chemoattractant protein expression (MCP-1)	
Rat Sprague Dawley Female	Autologous caudal NP grafted on the DRG	NP caudal DRG L5-L6	Epigallocatechin 3-gallate (EGCG)	Pain – Mechanical allodynia/hyperalgesia	Pain Behaviour: Treatment increased von Frey threshold on hind paw	[160]
Rat Wistar Male	Autologous caudal NP grafted on the DRG	NP S4-Co1 DRG L5	Antagonist: anti-TNF-α, anti-IL-1β and anti-CINC-1	Pain – Mechanical hyperalgesia Pain – Thermal hyperalgesia	Pain Behaviour: Treatment increased von Frey threshold on hind paw Treatment increased Hargreaves latency in plantar test on hind paw	[161]
Rat Sprague Dawley	Autologous lumbar NP grafted on the DRG	DRG Nerve root	-	Pain – central modulator-induced hyperalgesia	Injury increased immunoreactivity of BDNF in DRG by IHC	[162]

Table 1.1 (Continued)

Species characteristic	Model	Location	Treatment	Description of markers	Analysis and Results	Ref
Discogenic Pain Model						
Rat Sprague Dawley Male	Annular puncture with shallow needle depth (1.5 mm) to induce an incomplete AF injury, needle depth (3mm) to induce complete AF/NP injury and intradiscally injected with PBS, TNFα, and NGF and VEGF	IVD L3–L4, L4–L5, and L5–L6	-	Pain – Mechanical allodynia / hyperalgesia Loss disc height Anatomical degeneration Pain – Neurotransmiter and neuron	Pain Behaviour: Injury reduced von Frey threshold on hindpaw Injury induced degenerative changes indicated by lateral radiographs, Safranin O, fastgreen and H&E for disc morphology and GAG IHC: Toluidine blue and Substance P in L1 DRGs for evidence of neurotransmiter	[163]
Rat Sprague Dawley Male	Annular puncture with 26-gauge needle at a depth of 3 µm, guided by a needle stopper. 2.5 µl of PBS was injected into the IVDs	IVD L3–L4, L4–L5, and L5–L6	-	Pain – Mechanical hyperalgesia Pain – Thermal hyperalgesia Gait function	Pain Behaviour: Injury decreased von Frey threshold on hindpaw Injury decreased Hargreaves latency on hindpaw Injury altered walking stability of hindlimbs, swing duration, increased percentage of stride in stance and stance-to-swing ratio	[164]

Table 1.1 (Continued)

Species characteristic	Model	Location	Treatment	Description of markers	Analysis and Results	Ref
				General discomfort Motor function Loss disc height Hydration Anatomical degeneration	Spontaneous behaviours: Injury increased grooming and wet-dog shake Injury inclined plane test Injury incuded degeneration indicated by radiographic and postmortem MRI Histology (Safranin-O/fastgreen/H&E) shown fibrous nucleus pulposus, disorganized annular lamellae and decreased proteoglycan	
Rat Sprague Dawley Male	Annular puncture with 24-gauge needle,1.5 mm into the central portion of the anterior disc. Simultaneously, the neurotracer Fluoro-Gold injected into the disc	IVD L5-L6		Gait Function Pain - Neuropeptide for NGF-sensitive neurons	CatWalk Stride showed injury reduced length and swing speed of the front and hind paws DRGs: Injury increased immunohistochemistry for CGRP and FG-labeled neurons	[165]

Table 1.1 (Continued)

Species characteristic	Model	Location	Treatment	Description of markers	Analysis and Results	Ref
Rat Sprague Dawley	Annular puncture and NP removal with microsurgical drill (0.5 mm in diameter and 0.25 mm2 area, equivalent to a 25-gauge needle) inserted into the disc to a depth of 2 mm	IVD L4/L5 and L5/L6	Antagonist: Morphine (6.7 mg/kg)	Pain related Behaviour Pain – mechanical Allodynia Anatomical degeneration Disc height Inflammation Pain – Neurotransmitter and central modulator	Behavioral: Injury increased vocalization by applying force gauge, this was inhibited by Morphine Injury decreased von Frey threshold and high dose morphine relief pain Histology and grading: Safranin O stained loss of proteoglycan, Toluidine blue stained for mast cells; positive anti-CD11b Post-mortem x-ray showed loss of disc height qRT-PCR revealed increase expression of TLR4, MCP-1, TNF-α in DRG L4/L5 Substance P, neurokinin 1 in and L5/L6 DRG for neuropeptide Y, BDNF, voltage-gated calcium channel $\alpha_2\delta_1$	[166]

Table 1.1 (Continued)

Species characteristic	Model	Location	Treatment	Description of markers	Analysis and Results	Ref
Disc Degeneration Model						
Rat Sprague Dawley Male	Annular puncture with 23-gauge needle	IVD L5-L6	Antagonist: Anti-NaV1.7 Antibody	Pain - Neurotransmitter for NGF-sensitive neurons	Injury induced CGRP-IR in L1-L6 DRG and the expression was reduced by the treatment	[167]
Mice (C57BL/6NCr) Nine-week-old male	Percutaneous annular puncture three times using a 30-gauge needle	IVD Co3-Co4 Co4-Co5 Co5-Co6 Co6-Co7 Co7-Co8	Antagonist: anti-IL-6R monoclonal antibody	Inflammation Pain - Neurotransmitter for NGF-sensitive neurons	IHC and ELISA: Injury induced IL-6, IL-6R and CGRP and this was inhibited by antagonist	[168]
Rat Sprague Dawley Male	A perforation 0.5 mm in depth was made on the left ventrolateral surface of the disc using a 23-gauge needle, post-surgery 7 days injection of Freund's adjuvant	IVD L5–L6	-	Pain - Innervation Pain - Neurotransmitter for NGF-sensitive neurons Pain - Neurotransmiter for GDNF-sensitive neurons	Fluoro-Gold neurotracer, IHC: Injury induced expression of GAP43, CGRP and IB-4	[169]
Sheep Merino	Annular lesion in the outer one third of the left anterolateral, 4-mm deep	IVD L1–L2 L3–L4	-	Pain - Innervation	IHC: Injury induced expression of GAP43 and PGP 9.5	[170]

Table 1.1 (Continued)

Species characteristic	Model	Location	Treatment	Description of markers	Analysis and Results	Ref
Rat Sprague Dawley	Rat-tail model blade injury,1-inch longitudinal hemisection	IVD Co2–Co3 (normal) Co3–Co4 (Injury + MSC-transplantation) Co4–Co5 (Injury + saline)	Human MSC transplantation	Disc height Hydration Anatomical Degeneration	Post injury 2, 4, 6, and 8 weeks: Radiology by x-ray showed injury induced loss of disc height, but retained by the treatment MSC Histology: H&E indicated AF restoration by MSC IHC by nucleic antibody (ANA Ab) revealed MSC survived for 2 weeks	[171]
Rat Athymic Male	Annular puncture using18-gauge needle	IVD Co3-Co4	High density collagen gel of 15 mg/mL, riboflavin (RF) cross-linked (15 mg/mL): 9 with 0.25 mM RF, and 6 with 0.5 mM.	Disc height Hydration severity Anatomical degeneration	Radiology x-ray demonstrated loss of disc height in untreated disc compared to collagen gel MRI Pfirrmann grade of III with black disc in untreated group Histology: Safranin O stained fibrous cap, alcian blue presented NP extrudes through the annular defect into the paravertebral space and disorganised AF lamellar in the un-treated discs, but show tissue restoration by the collagen gel	[172]

Table 1.1 (Continued)

Species characteristic	Model	Location	Treatment	Description of markers	Analysis and Results	Ref
Rabbit New Zealand white	Annular puncture using 18-gauge needle at depths of 1 and 5-mm	IVD - L2–L3 or L4–L5	-	Disc Height Hydration Pain – Innervation	Radiographs x-ray showed loss of disc height MRI grade III Immunostaining PGP9.5 positive with scar tissue formation	[173]
Rabbit New Zealand white 8 month-old	Anular puncture using 18- gauge needle; anterolateral region of AF	IVD - L2/3 (punctured), L3/4 (non-punctured), L4/5 (punctured), L6/7 (non-punctured)	-	Disc height Hydration	Radiographs x-ray showed loss of disc height MRI T2 NP reduced Post-mortem: lower peel strength in the inter-lamellar matrix of the AF by 180-degree mechanical peel test	[174]
Rabbit New Zealand white 3.5 kg 4-5 month-old	Percutaneous annular puncture with 18-gauge angiography needle, inserted 3-4 cm ventral from the midline into the disc space under flouro scopic control	IVD L2-L3 L3-L4 L4-L5	-	Disc height Hydration ECM Anabolism	Post-surgery 4, 8, or 20 weeks: Radiographs x-ray showed narrowing of disc space MRI loss and mild Histology Safranin O, collagen I/II and PCR MMP-13, ACAN indicated degenerative changes upon injury	[175]

Table 1.1 (Continued)

Species characteristic	Model	Location	Treatment	Description of markers	Analysis and Results	Ref
Rabbit New Zealand white 3.5kg	Classical stab incision using scalpel 11 blade about 2 to 3 mm wide and 5 mm Annular puncture; 1–2mm diameter using16,18 and 21-gauge needle at depth of 5 mm	IVD - anterior approach L2–L3 L4–L5	-	Disc height Hydration severity Anatomical degeneration	Disc narrowing by lateral plain radiographs using x-ray MRI analysis 2, 4, or 8 weeks, grade IV 16G, grade III 18G, grade II 21G. Postmortem: 2, 4, 8, or 24 weeks histology showed degeneration	[176]
Rabbit New Zealand white 1.5 kg	NP removal (5–8mg wet weight) using a 21- gauge needle on a 10ml syringe	IVD antero-lateral approach L2–L3 L3–L4 L4–L5	LacZ expressing MSCs transplantation after 2 weeks induced degeneration	Disc height Hydration ECM anabolism	Plain radiograph X-ray T2-weighted by MRI Histology – Safranin O preserved nucleus with circular annulus structure in MSC-transplanted discs, IHC and matrix associated gene expressions - Restoration of proteoglycan accumulation by the MSC transplantation	[177]

Table 1.1 (Continued)

Species characteristic	Model	Location	Treatment	Description of markers	Analysis and Results	Ref
Rat Sprague Dawley Male	Static compression at 1.3 MPa loaded for up to 56 days	IVD Co8-Co10	-	Anatomical severity Loss notochordal cells Apoptosis Anti-apoptosis	Histology: Injury induced decreas of AF and NP cellularity IHC demonstrated cytokeratin-8- and galectin-3-co-positive cells, IHC revealed immuno-positive caspase-3/8, p53-regulated apoptosis-inducing protein 1 increase IHC: Decreased of B-cell lymphoma 2 (Bcl-2) and silent mating type information regulation 2 homolog 1 (SIRT1)	[178]
Rat Wistar 12 month-old	Static compression forces of 0.1, 0.2, 0.5, and 1.0 MPa were applied with springs at t = 46, 76, 106, and 136 min	IVD Co8-Co9 Co6-Co7, Co10-Co11 (control)	-	Disc height ECM anabolism ECM catabolism	Radiographs by x-ray showed loss of disc height qPCR revealed for aggrecan, collagen I/II qPCR indicated increase for MMP3, MMP-l3 and ADAMT-4	[179]

Table 1.1 (Continued)

Species characteristic	Model	Location	Treatment	Description of markers	Analysis and Results	Ref
Rat Sprague Dawley Male	Static or cyclic of 0.5, 1.5, or 2.5 Hz	IVD Co6-Co7	-	Mechanical intergrity	Angular compliance, angular laxity, and interpin distance	[180]
Rat Sprague Dawley Male	Cyclic rotation to ±5°, ±15°, and ±30°, static rotation to +30°	IVD Co8-Co9 Co6-Co7, Co10-Co11 (control)	-	Mechanical intergrity ECM catabolism ECM anabolism Inflammation	Cyclic torsion upregulated elastin expression in AF qPCR for ADAMTS4 and MMP12 qPCR for ACAN and TIMP3 qPCR for TNF-α, IL-1β	[181]
Rat (Sand) Psammomys obesus Male and female	Sand rat breed	IVD cervical, lumbar, thorasic level	-	Anatomical degeneration	Histology – H&E, Alcian blue and nuclear fast red: trabecular and osteoblastic surface, osteoclast containing lacunae	[182]
Rat (Sand) Psammomys obesus Male and female	Sand rat breed	IVD T12–L1, L1–L2, L2–L3, L3–L4, L4–L5, L5–L6, L6–L7, L7–S	-	Disc height Anatomical degeneration	Lateral radiographs Irregular disc margins, disc collapse, endplate calcification, ligament calcification, subchondral sclerosis, and osteophyte.	[183]

Table 1.1 (Continued)

Species characteristic	Model	Location	Treatment	Description of markers	Analysis and Results	Ref
Pintail mice (pt/+) and (Pt/Pt)	Mutation by carcinogen and methylcholanthrene	IVD lumbosacral level	-	Anatomical degeneration	Histology: H&E, alcian blue and chlorantine fast red – no notochordal and NP cells, contain fibrocytes and predominant cartilagous tissue with proteoglycan, increase collagen, AF differenciate normally, ossification in AF	[184]
Monkey Male and female	Mercury exposure on macaque (Macaca fascicularis)	IVD thoracolumbar level	-	Disc height Osteophytosis Mechanical properties	Radiography showed model induced disc space narrowing and osteophytosis Impulse and cyclic test – axial compression loading, cyclic sinusoidal loading – increase stiffness and alter energy absorption at advancing degeneration	[185]

Table 1.1 (Continued)

Species characteristic	Model	Location	Treatment	Description of markers	Analysis and Results	Ref
Canine	Chondrodystrophic (CD) dog breed	IVD C3-C4, T6-T7, T8-T9, T12-T13, L1-L2	-	Disc height Osteophytosis Anatomical degeneration Mechanical intergrity	Radiography – loss height and osteophytosis H&E - necrosis and calcification of the chondroid tissue, proliferation of cartilage, bone formation, and neovascularization Compression loading - increase strain and decrease peak stress and elastic modulus	[186]
Canine	Chondrodystrophic (CD) and non-chondrodystrophic (NCD) dog breeds, older than 1 year	IVD	-	Disc Height Anatomical degeneration Loss notochordal cells ECM anabolism ECM catabolism	Histological Thompson grade IV NP with increasing cell cluster size, disorganization of the AF, and increasing appearance of clefts and cracks in the disc, loss notochordal cells GAG content by DMMB assay Increased MMP-2 by zymography	[187]

Table 1.1 (Continued)

Species characteristic	Model	Location	Treatment	Description of markers	Analysis and Results	Ref
Canine	Chondrodystrophic (CD) and non-chondrodystrophic (NCD) dog breeds Degeneration and herniation	IVD cervical thoracolumbar lumbosacral	-	Hydration Severity ECM anabolism Inflammation Anatomical degeneration	MRI Pfirrmann grading IV, V GAG content in the NP reduce ELISA: Injury increased IL-2, IL-6, IL-7, IL-8, IL-10, IL-15, IL-18, IP-10, TNF-α, and GM-CSF,PGE_2, CXCL1 and CCL2 IHC: COX-2 Histology indicated degeneration	[188]
Canine	Chondrodystrophic (CD) and non-chondrodystrophic (NCD) dog breeds		-	Loss notochordal cells Anatomical degeneration	Histology: H&E displayed loss of notochordal cells, increase of chondrocyte-like cells, disorganization of the lamellar fibre Picrosirius red and Alcian blue showed no clear demarcation NP /AF, increase collagen	[189]

Nevertheless, none of these models have investigated pain related behaviour compared to that in rodent models. Therefore, a rat model of disc degeneration associated pain has been established in this study to further determine the therapeutic efficacy of potential intervention in the alleviation of pain for disc regeneration.

1.9 Current Clinical Treatment

Most discogenic back pain (90%) resolves within three months of onset. However, a number of patients with an acute episode of low back pain progress to chronic low back pain, which is associated with disability [14]. Surgical intervention such as spinal fusion is the last resort when conservative management fails [14]. Spinal surgery has traditionally worked best for spinal stenosis or radicular pain. Surgical decompression with or without discectomy has stood the test of time for compressive radiculopathy. Surgery for back pain, particularly mechanical back pain, is not quite so predictable. Spinal fusion techniques have evolved over the past hundred years and various biologic agents have been developed to promote bony fusion [190-193]. Clinical experience has demonstrated that mechanical back pain often persists despite bony fusion indicating that the disc is not necessarily the pain source. Far greater attention has recently been paid to the sagittal balance of the spine when planning surgical fusion as it has become apparent that the muscle is often the source of pain. If careful attention is paid to the sagittal balance of the spine then interbody fusion and elimination of the disc as a potential pain generator has been shown to significantly improve low back pain. A two-year clinical trial revealed pain reduction and a greater functional improvement among patients who had spinal fusion surgery compared to patients who had unstructured physical therapy [194]. Currently, multimodal conservative management including pharmacologic treatments and physiotherapy are the most satisfactory clinical modalities to relieve pain for patients especially at the early stage of degenerative disc disease [14]. Percutaneous minimally invasive treatments that target the underlying disease pathology specifically targeting innervation of the disc have recently been introduced.

Pharmacologic treatments include acetaminophen, nonsteroidal anti-inflammatory drugs (NSAIDs), muscle relaxants and opioid analgesics are only effective for short term treatment of acute low back pain [195][34]. A Cochrane

review (51 trials) from a systematic review of randomised controlled clinical trials found that non-selective NSAIDs are superior to placebo for the treatment of acute low back pain. For chronic low back pain, a NSAID (ibuprofen) is superior to placebo [34]. In the US, ibuprofen and naproxen account for most of the prescriptions for traditional NSAIDs (60%), while muscle relaxants including cyclobenzaprine, carisoprodol, and methocarbamol are also prescribed [35]. Treatment with benzodiazepines, non-benzodiazepines and anti-spasticity muscle relaxants results only in a marginal clinical reduction in acute low back pain for patients relative to placebo [196]. Opioid therapy has a short term analgesic efficacy for chronic back pain, which is moderately effective with a decrease in pain intensity of at least 30% reported [197]. In one US health plan, 87% of all morphine equivalents for pain were dispensed to patients receiving long term opioids[198]. Patients with back pain are more likely than other patients with common pain diagnoses to receive high doses of opioids [199]. Indeed, per capita the use of potent opiods (fentanyl, hydromorphone, methadone, morphine, oxycodone, and pethidine) is higher in Canada and North America, and double the rate in Germany, United Kingdom, Australia and New Zealand [197]. However, long-term treatment with opioids or sedatives is generally discouraged due to risks of tolerance and side effects [200]. Systemic corticosteroid treatment with intravenous pulse glucocorticoids has only a short term efficacy in treating acute pain. However no difference in alleviating chronic pain by a single intramuscular injection of methylprednisolone has been observed [34]. Antidepressants including tricyclic and tetracyclic drugs have demonstrated pain reduction in patients with chronic low back pain without clinical depression [201]; however there is no consistent evidence of a functional improvement [202]. Treatment with selective serotonin-reuptake inhibitors and trazodone are ineffective for patients with chronic low back pain [201].

Physical therapy, exercise and manipulation resulted in some improvement, but little is known as to their effects over the long term [93]. A Cochrane systematic review of randomized controlled trials revealed various exercises including strengthening, stretching exercises, and conventional physical therapy that consists of hot packs, massage, and stretching, flexibility, and coordination exercises, proved more effective in reducing pain and improving functional disability, than was achieved by placebo [203]. None of the less intensive rehabilitation programs,

especially those not recommended by extensive components of behavioural therapy, or pain management programmes relying on spinal injections and analgesic drugs, offer clear advantages over usual care for improving functional outcomes [200].

Epidural injections are commonly performed to treat chronic discogenic pain, administered via the lumbar epidural space by multiple routes including interlaminar, caudal, and transforaminal [93]. A systematic review study indicated the effectiveness of epidural injections with local anesthetics and steroids for the treatment of discogenic low back pain with radiculitis [204]. Hard evidence to support the use of injections of glucocorticoids or anesthetic agents into the epidural space, lumbar discs, lumbar facets, to treat chronic low back pain patients without radiculopathy [205-206]. Nevertheless, these methods are used universally in clinical practice due to the lack of effective treatments with at least anecdotal benefit reported by patients. The mechanism of action of epidurally administered local anesthetic injections is believed to be through inhibition of nociceptive input, the reflex mechanism of the afferent fibers, self-sustaining activity of the neurons, and the pattern of central neuronal sensitization [204][93]. Corticosteroids have been shown to reduce inflammation by inhibiting the synthesis or release of pro-inflammatory mediators and by causing a reversible local anesthetic effect [93].

Alternatively, percutaneous minimally invasive procedures such as annuloplasty, percutaneous disc decompression, intradiscal steroids, and intradiscal laser devices have been advocated for the treatment of discogenic back pain. The annulaplasty approach uses intradiscal electrothermal and radiofrequency annuloplasty. Intradiscal electrothermal therapy (IDET) modifies the collagen architecture of the disc making it thicker, and causing it to contract and decreasing its ability to revascularize [14]. IDET also destroys (coagulates) the nociceptors within the annular region, thus inhibiting transmission of nociceptive input chemically or mechanically, thereby alleviating pain [207]. In 2000, a prospective study reported significant pain reduction and improvement in the daily activities of patients who received IDET treatment [208]. One meta-analysis study reported some evidence for the efficacy and safety of IDET [209]. However in 2006, a critical appraisal concluded that the efficacy of IDET remains weak and is only moderately effective in managing chronic discogenic low back pain [210].

Percutaneous disc decompression includes laser discectomy, radiofrequency coblation, mechanical disc decompression and manual percutaneous lumbar

discectomy. The most common laser (Clarus Medical) for the lumbar spine is holmium: yttrium-aluminum-garnet (Ho:YAG). The others are potassium-titanyl-phosphate and neodymium (Nd:YAG) laser. A percutaneous nucleotomy using cannulas aims to decrease intradiscal pressure to reduce irritation of the nerve root and the nociceptive receptors in the AF. Then, the use of cannulas reduces the risk of nerve injury, facilitates removal of the NP with an all-in-one suction cutting device, and decreases surgical time [14]. Other devices such as Dekompressor® (Stryker Corporation, Kalamazoo, MI, U.S.A.) were developed to remove approximately 0.5 to 2 cc of NP tissue [14]. However the evidence base for these devices in the treatment of back pain is poor.

Spinal surgery has traditionally worked best for spinal stenosis or radicular pain. Surgical decompression with or without discectomy has stood the test of time for compressive radiculopathy. Surgery for back pain, particularly mechanical back pain, is not quite so predictable. Spinal fusion techniques have evolved over the past hundred years and biologic agents have been developed to promote bony fusion [190-193]. Clinical experience has demonstrated that mechanical back pain often persists despite bony fusion indicating that the disc is not necessarily the source of pain. Far greater attention has recently been paid to the sagittal balance of the spine when planning surgical fusion as it has become apparent that the muscle is often the source of pain. Paying careful attention to the sagittal balance of the spine facilitates interbody fusion and the elimination of the disc as a potential pain generator significantly improves low back pain. A two-year clinical trial revealed pain reduction and a greater functional improvement among patients who had spinal fusion surgery compared to patients who had unstructured physical therapy [194].

1.10 Tissue Engineering for Disc Regeneration

Research in tissue engineering has emerged over the past decade including biomaterial-based, cellular and molecular therapies for disc repair. To date, spinal intervention technologies are critically not regenerative in nature to treat degenerative disc patients with low back pain. Therefore, tissue-engineering strategies using biomaterials alone and enriched with cells and/or therapeutic molecules targeting the multiple signaling pathways underlying disease are potentially a therapeutic strategy to regenerate the degenerative disc and relieve pain (Figure 1.6). Cell-based therapies can be delivered alone or injection within a

biodegradable scaffold. Autologous AF and/or NP cell transplantation; exogenous cell transplantation including allogenic, xenogenic AF and/or NP cells, multipotent stem cells, cells activated or pre-differentiated *in vitro*; and endogenous cell stimulation and recruitment such as notochordal cells and MSCs using growth factors/proteins are potential pathways to replicate IVD homeostasis [211]. Since the degenerated disc is characterised by low cellularity and an environment with insufficient nutrients, incorporating therapeutic molecules such as growth factors [212-214], cellular regulator [215], and drug or inhibitor [216-217] exhibits potential as a therapeutic strategy for disc repair.

Biomaterials scaffolds act as a cell carrier by providing a physical support for cell placement, promoting specific cellular micro-environments and molecules that directly target cellular activity [218]. Biomaterials can transport exogenous proteins, genes, small molecules and drugs to the target site. This delivery system functions to protect and provide sustained release of the therapeutic agents over time for a continuous effect [24]. To date, numerous biomaterials including alginate [219-22-], chitosan [221-222], gellan gum [223], hyaluronan [224-226], collagen [177][227] and fibrin [228-229] have been used as tissue engineering strategies to repair the disc as summarized in Table 1.2. This biomaterial approach gives an advantage as a therapeutic strategy to modulate the ECM in the disc by providing an optimal micro-environment for cell adhesion and proliferation, synthesis of protein and macromolecules, that influences multiple signaling pathways and offer protection from hostile local injection/implantation environments [37][218].

Overall, the suitability of a biomaterials scaffold for tissue engineering should meet the requirement of biocompatibility, biodegradability, sufficient mechanical integrity, chemical or structural architecture that allows the diffusion of nutrients, metabolites and regulatory molecules to and from the cells, and availability for manufacture that is cost effective to scale up the technology [230]. The future direction of the biomaterial approach in tissue engineering is developing the therapeutic effectiveness of the biomaterial itself in modulating molecular, cellular and extracellular cell functions for disc repair. In particular, hyaluronic acid (HA) or hyaluronan has developed quickly over the years from mere scientific novelty to actual biomedical applications.

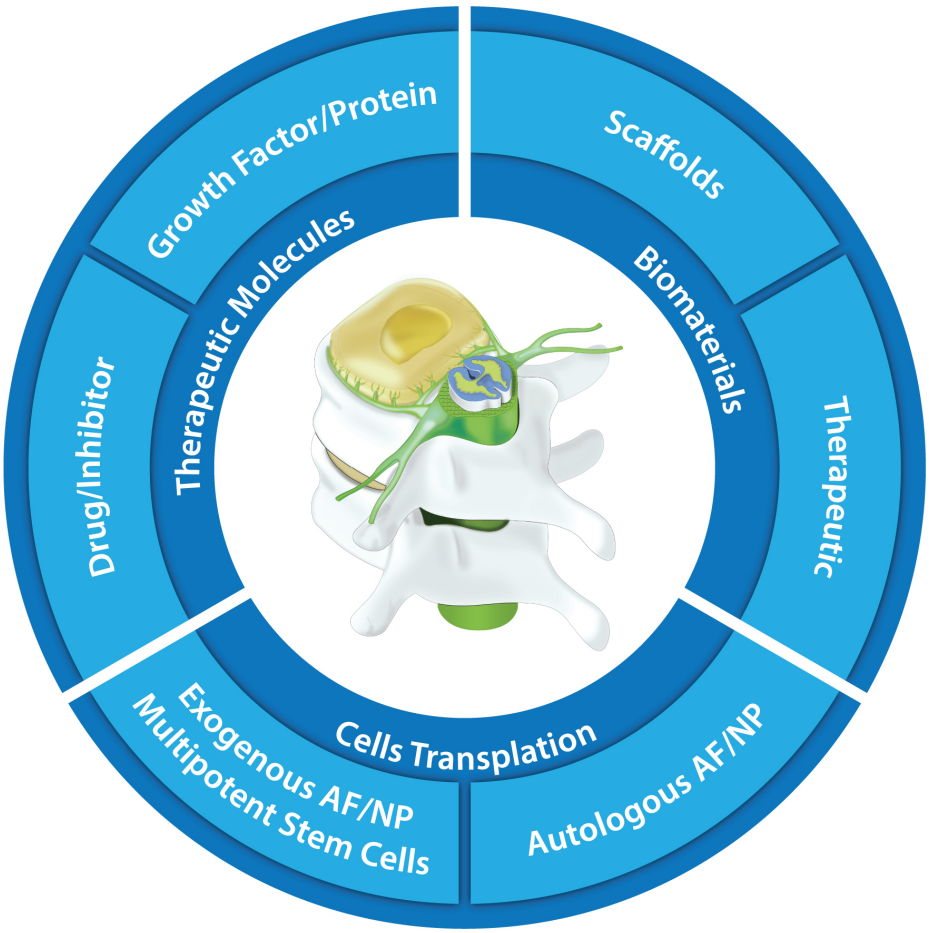

Figure 1.6 Tissue engineering strategies for IVD regeneration. Therapeutic molecules such as drug or inhibitor or growth factor can be incorporated to target specific signalling pathway underlying disc degeneration at early stage of the disease. Transplantation of cells either exogenous or autologous can be performed to re-populate native cells for disc tissue regeneration where it is required for mild or late stage of degeneration. Both therapeutic molecules and cell therapy can be delivered via biomaterials, for example scaffolds have been used to provide a conclusive microenviornment for AF and NP cells survival and release the cargo to the target site for the long term efficacy. Biomaterials platform can be utilised as a therapeutic strategy in alleviation of pain and promote disc repair.

Table 1.2 Example of biomaterials employed for disc tissue engineering.

Scaffold	Cell source	Descriptions	Analysis and Results	Ref
Cell-alginate construct	IVD cells (AF, TZ, and NP) from lumbar spine of 4-5 month-old pigs	Mechanical integrity ECM anabolism	3D *in vitro*: Decreased of compression and shear stress qPCR showed collagen I expression in AF and collagen II expression in transition zone	[219]
Alginate-collagen porous composite	AF and MSCs of porcine 4 months-old	Shape memory Microstructure Cell morphology ECM anabolism Mechanical integrity Cell migration Cell viability ECM anabolism Cell viability	Swelling ratio SEM: porosity H&E for cell colonization Picro-sirius red for collagen deposition Compressive equilibrium modulus Release profile from TGF-β3 *In vitro* AF cell migration: Cell cytoskeleton fluorescence staining, cell morphology using SEM, DNA content and *In vitro* cyto-compatibility of MSCs: Cell viability, biochemical content, and histology Fibroblastic-like cell morphology Cell proliferation and extracellular matrix deposition (collagen type I) TGF-B3 Bovine *ex vivo* organ defect model: maintained viability of transplanted MSCs	[220]
Chitosan hydrogel	Coccygeal IVDs from 2–4 year-old bovine	ECM anabolism	*In vitro*: DMMB: GAG retention in gel Histology Safranin O and fast green GAG Content	[221]

Table 1.2 (Continued)

Scaffold	Cell source	Descriptions	Analysis and Results	Ref
Chitosan–glycerophosphate hydrogels	Human MSCs, NP cells and Human articular chondrocytes	Cell viability Cell distribution and morphology Chondrgenic marker Osteogenic marker Fibroblastic marker ECM anabolism DNA content	*In vitro*: Live/dead assay Histology H&E and Masson trichrome RT-qPCR: SOX-9, type II collagen, aggrecan and type I collagen Conventional PCR: type X collagen DMMB: GAG Content Sircol assay: Collagen content Picogreen assay: DNA content	[222]
Ionic-(iGG–MA) and photo-crosslinked (phGG–MA) methacrylated gellan gum hydrogels	MSCs, Nasal chondrocyte, Human dermal microvascular endothelial cells	MSCs phenotype Cytotoxicity Inflammation ECM anabolism Apoptosis Microstructure Anatomical degeneration	*In vitro*: Surface marker CD29, 44, 73, 90, 105 Alizarin red for tri-lineage differentiation Von Kossa for osteogenic differentiation Oil red O for adipogenic differentiation Safranin O, alcian blue and collagen II for chondrogenic differentiation, MTS and crystal violet assays were ELISA for IL-8 and ICAM-1 IHC for collagen II, aggrecan and vimentin TUNEL assay for cell death TEM *In vivo* subcutaneous implantation in SCID mice: IHC	[223]

Table 1.2 (Continued)

Scaffold	Cell source	Descriptions	Analysis and Results	Ref
Hyaluronan-poly(N-isopropylacrylamide) (HA-pNIPAM)	Human MSCs		*In vitro*:	[224]
		Cell viability	Live/dead cytotoxicity
		DNA content	Quant-IT PicoGreen assay
		ECM anabolism	DMMB assay for sulfated GAG
		Disc phenotype	qPCR for collagen type I a1 and II a1 (COL1 and COL2), aggrecan (ACAN), cytokeratin-19 (KRT19), SOX9, cluster of differentiation 24 (CD24), fork-head box protein F1 (FOXF1), and CA12
			Bovine caudal *ex vivo*:
		Cell viability	Live/Dead assay, and DNA content, GAG and gene expression
		ECM anabolism	
Thiolated hyaluronic acid/poly(ethylene glycol)vinylsulfone hydrogel	AF and NP cells from lumbar spines of pig 3–6 month-old		*In vitro*:	[225]
		Mechanical integrity	Storage modulus torsional dynamic shear test by DMMB for sulfated GAG
		ECM anabolism	DNA contents
		DNA content	Lactate and pyruvate concentration
		Metabolites	Light microscopy
		Cell morphology	

Table 1.2 (Continued)

Scaffold	Cell source	Descriptions	Analysis and Results	Ref
Collagen I gel cross-linked riboflavin	-	Anatomical degeneration Hydration Mechanical integrity	*In vivo* of punctured IVD model: FITC-labeled collagen gel Safranin O and Alcian blue for tissue reorganization and retention of NP MRI Pfirrman grade Stress-relaxation tests; hydraulic permeability	[236]
Atelocollagen implant	MSCs from rabbit bone marrow	Adipogenesis Chondrogenesis Calcium deposition Disc height Hydration Adipogenesis Chondrogenesis ECM anabolism	*In vitro*: MSCs differentiation assay; Oil red O staining Immunostaining for type II collagen and keratan sulfate IHC Von Kossa staining *In vivo* rabbit model: Lateral plain radiographs MRI Histology Oil red O Von Kossa staining IHC keratan sulfate qPCR for COL1, COL2 and versican.	[177]

Table 1.2 (Continued)

Scaffold	Cell source	Descriptions	Analysis	Ref
Silk composite with Fibrin/HA composite gels	Human chondrocytes	HA functionalisation Composite volume Mechanical integrity Cell viability ECM anabolism DNA content ECM anabolism Chondrogenesis	*In vitro* characterisation: FTIR for amide I region components 3D volume measurement for surface area and volume Elastic modulus and compressive strength by unconfined compression tests Live/Dead assay Histology H&E, safranin-O, and Alcian blue for proteoglycan IHC for type II collagen Quant-iT PicoGreen reagent for DNA content DMMB for GAG qPCR for Collagen II a, aggrecan, SOX-9	[228]

1.11 Hyaluronic Acid

Hyaluronic acid (HA), *syn.* hyaluronan or hyaluronate [231] is a ubiquitous polysaccharide with diverse biological functions and which is found naturally in the ECM and pericellular matrix, and also occurs intracellularly [232]. In the body, HA is found primarily in high concentrations in connective tissue including the umbilical cord, skin, cartilage, nucleus pulposus of the disc, and synovial fluid [233]. It was first identified in the vitreous body of eye [234]. In body fluids, the concentration of HA ranges from 1400 to 3600 μg g^{-1} in synovial fluid, 8.5 to18 μg g^{-1} in the thoracic lymph, 0.1 to 0.3 μg g^{-1} in urine, 0.02 to 0.32 μg g^{-1} in CSF to 0.01 to 0.1 μg g^{-1} in the blood serum. A significant amount of HA is also found in the lung, kidney, brain, and muscle [233].

1.11.1 Physicochemical and structural properties

1.11.1.1 Chemical and polymer structure

HA comprises 10 000 repeating unit of glucuronic acid and *N*-acetyl glucosamine (GlcA), linked by alternate β-(1,3)- and β-(1,4)-linkages [235]. Both sugars are spatially related to glucose in which the beta configuration of this monosaccarides allow hydroxyls, carboxylate moiety and the anomeric carbon groups on the adjacent sugar contribute to sterically favorable equatorial reactions, while all of the small hydrogen atoms occupy the less sterically favourable axial reactions. Thus, the structure of the disaccharide is energetically very stable [237]. In physiological conditions, HA exists as a linear polysaccharide in a high molecular weight (HMW) form ranging from 20000 [238] to ~8 million daltons, with each disaccharide being approximately ~ 400 daltons. The average length of a disaccharide is ~1 nm and a diameter of 0.5 nm [239]. Therefore, a HA molecule could extend up to 10 μm length.

1.11.1.2 Biophysical properties

HA exists commonly as a sodium salt by interacting with polyelectrolyte cations [232]. HA forms the viscoelastic state at pH 2.5 in the presence of salt, and a gel state at pH 2.5 in a mixed organic/aqueous solution containing salt i.e NaCl. Ordered and associated structures have been observed for HA on the surfaces, especially in the presence of surface-structured water [239]. The helical appreance is found in the

HA network, with proteoglycan core protein aggregates around the HA chain [240]. In physiological solutions, the HA is supported by a combination of the chemical structure of the disaccharide, internal hydrogen bonds, and interactions with the solvent. The axial hydrogen atoms form a non-polar, hydrophobic face relatively, while the equatorial side chains form a more polar, hydrophilic face, thereby creating a helical structure [239]. A single helic of HA contains 2, 3, or 4 disaccharides per helical turn, depending on the ion present (H^+, Na^+, K^+, Ca^{2+}) [241-242]. All of these structures look like randomly stretched coils. A double helic, containing four disaccharides per turn, was also observed under unusual ionic conditions (mixed H^+/K^+, Rb^+, NH_4^+). These structures are stabilized by hydrogen bonds linking adjacent sugar residues across the glycosidic bonds [239].

1.10.2 Metabolism

Most of the GAGs are produced in the cell's Golgi apparatus and transported by the fusion of secretory vesicles with plasma membranes. Unlike other GAGs, HA is secreted by both mammalian cells and bacteria by other mechanisms.

1.10.2.1 Synthesis

HA is synthesized by an integral plasma membrane glycosyltransferases called hyaluronan synthases (HAS) within the inner side of plasma membranes e.g cytoplasm and extruded to the cell surface, which then resides extracellularly [243]. Currently, three isoforms of HAS have been identified in vertebrates known as HAS1, HAS2 and HAS3 [244]. These are highly homologous; however, they synthesis a similar HA product of varying molecular weight. HAS3 synthesized the lowest HA molecular weight (1×10^5 to 1×10^6Da), while HAS1 and HAS2 synthesized larger polymers (2×10^5 to 2×10^6Da) [245]. HAS synthesize HA by catalyzing the addition of UDP-D-glucuronic acid (GlcA) and UDP-N-acetyl-D-glucosamine (GlcNAC) monomers in an alternate assembly to form HA chains [237]. The cytoplasmic HA product is secreted into the pericellular space by multidrug resistance transporters, an energy dependent transport proteins that are responsible for transporting compounds through cell membranes [246].

1.11.2.2 Degradation

The half life ($t_{1/2}$) of HA in the circulation, skin and cartilage is 2±5 minutes, 1±2 days and 1±2 weeks respectively [247]. In physiological conditions, the turnover of

HA is through catabolism intead of through excretion, for approximately 5 g per day. Initial degradation occurs in the local tissue where it is synthesized (10-30%), in the lymph nodes after displacement from the tissues (50-90%) and clearance from the blood of that non-metabolised product by the lymph nodes by liver, kidneys and spleen [248]. The HMW HA polymer of ECM is tethered to the cell surface by CD44 and the GPI-anchored hyaluronidase of Hyal-2. The involvement of CD44 in the interaction Hyal-2 and NHE1 facilitates Hyal-2 which enzymatically cleaves the HMW HA (10^6 to10^7 Da) to oligosaccharides 20 kDa or about 50 disaccharides. These Hyal-2-generated HA fragments are internalized and delivered to lysosomes for further degradation by Hyal-1 of 20 kDa fragments to small tetrasaccharides 800 Da, which are also sequentially cleaved by β-D-glucuronidase and β-N-acetyl-D-hexosaminidase to the monosaccharides 200 Da. The single sugar product is D-glucuronic acid, and N-acetyl-D-glucosamine is released into the cytoplasm for phosphorylating to N-acetylglucosamine-6-P by N-acetylglucosamine deacetylase [247], and for processing to CO, ammonia, acetate and lactate [248]. The subsequent degradation occurs in lymph nodes and liver. It has been proposed that circulating HA levels and clearance of HA ECM breakdown products are regulated by scavenger receptors which are expressed on hepatic sinusoid endothelial cells (HSECs)/liver endothelial cells (LEC), in which HA binding activity on the surface of endothelial cells is mediated by non-endocytic (Ca^{2+}-dependent) and endocytic HA receptor such as stabilin 2 (STAB2) [247][249].

1.11.3 Therapeutic Applications

The unique viscoelastic nature of HA together with its biocompatibility and non-immunogenicity give it an advantage in clinical applications including the treatment of opthalmic diseases, osteoarthritis, pain, inflammation, respiratory disorders, wound and vascular healing, and immuno-modulation [250].

1.11.3.1 Opthalmic Treatment

HMW HA was first patented in medical treatment for ophthalmologic practice in 1979 [251] and was used for the treatment of corneal wound healing, optic nerve atrophy, malignant myopia, retinitis pigmentosa, neuroretinitis, iritis, uveitis, cataract and radial keratotamy surgeries. This is because of its viscoelastic properties which maintains intra-ocular pressure at an optimal level in the vitreous body, absorb shocks, and prevent the exfoliation of retina and pigmented epithelium [252].

1.11.3.2 Anti-nociception and Analgesics

HA has been reported to exhibit anti-inflammatory and anti-nociceptive effects in various pathologic conditions. Viscosupplementation with HA has also proved effective and safe for the treatment of osteoarthritic pain [253-255]. Intra-articular injection of HA solutions into the knee revealed a long-term beneficial effect by relieving pain [256], improving function, and reducing the volume of synovial fluid effusion without toxic effects [257]. In animal studies, HA reduced nociceptive nerve activity in a model of osteoarthritic knee joint pain in the guinea pig [258] and decreased the excitability of peripheral nociceptive neurons and joint sensory fibres in a knee joint rat model. It also reduced nociceptive behaviour in response to noxious stimuli in a mouse model [259-260]. The analgesic effect of HA has also induced stimulatory effects on the κ-opiod receptor in epithelial cell lines and rat DRG neurons [261].

1.11.3.3 Respiratory Applications

In respiratory diseases, exogenous administration of HA improves the mechanical properties of elastic fibres by preferentially adhering to the fibres from enzymatic breakdown (elastolysis) and preventing enlargement of the air-space through the increase of water content in the ECM, thereby preventing alveolar dilatation and rupture in pulmonary emphysema [262]. Thus, the administration of aerosolized HA alleviated bonchoconstriction in an airway hypersensitivity sheep model [263-264], which is postulated to be due to the binding of HA to tissue kallikrein, which reduces kinin-mediated inflammation in the bronchial walls [265].

1.11.3.4 Anti-neoplastics

Furthermore, HMW HA mediated cancer resistance via binding to the CD44 receptor and by reducing hyaluronidase activity in the naked mole rat [266]. Additionally, HA prevented tumour metastasis by elevating circulating HA levels through inhibition of its clearance receptor which is stabilin-2 in the mouse model [249][267]. Also, a cross-linked HA gel inhibited the migration and invasion activities of gastric and hepatic cancer cells, and blocked the activation of the HA cell membrane receptors of integrin α5β1, EGFR and VEGFR via downstream cascades *in vitro.* The cross-linked HA gel suppressed colonization, and the growth

and metastasis of gastric cancer in the peritoneal cavity in a nude mouse model [268]. Clinically, HA has aided the recovery of hematopoietic organ functions suppressed by chemotherapy in patients with malignant neoplasms. Irradiation facilitates HA displacement from peripheral to deeper zones of tumour cells. This restricted the growth of malignant cells in the zone of implantation and inhibited metastasis into the internal organs [250].

1.11.3.5 Anti-inflammatory

HA plays a critical role in modulating inflammation. The inflammatory activity of HA depends on its molecular weight, where HMW HA promotes an anti-inflammatory effect and tissue repair. HA is found to inhibit phagocytosis of macrophages in a dose and viscosity dependent manner [269]. In lung injury, HA protected against apoptosis through NF-kB Tlr2–/–Tlr4–/– and Myd88–/– pathways in mice [270]. In addition, it reduced pro-inflammatory cytokine plasma levels including TNF-α, IFN-γ, macrophage inflammatory protein 2, and IL-4 in a T-cell mediated liver injury of mouse model [271]. Conversely, low molecular weight (LMW) HA fragments stimulate an inflammatory response resulting in the production of pro-inflammatory cytokines (IL-1β, IL-6, IL-8, cyclooxygenase (COX)-2 and catabolic enzymes (MMP-1 and -13) via toll-like receptor 2 signalling pathways [272]. Moreover, it induces IFNβ via a novel TLR4-TRIF-TBK1-IRF3-dependent pathway [273].

1.11.3.6 Immunomodulation

In uninjured tissue, HA maintained immune homeostasis by regulating the adaptive immune system through regulatory T cells (T_{Reg}) after the tissue matrix integrity has been restored through a co-stimulatory signal of cross-linking CD44, which also promotes Foxp3 expression, a critical signalling molecule associated with T_{Reg} [274]. Also, HA promoted IL-10 producing regulatory T-cell (TR1) induction via a CD44-dependant fashion [275].

1.11.3.7 Wound Healing

HA is one of important ECM components for wound healing. The level of HA increases from initial clot and platelet plug through binding to fibrinogen, increases vascular permeability and edema by promoting endothelial integrity and inhibiting vascular leakiness, facilitates inflammatory responses by binding to CD44,

suppresses angiogenesis via inhibition of *c-Fos*, *c-Jun* and krox-20 signalling, and promotes keratinocyte proliferation for re-epithelialization. However, dysregulation of the HA metabolism is a feature of aging and diabetes and may underlie the chronic wound healing and contribute to complications such as hypertrophic scars in diabetic patients [276]. In an open wound rat model with abdominal sepsis, HA reduced damage and the size of the granulation tissue by attenuating free-radical-induced inflammation [277]. HA also promoted scarless foetal dermal healing by delaying the onset of foetal platelet aggregation and reducing its aggregation in a dose dependant manner. It also minimized inflammation by decreasing the release of platelet-derived growth factor (PDGF) [278].

1.11.3.8 Vascular Repair

For the repair of arterial injury, HA increased matrix contraction in both smooth muscle cells and adventitial fibroblasts by enhancing pericellular accumulation of collagen fibrils via CD44-receptor ligation, thus providing a potential target for therapies to prevent constrictive remodelling and restenosis [279].

1.12 Rationale for the Use of Hyaluronic Acid for Disc Regeneration

Various forms of HA have been used to study IVD regeneration, which maintain the IVD phenotype, compensate for the imbalance of ECM and cellular function, facilitate disc biomechanics, promotes disc tissue remodelling and combats the inflammatory response from further degeneration and pain, as summarised in Table 1.3.

1.12.1 Micro-environment Towards and/or Maintainance of Disc Phenotype

The capacity of the three dimensional (3D) scaffold to retain the biological function of the IVD environment makes it the most favourable platform for designing biomaterial systems for disc regeneration since the IVD is characterised as avascular with low oxygen supply. A thermoreversible hyaluronan-based hydrogel, hyaluronan-poly(N-isopropylacrylamide) (HA-pNIPAM) has been shown to induce differentiation of human mesenchymal stem cells (hMSC) to the IVD phenotype with the maintenance of cell viability, a higher GAG/DNA ratio, and an increased expression of collagen type II, SOX9, cytokeratin-19, CD 24, and forkhead box protein F1 compared to alginate hydrogels in both *in vitro* and *ex vivo* bovine models [224].

A Type II collagen hydrogel crosslinked with 4S-StarPEG enriched with HA did not influence the NP phenotype but increased NP cell viability and no cytotoxicity was observed against adipose-derived stem cells (ADSCs) [280]. A tuneable Type II collagen and hyaluronan (HA) microgel differentiated ADSCs towards a NP cell phenotype, maintained 80% cell viability and a rounder shape, and expressed high levels of collagen II, aggrecan, SOX9, and low levels of collagen I [281]. A MSC-seeded nanofibrous scaffold enveloping a HA hydrogel which resembles the native IVD was shown to undergo chondrogenesis *in vitro* with uniform cell distribution of elongated AF cells and rounded NP cells, increased ECM deposition and increased expression of IVD markers including Type I and Type II collagen, aggrecan and link protein [282]. Interestingly, a recent study reported that a bioengineered collagen Type II and HA hydrogel revealed inflammatory cross-talk on a molecular basis which modulates the production of ECM, key inflammatory pathways and altered the glycosylation profile in the inflamed IVD, thus providing an appropriate disease model *in vitro* to study disc inflammation [283].

1.12.2 Promotion of ECM Homeostasis and Cellular Function

An optimal and conducive micro-environment is essential for IVD repair to maintain ECM homeostasis, and thereby promote cellular function and provide mechanical support. A hydrogel scaffold exhibits the most promising results in IVD repair since the native NP tissue is composed of a highly hydrated ECM.

A gelatin/chondroitin-6-sulfate/hyaluronan tri-copolymer sponge maintained the NP phenotype and promoted ECM synthesis [284]. Functionalised HA/PEG hydrogels via thiolated HA or PEG vinylsulfone HA revealed higher NP and AF cell numbers with cell clustering on the HA/PEG hydrogels observed to be molecular weight dependent, with increased sulfated GAG production observed compared to a gelatin hydrogel [285]. Pentosan polysulphate (PPS) in PEG/HA based hydrogels enhanced mesenchymal progenitor cells (MPCs) towards chondrogenic differentiation, which retained good viability, adopted a rounded morphology and increased ECM deposition [286]. Interestingly, direct stimulation of human NP cells with HA induces chondrogenic differentiation and promotes proteoglycan and type II collagen deposition *in vitro* [287]. Incorporation of Bone morphogenetic protein (BMP)-2/7 heterodimer in a NP cell-seeded fibrin-hyaluronan (FBG-HA) hydrogel up-regulated mRNA expression of aggrecan and type II collagen, and

glycosaminoglycan synthesis *in vitro*. Under cyclic dynamic load in a nucleotomy bovine caudal *ex-vivo* model, the hydrogel stimulated proteoglycan synthesis with no increase in type I collagen and alkaline phosphatase expression observed, indicating no osteogenic effect [288].

1.12.3 Facilitation of Mechanical Integrity

Fine tuning of the macromolecular architecture includes viscoelasticity, injectability/implantability and physical/functional mechanical stability, all of which are key elements in developing a biomaterial scaffold for IVD repair. Enzymatically cross-linked collagen–hyaluronan gel-like scaffold maintained cell viability and retained the highest proteoglycan synthesis, thereby increasing mechanical strength [289]. A HA/gelatin hydrogel exhibited viscoelastic properties (11–14 kPa) under complex shear modulus similar to that of native tissue (11.3 kPa), which also maintaining the NP phenotype with a rounded morphology and the expression of NP specific markers such as type II collagen, aggrecan, SOX-9, and HIF-1α [290]. A Type II collagen/HA hydrogel supported the viability of rat MSCs and promoted their differentiation to a chondrogenic lineage and increased the hydrogel's compressive modulus and enzymatic stability [291]. An enzymatically-crosslinked PEG/HA hydrogel displayed a higher storage modulus ranging from 5.55 to 5.46 kPa, and exhibited predominantly elastic behaviour and hydrolytic stability over a period of three months. Furthermore, a MPC encapsulated hydrogel revealed good cell viability and promoted cartilage-like tissue with a rounded morphology, increased collagen II deposition *in vitro*, and did not exhibit any macroscopic signs of an inflammatory response in a rat subcutaneous implantation model [226].

1.12.4 Tissue Remodelling

The success of a tissue engineering strategy is determined by the capacity of the biomaterials scaffold to compensate for local tissue responses, maintain disc phenotype, attain tissue biochemical homeostasis and promote anatomical tissue repair to provide functional mechanical support. The NP cell-seeded collagen II/hyaluronan/chondroitin-6-sulfate tri-copolymer construct was shown to promote ECM deposition, and thereby increase the disc height index in a nucleotomy rabbit model [292]. In a lumbar nucleotomy porcine model, an injectable hyaluronan based photo-linked derivative of both cell-free HYAFF®120 and cell-loaded HYADD®3

prevented disc narrowing, the formation of fibrous tissue and the disruption of the bony end-plates, thereby promoting the NP-like matrix [293]. Polyglycolic acid-hyaluronan implants promoted tissue repair with an increase in type II collagen deposition in a nucleotomy rabbit model [294].

1.12.5 Attenuation of Inflammation

The anti-inflammatory effect of HA has been studied over the years in other pathological conditions. In an inflammation model of NP cells, a PEG crosslinked-HA based hydrogel has been demonstrated to reduce IL-1β signalling molecules and neurogenic inflammation markers including NGF and BDNF, possibly via binding to the cell surface HA receptor; CD44 [295]. The hydrogel down-regulated IFN-α signalling molecules, IGFBP3 and IFIT3, and reduced the catabolic phenotype to promote an ECM modulatory effect in the AF of a bovine caudal *ex-vivo* model [296].

1.12.6 Alleviation of Pain

In the study of pain, HA is well established in clinical practice in osteoarthritis; however a trial to test the effectiveness of stem cells with HA injections in patients with back pain due to disc degeneration has only been conducted recently with results yet to be published [297]. So far, only one study has demonstrated that the topical application of a HMW HA gel reduced post-operative fibrosis and radicular pain in a post-laminectomy rat model [298]. There is no evidence to date regarding discogenic as opposed to neurogenic back pain, not helped by the difficulty in distinguishing these two entities if indeed they are totally separate. Therefore, further research in this field needs to be undertaken for a better elucidation of discogenic pain caused by disc degeneration in order to develop future clinically relevant therapeutic interventions.

Table 1.3 Hyaluronic acid application in tissue engineering for IVD regeneration.

HA Scaffold	Cellular / Therapeutic Molecules	Model	Description of Markers	Analysis and Results	Ref
Micro-environment Towards/Maintains IVD Phenotype					
Hyaluronan-poly(N-isopropylacrylamide) (HA-pNIPAM) hydrogel	Human MSC	*In vitro* hMSC seeded hydrogel; *Ex-vivo* bovine caudal model	Cell viability DNA content GAG content IVD phenotype	hMSC viability by ethidium homodimer *in-vitro*, PKH26 red fluorescent dye *ex-vivo* DNA quantification by Quant-IT PicoGreen Sulfated GAG by 1,9-dimethylmethylene blue (DMMB) Gene expression by qPCR for collagen type I α1 and II α1 (COL1 and COL2), aggrecan (ACAN), cytokeratin-19 (KRT19), SOX9, cluster of differentiation 24 (CD24), fork- head box protein F1 (FOXF1), and CA12	[224]
Type II collagen hydrogel crosslinked PEG, enriched with HA	Rabbit ADSC and bovine NP cells	*In vitro* rabADSCs/ NP cells encapsulated in hydrogel	Functionalisation Enzymatic stability Gelation; Mechanical Cell viability Cell proliferation Cell distribution ECM anabolism	Characterisation: Primary amine groups of collagen by TNBSA assay Degradation by collagenase assay Gelation time and storage modulus by rheology rADSC viability by trypan blue NP cell viability by Live/Dead assay NP cell proliferation by PicoGreen assay NP distribution by dissector stereological qPCR of collagen I, collagen II and aggrecan	[280]

Table 1.3 (Continued)

HA Scaffold	Cellular / Therapeutic Molecules	Model	Description of Markers	Analysis and Results	Ref
Type II collagen and hyaluronan microgel	Rabbit ADSCs	*In vitro* rabADSCs encapsulated in microgel	Cell viability Cell proliferation Cell morphology Stress fibres Glycogen content NP phenotype	ADSCs viability by Live/Dead assay ADSCs proliferation by flow cytometry Live cell by calcein staining Cell's cytoskeleton with phalloidin staining Glycogen in cell's cytoplasm by TEM High levels of collagen II, aggrecan, SOX-9, and low levels of collagen I by qPCR	[281]
HA–nanofibrous scaffold amalgam	Human MSC	*In vitro* hMSC encapsulated in scaffold	Cell morphology Cell distribution ECM anabolism IVD phenotype	Uniform cell loading, elongated AF and rounded NP cells by H&E Uniform cell distribution by SEM ECM deposition with alcian blue staining Sulfated GAG content by DMMB IHC for collagen types I, II, and IX, aggrecan and link protein qPCR for collagen types I, II, IX, X, and XI; aggrecan and COMP	[282]

Table 1.3 (Continued)

HA Scaffold	Cellular / Therapeutic Molecules	Model	Description of Markers	Analysis and Results	Ref
Type II collagen/HA and collagen I hydrogel	Bovine AF and NP cells	Bimodular NP and AF cells encapsulated in collagen/HA hydrogel inflamed model	Cell morphology and distribution Cell viability Cell proliferation ECM anabolism Neurogenic inflammation Glycosylation	F-actin staining for cell shape and distribution Cell viability by live/dead assay PicoGreen for cell proliferation qPCR for collagen I, collagen II and aggrecan qPCR for NGF and BDNF IL-6 and TNF-α using ELISA Genomic profile by RNA sequencing Lectin histrochemistry of SNA-I (Sambucus nigra agglutinin I) MAA(Maackia amurensis agglutinin) WGA (Wheat germ agglutinin) Con A (Concanavalin A) UEA-I (Ulex europaeus agglutinin I) PNA(Peanut agglutinin) GS-IB4 (Griffonia simplicifolia isolectin) WFA (Wisteria floribunda agglutinin) LEA (Lycopersicon esculentum agglutinin)	[283]

Table 1.3 (Continued)

HA Scaffold	Cellular / Therapeutic Molecules	Model	Description of Markers	Analysis and Results	Ref
Promote ECM synthesis					
Gelatin/chondroitin-6-sulfate/hyaluronan tri-copolymer sponge	Human NP cells	Expand hNP cells seeded in scaffold *in vitro*	Morphology Cell viability Cell proliferation ECM anabolism NP phenotype ECM anabolism	SEM for polymer morphology hNP viability by trypan blue dye hNP proliferation by water soluble tetrazolium salt (WST-1) assay Increase in production of GAG by DMMB Higher mRNA expression in collagen II, aggrecan, SOX9, TGFβ-1, and TIMP1 by qPCR Histology for H&E, alcian blue staining and IHC for type II collagen	[284]
Thiolated HA/PEG hydrogel	Porcine AF and NP cells	AF and NP cells seeded on hydrogels *in vitro*	Mechanical integrity ECM anabolism DNA content Metabolite Cell morphology and distribution	Torsional dynamic shear for storage modulus (G') and complex modulus (G*) by rheology Sulfated GAG compositions DNA stained with Hoechst 33258 dye Lactate and pyruvate concentration by colorimetric reaction kit Cell clustering and spreading by light microscope	[285]

Table 1.3 (Continued)

HA Scaffold	Cellular / Therapeutic Molecules	Model	Description of Markers	Analysis and Results	Ref
Soluble or bound pentosan polysulphate (PPS) in PEG/HA based hydrogel	Human MPCs	MPCs encapsulated in hydrogel	Functionalisation	Amine-functionalised-HA measure by TNBSA Carboxylation of PPS and amine-functionalised-HA by FTIR, NMR	[286]
			Mechanical integrity	Gelation kinetics and final moduli by rheology	
			Swelling property	High degree of swelling in PBS	
			Hydrolytic stability	Degradation test in PBS	
			Cell proliferation	MPC proliferation by CCK8 and EdU assay	
			Cell viability	MPC viability with more spread and polygonal shape by Live/Dead assay	
			ECM anabolism	Increase GAG synthesis by DMMB Increase staining of alcian blue, toluidine blue and safranin O for HA-PPS	
			Mechanical integrity	Rheology: Time sweep analyses for elastic shear modulus, Frequency sweeps test for elasticity of materials	
			Cell viability	Viability of encapsulated cells in hydrogel by Live/Dead	
			Cell distribution	MPCs distribution in hydrogel by H&E	
			ECM anabolism	Turnover of the pericellular matrix, deposition of GAGs in hydrogel by safranin O, alcian blue, and picrosirius red Increase collagen I and II by immunostaining	

Table 1.3 (Continued)

HA Scaffold	Cellular / Therapeutic Molecules	Model	Description of Markers	Analysis and Results	Ref
HA solution	Human NP cell	hNP cells stimulated by HA	Cell migration Chondrogenesis ECM anabolism	ChemoTX® assay Chondrogenic marker mRNA of type I collagen, type II collagen, type III collagen, type IX collagen, cartilage link protein (LINK), COMP and aggrecan by qPCR IHC for type II collagen and alcian blue staining for GAG content	[287]
Incorporation of BMP-2/7 heterodimer in a NP cell-seeded fibrin-hyaluronan hydrogel	Bovine NP cells; BMP-2 and BMP-7	NP cell seeded in hydrogel in corporation with BMP *in vitro* and in nucleotomy bovine caudal *ex vivo*	ECM anabolism Disc height ECM anabolism	*In vitro*: qPCR for COL1A2, COL2A1 and ACAN GAG content in vitro and ex vivo by DMMB *Ex vivo*: Disc height using caliper ^{35}S sulfate incorporation for proteoglycan synthesis rate qPCR for versican, biglycan and ALP Collagen content by hydroxy-proline assay DNA content using Hoechst (33258) dye GAG conteny by Safranin O and collagen content by fast green, cell distribution by H&E Aggrecan, collagen type II and collagen type I content by IHC	[288]

Table 1.3 (Continued)

HA Scaffold	Cellular / Therapeutic Molecules	Model	Description of Markers	Analysis and Results	Ref
Mechanical Integrity					
mTGase cross-linked collagen/hyaluronan gel-like scaffold	Bovine NP cells	NP cells seeded in scaffold *in vitro*	Mechanical integrity	High storage modulus (G^0) by rheology Increase compressive strength by compression test	[289]
			Cell distribution	Homogeneous cell distribution in scaffold by Safranin O and fast green and stereology	
			DNA content	DNA stained with Hoechst (33258) dye	
			Cell viability	NP viability by AlamarBlue™	
			GAG content	Higher sulfated GAG by DMMB	
			GAG synthesis rate	^{35}S sulfate radiolabeling	
In situ oxidized HA/gelatin hydrogel	Rabbit NP cells	NP cells seeded on hydrogel; NP cells encapsulated in hydrogel *in vitro*	HA functionalisation	Confirm oxidized HA/gelatin by FTIR	[290]
			Mechanical integrity	Storage moduli (elasticity) and loss modulus (viscosity) under oscillation frequency sweep tests by rheology	
			Cell viability	NP viability by Live/Dead and Alexa Fluor 488® and rhodamine phalloidin	
			Cell morphology	Cell-seeded hydrogel morphology by SEM	
			NP phenotype	qPCR for HIF-1, SOX-9, BGN, DCN, ACAN, COL1A1 and COL2A1	

Table 1.3 (Continued)

HA Scaffold	Cellular / Therapeutic Molecules	Model	Description of Markers	Analysis and Results	Ref
Type II collagen/HA hydrogel	Rat MSCs	rMSCs encapsulated in hydrogel *in vitro*	HA functionalisation Physical properties Release ability Enzymatic stability Mechanical integrity Hydrogel morphology MSC markers Cell viability Cell proliferation Cell distribution NP phenotype	Confirm ester bond formation by FTIR Shrinking temperature; Degree of swelling HA release from hydrogel by ELISA Degradation by collagenase assay Confined compression test for modulus of elasticity Hydrogel porosity by SEM MSC cell surface markers (CD3, CD19, CD34, CD45, CD106, CD29, CD73, CD90, and CD105) by flow cytometry MSC viability by alamarBlue MSC proliferation by PicoGreen® assay MSC distribution by rhodamine phalloidin Chondrogenic differentiation of COL2A1, COL1A1 and ACAN by qPCR	[291]
Tyramine-functionalised HA / PEG (3-4-hydroxyphenylpropionic acid) crosslinked H_2O_2 hydrogel	Stro3-selected human MPCs	MPCs encapsulated in hydrogel *in vitro*; acellular hydrogel implantation in rat subcutaneous *in vivo*	HA functionalisation Mechanical integrity Swelling property Hydrolytic stability Injectable system Cell viability Cell distribution	Amine-functionalised-HA by NMR Gelation kinetics and final moduli by rheology High degree of swelling in PBS Degradation test in PBS *In vitro* injection in hydrated agarose gel MPC viability by Live/Dead assay Cell distribution in hydrogel by H&E	[226]

Table 1.3 (Continued)

HA Scaffold	Cellular / Therapeutic Molecules	Model	Description of Markers	Analysis	Ref
			ECM anabolism Local tissue response	GAG content by Alcian blue, collagen by Safranin O and Picrosirius red IHC for collagen I and II deposition H&E and IHC for CD68+ macrophage evident no inflammation for implanted hydrogel *in vivo*	
Tissue Remodelling					
Collagen II/HA/CS tri-copolymer	Rabbit NP cells	Implantable of allograft NP seeded scaffold in nucleotomy rabbit model	Cell morphology ECM anabolism Anatomical restoration Disc hydration	Viable allografted cells with chondrocyte-like shape by H&E staining Prominent staining of alcian blue for ECM Increase disc height index by plain radiograph Restore T2 signal intensity on MRI	[292]
HA based photo-linked derivative, cell-free HYAFF®120 and cell-loaded HYADD®3	Porcine bone marrow stem cells	Injectable of autologous stem cells seeded scaffold in nucleotomy porcine model	Anatomical restoration	Cellular tissue with chondrocytes producing matrix present in the centre of the disc, retention of the normal disc space and no vascular fibrous tissue evident by H&E and toluidine blue methods	[293]

Table 1.3 (Continued)

HA Scaffold	Cellular / Therapeutic Molecules	Model	Description of Markers	Analysis	Ref
Polyglycolic acid–hyaluronan (PGA/HA) implant	-	Scaffold implantation in nucleotomy rabbit model	Disc hydration Anatomical restoration ECM anabolism	T2-weighted signal intensity by MRI H&E to identify annulus fibrosus and nucleus pulposus region Safranin O for proteoglycans IHC for type I collagen and type II collagen	[294]
Attenuate Inflammation					
HA/PEG hydrogel	-	Normal and inflamed NP cells seeded on hydrogel *in vitro*	HA functionalisation Hydrolytic stability Enzymatic stability Cell viability Cell metabolism Inflammation Cell surface Neurogenic inflammation	Residual un-crosslinked carboxyl groups of HA by FTIR Amount of unreacted amine groups of PEG by TNBSA Incubation in PBS Incubation in hyaluronidase NP viability Live/Dead staining kit NP metabolic activity by alamarBlue assay IHC for IL-1R1, MyD88 IHC for CD44 qPCR for NGF and BDNF	[295]

Table 1.3 (Continued)

HA Scaffold	Cellular / Therapeutic Molecules	Model	Description of Markers	Analysis	Ref
HA/PEG hydrogel	-	Injectable hydrogel in annular defect/inflamed bovine caudal *ex vivo*	Inflammation Apoptosis ECM anabolism ECM catabolism	qPCR for IFNAR1, IFNAR2, STAT1/2, JAK1, IFIT3 and IGFBP3 IHC for IFIT3 and IGFBP3 IHC for caspase 3 qPCR and IHC for aggrecan and collagen I qPCR for ADAMTS4	[296]
Alleviate Pain					
HMW HA gel	-	L5-L6 rat laminectomy disc injury model: HA gel was layered over the dura and into the laminectomy canal	Nerve fibrosis Pain - Mechanical allodynia	Postoperative proliferative fibrosis of the L5 spinal nerves by hydroxyproline assessment for collagen content Von Frey test on hind paws	[298]

1.13 Ongoing/Concluded Therapeutic Trials

In recent years, there has been a growing interest in the paradigm shift from spinal surgeries towards biological therapies that promises to restore the disc anatomy and function. These emerging concepts are underpinned by the potential of bioengineered therapies to induce multi-tissue regeneration processes even at mechanically challenging sites such as the spinal column. Many of the scientific analyses performed over the past two decades have identified key signalling pathways as well as candidate biomolecules and pluripotent cells that could be of therapeutic interest. Nevertheless, questions remain on how many of the preclinical studies reported so far are reproducible in patients. Indeed, given the plethora of research work focusing on biological therapies to restore the disc anatomy and mechanical properties, only a handful of bioengineered therapies are currently undergoing clinical trials as revealed by a search of the websites www.ClinicalTrials.gov and http://stemcellsportal.com/clinical_trials_musculoskeletal_disease [299-302]. Of the 12 clinical trials reported so far in 2017 (www.clinicaltrials.gov) (Table 1.4), eight involve the implantation of cells while four involve the indradiscal application of a growth factor, recombinant human growth/differentiation factor 5 (rhGDF-5), to induce disc tissue regeneration. Of the eight cell studies, three studies have focused on the potential of adipose tissue derived autologous stem/stromal cells (NCT01643681, NCT02338271, NCT02097862), two are evaluating allogenic mesenchymal stromal/precursor cells (NCT01860417, NCT01290367) and one each is testing the use of either autologous disc chondrocytes (NCT01640457) or allogenic juvenile chondrocytes (NCT01771471) respectively to promote disc tissue repair (NCT01640457).

The first reported multicentre clinical trial study involved 32 patients conducted in the United States of America which started recruiting patients in 2008. It evaluated the safety and efficacy of a single injection of rhGDF5 into a degenerating single level spinal disc. The study was sponsored by DePuy Spine. Interestingly, although the findings from this maiden acellular biotherapy strategy were not made public, three similar studies recruiting 31, 40 and 24 patients respectively were subsequently commenced in the year 2010 by the same sponsor, DePuy Spine, respectively in Yeungnam University Medical Center of the Republic

of Korea, St. George Private Hospital Kogarah, New South Wales, Australia, and in a number of centres across the USA. All these studies are reported to have ended but their findings are yet to be published.

In 2012, three different cell-based clinical trials were launched to evaluate the efficacy and safety of injected cells to promote intervertebral disc regeneration (Table 1.4). At the University Anam Hospital in Seoul, Korea, a single centre non-randomized, non-blinded Phase I/II clinical trial (NCT01643681) evaluated the safety and efficacy of autologous adipose tissue derived mesenchymal stem cells transplanted into patients with lumbar intervertebral disc degeneration [303]. This 24-week long trial recruited a total of eight patients who experienced chronic low back pain for at least one year and who have radiographic evidence of degenerated intervertebral disc on T2-weighted MRI images confirmed by positive discography. All eight participants received 4 x 10^7 cells mL^{-1} autologous cells infusion into their diseased lumbar intervertebral disc. The participants were subsequently monitored for therapeutic changes as well as complications in their clinical condition. The outcome of the study has not yet been made public but given the small size of the study, the main expectation will be to focus on the safety of the technology.

A larger, multicentre study conducted in Austria and Germany recruited 120 patients. The cells implanted were autologous IVD chondrocytes. Similarly, another relatively large (44 patients) multicentre study in the USA loaded allogenic juvenile chondrocytes into a fibrin gel for implantation into patients. Both of these studies are still on-going but preliminary results showed no adverse effects of cell injection [304-305]. The most promising findings with cell therapy to treat the IVD pathology to date were reported from a study conducted in the USA [304]. The study enlisted 100 patients who were injected with autologous adipose stem cells. In addition to the favourable safety profile, the authors reported that patients demonstrated statistically significant improvements in several of the therapeutic parameters evaluated including: flexion, a number of pain rating scales, and psychometric response scales over the first twelve months. Finally, the largest cell-based study is currently recruiting a total of 360 patients in both Australia and the USA to evaluate the safety

Table 1.4 Clinical trials in degenerative disc disease

Clinical trial #	Biological agent (s)	Source	Eligibility	Enrolment (patients)	Country(ies)	Study period	Remarks
NCT02097862	Adipose Stem Cells	Cells, Autologous	18-85 years old	100	USA	March 2014-2017	Pain relief with no reported adverse effects [304]
NCT01643681	Adipose Stem Cells	Cells, Autologous	19-70, years old	8	Korea	July July 2012-2014	Awaiting publication of outcome [303]
NCT02338271	Adipose mesenchymal stem cell	Cells, Autologous	18-70 Years	10	Korea	January 2015-2017	Active
NCT01640457	IVD Chondrocytes NOVOCAR®	Cells, Autologous	18-60 years old	120	Austria Germany	August 2012-2021	Active: no adverse effects observed so far
NCT01860417	Mesenchymal Stromal Cells	Cells, Allogenic	18-75 years old	24	Spain	April 2013-2016	Completed. Awaiting open publication of outcome.
NCT01290367	Mesenchymal Precursor Cells + HA	Cells, Allogeneic+ Carrier	18 Years and older	100	USA	August 2011-2015	Completed. Awaiting open publication of outcome.

Table 1.4 (Continued)

Clinical trial #	Biological agent (s)	Source	Eligibility	Enrolment (patients)	Country(ies)	Study period	Remarks
NCT01771471	Chondrocytes in fibrin NuQu®	Cells, Allogenic Juvenile	21 Years and older	44	USA	November 2012-2016	Over 50% of patients continued to improve at 1 year follow-up [305]
NCT02412735	Mesenchymal Precursor Cells Rexlemestrocel-L® + HA	Cells, Allogeneic + Carrier	18 Years and older	360	USA, Australia	March 2015-2020	Active
NCT01158924	Intradiscal rhGDF-5	Drug	18 Years and older	40	Australia	March 2010-2014	Completed. Awaiting open publication of outcome.
NCT01182337	Intradiscal rhGDF-5	Drug	18 Years and older	31	Korea	June 2010-2014	Completed. Awaiting open publication of outcome.
NCT00813813	Intradiscal rhGDF-5	Drug	18 Years and older	32	USA	June 2008-2013	Completed. Awaiting open publication of outcome.
NCT01124006	Intradiscal rhGDF-5	Drug	18 Years and older	24	USA	January 2010-2014	Completed. Awaiting open publication of outcome.

and efficacy of allogenic mesenchymal precursor cell therapy. The results of this study when available will be important in determining the role of allogenic cell based mesenchymal cells in IVD therapy. Similarly, in January 2015, CHA Bundang Medical Center of CHA University Seongnam-si, Korea, began a Phase I clinical trial (NCT02338271) which enrolled 10 patients with low back pain and lumbar intervertebral disc degeneration. The main aim of this study was to evaluate the safety and efficacy of autologous adipose derived mesenchymal stem cells plus HA derivatives (Tissuefill) biotherapy in disc degenerated disc disease.

1.14 Future Directions

Given the current lack of a satisfactory therapeutic strategy that preserves the spinal joint anatomy and the enormous potential reported for regenerative strategies in various models of IVD degeneration, the future of discogenic pain therapy will lie with regenerative therapies despite the diversity of challenges it still faces today. The complexity of disc tissue composition and organization, the mechanical and other functional demands on the disc joints, the paucity of blood/nutrient supply to these tissues, and the difficulties in regulating the therapeutic activities of biological implants represent a challenging problem. The immediate future therefore lie in the ability of the scientific community to achieve one or all of the following three: 1) to prepare a “fertile ground” using biomaterials for survival of remaining disc cell populations to improve functionality *in situ*; and 2) to fine tune the functions of biomaterials to recruite specific cell populations that would produce therapeutic factors at efficacious doses to rescue degenerated disc tissues; 3) to elucidate long term efficacy of biomaterials and its mechanism of actions to promote disc regeneration and alleviate pain.

1.15. Conclusions

An understanding of the disc pathology is necessary to develop clinically relevant strategies for the treatment of discogenic back pain. Biomaterial-based tissue engineering strategies have demonstrated efficacy in compensating local tissue responses, maintaining disc phenotype, attaining tissue biochemical homeostasis and promoting anatomical tissue repair in pre-clinical models. However, despite intensive research efforts focused on biological therapies to halt or reverse the progression of disc degeneration, only a handful of bioengineered therapies are

currently undergoing open clinical trials – and these approaches have shown limited clinical effectiveness in patients – which is postulated to be due to the fact that they do not address the underlying disease pathology. Recent advances in our understanding of the cellular, biochemical, and molecular pathways of the pathogenesis of disc degeneration will offer future opportunities to develop therapeutic strategies targeting the treatment of discogenic pain to halt or reverse the progression of disc degeneration. Specifically hyaluronan modulates key inflammatory pathways of signalling molecules to respectively attenuate nociception, innervation, inflammation and regulate the deposition of ECM components. Well-controlled preclinical testing is needed to address the long-term efficacy and safety of hyaluronan to treat discogenic pain. Furthermore well-designed clinical trials will be crucial to translate the use of hyaluronan to treat patients in the clinical setting.

1.16 Objectives and Hypotheses

The aim of this study was to develop a therapeutic biomaterial system by using high molecular weight of HA hydrogel and to investigate its efficacy in alleviating inflammatory pain via glycome and proteome modulation in degenerative disc disease for treating discogenic back pain. This thesis consists of three research phases (Figure 1.7): I) The development of a HA Hydrogel in an Inflammation Milieu **(Chapter 2)**, II) The Establishment of a Pre-clinical Model of Pain in Disc Degeneration **(Chapter 3)** and III) The investigation of the efficacy of a HA Hydrogel in a Painful Disc Degeneration Model **(Chapter 4)**.

1.16.1 Phase I

Overall aim

To develop a therapeutic HA hydrogel that can modulate the key inflammatory pathways of IL-1β.

Hypothesis

HA hydrogel attenuates inflammatory receptor of IL-1R1 and MyD88 and neurotrophin expression of NGF and BDNF in IL-1β induced inflammation model on NP cells.

Objectives

I. Synthesize and optimise HA hydrogel at a various concentrations of crosslinker, 4-arm PEG amine.
II. Characterise optimally HA hydrogel in a study of hydrolytic stability and enzymatic degradability, and cytotoxicity in NP cells.
III. Determine efficacy of HA hydrogel in modulating IL-1β signalling molecules of IL-1R1 and MyD88.
IV. Determine mechanism of action of HA hydrogel through binding cell surface receptor, CD44.

1.16.2 Phase II

Overall aim

To develop and validate a clinically relevent painful disc degeneration *in vivo*.

Hypothesis

1. Surgical-puncture-induced disc injury in the rat-tail elicits robust nociceptive behaviour in rats, induces spinal molecular markers of nociception and anatomical disc degeneration, and differentially modulates glycosylation in AF and NP tissues.
2. Systemic acute administration of morphine reverses nociceptive behaviour following surgically punctured-induced disc injury in the rats.

Objectives

I. Investigate nociceptive behaviour following surgically puncture-induced disc injury in rats by assessing thermal hyperalgesia and mechanical allodynia or hyperalgesia.
II. Determine spinal molecular marker of nociception, *c-Fos* in dorsal horn of spinal cord.
III. Determine histological severity of induced disc degeneration by identifying AF morphology, NP cell cellularity and matrix, and annular demarcation.
IV. Identify distinct glycosignature of sialylation, high mannose, fucosylation and galactosylation in injured and healthy (sham) for AF and NP tissues at cellular ECM level using lectin histochemistry.
V. Quantify sulfation pattern of ECM chondroitin sulfate and HA compositions in injured and healthy (sham) AF and NP tissues.

VI. Validate surgically puncture-nduced disc injury through inhibition of nociceptive behaviour using morphine treatment.

1.16.3 Phase III

Overall aim

To evaluate efficacy of HA hydrogel in modulating inflammatory pain through regulation of regenerative glycome- and proteome- signatures in a painful disc degeneration.

Hypothesis

HA hydrogel treatment alleviates nociceptive behaviour, inhibits sensory hyper-innervation and expression of peripheral pro-nociceptive receptors TRPV1 and high afinity nerve growth factor receptor (Trk A) *in vivo*, down-regulates mRNA expression of spinal nociception markers *c-Fos* and *Tac1* (which encodes substance P) and regulates glycomic signature and proteomic expression to modulate inflammatory and protein-regulatory pathways in both NP and AF tissues.

Objectives

I. Determine the efficacy of HA hydrogel in alleviating nociceptive behaviour in rats by assessing thermal hyperalgesia and mechanical allodynia or hyperalgesia.
II. Determine the efficacy of HA hydrogel to down-regulate spinal nociception markers, *c-Fos* and *Tac1* (gene encodes substance P) in dorsal horn of spinal cord, and peripheral pro-nociceptor, TRPV1 and Trk A in AF and NP tissues.
III. Determine the efficacy of HA hydrogel in inhibiting sensory hyper-innervation markers of GAP43 and CGRP in AF and NP tissues.
IV. Determine the effect of a HA hydrogel in modulating IVD glyco-environment of sialylation, galactosylation and chondroitin/keratan sulfate expressions in AF and NP tissues.
V. Determine the mechanisma of action of HA in regulating cellular and ECM proteome expression so as to identify key inflammatory and regulatory pathways to respectively attenuate inflammation and regulate ECM content for disc repair.

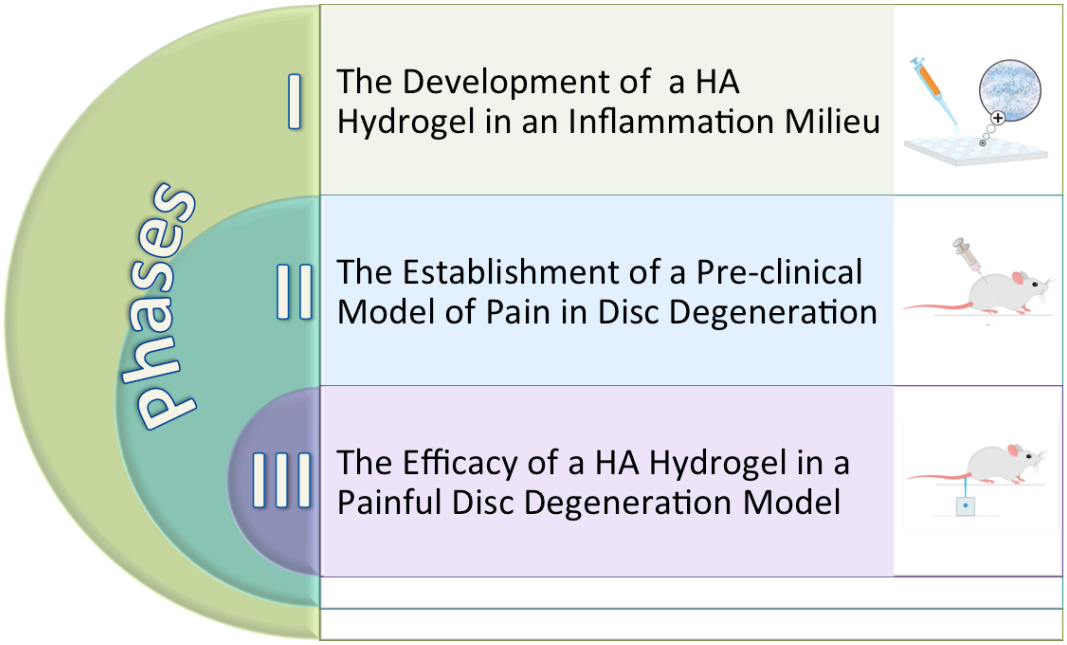

Figure 1.7. Thesis overview. The studies comprised of three research phases in which aim to modulate inflammatory pain for disc repair.

1.17 References

[1] L. Manchikanti, V. Singh, S. Datta, S. P. Cohen, and J. A. Hirsch, "Comprehensive review of epidemiology, scope, and impact of spinal pain," *Pain Physician*, vol. 12, pp. 35–70, 2009.

[2] G. B. Andersson, "Epidemiological features of chronic low-back pain," *Lancet*, vol. 354, no. 9178, pp. 581–585, 1999.

[3] M. L. Skovron, "Epidemiology of low back pain," *Baillieres. Clin. Rheumatol.*, vol. 6, no. 3, pp. 559–573, 1992.

[4] A. M. Elliott, B. H. Smith, K. I. Penny, W. C. Smith, and W. A. Chambers, "The epidemiology of chronic pain in the community," *Lancet*, vol. 354, no. 9186, pp. 1248–1252, 1999.

[5] D. Hoy, P. Brooks, F. Blyth, and R. Buchbinder, "The epidemiology of low back pain," *Best Pract. Res. Clin. Rheumatol.*, vol. 24, no. 6, pp. 769–781, 2010.

[6] B. I. Martin, R. A. Deyo, S. K. Mirza, J. A. Turner, B. A. Comstock, W. Hollingworth, and S. D. Sullivan, "Expenditures and health status among adults with back and neck problems," *J. Am. Med. Assoc.*, vol. 299, no. 6, pp. 656–664, 2013.

[7] D. Hoy, L. March, P. Brooks, F. Blyth, A. Woolf, C. Bain, G. Williams, E. Smith, T. Vos, J. Barendregt, C. Murray, R. Burstein, and R. Buchbinder, "The global burden of low back pain: Estimates from the Global Burden of Disease 2010 study," *Ann. Rheum. Dis.*, vol. 73, no. 6, pp. 968–974, 2014.

[8] N. Maniadakis and A. Gray, "The economic burden of back pain in the UK," *Pain*, vol. 84, no. 1, pp. 95–103, 2000.

[9] S. Dagenais, J. Caro, and S. Haldeman, "A systematic review of low back pain cost of illness studies in the United States and internationally," *Spine J.*, vol. 8, no. 1, pp. 8–20, 2008.

[10] M. Juniper, T. K. Le, and D. Mladsi, "The epidemiology, economic burden, and pharmacological treatment of chronic low back pain in France, Germany, Italy, Spain and the UK: A literature-based review.," *Expert Opin.*

Pharmacother., vol. 10, no. December 2015, pp. 2581–2592, 2009.

[11] K. M. C. Cheung, J. Karppinen, D. Chan, D. W. H. Ho, Y. Q. Song, P. Sham, K. S. E. Cheah, J. C. Y. Leong, and K. D. K. Luk, "Prevalence and pattern of lumbar magnetic resonance imaging changes in a population study of one thousand forty-three individuals.," *Spine (Phila. Pa. 1976).*, vol. 34, no. 9, pp. 934–40, 2009.

[12] K. Luoma, H. Riihimäki, R. Luukkonen, R. Raininko, E. Viikari-Juntura, and A. Lamminen, "Low back pain in relation to lumbar disc degeneration," *Spine (Phila. Pa. 1976).*, vol. 25, no. 4, pp. 487–492, Mar. 2000.

[13] C. J. Zheng and J. Chen, "Disc degeneration implies low back pain.," *Theor. Biol. Med. Model.*, vol. 12, no. 1, p. 24, 2015.

[14] R. P. Prithvi, "Intervertebral disc: anatomy-physiology-pathophysiology-treatment," *Pain Pract.*, vol. 8, no. 1, pp. 18–44, 2008.

[15] G. Pattappa, Z. Li, M. Peroglio, N. Wismer, M. Alini, and S. Grad, "Diversity of intervertebral disc cells: Phenotype and function," *J. Anat.*, vol. 221, no. 6, pp. 480–496, 2012.

[16] N. Inoue and A. Espinoza Orias, "Biomechanics of intervertebral disc degeneration," *Orthop Clin North Am*, vol. 42, no. 4, pp. 487–499, 2011.

[17] D. Sakai, Y. Nakamura, T. Nakai, T. Mishima, S. Kato, S. Grad, M. Alini, M. V Risbud, D. Chan, K. S. E. Cheah, K. Yamamura, K. Masuda, H. Okano, K. Ando, and J. Mochida, "Exhaustion of nucleus pulposus progenitor cells with ageing and degeneration of the intervertebral disc.," *Nat. Commun.*, vol. 3, no. May, p. 1264, 2012.

[18] K. Wuertz, N. Vo, D. Kletsas, and N. Boos, "Inflammatory and catabolic signalling in intervertebral discs: the roles of NF-κB and MAP kinases.," *Eur. Cell. Mater.*, vol. 23, pp. 103–120, Jan. 2012.

[19] J. P. Urban and S. Roberts, "Degeneration of the intervertebral disc," *Arthritis Res Ther*, vol. 5, no. 3, pp. 120–130, 2003.

[20] J. E. Mayer, J. C. Iatridis, D. Chan, S. A. Qureshi, O. Gottesman, and A. C. Hecht, "Genetic polymorphisms associated with intervertebral disc

degeneration," *Spine J*, vol. 13, no. 3, pp. 299–317, 2013.

[21] R. Shiri, J. Karppinen, P. Leino-Arjas, S. Solovieva, and E. Viikari-Juntura, "The association between smoking and low back pain: A Meta-analysis," *Am. J. Med.*, vol. 123, no. 1, p. 87.e7-87.e35, 2010.

[22] R. Shiri, J. Karppinen, P. Leino-Arjas, S. Solovieva, and E. Viikari-Juntura, "The association between obesity and low back pain: A meta-analysis," *Am. J. Epidemiol.*, vol. 171, no. 2, pp. 135–154, 2010.

[23] A. Hiyama, D. Sakai, and J. Mochida, "Cell signaling pathways related to pain receptors in the degenerated disk.," *Glob. spine J.*, vol. 3, no. 3, pp. 165–74, Jun. 2013.

[24] D. Sakai and S. Grad, "Advancing the cellular and molecular therapy for intervertebral disc disease.," *Adv. Drug Deliv. Rev.*, vol. 84, pp. 159–171, Jun. 2015.

[25] C. L. LeMaitre, A. J. Freemont, and J. A. Hoyland, "The role of interleukin-1 in the pathogenesis of human intervertebral disc degeneration.," *Arthritis Res. Ther.*, vol. 7, no. 4, pp. R732-45, Jan. 2005.

[26] J. Wang, D. Markova, D. G. Anderson, Z. Zheng, I. M. Shapiro, and M. V. Risbud, "TNF-alfa and IL-1beta promote a disintegrin-like and metalloprotease with thrombospondin type I motif-5-mediated aggrecan degradation through syndecan-4 in intervertebral disc," *J. Biol. Chem.*, vol. 286, no. 46, pp. 39738–39749, 2011.

[27] A. Hiyama, D. Sakai, M. Tanaka, F. Arai, D. Nakajima, K. Abe, and J. Mochida, "The relationship between the Wnt/β-catenin and TGF-β/BMP signals in the intervertebral disc cell.," *J. Cell. Physiol.*, vol. 226, no. 5, pp. 1139–48, May 2011.

[28] Z. Kazezian, R. Gawri, L. Haglund, J. Ouellet, F. Mwale, F. Tarrant, P. O'Gaora, A. Pandit, M. Alini, and S. Grad, "Gene expression profiling identifies interferon signalling molecules and IGFBP3 in human degenerative annulus fibrosus," *Sci. Rep.*, vol. 5, no. April, p. 15662, 2015.

[29] D. Purmessur, A. J. Freemont, and J. A. Hoyland, "Expression and regulation

of neurotrophins in the nondegenerate and degenerate human intervertebral disc.," *Arthritis Res. Ther.*, vol. 10, no. 4, p. R99, Jan. 2008.

[30] J. M. Lee, J. Y. Song, M. Baek, H. Y. Jung, H. Kang, I. B. Han, Y. Do Kwon, and D. E. Shin, "Interleukin-1β induces angiogenesis and innervation in human intervertebral disc degeneration.," *J. Orthop. Res.*, vol. 29, no. 2, pp. 265–9, Mar. 2011.

[31] A. J. Freemont, A. Watkins, C. LeMaitre, P. Baird, M. Jeziorska, M. T. N. Knight, E. R. S. Ross, J. P. O'Brien, and J. A. Hoyland, "Nerve growth factor expression and innervation of the painful intervertebral disc.," *J. Pathol.*, vol. 197, no. 3, pp. 286–92, Jul. 2002.

[32] A. J. Freemont, T. E. Peacock, P. Goupille, J. A. Hoyland, J. O. Brien, and M. I. V Jayson, "Early report nerve ingrowth into diseased intervertebral disc in chronic back pain," *Lancet*, vol. 350, pp. 178–181, 1997.

[33] C. G. Maher, "Effective physical treatment for chronic low back pain," *Orthop. Clin. North Am.*, vol. 35, no. 1, pp. 57–64, 2004.

[34] R. Chou and L. H. Huffman, "Medications for acute and chronic low back pain: A review of the evidence for an American Pain Society/American College of Physicians Clinical Practice Guideline," *Ann. Intern. Med.*, vol. 147, pp. 505–514, 2007.

[35] X. Luo, R. Pietrobon, L. H. Curtis, and L. A. Hey, "Prescription of nonsteroidal anti-inflammatory drugs and muscle relaxants for back pain in the United States," *Spine (Phila. Pa. 1976).*, vol. 29, no. 23, pp. E531–E537, Dec. 2004.

[36] F. Taher, D. Essig, D. R. Lebl, A. P. Hughes, A. A. Sama, F. P. Cammisa, and F. P. Girardi, "Lumbar degenerative disc disease: Current and future concepts of diagnosis and management," *Adv. Orthop.*, vol. 2012, p. 970752, Jan. 2012.

[37] D. M. O'Halloran and A. Pandit, "Tissue-engineering approach to regenerating the intervertebral disc.," *Tissue Eng.*, vol. 13, no. 8, pp. 1927–54, Aug. 2007.

[38] R. J. Kowalski, L. A. Ferrara, and E. C. Benzel, "Biomechanics of the Spine,"

Biomech. Spine, no. April, pp. 529–561, 2005.

[39] H. Shankar, J. A. Scarlett, and S. E. Abram, "Anatomy and pathophysiology of intervertebral disc disease," *Tech. Reg. Anesth. Pain Manag.*, vol. 13, no. 2, pp. 67–75, Apr. 2009.

[40] A. I. Chou, A. Bansal, G. J. Miller, and S. B. Nicoll, "The effect of serial monolayer passaging on the collagen expression profile of outer and inner anulus fibrosus cells.," *Spine (Phila. Pa. 1976).*, vol. 31, no. 17, pp. 1875–81, Aug. 2006.

[41] M. Francoise and A. Abdul M., "Investigation of the laminate structure of lumbar disc anulus fibrosus," *Spine (Phila. Pa. 1976).*, vol. 15, no. 5, pp. 402–410, 1990.

[42] J. L. Bron, M. N. Helder, H. J. Meisel, B. J. Van Royen, and T. H. Smit, "Repair, regenerative and supportive therapies of the annulus fibrosus: Achievements and challenges.," *Eur. spine J.*, vol. 18, no. 3, pp. 301–13, Mar. 2009.

[43] A. Maroudas, R. A. Stockwell, A. Nachemson, and J. Urban, "Factors involved in the nutrition of the human lumbar intervertebral disc: cellularity and diffusion of glucose *in vitro*," *Anatomy*, vol. 121, no. 1, pp. 113–130, 1975.

[44] P. Franco, B. Marinella, and M. Marco, "Morphologic changes in annulus fibrosus during aging. An ultrastructural study in rats.," *Spine (Phila. Pa. 1976).*, vol. 9, no. 6, pp. 596–603, 1984.

[45] D. G. Anderson and T. J. Albert, "The molecular basis of intervertebral disk degeneration," *Semin. Spine Surg.*, vol. 15, no. 4, pp. 352–360, Dec. 2003.

[46] J. P. Urban and S. Roberts, "Development and degeneration of the intervertebral discs.," *Mol. Med. Today*, vol. 1, no. 7, pp. 329–335, 1995.

[47] T. J. Freemont, C. LeMaitre, A. Watkins, and J. A. Hoyland, "Degeneration of intervertebral discs: current understanding of cellular and molecular events, and implications for novel therapies.," *Expert Rev. Mol. Med.*, vol. 2001, no. March, pp. 1–10, Mar. 2001.

[48] M. R. McCann and C. A. Séguin, "Notochord cells in intervertebral disc development and degeneration.," *J. Dev. Biol.*, vol. 4, no. 1, pp. 1–18, 2016.

[49] A. Colombini, G. Lombardi, M. M. Corsi, and G. Banfi, "Pathophysiology of the human intervertebral disc.," *Int. J. Biochem. Cell Biol.*, vol. 40, no. 5, pp. 837–42, Jan. 2008.

[50] J. Yu, "Elastic tissues of the intervertebral disc," *Biochem. Soc. Trans.*, vol. 30, pp. 848–852, 2002.

[51] M. V Risbud, A. Guttapalli, D. G. Stokes, D. Hawkins, K. G. Danielson, T. P. Schaer, T. J. Albert, and I. M. Shapiro, "Nucleus pulposus cells express HIF-1 alpha under normoxic culture conditions: A metabolic adaptation to the intervertebral disc microenvironment.," *J. Cell. Biochem.*, vol. 98, no. 1, pp. 152–9, May 2006.

[52] J. P. G. Urban, S. Smith, and J. C. T. Fairbank, "Nutrition of the intervertebral disc," *Spine (Phila. Pa. 1976).*, vol. 29, no. 23, pp. 2700–2709, 2004.

[53] M. H. Walker and D. G. Anderson, "Molecular basis of intervertebral disc degeneration.," *Spine J.*, vol. 4, no. 6 Suppl, p. 158S–166S, 2004.

[54] J. R. Taylor, "Growth of human intervertebral discs and vertebral bodies.," *J. Anat.*, vol. 120, no. Pt 1, pp. 49–68, 1975.

[55] S. Ohtori, K. Takahashi, T. Chiba, M. Yamagata, H. Sameda, and H. Moriya, "Sensory innervation of the dorsal portion of the lumbar intervertebral discs in rats.," *Spine (Phila. Pa. 1976).*, vol. 26, no. 8, pp. 946–950, 2001.

[56] S.-I. Nakamura, K. Takahashi, Y. Takahashi, M. Yamagata, and H. Moriya, "The afferent pathways of discogenic low-back pain," *J. Bone Jt. Surg.*, 1996.

[57] N. Bogduk, "Innervation of the lumbar spine.," *Spine (Phila. Pa. 1976).*, vol. 8, no. 3, pp. 286–293, 1983.

[58] N. Bogduk, W. Tynan, and A. S. Wilson, "The nerve supply to the human lumbar intervertebral discs," *J. Anat.*, vol. 132, no. 1, pp. 39–56, 1981.

[59] W. E. B. Johnson, H. Evans, J. Menage, S. M. Eisenstein, A. El Haj, and S. Roberts, "Immunohistochemical detection of Schwann cells in innervated and

vascularized human intervertebral discs," *Spine (Phila. Pa. 1976).*, vol. 26, no. 23, pp. 2550–2557, Dec. 2001.

[60] A. Dimitroulias, C. Tsonidis, K. Natsis, I. Venizelos, S. N. Djau, P. Tsitsopoulos, and P. Tsitsopoulos, "An immunohistochemical study of mechanoreceptors in lumbar spine intervertebral discs," *J. Clin. Neurosci.*, vol. 17, no. 6, pp. 742–745, 2010.

[61] A. Nachemson, "The effect of forward leaning on lumbar intradiscal pressure," *Acta Orthop. Scand.*, vol. 35, no. Nachemson 1960, pp. 314–28, 1965.

[62] H. J. Wilke, P. Neef, M. Caimi, T. Hoogland, and L. E. Claes, "New *in vivo* measurements of pressures in the intervertebral disc in daily life.," *Spine (Phila. Pa. 1976).*, vol. 24, no. 8, pp. 755–62, 1999.

[63] I. James C., S. Lori A., W. Mark, and M. Van C., "The viscoelastic behavior of the non-degenerate lumbar nucleus," *J. Biomech.*, vol. 9290, no. 97, pp. 1005–1013, 1996.

[64] B. Johnstone and M. T. Bayliss, "The large proteoglycans of the human intervertebral disc. Changes in their biosynthesis and structure with age, topography, and pathology.," *Spine*, vol. 20, no. 6. pp. 674–684, 1995.

[65] J. B. Lowe and J. D. Marth, "A genetic approach to Mammalian glycan function.," *Annu. Rev. Biochem.*, vol. 72, no. 1, pp. 643–691, 2003.

[66] R. Raman, S. Raguram, G. Venkataraman, J. C. Paulson, and R. Sasisekharan, "Glycomics: An integrated systems approach to structure-function relationships of glycans," *Nat. Methods*, vol. 2, no. 11, pp. 817–824, 2005.

[67] M. E. Griffin and L. C. Hsieh-Wilson, "Glycan engineering for cell and developmental biology," *Cell Chem Biol*, vol. 6, no. 2, pp. 356–372, 2015.

[68] P. R. Crocker, "Siglecs: Sialic-acid-binding immunoglobulin-like lectins in cell-cell interactions and signalling," *Curr. Opin. Struct. Biol.*, vol. 12, no. 5, pp. 609–615, 2002.

[69] J. Zaia, "At last, functional glycomics," *Nat. Methods*, vol. 8, no. 1, pp. 55–57, 2011.

[70] A. Varki and J. B. Lowe, "Chapter 6. Biological roles of glycans," in *Essentials of Glycobiology*, 2009.

[71] C. M. Galtrey and J. W. Fawcett, "The role of chondroitin sulfate proteoglycans in regeneration and plasticity in the central nervous system," *Brain Res. Rev.*, vol. 54, no. 1, pp. 1–18, 2007.

[72] R. Kleene and M. Schachner, "Glycans and neural cell interactions.," *Nat. Rev. Neurosci.*, vol. 5, no. 3, pp. 195–208, 2004.

[73] H. J. Gabius, S. André, J. Jiménez-Barbero, A. Romero, and D. Solís, "From lectin structure to functional glycomics: Principles of the sugar code," *Trends Biochem. Sci.*, vol. 36, no. 6, pp. 298–313, 2011.

[74] K. W. Moremen, M. Tiemeyer, and A. V Nairn, "Vertebrate protein glycosylation: Diversity, synthesis and function," *Nat. Rev. Mol. Cell Biol.*, vol. 13, no. July, pp. 448–462, 2012.

[75] C. Boscher, J. W. Dennis, and I. R. Nabi, "Glycosylation, galectins and cellular signaling," *Curr. Opin. Cell Biol.*, vol. 23, no. 4, pp. 383–392, 2011.

[76] P. Stanley, H. Schachter, and N. Taniguchi, "Chapter 8. N-Glycans," in *Essentials of Glycobiology*, 2009.

[77] P. Van Den Steen, P. M. Rudd, R. A. Dwek, and G. Opdenakker, "Concepts and principles of O-Linked glycosylation," *Crit. Rev. Biochem. Mol. Biol.*, vol. 33, no. 3, pp. 151–208, 1998.

[78] R. Raman, V. Sasisekharan, and R. Sasisekharan, "Structural insights into biological roles of protein-glycosaminoglycan interactions," *Chem. Biol.*, vol. 12, pp. 267–277, 2005.

[79] B. P. Toole, "Hyaluronan: From extracellular glue to pericellular cue," *Nat. Rev. Cancer*, vol. 4, no. July, pp. 528–539, 2004.

[80] C. Roch, J. Kuhn, K. Kleesiek, and C. Götting, "Differences in gene expression of human xylosyltransferases and determination of acceptor specificities for various proteoglycans," *Biochem. Biophys. Res. Commun.*, vol. 391, pp. 685–691, 2010.

[81] C. Gçtting, J. Kuhn, and K. Kleesiek, "Human xylosyltransferases in health and disease," *Cell. Mol. Life Sci.*, vol. 64, no. 2007, pp. 1498–1517, 2013.

[82] C. Malavaki, S. Mizumoto, N. Karamanos, and K. Sugahara, "Recent advances in the structural study of functional chondroitin sulfate and dermatan sulfate in health," *Connect. Tissue Res.*, vol. 49, pp. 133–139, 2008.

[83] R. V. Iozzo and L. Schaefer, "Proteoglycan form and function: A comprehensive nomenclature of proteoglycans," *Matrix Biol.*, vol. 42, pp. 11–55, 2015.

[84] W. E. B. Johnson, B. Caterson, S. M. Eisenstein, D. L. Hynds, D. M. Snow, and S. Roberts, "Human intervertebral disc aggrecan inhibits nerve growth in vitro.," *Arthritis Rheum.*, vol. 46, no. 10, pp. 2658–64, Oct. 2002.

[85] B. T. S. Sudarla, E. D. Laing, P. Yu, Y. Katagiri, H. M. Geller, and A. J. Symes, "Smad proteins differentially regulate transforming growth factor-beta-mediated induction of chondroitin sulfate proteoglycans," *J. Neurochem.*, vol. 119, pp. 868–878, 2011.

[86] G. Zimmer, S. M. Schanuel, S. Bürger, F. Weth, A. Steinecke, J. Bolz, and R. Lent, "Chondroitin sulfate acts in concert with semaphorin 3A to guide tangential migration of cortical interneurons in the ventral telencephalon.," *Cereb. Cortex*, vol. 20, no. 10, pp. 2411–22, Oct. 2010.

[87] D. Purmessur, M. C. Cornejo, S. K. Cho, P. J. Roughley, R. J. Linhardt, A. C. Hecht, and J. C. Iatridis, "Intact glycosaminoglycans from intervertebral disc-derived notochordal cell conditioned media inhibits neurite growth while maintaining neuronal cell viability," *Spine J.*, vol. 15, no. 5, pp. 1060–1069, 2015.

[88] J. L. Funderburgh, "Keratan sulfate biosynthesis," *IUBMB Life*, vol. 54, no. 4, pp. 187–194, 2002.

[89] P. Antonsson, D. Heinegird, and A. Oldberg, "Post-translational modifications of fibromodulin," *J. Biol. Chem.*, vol. 266, no. 25, pp. 16859–16861, 1991.

[90] I. A. Nieduszynski, T. N. Huckerby, J. Dickenson, G. M. Brown, T. Gui-Hua, and M. T. Bayliss, "Structural aspects of skeletal keratan sulphates," *Biochem.*

Soc. Trans, vol. 18, pp. 792–793, 1990.

[91] K. Siemionow, H. An, K. Masuda, G. B. Andersson, and G. Cs-Szabo, "The effects of age, gender, ethnicity, and spinal level on the rate of intervertebral disc degeneration. A review of 1712 intervertebral discs," *Spine (Phila Pa 1976)*, vol. 36, no. 17, pp. 1333–1339, 2012.

[92] N. Boos, S. Weissbach, H. Rohrbach, C. Weiler, K. F. Spratt, and A. G. Nerlich, "Classification of age-related changes in lumbar intervertebral discs," *Spine (Phila. Pa. 1976).*, vol. 27, no. 23, pp. 2631–2644, 2002.

[93] B.-G. Peng, "Pathophysiology, diagnosis, and treatment of discogenic low back pain.," *World J. Orthop.*, vol. 4, no. 2, pp. 42–52, 2013.

[94] J. H. Adler, M. Schoenbaum, and R. Silberberg, "Early onset of disk degeneration and spondylosis in sand rats (Psammomys obesus).," *Vet. Pathol.*, vol. 20, no. 1, pp. 13–22, 1983.

[95] K. Singh, K. Masuda, E. J. M. Thonar, H. S. An, and G. Cs-Szabo, "Age-related changes in the extracellular matrix of nucleus pulposus and anulus fibrosus of human intervertebral disc," *Spine (Phila Pa 1976)*, vol. 34, no. 1, pp. 10–16, 2010.

[96] S. Roberts, B. Caterson, J. Menage, E. H. Evans, D. C. Jaffray, and S. M. Eisenstein, "Matrix metalloproteinases and aggrecanase: Their role in disorders of the human intervertebral disc.," *Spine (Phila. Pa. 1976).*, vol. 25, no. 23, pp. 3005–3013, 2000.

[97] A. J. Freemont, "The cellular pathobiology of the degenerate intervertebral disc and discogenic back pain.," *Rheumatology (Oxford).*, vol. 48, no. 1, pp. 5–10, Jan. 2009.

[98] G. Cs-Szabo, D. Ragasa-San Juan, V. Turumella, K. Masuda, E. J. M. A. Thonar, and H. S. An, "Changes in mRNA and protein levels of proteoglycans of the anulus fibrosus and nucleus pulposus during intervertebral disc degeneration.," *Spine (Phila. Pa. 1976).*, vol. 27, no. 20, pp. 2212–2219, 2002.

[99] C. L. Le Maitre, A. Pockert, D. J. Buttle, A. J. Freemont, and J. A. Hoyland,

"Matrix synthesis and degradation in human intervertebral disc degeneration.," *Biochem. Soc. Trans.*, vol. 35, no. Part 4, pp. 652–5, Aug. 2007.

[100] J. P. G. Urban and S. Roberts, "Degeneration of the intervertebral disc.," *Arthritis Res. Ther.*, vol. 5, no. 3, pp. 120–30, Jan. 2003.

[101] M. V Risbud and I. M. Shapiro, "Role of cytokines in intervertebral disc degeneration: pain and disc content.," *Nat. Rev. Rheumatol.*, vol. 10, no. 1, pp. 44–56, 2014.

[102] J. Yamamoto, K. Maeno, T. Takada, K. Kakutani, T. Yurube, Z. Zhang, H. Hirata, T. Kurakawa, D. Sakai, J. Mochida, M. Doita, M. Kurosaka, and K. Nishida, "Fas ligand plays an important role for the production of pro-inflammatory cytokines in intervertebral disc nucleus pulposus cells," *J. Orthop. Res.*, vol. 31, no. 4, pp. 608–615, 2013.

[103] J. G. Burke, R. W. G. Watson, D. McCormack, F. E. Dowling, M. G. Walsh, and J. M. Fitzpatrick, "Intervertebral discs which cause low back pain secrete high levels of proinflammatory mediators.," *J. Bone Joint Surg. Br.*, vol. 84, no. 2, pp. 196–201, Mar. 2002.

[104] M. F. Shamji, L. A. Setton, W. Jarvis, S. So, J. Chen, L. Jing, R. Bullock, R. E. Isaacs, C. Brown, and W. J. Richardson, "Proinflammatory cytokine expression profile in degenerated and herniated human intervertebral disc tissues," *Arthritis Rheum.*, vol. 62, no. 7, pp. 1974–1982, 2010.

[105] I. Altun, "Cytokine profile in degenerated painful intervertebral disc: variability with respect to duration of symptoms and type of disease.," *Spine J.*, vol. 16, no. 7, pp. 857–861, 2016.

[106] C. K. Kepler, D. Z. Markova, F. Dibra, S. Yadla, A. R. Vaccaro, M. V Risbud, T. J. Albert, and D. G. Anderson, "Expression and relationship of proinflammatory chemokine RANTES/CCL5 and cytokine IL-1β in painful human intervertebral discs.," *Spine (Phila. Pa. 1976).*, vol. 38, no. 11, pp. 873–80, 2013.

[107] J. A. Hoyland, C. Le Maitre, and A. J. Freemont, "Investigation of the role of

IL-1 and TNF in matrix degradation in the intervertebral disc.," *Rheumatology (Oxford).*, vol. 47, no. 6, pp. 809–14, Jun. 2008.

[108] D. Purmessur, B. a Walter, P. J. Roughley, D. M. Laudier, A. C. Hecht, and J. Iatridis, "A role for TNFα in intervertebral disc degeneration: a non-recoverable catabolic shift.," *Biochem. Biophys. Res. Commun.*, vol. 433, no. 1, pp. 151–6, Mar. 2013.

[109] C. L. Le Maitre, J. A. Hoyland, and A. J. Freemont, "Interleukin-1 receptor antagonist delivered directly and by gene therapy inhibits matrix degradation in the intact degenerate human intervertebral disc: an in situ zymographic and gene therapy study.," *Arthritis Res. Ther.*, vol. 9, no. 4, p. R83, 2007.

[110] Y. Tian, W. Yuan, N. Fujita, J. Wang, H. Wang, I. M. Shapiro, and M. V. Risbud, "Inflammatory cytokines associated with degenerative disc disease control aggrecanase-1 (ADAMTS-4) expression in nucleus pulposus cells through MAPK and NF-κB," *Am. J. Pathol.*, vol. 182, no. 6, pp. 2310–2321, 2013.

[111] X. Wang, H. Wang, H. Yang, J. Li, Q. Cai, I. M. Shapiro, and M. V Risbud, "Tumor necrosis factor-α- and interleukin-1β-dependent matrix metalloproteinase-3 expression in nucleus pulposus cells requires cooperative signaling via syndecan 4 and mitogen-activated protein kinase-NF-κB axis: implications in inflammatory disc disease.," *Am. J. Pathol.*, vol. 184, no. 9, pp. 2560–72, Sep. 2014.

[112] J. Li, L. Nie, Y. Zhao, Y. Zhang, X. Wang, S. Wang, and Y. Liu, "IL-17 mediates inflammatory reactions via p38/c-Fos and JNK/c-Jun activation in an AP-1-dependent manner in human nucleus pulposus cells," *J. Transl. Med.*, pp. 1–10, 2016.

[113] M. Stefanakis, M. Al-Abbasi, I. Harding, P. Pollintine, P. Dolan, J. Tarlton, and M. a. Adams, "Annulus fissures are mechanically and chemically conducive to the ingrowth of nerves and blood vessels," *Spine (Phila. Pa. 1976).*, vol. 37, no. 22, pp. 1883–1891, 2012.

[114] K. T. Weber, D. O. Alipui, C. P. Sison, O. Bloom, S. Quraishi, M. C. Overby, M. Levine, and N. O. Chahine, "Serum levels of the proinflammatory

cytokine interleukin-6 vary based on diagnoses in individuals with lumbar intervertebral disc diseases," *Arthritis Res. Ther.*, vol. 18, no. 1, p. 3, 2016.

[115] J. García-Cosamalón, M. E. del Valle, M. G. Calavia, O. García-Suárez, A. López-Muñiz, J. Otero, and J. a Vega, "Intervertebral disc, sensory nerves and neurotrophins: Who is who in discogenic pain?," *J. Anat.*, vol. 217, no. 1, pp. 1–15, Jul. 2010.

[116] Y. Abe, K. Akeda, H. S. An, Y. Aoki, R. Pichika, C. Muehleman, T. Kimura, and K. Masuda, "Proinflammatory cytokines stimulate the expression of nerve growth factor by human intervertebral disc cells," *Spine (Phila. Pa. 1976).*, vol. 32, no. 6, pp. 635–642, 2007.

[117] C. E. Steeds, "The anatomy and physiology of pain," *Basic Sci.*, vol. 34, no. 2, pp. 55–59, 2016.

[118] Echlin F, "Pain responses on stimulation of the lumbar sympathetic chain under local anesthesia," *J Neurosurgery.*, vol. 6. pp. 530–533, 1949.

[119] A. J. Todd, "Neuronal circuitry for pain processing in the dorsal horn," *Nat. Rev. Neurosci.*, vol. 11, no. 12, pp. 823–836, 2010.

[120] A. I. Basbaum, D. M. Bautista, G. Scherrer, and D. Julius, "Cellular and molecular mechanisms of pain," *Cell*, vol. 139, no. 2, pp. 267–284, 2010.

[121] S. Neumann, T. P. Doubell, T. Leslie, and C. J. Woolf, "Inflammatory pain hypersensitivity mediated by phenotypic switch in myelinated primary sensory neurons.," *Nature*, vol. 384, no. 6607, pp. 360–364, 1996.

[122] M. J. Millan, "The induction of pain: An integrative review.," *Prog. Neurobiol.*, vol. 57, no. 1, pp. 1–164, Jan. 1999.

[123] S. Ohtori, K. Takahashi, H. Ino, T. Chiba, M. Yamagata, H. Sameda, and H. Moriya, "Up-regulation of substance P and NMDA receptor mRNA in dorsal horn and pre-gang," *Ann. Anat.*, vol. 184, pp. 71–76, 2002.

[124] A. Merighi, C. Salio, A. Ghirri, L. Lossi, F. Ferrini, C. Betelli, and R. Bardoni, "BDNF as a pain modulator.," *Prog. Neurobiol.*, vol. 85, no. 3, pp. 297–317, Jul. 2008.

[125] S. P. Hunt, A. Pini, and G. Evan, "Induction of c-fos-like protein in spinal cord neurons following sensory stimulation," *Nature*, vol. 328, no. 6131, pp. 632–634, 1987.

[126] M. J. Millan, "Descending control of pain," *Prog. Neurobiol.*, vol. 66, no. 6, pp. 355–474, 2002.

[127] K. Takahashi, Y. Aoki, and S. Ohtori, "Resolving discogenic pain.," *Eur. Spine J.*, vol. 17 Suppl 4, pp. 428–31, Dec. 2008.

[128] D. Chou, D. Samartzis, C. Bellabarba, A. Patel, K. D. K. Luk, J. M. S. Kisser, and A. C. Skelly, "Degenerative magnetic resonance imaging changes in patients with chronic low back pain," *Spine (Phila. Pa. 1976).*, vol. 36, no. 21, pp. S43–S53, 2011.

[129] G. A. Von Forell, T. K. Stephens, D. Samartzis, and A. E. Bowden, "Low Back Pain," *Spine (Phila. Pa. 1976).*, vol. 40, no. 15, pp. 1165–1172, 2015.

[130] K. Ito and L. Creemers, "Mechanisms of intervertebral disk degeneration/injury and pain: A review.," *Glob. spine J.*, vol. 3, no. 3, pp. 145–52, Jun. 2013.

[131] F. Alyas, D. Connell, and A. Saifuddin, "Upright positional MRI of the lumbar spine," *Clin. Radiol.*, vol. 63, no. 9, pp. 1035–1048, 2008.

[132] D. G. Blankenbaker, V. M. Haughton, B. P. Rogers, M. E. Meyerand, and J. P. Fine, "Axial rotation of the lumbar spinal motion segments correlated with concordant pain on discography: A preliminary study," *Am. J. Roentgenol.*, vol. 186, no. 3, pp. 795–799, 2006.

[133] N. C. Gries, U. Berlemann, R. J. Moore, and B. Vernon-Roberts, "Early histologic changes in lower lumbar discs and facet joints and their correlation.," *Eur. Spine J.*, vol. 9, no. 1, pp. 23–9, 2000.

[134] P. Goupille, D. Mulleman, G. Paintaud, H. Watier, and J. P. Valat, "Can sciatica induced by disc herniation be treated with tumor necrosis factor α blockade?," *Arthritis Rheum.*, vol. 56, no. 12, pp. 3887–3895, 2007.

[135] M. F. Brown, M. V Hukkanen, I. D. McCarthy, D. R. Redfern, J. J. Batten, H. V Crock, S. P. Hughes, and J. M. Polak, "Sensory and sympathetic

innervation of the vertebral endplate in patients with degenerative disc disease," *J. Bone Jt. Surgery, Br. Vol.*, vol. 79, no. 1, pp. 147–153, 1997.

[136] S. K. Tolofari, S. M. Richardson, A. J. Freemont, and J. A. Hoyland, "Expression of semaphorin 3A and its receptors in the human intervertebral disc: potential role in regulating neural ingrowth in the degenerate intervertebral disc.," *Arthritis Res. Ther.*, vol. 12, no. 1, p. R1, Jan. 2010.

[137] D. Purmessur, C. C. Guterl, S. K. Cho, M. C. Cornejo, Y. W. Lam, B. A. Ballif, D. M. Laudier, and J. C. Iatridis, "Dynamic pressurization induces transition of notochordal cells to a mature phenotype while retaining production of important patterning ligands from development," *Arthritis Res. Ther.*, vol. 15, no. 5, p. R122, 2013.

[138] W. D. Snider and S. B. McMahon, "Tackling pain at the source: New ideas about nociceptors," *Neuron*, vol. 20, no. 4, pp. 629–632, 1998.

[139] Y. Aoki, H. S. An, K. Takahashi, K. Miyamoto, M. E. Lenz, H. Moriya, and K. Masuda, "Axonal growth potential of lumbar dorsal root ganglion neurons in an organ culture system: Response of nerve growth factor-sensitive neurons to neuronal injury and an inflammatory cytokine.," *Spine (Phila. Pa. 1976).*, vol. 32, no. 8, pp. 857–63, Apr. 2007.

[140] P. W. McCarthy, B. Carruthers, D. Martin, and P. Petts, "Immunohistochemical demonstration of sensory nerve fibers and endings in lumbar intervertebral discs of the rat.," *Spine*, vol. 16, no. 6. pp. 653–5, 1991.

[141] Y. Aoki, S. Ohtori, K. Takahashi, H. Ino, Y. Takahashi, T. Chiba, and H. Moriya, "Innervation of the lumbar intervertebral disc by nerve growth factor-dependent neurons related to inflammatory pain.," *Spine (Phila. Pa. 1976).*, vol. 29, no. 10, pp. 1077–81, May 2004.

[142] S. M. Richardson, D. Purmessur, P. Baird, B. Probyn, A. J. Freemont, and J. A. Hoyland, "Degenerate human nucleus pulposus cells promote neurite outgrowth in neural cells.," *PLoS One*, vol. 7, no. 10, p. e47735, Jan. 2012.

[143] X. Zhang, J. Huang, and P. A. McNaughton, "NGF rapidly increases membrane expression of TRPV1 heat-gated ion channels.," *EMBO J.*, vol. 24,

no. 24, pp. 4211–23, Dec. 2005.

[144] R. R. Ji, T. A. Samad, S. X. Jin, R. Schmoll, and C. J. Woolf, "p38 MAPK activation by NGF in primary sensory neurons after inflammation increases TRPV1 levels and maintains heat hyperalgesia," *Neuron*, vol. 36, no. 1, pp. 57–68, 2002.

[145] K. L. Byron, C. Overland, T. W. Vanderah, and R. H. Spencer, "Peripheral mechanisms of pain and analgesia," *Brain Res. Rev.*, vol. 60, no. 1, pp. 90–113, 2010.

[146] R. J. Mannion, M. Costigan, I. Decosterd, F. Amaya, Q. P. Ma, J. C. Holstege, R. R. Ji, A. Acheson, R. M. Lindsay, G. A. Wilkinson, and C. J. Woolf, "Neurotrophins: Peripherally and centrally acting modulators of tactile stimulus-induced inflammatory pain hypersensitivity.," *Proc. Natl. Acad. Sci. U. S. A.*, vol. 96, no. 16, pp. 9385–90, 1999.

[147] F. Lembeck, J. Donnerer, M. Tsuchiya, and A. Nagahisa, "Inhibitor of Neurogenic Inflammation," *Br. J. Pharmacol.*, vol. 105, pp. 527–530, 1992.

[148] C. K. Kepler, D. Z. Markova, A. S. Hilibrand, A. R. Vaccaro, M. V Risbud, T. J. Albert, and D. G. Anderson, "Substance P stimulates production of inflammatory cytokines in human disc cells.," *Spine (Phila. Pa. 1976).*, vol. 38, no. 21, pp. E1291-9, 2013.

[149] Q. P. Ma and C. J. Woolf, "Tachykinin NK1 receptor antagonist RP67580 attenuates progressive hypersensitivity of flexor reflex during experimental inflammation in rats," *Eur. J. Pharmacol.*, vol. 322, no. 2–3, pp. 165–171, 1997.

[150] S. Kimura, Y. Sakuma, M. Suzuki, S. Orita, K. Yamauchi, G. Inoue, Y. Aoki, T. Ishikawa, M. Miyagi, H. Kamoda, G. Kubota, Y. Oikawa, K. Inage, T. Sainoh, J. Sato, J. Nakamura, T. Toyone, K. Takahashi, and S. Ohtori, "Evaluation of pain behavior and calcitonin gene-related peptide immunoreactive sensory nerve fibers in the spinal dorsal horn after sciatic nerve compression and application of nucleus pulposus in rats.," *Spine (Phila. Pa. 1976).*, vol. 39, no. 6, pp. 455–462, 2014.

[151] Y. Uchiyama, C. C. Cheng, K. G. Danielson, J. Mochida, T. J. Albert, I. M. Shapiro, and M. V Risbud, "Expression of acid-sensing ion channel 3 (ASIC3) in nucleus pulposus cells of the intervertebral disc is regulated by p75NTR and ERK signaling.," *J. Bone Miner. Res.*, vol. 22, no. 12, pp. 1996–2006, Dec. 2007.

[152] S. Y. Park, J. Y. Choi, R. U. Kim, Y. S. Lee, H. J. Cho, and D. S. Kim, "Downregulation of voltage-gated potassium channel alpha gene expression by axotomy and neurotrophins in rat dorsal root ganglia.," *Mol. Cells*, vol. 16, no. 2, pp. 256–9, 2003.

[153] D. Le Bars, M. Gozariu, and S. W. Cadden, "Animal models of nociception.," *Pharmacol. Rev.*, vol. 53, no. 4, pp. 597–652, 2001.

[154] M. Alini, S. M. Eisenstein, K. Ito, C. Little, A. A. Kettler, K. Masuda, J. Melrose, J. Ralphs, I. Stokes, and H. J. Wilke, "Are animal models useful for studying human disc disorders/degeneration?," *Eur. Spine J.*, vol. 17, no. 1, pp. 2–19, Jan. 2008.

[155] T. Nakamae, M. Ochi, and K. Olmarker, "Pharmacological inhibition of tumor necrosis factor may reduce pain behavior changes induced by experimental disc puncture in the rat: An experimental study in rats.," *Spine (Phila. Pa. 1976).*, vol. 36, no. 4, pp. E232–E236, 2011.

[156] K. Olmarker, "Puncture of a lumbar intervertebral disc induces changes in spontaneous pain behavior: an experimental study in rats," *Spine (Phila Pa 1976.)*, vol. 33, no. 1528–1159 (Electronic), pp. 850–855, 2008.

[157] E. Nilsson, T. Nakamae, and K. Olmarker, "Pain behavior changes following disc puncture relate to nucleus pulposus rather than to the disc injury per se: An experimental study in rats.," *Open Orthop. J.*, vol. 5, pp. 72–7, 2011.

[158] S. J. Kim, W. R. Kim, H. S. Kim, H. W. Park, Y. W. Cho, S. H. Jang, S. J. Hwang, and S. H. Ahn, "Abnormal spontaneous activities on needle electromyography and their relation with pain behavior and nerve fiber pathology in a rat model of lumbar disc herniation.," *Spine (Phila. Pa. 1976).*, vol. 36, no. 24, pp. E1562-7, 2011.

[159] P. Y. Hwang, K. D. Allen, M. F. Shamji, L. Jing, B. A. Mata, M. A. Gabr, J. L. Huebner, V. B. Kraus, W. J. Richardson, and L. A. Setton, "Changes in midbrain pain receptor expression, gait and behavioral sensitivity in a rat model of radiculopathy," *Open Orthop. J.*, vol. 6, pp. 383–391, 2012.

[160] O. Krupkova, M. Sekiguchi, J. Klasen, O. Hausmann, S. Konno, and S. J. Ferguson, "Epigallocatechin 3-gallate supresses interleukin-1β-induced inflammatory responses in intervertebral disc cells in vitro and reduces radiculopathic in rats," *Eur. Cells Mater.*, vol. 28, pp. 372–386, 2014.

[161] A. L. de Souza Grava, L. F. Ferrari, and H. L. A. Defino, "Cytokine inhibition and time-related influence of inflammatory stimuli on the hyperalgesia induced by the nucleus pulposus.," *Eur. Spine J.*, vol. 21, no. 3, pp. 537–45, Mar. 2012.

[162] A. Onda, Y. Murata, B. Rydevik, K. Larsson, S. Kikuchi, and K. Olmarker, "Immunoreactivity of brain-derived neurotrophic factor in rat dorsal root ganglion and spinal cord dorsal horn following exposure to herniated nucleus pulposus," *Neurosci. Lett.*, vol. 352, pp. 49–52, Sep. 2003.

[163] A. Lai, A. Moon, D. Purmessur, B. Skovrlj, D. M. Laudier, B. A. Winkelstein, S. K. Cho, A. C. Hecht, and J. C. Iatridis, "Annular puncture with tumor necrosis factor-alpha injection enhances painful behavior with disc degeneration in-vivo," *Spine J.*, pp. 1–12, 2015.

[164] A. Lai, A. Moon, D. Purmessur, B. Skovrlj, B. A. Winkelstein, S. K. Cho, A. C. Hecht, and J. C. Iatridis, "Assessment of functional and behavioral changes sensitive to painful disc degeneration," *J Orthop Res*, vol. 33, no. 5, pp. 755–764, 2015.

[165] M. Miyagi, T. Ishikawa, H. Kamoda, M. Suzuki, Y. Sakuma, S. Orita, Y. Oikawa, Y. Aoki, T. Toyone, K. Takahashi, G. Inoue, and S. Ohtori, "Assessment of pain behavior in a rat model of intervertebral disc injury using the CatWalk gait analysis system.," *Spine (Phila. Pa. 1976).*, vol. 38, no. 17, pp. 1459–65, 2013.

[166] J. S. Kim, J. S. Kroin, X. Li, H. S. An, A. Buvanendran, D. Yan, K. J. Tuman, A. J. van Wijnen, D. Chen, and H. J. Im, "The rat intervertebral disk

degeneration pain model: relationships between biological and structural alterations and pain.," *Arthritis Res. Ther.*, vol. 13, no. 5, p. R165, Jan. 2011.

[167] D. Nojima, K. Inage, Y. Sakuma, J. Sato, S. Orita, K. Yamauchi, Y. Eguchi, N. Ochiai, K. Kuniyoshi, Y. Aoki, J. Nakamura, M. Miyagi, M. Suzuki, G. Kubota, T. Sainoh, K. Fujimoto, Y. Shiga, K. Abe, H. Kanamoto, G. Inoue, K. Takahashi, and S. Ohtori, "Efficacy of anti-NaV1.7 antibody on the sensory nervous system in a rat model of lumbar intervertebral disc injury," *Yonsei Med. J.*, vol. 57, no. 3, pp. 748–753, 2016.

[168] T. Sainoh, S. Orita, M. Miyagi, Y. Sakuma, K. Yamauchi, M. Suzuki, G. Kubota, Y. Oikawa, K. Inage, J. Sato, K. Fujimoto, Y. Shiga, G. Inoue, Y. Aoki, K. Takahashi, and S. Ohtori, "Interleukin-6 and interleukin-6 receptor expression, localization, and involvement in pain-sensing neuron activation in a mouse intervertebral disc injury model," *J. Orthop. Res.*, p. n/a-n/a, 2015.

[169] Y. Aoki, S. Ohtori, H. Ino, H. Douya, T. Ozawa, T. Saito, H. Moriya, and K. Takahashi, "Disc inflammation potentially promotes axonal regeneration of dorsal root ganglion neurons innervating lumbar intervertebral disc in rats.," *Spine (Phila. Pa. 1976).*, vol. 29, no. 23, pp. 2621–6, Dec. 2004.

[170] J. Melrose, S. Roberts, S. Smith, J. Menage, and P. Ghosh, "Increased nerve and blood vessel ingrowth associated with proteoglycan depletion in an ovine anular lesion model of experimental disc degeneration.," *Spine (Phila. Pa. 1976).*, vol. 27, no. 12, pp. 1278–85, Jun. 2002.

[171] J. H. Jeong, E. S. Jin, J. K. Min, S. R. Jeon, C. S. Park, H. S. Kim, and K. H. Choi, "Human mesenchymal stem cells implantation into the degenerated coccygeal disc of the rat.," *Cytotechnology*, vol. 59, no. 1, pp. 55–64, Jan. 2009.

[172] P. Grunert, B. H. Borde, K. D. Hudson, M. R. Macielak, L. J. Bonassar, and R. Härtl, "Annular repair using high-density collagen gel: A rat-tail *in vivo* model.," *Spine (Phila. Pa. 1976).*, vol. 39, no. 3, pp. 198–206, Mar. 2014.

[173] Y. Aoki, K. Akeda, H. An, C. Muehleman, K. Takahashi, H. Moriya, and K. Masuda, "Nerve fiber ingrowth into scar tissue formed following nucleus pulposus extrusion in the rabbit anular-puncture disc degeneration model:

effects of depth of puncture.," *Spine (Phila. Pa. 1976).*, vol. 31, no. 21, pp. E774-80, Oct. 2006.

[174] D. E. Gregory, W. C. Bae, R. L. Sah, and K. Masuda, "Disc degeneration reduces the delamination strength of the annulus fibrosus in the rabbit annular disc puncture model.," *Spine J.*, vol. 14, no. 7, pp. 1265–71, Jul. 2014.

[175] Y. J. Kwon, "A minimally invasive rabbit model of progressive and reproducible disc degeneration confirmed by radiology, gene expression, and histology.," *J. Korean Neurosurg. Soc.*, vol. 53, no. 6, pp. 323–30, Jun. 2013.

[176] K. Masuda, Y. Aota, C. Muehleman, Y. Imai, M. Okuma, E. J. Thonar, G. B. Andersson, and H. S. An, "A novel rabbit model of mild, reproducible disc degeneration by an anulus needle puncture: correlation between the degree of disc injury and radiological and histological appearances of disc degeneration.," *Spine (Phila. Pa. 1976).*, vol. 30, no. 1, pp. 5–14, 2005.

[177] D. Sakai, J. Mochida, T. Iwashina, A. Hiyama, H. Omi, M. Imai, T. Nakai, K. Ando, and T. Hotta, "Regenerative effects of transplanting mesenchymal stem cells embedded in atelocollagen to the degenerated intervertebral disc.," *Biomaterials*, vol. 27, no. 3, pp. 335–45, Jan. 2006.

[178] T. Yurube, H. Hirata, K. Kakutani, K. Maeno, T. Takada, Z. Zhang, K. Takayama, T. Matsushita, R. Kuroda, M. Kurosaka, and K. Nishida, "Notochordal cell disappearance and modes of apoptotic cell death in a rat tail static compression-induced disc degeneration model.," *Arthritis Res. Ther.*, vol. 16, no. 1, p. R31, Jan. 2014.

[179] J. J. MacLean, C. R. Lee, M. Alini, and J. C. Iatridis, "The effects of short-term load duration on anabolic and catabolic gene expression in the rat tail intervertebral disc.," *J. Orthop. Res.*, vol. 23, no. 5, pp. 1120–7, Sep. 2005.

[180] C. T. S. Ching, D. H. K. Chow, F. Y. D. Yao, and A. D. Holmes, "The effect of cyclic compression on the mechanical properties of the inter-vertebral disc: An *in vivo* study in a rat tail model," *Clin. Biomech.*, vol. 18, no. 3, pp. 182–189, Mar. 2003.

[181] A. Barbir, K. E. Godburn, A. J. Michalek, A. Lai, R. D. Monsey, and J. C.

Iatridis, “Effects of torsion on intervertebral disc gene expression and biomechanics, using a rat tail model,” *Spine (Phila Pa 1976)*, vol. 36, no. 8, pp. 607–614, 2011.

[182] R. Silberberg, “Histologic and morphometric observationson vertebral bone of aging sand rats,” *Spine (Phila. Pa. 1976).*, vol. 13, no. 2, pp. 202–208, 1998.

[183] H. E. Gruber, T. Johnson, H. J. Norton, and E. N. Hanley, “The sand rat model for disc degeneration: radiologic characterization of age-related changes: Cross-sectional and prospective analyses,” *Spine (Phila. Pa. 1976).*, vol. 27, no. 3, pp. 230–4, 2002.

[184] R. J. Berry, “Genetically controlled degeneration of the nucleus pulposus in the mouse,” *J Bone Jt. Surg*, vol. 43, no. 2, pp. 387–393, 1961.

[185] D. J. Nuckley, P. A. Kramer, A. Del Rosario, N. Fabro, S. Baran, and R. P. Ching, “Intervertebral disc degeneration in a naturally occurring primate model: Radiographic and biomechanical evidence,” *J. Orthop. Res.*, vol. 26, no. 9, pp. 1283–1288, 2008.

[186] N. A. Gillett, R. Gerlach, J. J. Cassidy, and S. A. Brown, “Age-related changes in the beagle spine,” *Acta Orthop. Scand.*, vol. 59, no. 5, pp. 503–507, 1988.

[187] N. Bergknut, J. P. H. J. Rutges, H. J. C. Kranenburg, L. A. Smolders, R. Hagman, H. J. Smidt, A. S. Lagerstedt, L. C. Penning, G. Voorhout, H. A. W. Hazewinkel, G. C. M. Grinwis, L. B. Creemers, B. P. Meij, and W. J. A. Dhert, “The Dog as an Animal Model for Intervertebral Disc Degeneration?,” *Spine (Phila. Pa. 1976).*, vol. 37, no. 5, pp. 351–358, 2012.

[188] N. Willems, A. R. Tellegen, N. Bergknut, L. B. Creemers, J. Wolfswinkel, C. Freudigmann, K. Benz, G. C. M. Grinwis, M. A. Tryfonidou, and B. P. Meij, “Inflammatory profiles in canine intervertebral disc degeneration,” *BMC Vet. Res.*, vol. 12, no. 1, p. 10, 2016.

[189] N. Bergknut, L. A. Smolders, G. C. M. Grinwis, R. Hagman, A. S. Lagerstedt, H. A. W. Hazewinkel, M. A. Tryfonidou, and B. P. Meij, “Intervertebral disc degeneration in the dog. Part 1: Anatomy and physiology of the intervertebral

disc and characteristics of intervertebral disc degeneration," *Vet. J.*, vol. 195, no. 3, pp. 282–291, 2013.

[190] Medtronic, "InFUSE™ bone graft/LT-CAGE™ lumbar tapered fusion device," 2002.

[191] J. K. Burkus, E. E. Transfeldt, S. H. Kitchel, R. G. Watkins, and R. a Balderston, "Clinical and radiographic outcomes of anterior lumbar interbody fusion using recombinant human bone morphogenetic protein-2," *Spine (Phila. Pa. 1976).*, vol. 27, no. 21, pp. 2396–2408, 2002.

[192] Stryker, "AccuLIF® TL Cage System," 2014.

[193] C. W. B. Peng, W. M. Yue, S. Y. Poh, W. Yeo, and S. B. Tan, "Clinical and radiological outcomes of minimally invasive versus open transforaminal lumbar interbody fusion.," *Spine (Phila. Pa. 1976).*, vol. 34, no. 13, pp. 1385–9, 2009.

[194] P. Fritzell, O. Hagg, P. Wessberg, A. Nordwall, and S. L. S. S. Group, "2001 Volvo award winner in clinical studies: Lumbar fusion versus nonsurgical treatment for chronic low back pain: A multicenter randomized controlled trial from the Swedish Lumbar Spine study group," *Spine (Phila. Pa. 1976).*, vol. 26, no. 23, pp. 2521–2534, 2001.

[195] D. C. Cherkin, K. J. Wheelar, W. Barlow, and R. A. Deyo, "Medication use for low back pain in primary care," *Spine (Phila. Pa. 1976).*, vol. 23, no. 5, pp. 607–614, 1998.

[196] M. W. Van Tulder, T. Touray, A. D. Furlan, S. Solway, and L. M. Bouter, "Muscle relaxants for non-specific low-back pain," *The Cochrane Collaberation*, no. 4, pp. 4–6, 2008.

[197] R. A. Deyo, M. Von Korff, and D. Duhrkoop, "Opioids for low back pain," *BMJ*, vol. 350, p. g6380, 2015.

[198] M. von Korff, A. Kolodny, R. A. Deyo, and R. Chou, "Long-term opioid therapy reconsidered," *Ann. Intern. Med.*, vol. 155, no. 5, pp. 325–328, 2011.

[199] B. Morasco, J. P. Duckart, T. P. Carr, R. A. Deyo, and S. K. Dobscha, "Clinical characteristics of veterans prescribed high doses of opioid

medications for chronic non-cancer pain," *Pain*, vol. 151, no. 3, pp. 625–632, 2010.

[200] E. J. Carragee, "Persistent Low Back Pain," *N Engl J Med*, vol. 35218352, pp. 1891–8, 2005.

[201] T. O. Staiger, B. Gaster, M. D. Sullivan, and R. A. Deyo, "Systematic Review of Antidepressants in the Treatment of Chronic Low Back Pain," *Spine (Phila. Pa. 1976).*, vol. 28, no. 22, pp. 2540–2545, 2003.

[202] S. M. Salerno, R. Browning, and J. L. Jackson, "The effect of antidepressant treatment on chronic back pain: A meta-analysis," *Arch. Intern. Med.*, vol. 162, no. 1, pp. 19–24, 2002.

[203] M. Van Tulder, A. Malmivaara, R. Esmail, and B. Koes, "Exercise therapy for low-back pain (Review)," *Cochrane Database Syst Rev*, no. 2, 2005.

[204] R. M. Benyamin, L. Manchikanti, A. T. Parr, S. Diwan, V. Singh, F. J. E. Falco, S. Datta, S. Abdi, and J. A. Hirsch, "The effectiveness of lumbar interlaminar epidural injections in managing chronic low back and lower extremity pain.," *Pain Physician*, vol. 15, no. 4, pp. E363-404, 2012.

[205] S. Carette, S. Marcoux, R. Truchon, C. Grondin, J. Gagnon, Y. Allard, and M. Latulippe, "A controlled trial of corticosteroid injec- tions into facet joints for chronic low back pain," *N. Engl. J. Med.*, vol. 325, no. 14, pp. 1002–1007, 1991.

[206] P. J. Nelemans, R. A. de Bie, H. C. de Vet, and F. Sturmans, "Injection therapy for subacute and chronic benign low-back pain.," *Cochrane Database Syst. Rev.*, no. 4, 2006.

[207] J. S. Saal and J. A. Saal, "Management of chronic discogenic low back pain with a thermal intradiscal catheter: A preliminary report," *Spine (Phila. Pa. 1976).*, vol. 25, no. 3, pp. 382–388, 2000.

[208] R. Derby, B. Eek, Y. Chen, C. O'Neill, and D. Ryan, "Intradiscal electrothermal annuloplasty (IDET): A novel approach for treating chronic discogenic back pain," *Neuromodulation*, vol. 3, no. 2, pp. 82–88, 2000.

[209] D. Appleby, G. B. Andersson, and M. Totta, "Metaanalysis of the efficacy and

safety of intradiscal electrothermal therapy (IDET)," *Pain Med.*, vol. 7, no. 4, pp. 308–316, 2006.

[210] B. J. C. Freeman, "IDET: A critical appraisal of the evidence," *Eur. Spine J.*, vol. 15, no. Suppl. 3, pp. 448–457, 2006.

[211] D. Sakai and G. B. J. Andersson, "Stem cell therapy for intervertebral disc regeneration: obstacles and solutions," *Nat. Rev. Rheumatol.*, vol. 11, no. 4, pp. 243–256, 2015.

[212] H. Pratsinis and D. Kletsas, "PDGF, bFGF and IGF-I stimulate the proliferation of intervertebral disc cells in vitro via the activation of the ERK and Akt signaling pathways.," *Eur. Spine J.*, vol. 16, no. 11, pp. 1858–66, Nov. 2007.

[213] Z. Bian and J. Sun, "Development of a KLD-12 polypeptide/TGF-β1-tissue scaffold promoting the differentiation of mesenchymal stem cell into nucleus pulposus-like cells for treatment of intervertebral disc degeneration," *Int J Clin Exp Pathol*, vol. 8, no. 2, pp. 1093–1103, 2015.

[214] Y. Gan, S. Li, P. Li, Y. Xu, L. Wang, C. Zhao, B. Ouyang, B. Tu, C. Zhang, L. Luo, X. Luo, X. Mo, and Q. Zhou, "A controlled release codelivery system of MSCs encapsulated in dextran/gelatin hydrogel with TGF-B3-loaded nanoparticles for nucleus pulposus regeneration," *Stem Cells Int*, vol. 9042019, 2016.

[215] S. Tim Yoon and N. M. Patel, "Molecular therapy of intervertebral disc," *Eur. Cells Mater.*, vol. 10, no. SUPPL.3, p. 40, 2005.

[216] M. Likhitpanichkul, Y. Kim, O. M. Torre, E. See, Z. Kazezian, A. Pandit, A. C. Hecht, and J. C. Iatridis, "Fibrin-genipin annulus fibrosus sealant as a delivery system for anti-TNFα drug," *Spine J.*, vol. 15, no. 2015, pp. 2045–2054, 2015.

[217] D. J. Gorth, R. L. Mauck, J. A. Chiaro, B. Mohanraj, N. M. Hebela, G. R. Dodge, D. M. Elliott, and L. J. Smith, "IL-1ra delivered from poly(lactic-co-glycolic acid) microspheres attenuates IL-1beta mediated degradation of nucleus pulposus in vitro," *Arthritis Res. Ther.*, vol. 14, no. 4, p. R179, 2012.

[218] H. E. Gruber, K. Leslie, J. Ingram, H. J. Norton, and E. N. Hanley, "Cell-based tissue engineering for the intervertebral disc: in vitro studies of human disc cell gene expression and matrix production within selected cell carriers," *Spine J*, vol. 4, no. 1, pp. 44–55, 2004.

[219] A. E. Baer, J. Y. Wang, V. B. Kraus, and L. A. Setton, "Collagen gene expression and mechanical properties of intervertebral disc cell-alginate cultures," *J Orthop Res*, vol. 19, no. 1, pp. 2–10, 2001.

[220] O. Guillaume, S. M. Naqvi, K. Lennon, and C. T. Buckley, "Enhancing cell migration in shape-memory alginate-collagen composite scaffolds: In vitro and ex vivo assessment for intervertebral disc repair.," *J. Biomater. Appl.*, vol. 29, no. 9, pp. 1230–46, 2015.

[221] P. Roughley, C. Hoemann, E. DesRosiers, F. Mwale, J. Antoniou, and M. Alini, "The potential of chitosan-based gels containing intervertebral disc cells for nucleus pulposus supplementation.," *Biomaterials*, vol. 27, no. 3, pp. 388–96, Jan. 2006.

[222] S. M. Richardson, N. Hughes, J. A. Hunt, A. J. Freemont, and J. A. Hoyland, "Human mesenchymal stem cell differentiation to NP-like cells in chitosan-glycerophosphate hydrogels.," *Biomaterials*, vol. 29, no. 1, pp. 85–93, Jan. 2008.

[223] R. Tsaryk, J. Silva-Correia, J. Minguel Oliveira, R. E. Unger, C. Landes, C. Brochhausen, S. Ghanaati, R. L. Ries, and C. J. Kirkpatrick, "Biological performance of cell-encapsulated methacrylated gellan gum-based hydrogels for nucleus pulposus regeneration," *J. Tissue Eng. Regen. Med.*, vol. 11, no. 3, pp. 637–648, 2014.

[224] M. Peroglio, D. Eglin, L. M. Benneker, M. Alini, and S. Grad, "Thermoreversible hyaluronan-based hydrogel supports in vitro and ex vivo disc-like differentiation of human mesenchymal stem cells.," *Spine J.*, vol. 13, no. 11, pp. 1627–39, Nov. 2013.

[225] C. G. Jeong, A. T. Francisco, Z. Niu, R. L. Mancino, S. L. Craig, and L. A. Setton, "Screening of hyaluronic acid-poly(ethylene glycol) composite hydrogels to support intervertebral disc cell biosynthesis using artificial neural

network analysis," *Acta Biomater*, vol. 10, no. 8, pp. 3421–3430, 2014.

[226] J. E. Frith, A. R. Cameron, D. J. Menzies, P. Ghosh, D. L. Whitehead, S. Gronthos, A. C. W. Zannettino, and J. J. Cooper-White, "An injectable hydrogel incorporating mesenchymal precursor cells and pentosan polysulphate for intervertebral disc regeneration.," *Biomaterials*, vol. 34, no. 37, pp. 9430–40, Dec. 2013.

[227] P. Grunert, B. H. Borde, S. B. Towne, Y. Moriguchi, K. D. Hudson, L. J. Bonassar, and R. Härtl, "Riboflavin crosslinked high-density collagen gel for the repair of annular defects in intervertebral discs: An *in vivo* study," *Acta Biomater.*, vol. 26, pp. 215–224, 2015.

[228] S. H. Park, H. Cho, E. S. Gil, B. B. Mandal, B. H. Min, and D. L. Kaplan, "Silk-fibrin/hyaluronic acid composite gels for nucleus pulposus tissue regeneration.," *Tissue Eng. Part A*, vol. 17, no. 23–24, pp. 2999–3009, Dec. 2011.

[229] C. Zeng, Q. Yang, M. Zhu, L. Du, J. Zhang, X. Ma, B. Xu, and L. Wang, "Silk fibroin porous scaffolds for nucleus pulposus tissue engineering," *Mater. Sci. Eng. C*, vol. 37, pp. 232–240, 2014.

[230] F. J. O'Brien, "Biomaterials & scaffolds for tissue engineering," *Mater. Today*, vol. 14, no. 3, pp. 88–95, 2011.

[231] E. A. Balazs, T. C. Laurent, and R. W. Jeanloz, "Nomenclature of hyaluronic acid," *Biochem. J.*, vol. 235, p. 903, 1985.

[232] K. T. Dicker, L. A. Gurski, S. Pradhan-Bhatt, R. L. Witt, M. C. Farach-Carson, and X. Jia, "Hyaluronan: A simple polysaccharide with diverse biological functions," *Acta Biomater.*, vol. 10, no. 4, pp. 1558–1570, 2014.

[233] J. R. E. Fraser, T. C. Laurent, and U. B. G. Laurent, "Hyaluronan: Its nature, distribution, functions and turnover," *J. Intern. Med.*, vol. 242, pp. 27–33, 1997.

[234] M. Karl and J. W. Palmer, "The polysaccharide of the vitreous humor," *J Biol Chem*, vol. 107, pp. 629–634, 1934.

[235] A. J. Day and J. K. Sheehan, "Hyaluronan: Polysaccharide chaos to protein

organisation," *Curr. Opin. Struct. Biol.*, vol. 11, no. 5, pp. 617–622, Sep. 2001.

[236] P. Grunert, B. H. Borde, S. B. Towne, Y. Moriguchi, K. D. Hudson, L. J. Bonassar, and R. Härtl, "Riboflavin crosslinked high-density collagen gel for the repair of annular defects in intervertebral discs: An *in vivo* study," *Acta Biomater.*, no. June, 2015.

[237] J. Necas, L. Bartosikova, P. Brauner, and J. Kolar, "Hyaluronic acid (hyaluronan): A review," *Vet. Med. (Praha).*, vol. 8, no. 53, pp. 397–411, 2008.

[238] R. Stern, A. A Asari, and K. N. Sugahara, "Hyaluronan fragments: An information-rich system.," *Eur. J. Cell Biol.*, vol. 85, no. 8, pp. 699–715, Aug. 2006.

[239] M. K. Cowman and S. Matsuoka, "Experimental approaches to hyaluronan structure," *Carbohydr. Res.*, vol. 340, no. 5, pp. 791–809, 2005.

[240] M. Mörgelin, M. Paulsson, T. E. Hardingham, D. Heinegård, and J. Engel, "Cartilage proteoglycans. Assembly with hyaluronate and link protein as studied by electron microscopy," *Biochem J*, vol. 253, no. 1, pp. 175–185, 1988.

[241] M. A. Napier and N. M. Hadler, "Effect of calcium on structure and function of a hyaluronic acid matrix: Carbon-13 nuclear magnetic resonance analysis and the diffusional behavior of small solutes," *Proc. Natl. Acad. Sci.*, vol. 75, no. 5, pp. 2261–2265, 1978.

[242] N. M. Hadler, R. R. Dourmashkin, M. V Nermut, and L. D. Williams, "Ultrastructure of a hyaluronic acid matrix.," *Proc. Natl. Acad. Sci. U. S. A.*, vol. 79, no. 2, pp. 307–309, 1982.

[243] P. Prehm, "Hyaluronate is synthesized at plasma membranes," *J. Biomech.*, vol. 220, pp. 597–600, 1984.

[244] J. Y. Lee and A. P. Spicer, "Hyaluronan: A multifunctional, megaDalton, stealth molecule," *Curr. Opin. Cell Biol.*, vol. 12, no. 5, pp. 581–586, Oct. 2000.

[245] J. M. Cyphert, C. S. Trempus, and S. Garantziotis, "Size matters: Molecular weight specificity of hyaluronan effects in cell biology," *Int. J. Cell Biol.*, vol. 2015, no. Oct. 2015.

[246] P. Prehm and U. Schumacher, "Inhibition of hyaluronan export from human fibroblasts by inhibitors of multidrug resistance transporters.," *Biochem. Pharmacol.*, vol. 68, no. 7, pp. 1401–10, Oct. 2004.

[247] R. Stern, "Hyaluronan catabolism: A new metabolic pathway," *Eur. J. Cell Biol.*, vol. 83, no. 7, pp. 317–325, 2004.

[248] P. A. G. McCourt, "How does the hyaluronan scrap-yard operate?," *Matrix Biol.*, vol. 18, no. 5, pp. 427–432, 1999.

[249] S. Seton-Rogers, "Metastasis: multitasking hyaluronic acid.," *Nat. Rev. Cancer*, vol. 12, no. 4, p. 228, 2012.

[250] I. F. I. Radaeva and G. A. Kostina, "Use of hyaluronic acid for the treatment of various pathologic states," *Pharm. Chem. J.*, vol. 32, no. 9, pp. 492–494, 1999.

[251] E. A. Balazs, "US Patent No. 4141973; Chem. Abstr., 90, 174663 (1979)," 1979.

[252] D. R. Gibson, "US Patent No. 4983580," 1991.

[253] C. A. Cefalu and D. S. Waddell, "Viscosupplementation for the treatment of osteoarthritis of the knee," *Geriatrics*, vol. 54, no. 10, pp. 51–57, 1999.

[254] N. Evaniew, N. Simunovic, and J. Karlsson, "Cochrane in CORR®: Viscosupplementation for the treatment of osteoarthritis of the knee," *Clin. Orthop. Relat. Res.*, vol. 472, pp. 2028–2034, 2014.

[255] C. Weiss, "Viscosupplementation in the older patient with osteoarthritis," *Oper. Tech. Orthop.*, vol. 12, no. 2, pp. 124–130, 2002.

[256] M. Wobig, A. Dickhut, R. Maier, and G. Vetter, "Viscosupplementation with Hylan G-F 20: A 26-week controlled trial of efficacy and safety in the osteoarthritic knee," *Clin. Ther.*, vol. 20, no. 3, pp. 410–423, 1998.

[257] M. Dougados, M. Nguyen, V. Listrat, and B. Amor, "High molecular weight

sodium hyaluronate (hyalectin) in osteoarthritis of the knee: A 1 year placebo-controlled trial," *Osteoarthritis Cartilage*, vol. 1, pp. 97–103, 1993.

[258] A. Gomis, A. Miralles, R. F. Schmidt, and C. Belmonte, "Intra-articular injections of hyaluronan solutions of different elastoviscosity reduce nociceptive nerve activity in a model of osteoarthritic knee joint of the guinea pig," *Osteoarthr. Cartil.*, vol. 17, no. 6, pp. 798–804, Jun. 2009.

[259] R. Caires, E. Luis, F. J. Taberner, G. Fernandez-Ballester, A. Ferrer-Montiel, E. A. Balazs, A. Gomis, C. Belmonte, and E. de la Pena, "Hyaluronan modulates TRPV1 channel opening, reducing peripheral nociceptor activity and pain," *Nat. Commun.*, vol. 6, p. 8095, 2015.

[260] E. de la Pena, A. Gomis, A. Ferrer-Montiel, and C. Belmonte, "TRPV1 channel modulation by hyaluronan reduces pain," *Channels*, vol. 10, no. 2, pp. 81–82, 2016.

[261] B. Zavan, L. Ferroni, C. Giorgi, G. Calo, P. Brun, R. Cortivo, G. Abatangelo, and P. Pinton, "Hyaluronic acid induces activation of the k-Opioid receptor," *PLoS One*, vol. 8, no. 1, pp. 1–8, 2013.

[262] J. O. Cantor, "Potential therapeutic applications of hyaluronan in the lung," *Int. J. COPD*, vol. 2, no. 3, pp. 283–288, 2007.

[263] M. Scuri and W. M. Abraham, "Hyaluronan blocks human neutrophil elastase (HNE)-induced airway responses in sheep," *Pulm. Pharmacol. Ther.*, vol. 16, pp. 335–340, 2003.

[264] M. Scuri, W. M. Abraham, Y. Botvinnikova, and R. Forteza, "Hyaluronic acid blocks porcine pancreatic elastase (PPE)-induced bronchoconstriction in sheep," *Am. J. Respir. Crit. Care Med.*, vol. 164, no. 10 I, pp. 1855–1859, 2001.

[265] R. Forteza, I. Lauredo, W. M. Abraham, and G. E. Conner, "Bronchial tissue kallikrein activity is regulated by hyaluronic acid binding," *Am J Respir Cell Mol Biol*, vol. 21, no. 666, p. 674, 1999.

[266] X. Tian, J. Azpurua, C. Hine, A. Vaidya, M. Myakishev-Rempel, J. Ablaeva, Z. Mao, E. Nevo, V. Gorbunova, and A. Seluanov, "High-molecular-mass

hyaluronan mediates the cancer resistance of the naked mole rat.," *Nature*, vol. 499, no. 7458, pp. 1–6, 2013.

[267] Y. Hirose, E. Saijou, Y. Sugano, F. Takeshita, S. Nishimura, H. Nonaka, Y.-R. Chen, K. Sekine, T. Kido, T. Nakamura, S. Kato, T. Kanke, K. Nakamura, R. Nagai, T. Ochiya, and A. Miyajima, "Inhibition of Stabilin-2 elevates circulating hyaluronic acid levels and prevents tumor metastasis," *Proc. Nati. Acad. Sci. U.S.A*, vol. 109, no. 11, pp. 4263–4268, 2012.

[268] T. Lan, J. Pang, Y. Wu, M. Zhu, X. Yao, M. Wu, H. Qian, Z. Zhang, J. Gao, and Y. Chen, "Cross-linked hyaluronic acid gel inhibits metastasis and growth of gastric and hepatic cancer cells: in vitro and in vivo studies.," *Oncotarget*, vol. 7, no. 40, pp. 65418–65428, 2016.

[269] J. V. Forrester and E. A. Balazs, "Inhibition of phagocytosis by high molecular weight hyaluronate," *J. Immunol.*, vol. 40, no. January, p. 435, 1980.

[270] D. Jiang, J. Liang, J. Fan, S. Yu, S. Chen, Y. Luo, G. D. Prestwich, M. M. Mascarenhas, H. G. Garg, D. A. Quinn, R. J. Homer, D. R. Goldstein, R. Bucala, P. J. Lee, R. Medzhitov, and P. W. Noble, "Regulation of lung injury and repair by Toll-like receptors and hyaluronan," *Nat. Med.*, vol. 11, no. 11, pp. 1173–1179, 2005.

[271] K. Nakamura, S. Yokohama, M. Yoneda, S. Okamoto, Y. Tamaki, T. Ito, M. Okada, K. Aso, and I. Makino, "High, but not low, molecular weight hyaluronan prevents T-cell-mediated liver injury by reducing proinflammatory cytokines in mice," *J. Gastroenterol.*, vol. 39, no. 4, pp. 346–354, 2004.

[272] L. Quero, M. Klawitter, A. Schmaus, M. Rothley, J. Sleeman, A. N. Tiaden, J. Klasen, N. Boos, M. O. Hottiger, K. Wuertz, and P. J. Richards, "Hyaluronic acid fragments enhance the inflammatory and catabolic response in human intervertebral disc cells through modulation of toll-like receptor 2 signalling pathways.," *Arthritis Res. Ther.*, vol. 15, no. 4, p. R94, Jan. 2013.

[273] K. E. Black, S. L. Collins, R. S. Hagan, M. J. Hamblin, Y. Chan-Li, R. W. Hallowell, J. D. Powell, and M. R. Horton, "Hyaluronan fragments induce

IFNβ via a novel TLR4-TRIF-TBK1-IRF3-dependent pathway.," *J. Inflamm. (Lond).*, vol. 10, no. 1, p. 23, Jan. 2013.

[274] P. L. Bollyky, B. A. Falk, R. P. Wu, J. H. Buckner, T. N. Wight, and G. T. Nepom, "Intact extracellular matrix and the maintenance of immune tolerance: high molecular weight hyaluronan promotes persistence of induced CD4+CD25+ regulatory T cells," *J. Leukoc. Biol.*, vol. 86, no. 3, pp. 567–572, 2009.

[275] P. L. Bollyky, R. P. Wu, B. A. Falk, J. D. Lord, S. A. Long, A. Preisinger, B. Teng, G. E. Holt, N. E. Standifer, K. R. Braun, C. F. Xie, P. L. Samuels, R. B. Vernon, J. A. Gebe, T. N. Wight, and G. T. Nepom, "ECM components guide IL-10 producing regulatory T-cell (TR1) induction from effector memory T-cell precursors," *Proc. Nati. Acad. Sci. U.S.A*, vol. 108, no. 19, pp. 7938–7943, 2011.

[276] K. L. Aya and R. Stern, "Hyaluronan in wound healing: Rediscovering a major player.," *Wound Repair Regen.*, vol. 22, no. 5, pp. 579–93, Sep. 2014.

[277] D. Foschi, L. Castoldi, E. Radaelli, P. Abelli, G. Calderini, A. Rastrelli, C. Mariscotti, M. Marazzi, and E. Trabucchi, "Hyaluronic acid prevents oxygen free-radical damage to granulation tissue: A study in rats," *Int J Tissue React*, vol. 12, no. 6, pp. 333–339, 1990.

[278] J. Barone, D. R. Yager, R. F. Diegelmann, and I. Kelman, "Hyaluronic acid inhibits fetal platelet function: Implications in scarless healing," *J. Pediatr. Surg.*, vol. 32, no. 7, pp. 1037–1040, 1997.

[279] J. A. Travis, M. G. Hughes, J. M. Wong, W. D. Wagner, and R. L. Geary, "Hyaluronan enhances contraction of collagen by smooth muscle cells and adventitial fibroblasts: Role of CD44 and implications for constrictive remodeling," *Circ. Res.*, vol. 88, no. 1, pp. 77–83, Jan. 2001.

[280] E. C. Collin, S. Grad, D. I. Zeugolis, C. S. Vinatier, J. R. Clouet, J. J. Guicheux, P. Weiss, M. Alini, and A. Pandit, "An injectable vehicle for nucleus pulposus cell-based therapy.," *Biomaterials*, vol. 32, no. 11, pp. 2862–70, Apr. 2011.

[281] G. Fontana, D. Thomas, E. Collin, and A. Pandit, "Microgel microenvironment primes adipose-derived stem cells towards an NP cells-like phenotype," *Adv. Healthc. Mater.*, vol. 3, no. 12, pp. 2012–2022, 2014.

[282] L. J. Nesti, W. J. J. Li, R. M. Shanti, Y. J. Jiang, W. Jackson, B. A. Freedman, T. R. Kuklo, J. R. Giuliani, and R. S. Tuan, "Intervertebral disc tissue engineering using a novel hyaluronic acid-nanofibrous scaffold (HANFS) amalgam.," *Tissue Eng Part A*, vol. 14, no. 9, pp. 1527–1537, 2008.

[283] A. Srivastava, I. L. M. Isa, P. Rooney, and A. Pandit, "Bioengineered three-dimensional diseased intervertebral disc model revealed inflammatory crosstalk," *Biomaterials*, vol. 123, pp. 127–141, 2017.

[284] S. Yang, P. Chen, Y. Chen, and F. Lin, "An *in-vitro* study on regeneration of human nucleus pulposus by using gelatin/chondroitin-6-sulfate /hyaluronan tri-copolymer scaffold," *Artif. Organs*, vol. 29, no. 10, pp. 806–814, 2005.

[285] C. G. Jeong, A. T. Francisco, Z. Niu, R. L. Mancino, S. L. Craig, and L. A. Setton, "Screening of hyaluronic acid-poly(ethylene glycol) composite hydrogels to support intervertebral disc cell biosynthesis using artificial neural network analysis," *Acta Biomater.*, vol. 10, no. 8, pp. 3421–3430, 2014.

[286] J. E. Frith, D. J. Menzies, A. R. Cameron, P. Ghosh, D. L. Whitehead, S. Gronthos, A. C. W. Zannettino, and J. J. Cooper-White, "Effects of bound versus soluble pentosan polysulphate in PEG/HA-based hydrogels tailored for intervertebral disc regeneration.," *Biomaterials*, vol. 35, no. 4, pp. 1150–62, Jan. 2014.

[287] K. Haberstroh, A. Enz, M. L. Zenclussen, A. A. Hegewald, K. Neumann, A. Abbushi, C. Thomé, M. Sittinger, M. Endres, and C. Kaps, "Human intervertebral disc-derived cells are recruited by human serum and form nucleus pulposus-like tissue upon stimulation with TGF-β3 or hyaluronan in vitro," *Tissue Cell*, vol. 41, no. 6, pp. 414–420, 2009.

[288] Z. Li, G. Lang, L. S. Karfeld-Sulzer, K. T. Mader, R. G. Richards, F. E. Weber, C. Sammon, H. Sacks, A. Yayon, M. Alini, and S. Grad, "Heterodimeric BMP-2/7 for nucleus pulposus regeneration - *in vitro* and *ex vivo* studies," *J. Orthop. Res.*, pp. 1–10, 2016.

[289] D. O. Halloran, S. Grad, M. Stoddart, P. Dockery, M. Alini, and A. Pandit, "An injectable cross-linked scaffold for nucleus pulposus regeneration.," *Biomaterials*, vol. 29, no. 4, pp. 438–47, Mar. 2008.

[290] C. Yu-Chun, S. We-Yu, Y. Shu-Hua, G. Amit, and L. Feng-Huei, "In situ forming hydrogels composed of oxidized high molecular weight hyaluronic acid and gelatin for nucleus pulposus regeneration.," *Acta Biomater.*, vol. 9, no. 2, pp. 5181–93, Mar. 2013.

[291] L. Calderon, E. Collin, D. Velasco-Bayon, M. Murphy, D. O'Halloran, and A. Pandit, "Type II collagen-hyaluronan hydrogel - A step towards a scaffold for intervertebral disc tissue engineering," *Eur. Cells Mater.*, vol. 20, pp. 134–148, 2010.

[292] B. Huang, Y. Zhuang, C.-Q. Li, L. T. Liu, and Y. Zhou, "Regeneration of the intervertebral disc with nucleus pulposus cell-seeded collagen II/hyaluronan/chondroitin-6-sulfate tri-copolymer constructs in a rabbit disc degeneration model," *Spine (Phila. Pa. 1976).*, vol. 36, no. 26, pp. 2252–2259, 2011.

[293] P. A. Revell, E. Damien, L. Di Silvio, N. Gurav, C. Longinotti, and L. Ambrosio, "Tissue engineered intervertebral disc repair in the pig using injectable polymers," *J. Mater. Sci. Mater. Med.*, vol. 18, no. 2, pp. 303–308, 2007.

[294] M. Endres, M. L. Zenclussen, P. A. Casalis, U. Freymann, S. Gil Garcia, J. P. Krueger, U. W. Thomale, C. Woiciechowsky, and C. Kaps, "Augmentation and repair tissue formation of the nucleus pulposus after partial nucleotomy in a rabbit model," *Tissue Cell*, vol. 46, no. 6, pp. 505–513, 2014.

[295] I. L. M. Isa, A. Srivastava, D. Tiernan, P. Owens, P. Rooney, P. Dockery, and A. Pandit, "Hyaluronic acid based hydrogels attenuate inflammatory receptors and neurotrophins in interleukin-1β induced inflammation model of nucleus pulposus cells," *Biomacromolecules*, vol. 16, no. 6, pp. 1714–1725, 2015.

[296] Z. Kazezian, Z. Li, M. Alini, S. Grad, and A. Pandit, "Injectable hyaluronic acid down-regulates interferon signaling molecules , IGFBP3 and IFIT3 in the bovine intervertebral disc," *Acta Biomater.*, 2017.

[297] NCT01290367, "Safety and preliminary efficacy study of mesenchymal precursor cells (MPCs) in subjects with lumbar back pain," 2017.

[298] J. B. Massie, A. L. Schimizzi, B. Huang, C. W. Kim, S. R. Garfin, and W. H. Akeson, "Topical high molecular weight hyaluronan reduces radicular pain post laminectomy in a rat model," *Spine J.*, vol. 5, no. 5, pp. 494–502, 2005.

[299] A. Wei, B. Shen, L. Williams, and A. Diwan, "Mesenchymal stem cells: Potential application in intervertebral disc regeneration.," *Transl. Pediatr.*, vol. 3, no. 2, pp. 71–90, 2014.

[300] H. Yong-Can, L. Victor Y. L., L. William W., and L. Keith D. K., "The effects of microenvironment in mesenchymal stem cell-based regeneration of intervertebral disc.," *Spine J.*, vol. 13, no. 3, pp. 352–62, Mar. 2013.

[301] F. Yang, V. Y. Leung, K. D. Luk, D. Chan, and K. M. Cheung, "Mesenchymal stem cells arrest intervertebral disc degeneration through chondrocytic differentiation and stimulation of endogenous cells," *Mol. Ther.*, vol. 17, no. 11, pp. 1959–1966, 2009.

[302] S. Sobajima, G. Vadala, A. Shimer, J. S. Kim, L. G. Gilbertson, and J. D. Kang, "Feasibility of a stem cell therapy for intervertebral disc degeneration.," *Spine J.*, vol. 8, no. 6, pp. 888–896, 2008.

[303] NCT01643681, "Autologous adipose tissue derived mesenchymal stem cells transplantation in patient with lumbar intervertebral disc degeneration.," 2014.

[304] C. Kristin, S. Robert, and P. Michelle, "Effects of the intradiscal implantation of stromal vascular fraction plus platelet rich plasma in patients with degenerative disc disease," *J. Transl. Med.*, vol. 15, no. 1, p. 12, 2017.

[305] D. Coric, K. Pettine, A. Sumich, and M. O. Boltes, "Prospective study of disc repair with allogeneic chondrocytes presented at the 2012 Joint Spine Section Meeting.," *J. Neurosurg. Spine*, vol. 18, no. 1, pp. 85–95, 2013.

Chapter 2

Development of Hyaluronic Acid Hydrogel in an Inflammation Nucleus Pulposus Cell Model

Sections of this chapter have been published:

Isa I. L. M., Srivastava A., Tiernan D., Owens P., Rooney P., Dockery P., and Pandit A. Hyaluronic Acid Based Hydrogels Attenuate Inflammatory Receptors and Neurotrophins in Interleukin-1β Induced Inflammation Model of Nucleus Pulposus Cells. *Biomacromolecules*. 2015, 16, 1714−1725.

2.1 Introduction

The inflammatory process determines the severity and pain development in IVD degeneration [1-2]. Interleukin (IL)-1 is one of the most prominent pro-inflammatory cytokine expressed in IVD [1][3-4] and controls the inflammatory processes by activating receptor IL-1R1 and IL-1R antagonist [4]. The study, by Le Maitre *et al.* demonstrated that IL-1β and its receptor, IL-1R1, are increased by severity of degeneration in human disc samples [5]. These pro-inflammatory cytokines also correlate with the presence of neurotrophins or pain-related molecules and hyper-innervation in the IVD [6]. A recent study illustrated that IL-1β induces mRNA expression of neurotrophins' nerve growth factor (NGF) and brain-derived neurotrophic factor (BDNF) in NP cells extracted from degenerated human IVD. Hence, both NGF and BDNF indicate correlation with innervations via staining for an axonal growth marker such as protein gene product (PGP) 9.5 and growth-associated protein 43 (GAP43) [7-9]. Therefore, these inflammatory and neurotrophic factors are considered pathologic pathways of discogenic pain.

The neurotrophins NGF and BDNF are neuronal survival and growth factors that support neuronal development, function, nociception and have been shown to induce nerve ingrowth into the IVD [10]. A large number of non-myelinated sensory nerve fibres have been reported in the normal avascular and aneural IVD tissue, which is deeply projected into inner third AF and NP region in a painful degenerated human IVD [11]. Studies demonstrate that NGF stimulates nerve ingrowth into the disc from the painful degenerated human disc [12] by promoting collateral sprouting of nociceptive nerve fibres [13] and modulating its function so as to generate pain [14]. Thus, neurons innervating the IVD are NGF sensitive and show higher distribution of neurotransmitter calcitonin gene-related peptide (CGRP) in the dorsal root ganglion (DRG) neurons [9]. The nociceptive DRG neurons are categorized as NGF-sensitive neurons that conduct the pain information from peripheral region to the brain [15]. Similar to NGF, Gruber *et al.* showed that BDNF was expressed in culture in degenerated human and rat disc samples, also triggers innervation and correlates with the severity of disc degeneration [16]. BDNF regulates differentiation and survival of sensory neuron, and inflammatory pain hypersensitivity [17-19]. As a pain modulator, BDNF exerts fast excitatory (glutamatergic) and inhibitory (GABAergic/glycinergic) signals, and in contrast slows the peptidergic

neurotransmission in spinal cord. Therefore, BDNF plays a role in the synaptic junction in pain pathways in the central nervous system [20].

Hence, there is a compelling need to develop a therapy for painful IVD degeneration since the current treatment options, relieve the pain symptoms but do not treat the underlying degeneration and do not restore the native function of IVD. A tissue engineering approach targeting the multiple disrupted pathways underlying the cause of the disease is potentially a therapeutic strategy. A study from Andre *et al.* demonstrate a reduction of hyperalgesia in an inflammatory pain NP model of rat after treatment with antibodies specific to IL-1β and TNF-α [21]. Apart from that, the use of stem cells such as mesenchymal stem cells (MSCs) and adipose-derived stem cells (ADSC) were also shown promising results in IVD regeneration [22]. The injectable crosslinked polyethylene glycol (PEG) and hyaluronic acid (HA) hydrogel incorporating mesenchymal precursor cells (MPCs) maintained cell viability and formed a chondrocyte-like tissue in IVD degeneration [23]. In a recent study, human MSCs embedded in atelocollagen increased the disc height, preserved the NP tissue and restored the proteoglycan content in an *in vivo* model of IVD degeneration [24]. Previous work in the Pandit laboratory has also demonstrated that NP cells seeded in crosslinked PEG and collagen type II enriched with HA had maintained the NP cell viability and up-regulated mRNA of type II collagen for matrix synthesis [25]. In addition, ADSC encapsulated three dimensional (3D) type II collagen/HA microgels enhanced ECM production and mimicked the NP-like phenotype [26]. In this study, it has been proposed to investigate the therapeutic effect of acellular crosslinked PEG HA hydrogels in an inflammation milieu.

HA is a type of non-sulphated GAG composed of repeating units of glucuronic acid and N-acetyl-D-glucosamine connected through β-linkages [27]. At cellular level, HA is synthesized in plasma membrane by HA synthases (HAS) [28] and is transported out from cells to pericellular space through a multidrug resistant transporter [29]. In NP tissue, HA is the backbone of proteoglycan aggregate that hold aggrecan molecules which are attached with highly anionic sulphated GAG [30]. The use of high molecular weight (HMW) HA ($>1.0 \times 10^6$ Da) in osteoarthritis patients has been demonstrated to result in long-term functional improvement by reducing inflammation and pain [31]. HA also promotes tissue repair by stimulating matrix synthesis of collagen type II in NP cells and chondrocytes [25][32]

modulating cellular function such as migration of aortic smooth muscle cells [33] and maintaining NP cells' phenotype [25][34]. However, the mechanism of HA in modulating cellular functions in disease systems remains unclear. The binding of the cell surface receptor of CD44 with HA has been implicated in cellular signaling and subsequently in regulating multiple cellular functions [35]. It has been previously shown that chondrocytes adhere to HA through binding to CD44 and thus induce cell proliferation and matrix synthesis [36]. Furthermore, the HA network in normal ECM promotes clustering of the CD44 receptor to protect cells in response to the inflammation [37]. Nevertheless, none have been reported in NP tissue so far. The binding of CD44 and HA may play a key role in the mechanism of HA either in normal or in pathologic condition.

This biomaterial approach is based on supplementing inflamed NP cells with optimally crosslinked HMW HA hydrogels. Therefore, it was hypothesized that crosslinked HMW HA hydrogels alter the inflammatory receptor and neurotrophins expression in an IL-1β induced inflammation model of NP cells. To test this hypothesis specifically, a crosslinked HMW HA hydrogel system was developed by optimising the crosslinking system using various concentration of crosslinker and characterising the optimally crosslinked HA hydrogels in a study of *in vitro* degradation and cytotoxicity. The therapeutic effect of crosslinked HMW HA hydrogels in inflamed NP cells was investigated by evaluating expression of inflammatory receptors of IL-1R1 and MyD88, neurotrophins' mRNA expression of NGF and BDNF, and the mechanism of action of HA through expression of cell surface receptor of CD44.

2.2 Materials and Methods

2.2.1 Material and Reagents

HMW sodium hyaluronate (MW 1.19×10^6 Da) was purchased from Lifecore Biomedical, USA. 4-arm PEG-amine MW 2000 Da was purchased from JenKem Technology, USA Teflon™ tape was purchased from Fisher Scientific, Ireland. Live/Dead® staining kit, alamarBlue® assay, Alexa Fluor® 488, Alexa Fluor® 564 and rhodamine phalloidin were purchased from Life Technologies, Ireland. Human recombinant IL-1β cytokine was purchased from PeproTech, USA. Anti-IL-1R1 antibody was purchased from Novus Biologicals, USA. Anti-MyD88 antibody and

anti-CD44 antibody conjugated FITC were purchased from Abcam, UK. miRNeasy mini kit was purchased from Qiagen (Germany). TNBSA (2,4,6-trinitrobenzene sulfonic acid) was purchased from Thermo Scientific, USA. All other materials and reagents were purchased from Sigma Aldrich (Ireland) unless otherwise stated.

2.2.2 Synthesis of Crosslinked HA Hydrogels

Sodium hyaluronate 0.75% (w/v) was dissolved in 1 mL distilled water and then mixed with various final concentrations of 4-arm PEG-amine at 25 mM, 50 mM, 75 mM, 100 mM and 50 mM 0.625% glutaraldehyde (GTA). After complete mixing, N-hydroxysuccinimide (NHS) 15% (w/v) and 1-ethyl-3-(3-dimethylaminopropyl)carbodiimide (EDC) 9% (w/v) were added to initiate the crosslinking (Figure 2.a). Consistent with the previous method of hydrogel preparation [26], spherical-shaped hydrogels were then obtained through pipetting a channel volume of 5 µl onto a hydrophobically modified glass slide prepared by layering Teflon™ tape. The spherical-shaped droplets of the reaction mixture were then incubated for one hour at 37°C to allow complete crosslinking (Figure 2.1b). After complete fabrication, the HA hydrogels were washed in PBS overnight to remove the un-reactant and then dried and stored at 4°C for further analyses. After complete fabrication, the HA hydrogels were washed in PBS overnight to remove the un-reactant and then dried and stored at 4°C for further analyses.

2.2.3 Optimisation of the Cross-Linking System

The synthesis of crosslinked HA hydrogels was optimised using different concentrations of 4-arm PEG-amine at 25 mM, 50 mM, 75 mM, 100 mM and 50 mM 0.625% GTA, by estimation of free carboxyl groups of HA, quantification of unreacted amine group of PEG and HA hydrogel morphology by scanning electron microscope.

The residual un-crosslinked carboxyl groups of HA was measured by fourier transformed infrared spectroscopy (FTIR). Each hydrogel prepared at different ratios of PEG/HA was dried under vacuum and then studied by FTIR spectrometer (Varian 660-IR, Agilent Technology, Ireland) against a blank KBr pellet background.

A 2,4,6-trinitrobenzene sulfonic acid (TNBSA) assay (Thermo Scientific, USA) was performed to determine the amount of unreacted amine groups of PEG during the coupling reaction. Briefly, 1 mg hydrogel was dissolved in 1 mL reaction

buffer of 0.1 M sodium bicarbonate, pH 8.5. Each 200 µL sample was mixed with 100 µL 0.01% TNBSA and then incubated at 37°C for 2 hours. 100 µL 10% solution of SDS and 50 µL 1 N HCl was added for every 100 µL sample. Samples were run in triplicate and the amount of free amine groups in the hydrogel was determined by measuring the UV absorbance (Varioskan Flash, Thermofisher Scientific, Finland) of the supernatant at 335 nm and compared to a standard curve produced using glycine as a reference.

The surface morphology of crosslinked HA hydrogels at different concentrations of PEG was imaged by scanning electron microscopy (SEM). The hydrogels were dehydrated in a series of increasing ethanol concentrations in water and then freeze-dried. Dried samples were gold-coated before being analysed by Hitachi S-4700 SEM operated at 10 kV accelerating voltage.

2.2.4 *In Vitro* Degradation

The optimally crosslinked HA hydrogel was obtained using 75 mM PEG-amine and stability was determined by hydrolytic and enzymatic degradation. Pre-weighed (W_1) HA hydrogels were incubated in PBS and hyaluronidase (5 U/mL) respectively at 37°C using a water bath. The degradation medium was replenished with either PBS or a freshly prepared enzyme solution every two days. The hydrogels were recovered after 1, 3, 7, 14 and 28 days and dried under vacuum. The dry weight of HA gels (W_2) at each time point was measured and the weight-percentage of remaining hydrogels (wt%) was calculated using:

$$\text{wt\%} = \frac{W_1 - W_2 \times 100\%}{W_1}$$

2.2.5 NP Cell Isolation

The discs from T9-S1 spine were isolated from freshly obtained five-month-old bovine tails that were collected directly after sacrifice from a local slaughterhouse. Soft tissues surrounding the disc (muscles, tendons and ligaments) were manually dissected. The discs were cut into mid-sagittal and coronal sections (4 mm wide) using custom dissection tools. The NP tissues were harvested from each section. Tissues were washed twice with Hanks' Balanced Salt Solution (HBSS) and once using blank high glucose (HG) Dulbecco's modified Eagle's medium (DMEM). NP tissues were digested with 0.19% pronase prepared in HGDMEM media for

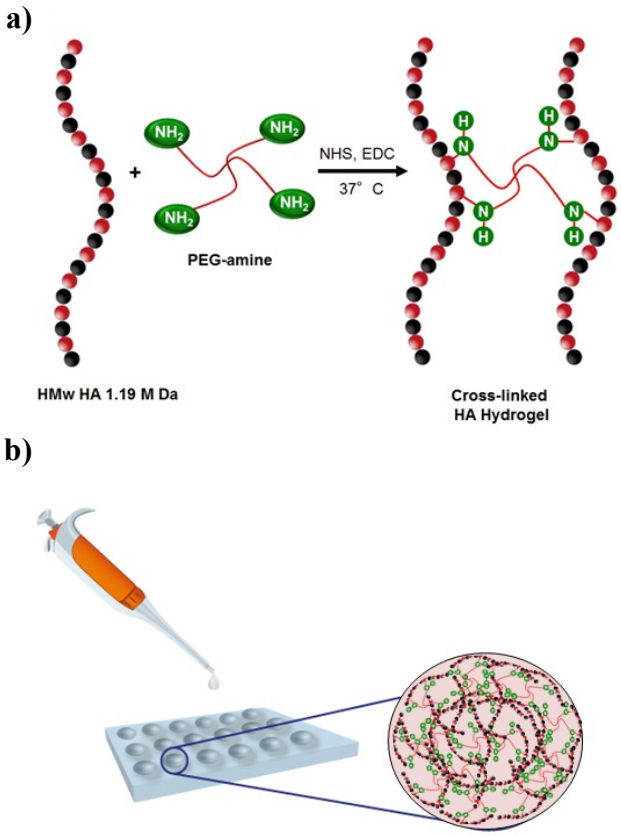

Figure 2.1 Schematic representation of crosslinked HA hydrogel system. (a) Crosslinking of high molecular weight hyaluronic acid and 4-arm PEG-amine. The succinimidyl groups of PEG-amine react with the amine groups on the HA molecules after carboxyl groups are functionalized with EDC and NHS. (b) 3D spherical shaped hydrogel preparation. 5 µL of mixed hydrogel solution containing HA, PEG-amine, EDC and NHS was dropped onto hydrophobic modified surface through pipette channel and incubated at 37°C for one hour to allow crosslinking reaction to complete.

one hour under agitation at 37°C in a humidified atmosphere of 5% CO_2 and were then centrifuged for five minutes at 1200 rpm. The pellets were washed three times with complete medium to inhibit pronase activity and then were resuspended in 0.025% collagenase type IV (327I U/mL) prepared in complete media. The mixture was incubated under agitation overnight at 37°C in a humidified atmosphere of 5% CO_2. The suspensions were filtered through a 70 μm cell strainer and centrifuged for eight minutes at 1200 rpm. Pellets were washed once, resuspended with complete media and grown in tissue culture flask for ten days until confluent. The cells were then passaged for subsequent experiments.

2.2.6 Viability of NP Cells

The cytotoxicity of crosslinked hydrogels at different concentrations of HA 0.75 mg (in 100 μL) and 1.5 mg (in 200 μL) was investigated on NP cells *in vitro*. Briefly, the 5×10^3 cells were seeded on four well chambers and allowed to grow for 1, 3 and 7 days in the presence of crosslinked hydrogels at 37°C in a humidified atmosphere of 5% CO_2. The NP cell morphology was observed using Live/Dead® staining kit, after which cell viability was determined using alamarBlue® assay.

2.2.7 *In vitro* Inflammation Model of NP cells

NP cells (1×10^4) were seeded on a modified glass surface 24 well cell culture plate prepared by putting 13 mm sterile glass cover slips onto cell culture well. The cells were grown in complete medium containing DMEM, 10% fetal bovine serum (FBS) and 1% penicillin/streptomycin (P/S) at 37°C in a humidified atmosphere of 5% CO_2. After one day in culture, the cells were stimulated with IL-1β (10 ng/mL) prepared in complete medium to create an inflammatory milieu to mimic the disease environment of the IVD degeneration. Subsequently, after 24 h cytokine stimulation, cells were treated with HA hydrogels for three and seven days. The concentration of HA to use in the inflammation study was finalized at 0.75 mg in 100 μL (5 μL × 20 hydrogels) based on NP viability results.

2.2.8 Analysis of Immunoreactivity of IL-1R1, MyD88 and CD44

The protein expression of immunoreactive inflammatory receptors was determined by immunofluorescence staining in inflamed NP cells after a three-day treatment with non-crosslinked HA and crosslinked HA hydrogels. Briefly, normal and

inflamed NP cells were incubated with non-crosslinked HA and crosslinked HA hydrogel (0.75 mg in 100 µL) in DMEM media supplemented with 10% FBS and 1% P/S. After three days' incubation, the modified cell culture plates were transferred from incubator to room temperature. The cells were washed three times with phosphate buffered saline (PBS) 1M for five minutes and then fixed with 3.7% paraformaldehyde (PFA) for fifteen minutes. After complete washing with PBS 1M three times for five minutes each, antigen retrieval was performed using Triton 0.1% for five minutes to permeate the cell membrane. Cells were then washed with PBS 1M three times for five minutes and incubated overnight at 4°C with primary rabbit anti-IL1R1 antibody (1:200) and rabbit anti-MyD88 antibody (1:200). After washing with PBS 1M three times for five minutes each, cells were incubated with Alexa Fluor® 488 and Alexa Fluor® 564 secondary anti-rabbit antibodies respectively at room temperature for one hour. For CD44 antibody staining, cells were incubated overnight at 4°C with anti-CD44 antibody conjugated with FITC (1:100) and the cells were incubated at room temperature for one hour with rhodamine phalloidin (1:200) after washing with PBS 1M three times. The cells were washed with PBS 1M three times and the cover slips with cells were carefully removed onto glass slides containing anti-fade mounting medium with 4,6-diamidino-2-phenylindole (DAPI). The slides were protected from light overnight at 4°C and staining for IL-1R1 and MyD88 was observed using a laser confocal microscope (Olympus Fluoview 1000). The mean fluorescence intensity of detectable receptors from three areas of each slide was further analysed using software imageJ version 1.48 (National Institutes of Health, USA). This experiment was carried out in triplicate.

2.2.9 Neurotrophins mRNA Expression

Normal and inflamed NP cells were incubated with non-crosslinked HA and crosslinked HA hydrogels (0.75 mg in 100 µL) in DMEM media supplemented with 10% FBS and 1% P/S. After a seven-day treatment with HA hydrogels, total RNA was extracted from NP cells in monolayer culture using Trizol® reagent (Invitrogen) and miRNeasy mini kit following the manufacturer's protocol. Total RNA of 100 ng/µL was reverse-transcribed with random primer (Promega) and subsequently with reverse transcriptase (Promega) in a 20 µL reaction mixture using PTC DNA Engine™ System (PTC-200, Peltier Thermal Cycler, MJ Research Inc., USA). The cDNA products were amplified using SYBR green PCR Master Mix (Promega) and

following specific primers (Table 2.). Reactions were conducted in triplicate using StepOnePlus™ Real-Time PCR System (Applied Biosystems®). The results were analysed using the $2^{-\Delta\Delta Ct}$ method and presented as fold change (relative gene expression) normalized to 18S and basal control.

2.3 Statistical Analysis

Statistical analysis was performed using software GraphPad Prism version 5.00. Data were compared by a one-way analysis of variance (ANOVA) and multiple pairwise comparisons were carried out using the Bonferroni post-hoc t-test. Statistical significance was set at $p < 0.05$.

2.4 Results

2.4.1 Optimisation of Cross-Linked HA Hydrogel

The carboxyl (C=O) stretch of un-crosslinked carboxyl groups of HA after the crosslinking reaction with 4-arm PEG-amine (Figure 2.2a) was observed at a peak of 1720 nm. A decrease in absorbance of carboxyl groups at 1720 nm was observed for all the concentrations of 4-arm PEG-amine used for the optimisation of HA hydrogel crosslinking. Un-crosslinked residual amine groups in HA hydrogel were estimated by TNBSA have shown significant decrease in amine group concentration. A plateau was reached after 75 mM of 4-arm PEG-amine (Figure 2.2b); demonstrating maximum crosslinking was achieved at that 4-arm PEG-amine concentration. Furthermore, the surface images of the HA hydrogels presented in Figure 2.3 with a micro-pits structure were observed in SEM images, when using low concentration PEG-amine. The use of high concentration PEG-amine, however, resulted in the formation of a smooth surface structure.

2.4.2 Hydrolytic and Enzymatic Degradability

The optimally crosslinked HA hydrogel was determined to be stable in *in vitro* degradation. Hydrogels incubated in PBS showed significant decrease in weight up to 30% after one day and were stable thereafter with no significant difference. Alternatively, hydrogels were degraded more in the presence of hyaluronidase at 44.07% ± 2.14%, 42.36% ± 2.58%, 40.89% ± 1.79%, 43.40% ± 0.28%, and 44.67% ± 0.73% after 1, 3, 7, 14 and 28 days' incubation respectively. The degradation of

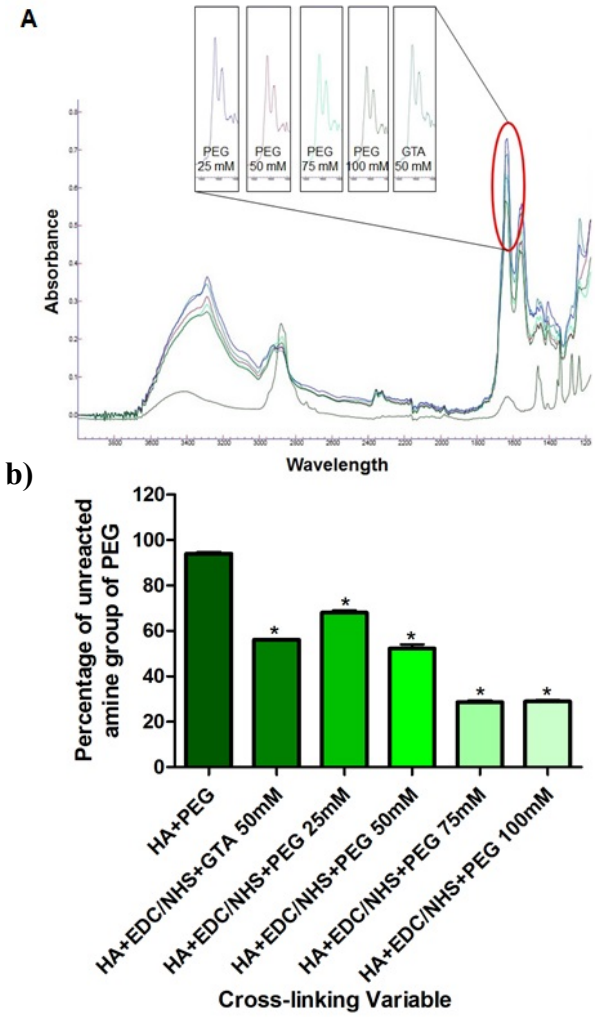

Figure 2.2 Optimisation of crosslinking system using different concentrations 4-arm PEG-amine of 25, 50, 75 and 100 mM. GTA was used as a control. (a) Determination of un-crosslinked carboxyl groups of HA after crosslinking reaction at a peak of 1720 nm, corresponding to the C=O stretch from the acid group. A decreasing pattern of peak in carboxyl groups as the PEG concentration increased. (b) Quantification of residual unreacted amine groups of PEG after crosslinkage. Free amine group was decreased with increasing of PEG concentration. *Significant statistical different for different concentrations of PEG-amine. (n = 3, one-way ANOVA, $p < 0.05$). Data presented as the mean ± standard error of the mean.

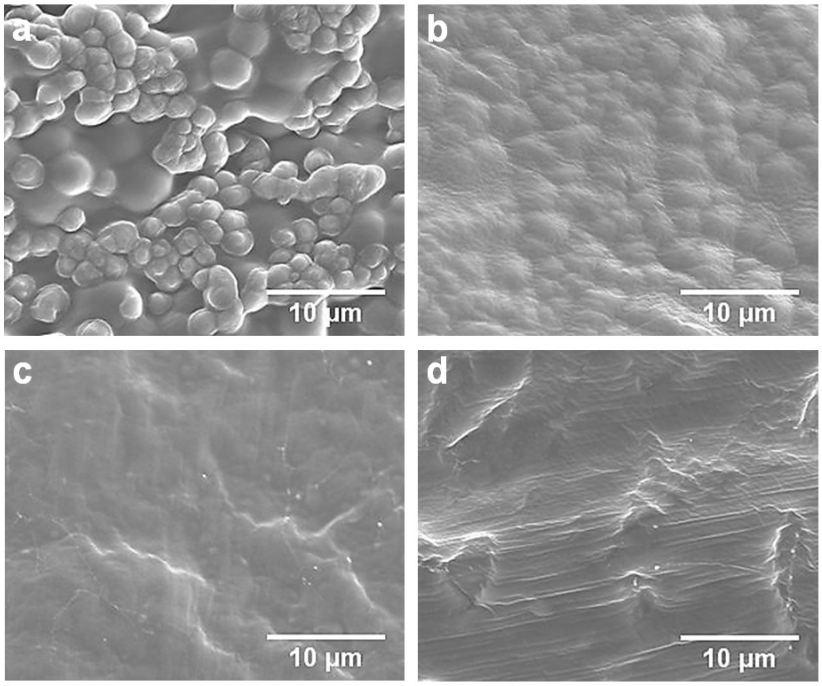

a. HA+EDC/NHS+PEG 25 mM b. HA+EDC/NHS+ PEG 50 mM
c. HA+EDC/NHS+PEG 75 mM d. HA+EDC/NHS+ PEG 100 mM

Figure 2.3 Physical properties of hydrogels at different concentrations 4-arm PEG-amine: 25, 50, 75 and 100 mM. GTA was used as a control. Surface morphology of the crosslinked HA hydrogels was presented as a micro-pits structure to a smooth surface layer at lower to higher concentrations of PEG-amine.

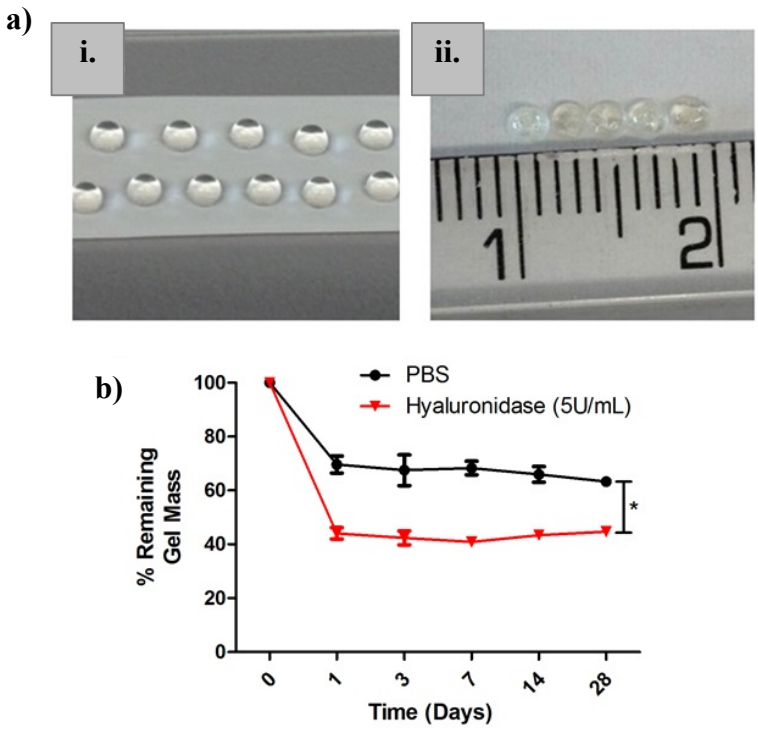

Figure 2.4 Characterisation of optimal 75 mM 4-arm PEG HA hydrogels. (a) Spherical-shaped hydrogels were obtained on modified hydrophobic surface using Teflon tape at room temperature (i) and the hydrogels maintained a 3D spherical shape after complete crosslinking at 37°C (ii). (b) Over 70% and 40% remaining gel mass of hydrogels in PBS and hyaluronidase over 28 days respectively *Significant differences were noted between the different groups (n = 3, one-way ANOVA, p < 0.05). Data presented as the mean ± standard error of the mean.

hydrogels was significantly different when treated with hyaluronidase respectively (Figure 2.4b).

2.4.3 NP Cell Morphology and Viability

Microscopically, the individual cells and clusters of cells with round morphology were observed in basal control of NP cells after three days in normal culture (Figure 2.5a). In hydrogel treatment at different doses of HA, NP cells maintained a chondrocyte-like rounded shape, and some of the cells showed short cytoplasmic extensions in normal culture (Figure 2.5a).

In the presence of crosslinked hydrogels containing HA dose (0.75 mg in 100 μL), NP cells demonstrated 94.16% ± 4.56% (day one), 89.79 ± 4.42% (3 day), 88.77 ± 7.44% (day seven) viability, while doubling the HA dose (1.5 mg in 200 μL) showed 80.51% ± 2.58% (day one), 74.08 ± 4.22% (3 day), 79.87 ± 3.64% (day seven) in normal monolayer culture respectively (Figure 2.5b).

2.4.4 Suppression of Inflammatory Receptor

Examination of IL1R1 and MyD88 protein expression in basal condition and IL-1β induced inflammation on NP cells with or without a HA hydrogels dose of 0.75 mg (in 100 μL) was performed by assessing immunofluorescence staining, illustrated in Figure 2.6a. It confirms immunoreactivity to IL1R1 and MyD88 as shown by green fluorescence corresponding to IL1R1, co-localized with red fluorescence corresponding to MyD88. Immunoreactive IL1R1 and MyD88 were detectable throughout basal and inflamed NP cells, but were more prominent in inflamed NP cells. Both IL1R1 and MyD88 appeared to be less intense in NP cells treated with crosslinked HA hydrogels than in non-crosslinked HA treatment and IL-1β control groups. The mean values with standard error of the mean (±S.E.M) fluorescence intensity of detectable immunoreactive IL-1R1 and MyD88 were further analysed to quantify the magnitude of protein expression. Figure 2.6b demonstrates that fluorescence intensity of IL-1R1 decreased significantly in NP cells with crosslinked hydrogels treatment. A consistent result was particularly noted for MyD88 expression, in which fluorescence intensity was significantly reduced in NP cells after crosslinked and non-crosslinked HA hydrogels treatment (Figure 2.6c).

Table 2.1 Primers utilised in qRT-PCR analysis.

Gene	Primer sequence		Base pair
	Forward	Reverse	
NGF	5′ AAG GGC AAG GAG GTG ATG 3′	5′ CTT GAC GAA GGT GTG GGT 3′	18
BDNF	5′ TAT TGG CTG GCG GTT CAT AC 3′	5′ TCC CTT CTG GTC ATG GAA ATG 3′	20
18S	5′ TCA ACA CGG GAA ACC TCA C 3′	5′ CGC TCC ACC AAC TAA GAA C 3′	19

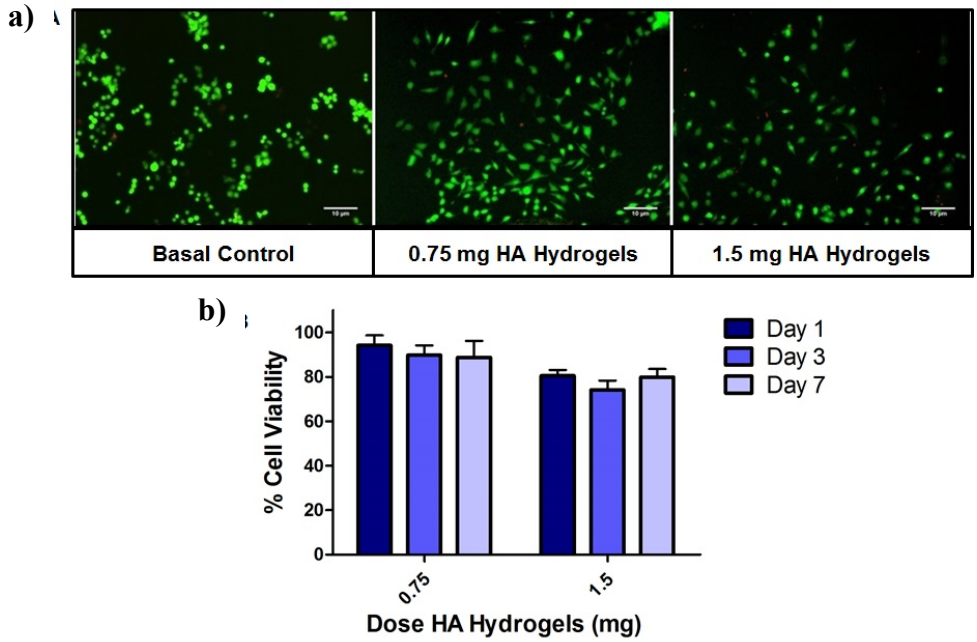

Figure 2.5 Viability study of NP cells after treatment of optimally crosslinked HA hydrogels. (a) NP cell morphology in the presence of hydrogels containing different doses of HA stained by Live/Dead® assay after 3 days in culture. Viable cells appear in green (calcein staining) and dead cells in red (ethidium bromide staining). (b) NP cells showed over 88% and 74% cell viability in the treatment of 0.75 mg (in 100 µL) and 1.5 mg (in 200 µL) crosslinked HA hydrogels respectively as measured by alamarBlue® assay. There was no significant difference between the groups (n = 3, one-way ANOVA, $p < 0.05$). Data presented as the mean ± standard error of the mean.

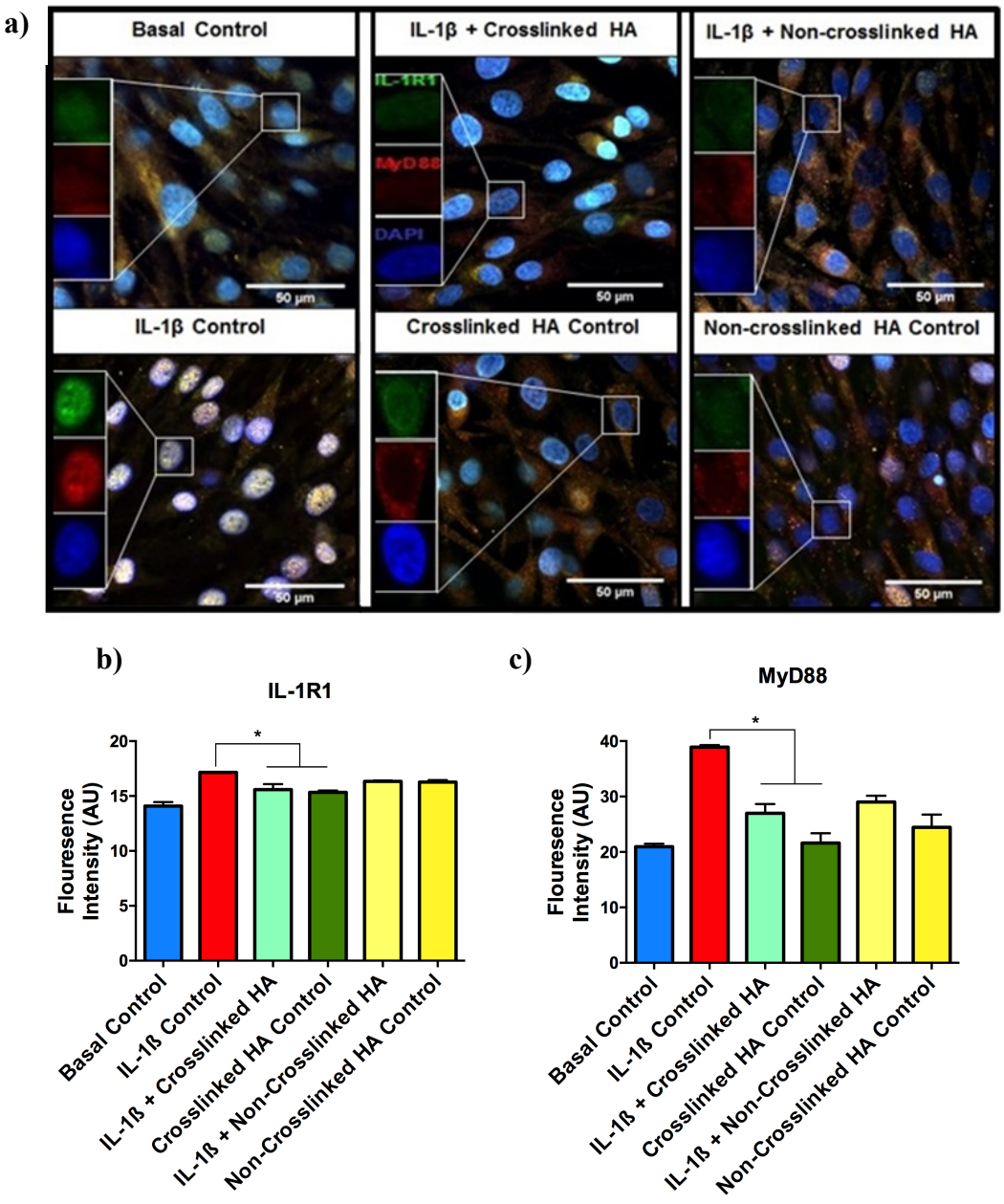

Figure 2.6 Expression of IL-1R1 and MyD88 in NP cells after HMw HA treatment. (a) Confocal micrograph showing IL-1R1 (green) co-localized with MyD88 (red) in IL-1β induced inflammation and normal NP cells in the treatment of 0.75 mg (in 100 µL) crosslinked and non-crosslinked HA after 3 days in culture. (b) Mean fluorescence intensity showing IL-1R1 receptor was significantly suppressed in the treatment of crosslinked HA hydrogels compared to IL-1β control group. (c) Mean fluorescence intensity of MyD88 significantly decreased after being treated with HA compared to IL-1β control group. *Significant differences were noted between the different groups (n = 3, one-way ANOVA, $p < 0.05$). Data presented as the mean ± standard error of the mean.

2.4.5 Down-regulation of Neurotrophins

The expression of NGF and BDNF at the mRNA level in basal condition or inflamed NP cells after treating with or without non-crosslinked HA and crosslinked HA hydrogels was performed by qRT-PCR using cDNA extracted from cell monolayer cultures. Figure 2.7a-b indicates that NGF mRNA was constitutively expressed in basal NP cells and highly up-regulated after being induced by IL-1β (10 ng/mL). However, NGF mRNA expression was down-regulated in all HA treatments and was significantly down-regulated in crosslinked HA hydrogels treatment groups. A pattern similar to BDNF mRNA expression shown in Figure 2.7b was expressed in basal NP cells. This confirmed that IL-1β up-regulated BDNF mRNA expression in NP cells. Nonetheless, the expression was significantly down-regulated in NP cells after treatment with crosslinked HA hydrogels.

2.4.6 Mechanism of Action of HA

This is the first study to examine expression of CD44 receptor of NP cell after HA treatment by investigating specific binding of antibody to antigen cell surface receptor CD44 in the basal condition and inflamed NP cells. This was carried out by immunofluorescence staining of the receptors. Figure 2.8a represents immunoreactive FITC labelled CD44 co-localized with rhodamine phalloidin (for cellular cytoskeleton). CD44 protein was expressed in basal NP cells and was most intense after treatment with crosslinked HA hydrogels. These results suggest that crosslinked HA bind to NP cells through CD44 (shown with a black arrow). To further analyse the strength of protein expression, the mean value with SEM (standard error mean) of fluorescence intensity of expressed immunoreactive CD44 was quantified for each group of HA treatment. Figure 2.8b shows a fluorescence intensity of CD44 at almost the same level as that in basal control, IL-1β control and NP cells treated with non-crosslinked HA. However, this intensity was significantly increased in NP cells after treatment with crosslinked HA hydrogels.

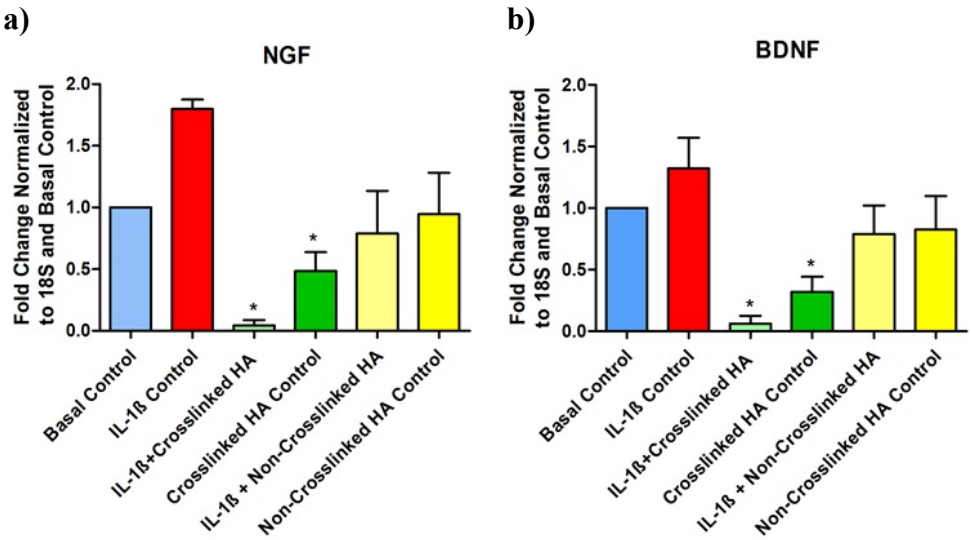

Figure 2.7 Effect of HMW HA treatment on neurotrophin mRNA expression of NP cells normalized to 18S and basal control. Histograms illustrating the fold change of (a) nerve growth factor and (b) brain derived neurotrophic factor down-regulated in IL-1β induced inflammation and normal NP cells in the treatment of crosslinked HA hydrogels after day 7. *Significant differences were noted between the different groups (n = 3, one-way ANOVA, $p < 0.05$). Data presented as the mean ± standard error of the mean.

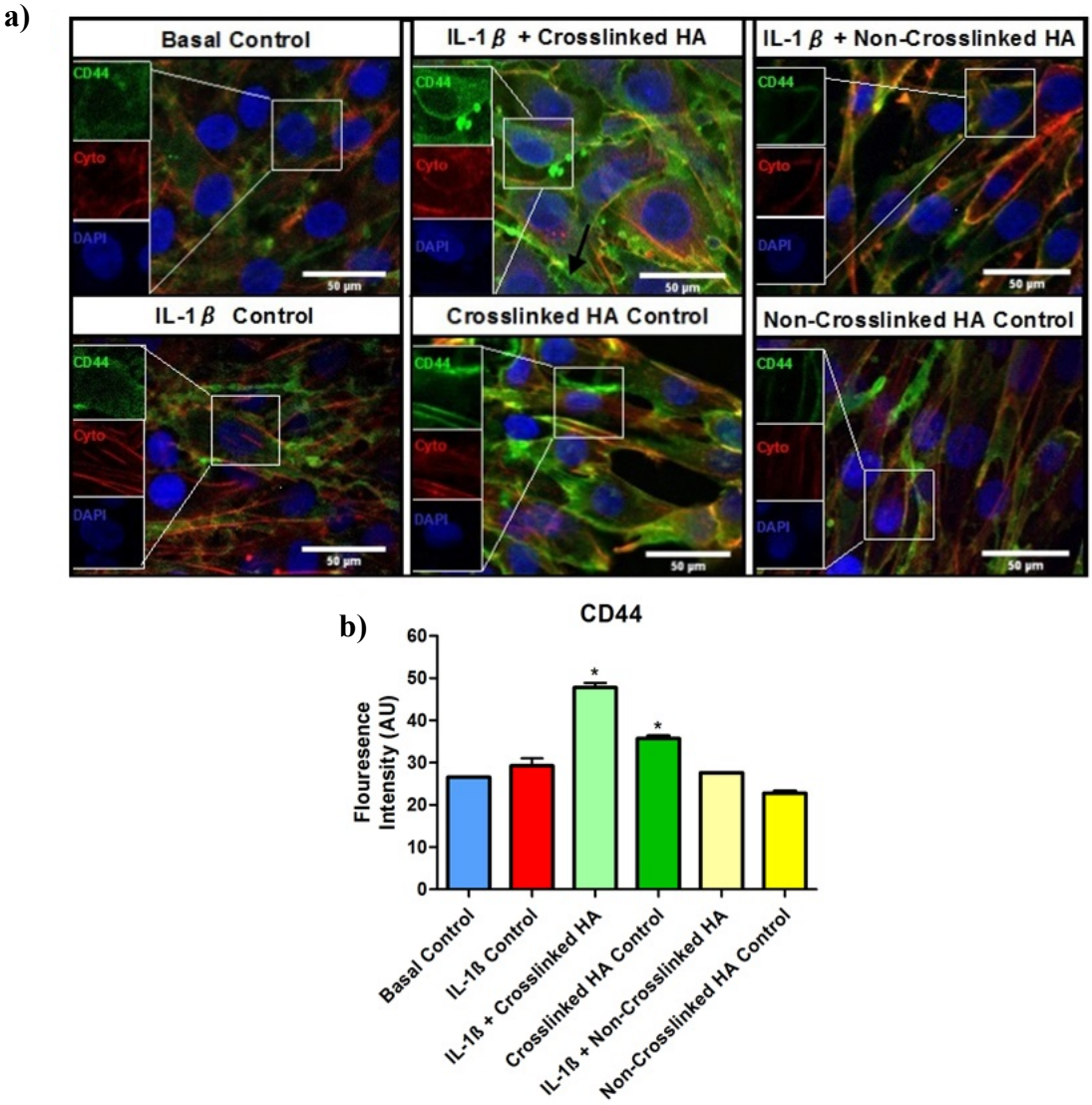

Figure 2.8 Antibody binding of CD44 in NP cells after HMW HA treatment. (a) Confocal micrograph showing distribution and co-localization of CD44 (green) and cellular cytoskeleton (red) in IL-1β induced inflammation and normal NP cells in the treatment of 0.75 mg (in 100 μL) crosslinked hydrogels and non-crosslinked HA after 3 days culture. The binding of crosslinked HA to CD44 receptor of NP cells which is shown by the black arrow. (b) Histogram illustrating mean fluorescence intensity of CD44 receptor significantly activated in crosslinked HA hydrogels treatment compared to IL-1β control group. *Significant differences were noted between the different groups (n = 3, one-way ANOVA, $p < 0.05$). Data presented as the mean ± standard error of the mean.

2.5 Discussion

An optimally crosslinked HA hydrogel system was developed in this study to evaluate the therapeutic effect of hydrogels in response to inflammation-associated pain and investigate the expression of CD44 in NP cells after HA treatment. The structure of multi-arm PEG-amine was important in optimising the hydrogel crosslinking system. 4-arm PEG-amine in hydrogel has been proved to enhance cell adhesion on the hydrogel surface to support biological properties in the system [38]. biodegradable hydrogels [39]. For this reason, 4-arm PEG-amine was used as a It can be easily crosslinked with naturally derived biomaterial such as HA to form crosslinking agent in this study. HA was covalently crosslinked with 4-arm PEG-amine after the carboxyl group of HA was functionalized using EDC coupling in the presence of NHS to stabilize the intermediate in the crosslinking reaction (Figure 2.1a). EDC and NHS activated carboxyl groups of HA facilitate the amide bond formation with primary amines of 4-arm PEG-amine. The remaining unreacted carboxyl groups of HA were determined by analysis of the FTIR at peak 1720 nm. The carboxyl groups of HA were decreased as PEG-amine concentration increased (Figure 2.2a). Similarly, the unreacted amine groups of 4-arm PEG-amine that do not participate in crosslinking reaction were found to decrease with increasing PEG-amine concentration. No further changes occurred after 75 mM PEG-amine, which suggests that the maximum crosslinking was reached at this point (Figure 2.2b). The microstructure of hydrogel was dependent on the concentration of PEG-amine used in the crosslinking reaction. Surface morphology SEM images display a micro-pits structure to a smooth surface layer at lower to higher concentration PEG-amine (Figure 2.3). These surface morphology changes are probably due to the sufficient crosslinking reaction.

The optimally crosslinked HA hydrogels was determined when using 75 mM PEG-amine. 3D sphere shape of these hydrogel was obtained when apply on hydrophobic surface at room temperature (Figure 2.4a, i) and maintained physical structure after complete crosslinking at 37°C (Figure 2.4a, ii). Hydrogel was also stable to the hydrolytic process in PBS and showed resistance to enzymatic degradation over 28 days (Figure 2.4b). Physiologically, HA is degraded predominantly by an enzymatic reaction through hyaluronidase [40]. The results of this finding may be due to the use of PEG in the crosslinking system that can

maintain the *in vitro* degradation rate of hydrogels. Therefore, in the present study, an optimally crosslinked HA hydrogels were formulated by controlling the degradation profile that are suitable for targeted controlled release drugs or other therapeutic molecules in NP regeneration.

At a cellular level, the clustering of NP cells with chondrocyte-like round shape was observed in basal control. With hydrogel treatment of 0.75 mg (in 100 μL) and 1.5 mg (in 200 μL) doses of HA, the cells maintained round morphology as normal and some of cells adopted a slightly fibroblastic-shape with short cytoplasmic extensions after three days culture (Figure 2.5a). This appears to be because of the binding with HA hydrogels [27], and the presence of oxygen in the cell culture system. Additionally, no statistical difference in viability of NP cells was observed after crosslinked HA hydrogel treatment (Figure 2.5b). This indicates no cytotoxicity was occurred. These recent results were supported by the previous studies showing that HA/type II collagen hydrogel maintained NP cell phenotype [34] and did not influence NP cell viability [25].

Apart from the physical properties of hydrogel, HA with a different molecular weight affects cellular responses such as cell adhesion, migration, proliferation and also maintains tissue structure [27]. In healthy tissue, HA presents high molecular weight with an average ~10^7 Da which can maintain tissue integrity and thus suppress the inflammatory response [41]. In this study, IL-1β was used to create an inflammation microenvironment of NP cells since IL-1β is one of main pro-inflammatory cytokine significantly increased in gene and protein expression [3] in symptomatic disc degeneration [42]. These current results demonstrated that the inflammatory receptor of IL-1R1 and MyD88 were highly expressed in NP cells after being stimulated by IL-1β. However, in treatment of HA hydrogels, these receptors were suppressed after three days in culture (Figure 2.6). Other supported findings showed that the use of HMW HA in the case of inflammation and tissue injury is through blocking neutrophil and macrophage infiltration in sepsis induced lung injury [43], inhibiting phagocytosis of peritoneal macrophages [44], decreasing production of pro-inflammatory cytokines (IL-1β and IL-6) and migration of macrophages in a post-laminectomy rat model [45].

The inflammatory process also induces neuronal sensitization of nociceptors that can increase synaptic conduction and result in pain sensation. The pro-inflammatory cytokine such as IL-1β is associated with the mechanism of nociception [21] by correlating the local production of neurotrophins and innervation of nociceptive nerve fibres into the disc. IL-1β induces neurotrophin expression of NGF and BDNF, resulting in innervation of human disc samples [8][46]. The current results show that NGF gene was expressed in basal NP cells and greatly increased regulation after being stimulated by IL-1β. These findings are supported by other studies and indicate that NGF-dependent neurons play a key role in inflammatory pain responses. In dorsal root ganglion (DRG), neurons innervating the disc, neuropeptides or markers for NGF-dependent neurons such as substance P (SP) and calcitonin-gene related peptide (CGRP) were mainly localised in small DRG neurons which are nociceptive neuron [47]. As with NGF, BDNF mRNA expression also up-regulated after being treated by IL-1β. BDNF is known a central nervous system modulator of nociception by binding to full-length receptor tropomyosin-related kinase B [48]. Conversely, both NGF and BDNF mRNA expression was down-regulated in all HA treatment and significantly down-regulated in crosslinked HA hydrogel treatment (Figure 2.7). These finding are supported by a previous study in which HA effectively reduced pain in osteoarthritic patients [31] and promoted an analgesic effect by activating the opioid receptor [49].

HA is known to bind to a specific cell surface receptor notably to CD44, that modulates cellular signaling in regulating cell adhesion, growth, survival, migration and differentiation and HA metabolism [50-51]. The architecture of HA crosslinking network functions as an anti-inflammatory cascade in response to tissue inflammation and is also mediated through CD44 [37]. Here, it was demonstrated that immuno-reactivity of CD44 receptor in normal and inflamed NP cells treated with non-crosslinked HA and crosslinked HA hydrogels. However, it was increased significantly in NP cells after treating with crosslinked HA hydrogels (Figure 2.8). These results suggest that crosslinked HA hydrogels bind to NP cells bind through CD44 and interfere pro-inflammatory cytokines binding to their receptors [37]. It has previously been shown that HA crosslinking network interacts with mononuclear leukocytes through CD44 in response to viral infection [52]. Furthermore, the architecture of HA in crosslinked form also stabilises the ECM during ovulation and

inflammation, regulates the hydrodynamic effect in the synovial joint, prevents loss of matrix components and thus promotes tissue repair [37].

The possible protective mechanism of crosslinked HA hydrogels is summarized in Figure 2.9. Nuclear factor-kappa B (NF-κB) is the major intracellular signalling pathway in mediating the molecular event for pathogenesis of disc degeneration. In the case of inflammation and pain, IL-1β is a pro-inflammatory mediator known to stimulate activation of NF-κB pathway in disc cells. Basically, IL-1β binds to IL-1R1 as part of the MyD88 complex. The active MyD88 induces signal transduction of IκB kinase (IKK) formation. Once IKK becomes activated and phosphorylates IκB to specific serine residues, this results in degradation. IκB degradation causes NF-κB to undergo translocation into the nucleus and subsequently bind to cDNA sequence that transcribes for specific gene expression [1]. Here, IL-1β induces activation of NF-κB to up-regulate transcription gene expression of pain mediators such as NGF and BDNF. However, in the presence of the hydrogel system, this crosslinked HMW HA possibly provides a protective mechanism in response to inflammation-associated pain through binding of the CD44 receptor on NP cells. The data, together wit available evidence suggests that HA may prevent the pro-inflammatory cytokines from binding to their receptors and thus inhibits transcription gene expression of neurotrophins to protect NP cells from further inflammation.

2.6 Conclusions

The formulated optimally crosslinked HMW HA hydrogels were stable, maintained a three-dimentional structure and demonstrated enzymatic resistance to degradation. No cytotoxicity of HA hydrogels was observed in NP cells after seven days in culture. Additionally, hydrogels showed a therapeutic effect by suppressing the inflammatory receptor of IL-1R1, MyD88 and down-regulated NGF and BDNF gene expression. Possible mechanism of HA in response to inflammation-associated pain is shown by highly expression of CD44 receptor after HA hydrogel treatment. Therefore, this biophysical and therapeutic effect of HA-based hydrogel provides a suitable microenvironment for NP regeneration.

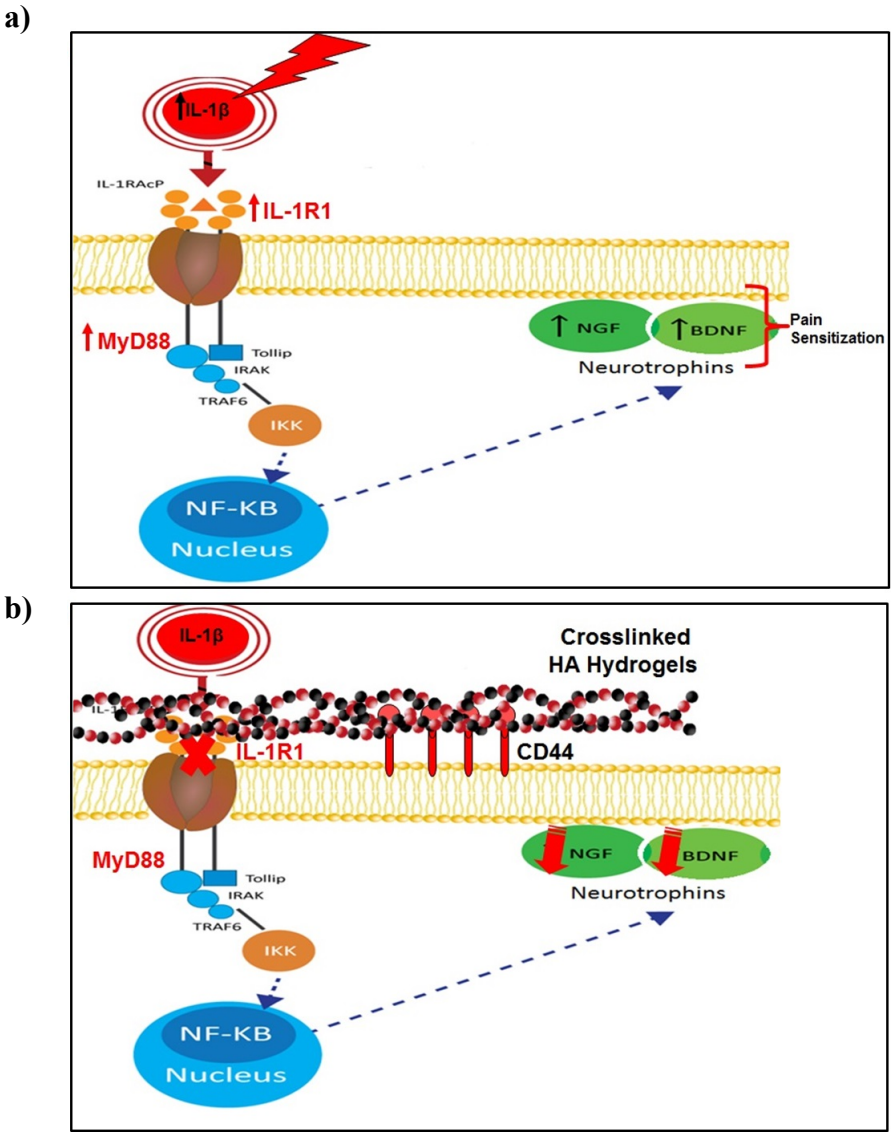

Figure 2.9 Schematic representation of possible protective mechanism of optimally crosslinked HA hydrogels in response to inflammation-associated pain. (a) At a molecular level, IL-1β binds to IL-1R1 to form MyD88 complex. The active MyD88 induces signal transduction of IKK and transcription factor of NF-κB to up-regulate neurotrophins of NGF and BDNF. These neurotrophins promote pain development during NP degeneration. (b) In the hydrogel system, these crosslinked HA hydrogel possibly bind to CD44 receptor of NP cells. Consequently, it interfere pro-inflammatory cytokines from binding to their receptors and inhibits transcription of neurotrophins to protect NP cells from further inflammation.

2.7 References

[1] K. Wuertz, N. Vo, D. Kletsas, and N. Boos, "Inflammatory and catabolic signalling in intervertebral discs: The roles of NF-κB and MAP kinases," *Eur. Cell. Mater.*, vol. 23, pp. 103-19-20, Jan. 2012.

[2] E. Krock, D. H. Rosenzweig, A. J. Chabot-Doré, P. Jarzem, M. H. Weber, J. A. Ouellet, L. S. Stone, and L. Haglund, "Painful, degenerating intervertebral discs up-regulate neurite sprouting and CGRP through nociceptive factors," *J. Cell. Mol. Med.*, vol. 18, no. 6, pp. 1213–25, Jun. 2014.

[3] C. L. Le Maitre, J. A. Hoyland, and A. J. Freemont, "Catabolic cytokine expression in degenerate and herniated human intervertebral discs: IL-1beta and TNFalpha expression profile," *Arthritis Res. Ther.*, vol. 9, no. 4, p. R77, Jan. 2007.

[4] C. K. Kepler, R. K. Ponnappan, C. A. Tannoury, M. V Risbud, and D. G. Anderson, "The molecular basis of intervertebral disc degeneration," *Spine J.*, vol. 13, no. 3, pp. 318–30, Mar. 2013.

[5] C. L. Le Maitre, A. J. Freemont, and J. A. Hoyland, "The role of interleukin-1 in the pathogenesis of human intervertebral disc degeneration," *Arthritis Res. Ther.*, vol. 7, no. 4, pp. R732-45, Jan. 2005.

[6] K. Wuertz and L. Haglund, "Inflammatory mediators in intervertebral disk degeneration and discogenic pain," *Glob. spine J.*, vol. 3, no. 3, pp. 175–84, Jun. 2013.

[7] Y. Abe, K. Akeda, H. S. An, Y. Aoki, R. Pichika, C. Muehleman, T. Kimura, and K. Masuda, "Proinflammatory cytokines stimulate the expression of nerve growth factor by human intervertebral disc cells," *Spine (Phila. Pa. 1976).*, vol. 32, no. 6, pp. 635–642, 2007.

[8] J. M. Lee, J. Y. Song, M. Baek, H. Y. Jung, H. Kang, I. B. Han, Y. Do Kwon, and D. E. Shin, "Interleukin-1β induces angiogenesis and innervation in human intervertebral disc degeneration," *J. Orthop. Res.*, vol. 29, no. 2, pp. 265–9, Mar. 2011.

[9] Y. Aoki, H. S. An, K. Takahashi, K. Miyamoto, M. E. Lenz, H. Moriya, and

K. Masuda, "Axonal growth potential of lumbar dorsal root ganglion neurons in an organ culture system: response of nerve growth factor-sensitive neurons to neuronal injury and an inflammatory cytokine," *Spine (Phila. Pa. 1976).*, vol. 32, no. 8, pp. 857–63, Apr. 2007.

[10] M. Gingras, J. Bergeron, J. Dery, H. D. Durham, and F. Berthod, "*In vitro* development of a tissue-engineered model of peripheral nerve regeneration to study neurite growth," *FASEB J.*, no. 17, pp. 2124–2126, 2003.

[11] A. J. Freemont, T. E. Peacock, P. Goupille, J. A. Hoyland, J. O. Brien, and M. I. V Jayson, "Early report nerve ingrowth into diseased intervertebral disc in chronic back pain," *Lancet*, vol. 350, pp. 178–181,1997.

[12] A. J. Freemont, A. Watkins, C. LeMaitre, P. Baird, M. Jeziorska, M. T. N. Knight, E. R. S. Ross, J. P. O'Brien, and J. A. Hoyland, "Nerve growth factor expression and innervation of the painful intervertebral disc," *J. Pathol.*, vol. 197, no. 3, pp. 286–92, Jul. 2002.

[13] J. Diamond, M. Coughlin, L. Macintyre, M. Holmes, and B. Visheau, "Evidence that endogenous beta nerve growth factor is responsible for the collateral sprouting, but not the regeneration, of nociceptive axons in adult rats," *Proc. Nati. Acad. Sci.*, vol. 84, no. September, pp. 6596–6600, 1987.

[14] C. J. Woolf, Q. P. Ma, A. Allchorne, and S. Poole, "Peripheral cell types contributing to the hyperalgesic action of nerve growth factor in inflammation," *J. Neurosci.*, vol. 16, no. 8, pp. 2716–2723, 1996.

[15] W. D. Snider and S. B. McMahon, "Tackling pain at the source: New ideas about nociceptors," *Neuron*, vol. 20, pp. 629–632, 1998.

[16] H. E. Gruber, J. A. Ingram, G. Hoelscher, N. Zinchenko, H. J. Norton, and E. N. Hanley, "Brain-derived neurotrophic factor and its receptor in the human and the sand rat intervertebral disc," *Arthritis Res. Ther.*, vol. 10, no. 4, pp. R82, Jan. 2008.

[17] B. Kirschenbaum and S. A. Goldman, "Brain-derived neurotrophic factor promotes the survival of neurons arising from the adult rat forebrain subependymal zone," *Proc. Natl. Acad. Sci.*, vol. 92, pp. 210–214, 1995.

[18] C. Q. Li, J. M. Xu, D. Liu, J. Y. Zhang, and R. P. Dai, "Brain derived

neurotrophic factor (BDNF) contributes to the pain hypersensitivity following surgical incision in the rats," *Mol. Pain*, vol. 4, pp. 27, Jan. 2008.

[19] D. Hellard, T. Brosenitsch, B. Fritzsch, and D. M. Katz, "Cranial sensory neuron development in the absence of brain-derived neurotrophic factor in BDNF/Bax double null mice," *Dev. Biol.*, vol. 275, pp. 34–43, 2004.

[20] A. Merighi, C. Salio, A. Ghirri, L. Lossi, F. Ferrini, C. Betelli, and R. Bardoni, "BDNF as a pain modulator," *Prog. Neurobiol.*, vol. 85, no. 3, pp. 297–317, Jul. 2008.

[21] A. L. de Souza Grava, L. F. Ferrari, and H. L. A. Defino, "Cytokine inhibition and time-related influence of inflammatory stimuli on the hyperalgesia induced by the nucleus pulposus," *Eur. Spine J.*, vol. 21, no. 3, pp. 537–45, Mar. 2012.

[22] D. Purmessur, M. C. Cornejo, S. K. Cho, P. J. Roughley, R. J. Linhardt, A. C. Hecht, and J. C. Iatridis, "Intact Glycosaminoglycans from intervertebral disc-derived notochordal cell conditioned media inhibits neurite growth while maintaining neuronal cell viability," *Spine J.*, vol. 15, no. 5, pp. 1060–1069, 2015.

[23] J. E. Frith, A. R. Cameron, D. J. Menzies, P. Ghosh, D. L. Whitehead, S. Gronthos, A. C. W. Zannettino, and J. J. Cooper-White, "An injectable hydrogel incorporating mesenchymal precursor cells and pentosan polysulphate for intervertebral disc regeneration," *Biomaterials*, vol. 34, no. 37, pp. 9430–40, Dec. 2013.

[24] D. Sakai, J. Mochida, T. Iwashina, A. Hiyama, H. Omi, M. Imai, T. Nakai, K. Ando, and T. Hotta, "Regenerative effects of transplanting mesenchymal stem cells embedded in atelocollagen to the degenerated intervertebral disc," *Biomaterials*, vol. 27, no. 3, pp. 335–45, Jan. 2006.

[25] E. C. Collin, S. Grad, D. I. Zeugolis, C. S. Vinatier, J. R. Clouet, J. J. Guicheux, P. Weiss, M. Alini, and A. Pandit, "An injectable vehicle for nucleus pulposus cell-based therapy," *Biomaterials*, vol. 32, no. 11, pp. 2862–70, Apr. 2011.

[26] G. Fontana, A. Srivastava, D. Thomas, P. Lalor, P. Dockery, and A. Pandit, "Three-dimensional microgel platform for the production of cell factories

tailored for the nucleus pulposus," *Bioconjug. Chem.*, 2014.

[27] J. Y. Lee and A. P. Spicer, "Hyaluronan: A multifunctional, megaDalton, stealth molecule," *Curr. Opin. Cell Biol.*, vol. 12, no. 5, pp. 581–586, Oct. 2000.

[28] P. Prehm, "Hyaluronate is synthesized at plasma membranes," *J. Biomech.*, vol. 220, pp. 597–600, 1984.

[29] P. Prehm and U. Schumacher, "Inhibition of hyaluronan export from human fibroblasts by inhibitors of multidrug resistance transporters," *Biochem. Pharmacol.*, vol. 68, no. 7, pp. 1401–10, Oct. 2004.

[30] H. Shankar, J. A. Scarlett, and S. E. Abram, "Anatomy and pathophysiology of intervertebral disc disease," *Tech. Reg. Anesth. Pain Manag.*, vol. 13, no. 2, pp. 67–75, Apr. 2009.

[31] M. Dougados, M. Nguyen, V. Listrat, and B. Amor, "High molecular weight sodium hyaluronate (hyalectin) in osteoarthritis of the knee: A 1 year placebo-controlled trial," *Osteoarthritis Cartilage*, vol. 1, pp. 97–103, 1993.

[32] E. Karna, W. Miltyk, J. A. Pałka, K. Jarzabek, and S. Wołczyński, "Hyaluronic acid counteracts interleukin-1-induced inhibition of collagen biosynthesis in cultured human chondrocytes," *Pharmacol. Res.*, vol. 54, no. 4, pp. 275–81, Oct. 2006.

[33] R. C. Savani, C. Wang, B. Yang, S. Zhang, M. G. Kinsella, T. N. Wight, R. Stem, D. M. Nance, and E. A. Turley, "Migration of bovine aortic smooth muscle cells after wounding injury. The role of hyaluronan and RHAMM," *J. Clin. Investig.*, vol. 95, pp. 1158–1168, 1995.

[34] D. O. Halloran, S. Grad, M. Stoddart, P. Dockery, M. Alini, and A. Pandit, "An injectable cross-linked scaffold for nucleus pulposus regeneration," *Biomaterials*, vol. 29, no. 4, pp. 438–47, Mar. 2008.

[35] J. A. Travis, M. G. Hughes, J. M. Wong, W. D. Wagner, and R. L. Geary, "Hyaluronan enhances contraction of collagen by smooth muscle cells and adventitial fibroblasts : Role of CD44 and implications for constrictive remodeling," *Circ. Res.*, vol. 88, no. 1, pp. 77–83, Jan. 2001.

[36] O. Ishida, Y. Tanaka, I. Morimoto, M. Takigawa, and S. Eto, "Chondrocytes

are regulated by cellular adhesion through CD44 and hyaluronic acid pathway," *J. Bone Miner. Res.*, vol. 12, no. 10, pp. 1657–1663, 1997.

[37] A. J. Day and C. A. de La Motte, "Hyaluronan cross-linking: A protective mechanism in inflammation?," *Trends Immunol.*, vol. 26, no. 12, pp. 637–43, Dec. 2005.

[38] H. Tan, A. DeFail, J. P. Rubin, C. R. Chu, and K. G. Marra, "Novel multi-arm PEG-based hydrogels for tissue engineering," *J. Biomed. Mater. Res. A*, vol. 92, no. 3, pp. 979–987, 2011.

[39] J. A. Wieland, T. L. Houchin-Ray, and L. D. Shea, "Non-viral vector delivery from PEG-hyaluronic acid hydrogels," *J. Control. Release*, vol. 120, no. 3, pp. 233–241, 2009.

[40] R. Stern, A. A. Asari, and K. N. Sugahara, "Hyaluronan fragments: An information-rich system," *Eur. J. Cell Biol.*, vol. 85, no. 8, pp. 699–715, Aug. 2006.

[41] A. C. Petrey and C. A. de La Motte, "Hyaluronan, a crucial regulator of inflammation," *Front. Immunol.*, vol. 5, no. March, p. 101, Jan. 2014.

[42] J. A. Hoyland, C. Le Maitre, and A. J. Freemont, "Investigation of the role of IL-1 and TNF in matrix degradation in the intervertebral disc," *Rheumatology (Oxford).*, vol. 47, no. 6, pp. 809–14, Jun. 2008.

[43] Y. Y. Liu, C. H. Lee, R. Dedaj, H. Zhao, H. Mrabat, A. Sheidlin, O. Syrkina, P.-M. Huang, H. G. Garg, C. A. Hales, and D. A. Quinn, "High-molecular-weight hyaluronan- a possible new treatment for sepsis-induced lung injury: A preclinical study in mechanically ventilated rats," *Crit. Care*, vol. 12, no. 4, p. R102, Jan. 2008.

[44] J. V. Forrester and E. A. Balazs, "Inhibition of phagocytosis by high molecular weight hyaluronate," *J. Immunol.*, vol. 40, no. January, p. 435, 1980.

[45] A. L. Schimizzi, J. B. Massie, M. Murphy, A. Perry, C. W. Kim, S. R. Garfin, and W. H. Akeson, "High-molecular-weight hyaluronan inhibits macrophage proliferation and cytokine release in the early wound of a preclinical postlaminectomy rat model," *spine J.*, vol. 6, no. 5, pp. 550–6, 2006.

[46] Y. Abe, K. Akeda, H. S. An, Y. Aoki, R. Pichika, C. Muehleman, T. Kimura, and K. Masuda, "Proinflammatory cytokines stimulate the expression of nerve growth factor by human intervertebral disc cells," *Spine (Phila. Pa. 1976).*, vol. 32, no. 6, pp. 635–42, Mar. 2007.

[47] Y. Aoki, Y. Takahashi, S. Ohtori, H. Moriya, and K. Takahashi, "Distribution and immunocytochemical characterization of dorsal root ganglion neurons innervating the lumbar intervertebral disc in rats: a review.," *Life Sci.*, vol. 74, no. 21, pp. 2627–42, Apr. 2004.

[48] C. L. Renn, C. C. Leitch, and S. G. Dorsey, "*In vivo* evidence that truncated trkB.T1 participates in nociception," *Mol. Pain*, vol. 5, p. 61, Jan. 2009.

[49] B. Zavan, L. Ferroni, C. Giorgi, G. Calo, P. Brun, R. Cortivo, G. Abatangelo, and P. Pinton, "Hyaluronic acid induces activation of the k-opioid receptor," *PLoS One*, vol. 8, no. 1, pp. 1–8, 2013.

[50] H. Ponta, L. Sherman, and P. A. Herrlich, "CD44: From adhesion molecules to signalling regulators," *Nat. Rev. Mol. Cell Biol.*, vol. 4, no. 1, pp. 33–45, Jan. 2003.

[51] K. Svee, J. White, P. Vaillant, J. Jessurun, U. Roongta, M. Krumwiede, D. Johnson, and C. Henke, "Acute lung injury fibroblast migration and invasion of a fibrin matrix is mediated by CD44," *J. Clin. Invest.*, vol. 98, no. 8, pp. 1713–27, Oct. 1996.

[52] C. A. de La Motte, V. C. Hascall, J. Drazba, S. K. Bandyopadhyay, and S. A. Strong, "Mononuclear leukocytes bind to specific hyaluronan structures on colon mucosal smooth muscle cells treated with polyinosinic acid: polycytidylic acid," *Am. J. Pathol.*, vol. 163, no. 1, pp. 121–133, 2003.

Chapter 3

The Establishment of a Pre-clinical Model of Pain in Intervertebral Disc Degeneration

Sections of this chapter are in preparation for submission:

Isa I. L. M., Abbah S. A., Kilcoyne M., Sakai D., Dockery P., Finn D. P., Pandit A. Implantation of hyaluronic acid hydrogel prevents the pain phenotype in a rat model with intervertebral disc injury, to be submitted to

3.1 Introduction

Discogenic low back pain is a very common problem that imposes enormous health and economic burdens on society, accounting for ~26–42% of patients with chronic low-back pain [1]. Pathological insults, such as catabolic imbalance and inflammatory response, result in degradation of high molecular weight of hyaluronic acid (HA) to low-molecular-weight HA, which contributes to disc degeneration by enhancement expression of matrix-degradative enzymes, induction of inflammatory responses and reduction of water retention in the discs [2]. The release of neurogenic mediators, such as pro-inflammatory cytokines (including interleukin (IL-1β) and tumor necrosis factor (TNF)) [3], neurotrophins (including beta-nerve growth factor (NGF) and brain-derived neurotrophic factor (BDNF)) [4-5] and neuropeptides (including calcitonin gene-related peptide (CGRP) and substance P) [6], can promote the innervation of peptidergic small neurons into aneural IVDs [7][3]. These changes sensitize nociceptive terminals and facilitate the development of discogenic back pain [8].

The development of a pre-clinical model of discogenic pain is necessary to enable study of the pathogenesis of symptomatic or painful disc degeneration, and to provide a platform to determine the effectiveness of potential therapeutic interventions. To date, however, few models have been developed to investigate pain associated with disc degeneration. Currently, surgically induced disc injury, or annulus fibrosus (AF) injury, is commonly used for induction of anatomical disruption, because damage to the AF is also known to affect human discs. This injury model is fairly quick to develop degeneration, and can be precisely controlled [9]. The rat tail model has also been widely adopted for the study of disc degeneration, because of the ability to avoid surrounding tissue damage, and the accessibility for intervention [9]. Reliable signs of pain (nociceptive behavioral responses) in rodents have been well characterized [10], making these animals highly appropriate for the investigation of painful disc degeneration.

Nevertheless, study of pain associated with disc degeneration in the rat tail is not reported at present. Herein, for the first time, a pre-clinical model of pain associated with symptomatic disc degeneration in the rat tail was developed. It was hypothesized that surgical puncture-induced disc injury elicits robust pain-related

behaviour in rats, induces spinal molecular markers of pain and structural degeneration, and differencially modulates glycosylation in both AF and NP tissues.

3.2 Materials and Methods

3.2.1 Materials and Reagents

Superfrost™ Plus slides, 3 kDa centrifugal filters and scalpel handle number 3 were purchased from Fisher Scientific (Dublin, Ireland). The RNeasy Mini kit was purchased from Qiagen (Hilden, Germany). Carprofen was purchased from Pfizer (Sandwich, UK). Isoflurane was purchased from Chanelle Group (Loughrea, Ireland). Morphine sulfate was purchased from Mercury Pharma Group (London, UK). Saline (0.9% (w/v) sodium chloride) was purchased from B. Braun Medical (Dublin, Ireland). Bone-cutting forceps, teeth forceps and iris scissors were purchased from Fine Science Tools (Heidelberg, Germany). A 1-mm biopsy puncher with a plunger, artery forceps and a needle holder were purchase from Medguard (Ashbourne, Ireland). von Frey filaments was purchased from North Coast Medical Inc. (Gilroy, CA, USA). An analgesic meter, six-compartment of rat enclosure (arena), mesh floor of von Frey and glass floor of Hargreaves test were purchased from IITC Life Science (Woodland Hills, CA, USA). Random primers, reverse transcriptase, 5× Reaction Buffer, 25 mM $MgCl_2$, dNTP mix and recombinant RNasin ribonuclease were purchased from Bioline (Dublin, Ireland). TaqMan® FAM™-labelled *c-Fos* primers (Rn00487426_g1) was purchased from Life Technologies (Dublin, Ireland). TaqMan VIC™-labeled rodent glyceraldehyde-3-phosphate dehydrogenase (*Gapdh*) primer and Universal PCR Master Mix were purchased from Applied Biosystems (Dublin, Ireland). Lectins conjugated with fluorescein isothiocyanate (FITC) or tetramethylrhodamine isothiocyanate (TRITC) were purchased from EY Laboratories (San Mateo, CA, USA). 4,6-diamidino-2-phenylindole (DAPI) was purchased from Life Technologies. Other materials and reagents were purchased from Sigma-Aldrich.

3.2.2 Animals

All animal-related protocols were performed in accordance with national guidelines and approved by the Animal Care Research Ethic Committee (ACREC) at the National University of Ireland, Galway and the Health Product Regulatory Authority (HPRA) Ireland. Experiments involved 50 adult (12-week-old) female Sprague–

Dawley rats, which were housed two to three per cage in individually ventilated cages, with wood-chip bedding, enriched with a wooden stick. Food and centralized tap water were available *ad libitum*, lights were turned on at 06:00 h, the temperature was maintained at 21 ± 2°C, and the husbandry was provided by female staff. Rats were purchased from Charles River (Margate, UK), and acclimated to the vivarium for at least 7 days prior to testing. For establishment of the disc-pain model, sample sizes were $n = 5$ for each of the three groups (Co4–Co5 NP injury; Co4–Co5 + Co5–Co6 NP injury; sham controls receiving isoflurane, but no surgical incision (sham–isoflurane); and sham controls receiving isoflurane and a skin incision, but no injury to the disc tissues (sham–incision)) with time-point day 29 (Figure 3.1a, i; Table 3.1a). To validate the disc-pain model using a reversible analgesic, sample sizes were $n = 5$ for each of the six groups (sham isoflurane + saline; sham isoflurane + low-dose (2 mg/kg) morphine; sham isoflurane + high-dose (10 mg/kg) morphine; Co4–Co5 + Co5–Co6 NP injury + saline; Co4–Co5 + Co5–Co6 NP injury + low-dose morphine; and Co4–Co5 + Co5–Co6 NP injury + high-dose morphine) with time-point day 29 (Figure 3.1a, ii; Table 3.1b).

3.2.3 Surgical-puncture-induced IVD Injury

On day 0, general health measurements, including body weight and temperature, were recorded prior to surgery. A single administration of the non-steroidal anti-inflammatory drug carprofen (5 mg/kg subcutaneous) was given to the rats 15 min before surgery, to manage post-operative pain in the early recovery phase. The rats were briefly anesthetized with inhalation of isoflurane (5% for induction and 1.8–2% for maintenance). The depth of anesthesia was determined by the loss of the pedal withdrawal (toe pinch) reflex. Moisturizer was dropped into the eyes if they remained open. The surgical site of the dorsal rat tail was washed with a betadine solution with gauze. The coccygeal discs Co4–Co5 and Co5–Co6 were identified by anatomical surface markings between two vertebral bones through the tail skin. The first disc between these two vertebral bodies counting from the base of the tail is Co4–Co5, followed by Co5–Co6. A rubber band was applied at the base of the tail not later than 30 minutes after identification of the discs (Figure 3.1b, i).

Surgery began with dissection with the aid of a binocular surgical loupe, and all surgical instruments were handled using aseptic technique. A longitudinal incision was introduced in the skin and at the connective tissue of the dorsal side of

the tail covering the discs. The tendons were pushed aside until the AF tissue (ivory matter) was reached (Figure 3.1b, ii). The injury was performed by punching defective NP tissue through the AF tissue at a diameter of 1 mm and a depth of 2 mm using a biopsy needle puncture (Figure 3.1b, iii). After injury, the discs were either left alone or implanted with HA hydrogel. The tendons were layer sutured to close the injury site, thereby covering the discs, and the animals were marked to show that the procedure had been performed. The wound was closed by suturing the skin with nylon suture using the interrupted horizontal mattress suturing method, and the rubber band was then removed from the tail to enable recovery of blood flow.

For post-operative care, the rats were closely monitored until they were completely recovered from anesthesia, then placed singly in individually ventilated cages until the wounds healed satisfactorily, which took approximately 1 week. Then, the rats were housed two to three per cage in individually ventilated cages for the recovery until day 29. Wounds were examined for signs of inflammation or infection, such as redness, swelling and/or purulent or serous discharge. General health-assessment details, such as tail-skin complications, body weight and temperatures, along with distress scores, were recorded on days 2, 7, 14 and 28 after the operation. The temperature and humidity of the housing environment were monitored, and appropriate bedding materials were provided during the studies.

3.2.4 Quantitative Behavioural Nociception Assays

Rats were habituated to the arena test environment for 20 min, 24 h prior to the commencement of testing, which minimized locomotor activity and stress-induced analgesia during testing. The same investigator performed the scoring in all behavioral tests, and was blinded to the experimental groups. The rats were assessed by the Hargreaves, von Frey and tail-flick tests (Figure 3.2b-d).

3.2.4.1 von Frey Test

The von Frey test was carried out on days −3, 2, 7, 14 and 29. The rats were individually placed into six-compartment of rat enclosure (arena) with wire-mesh floors and lids with air holes for a twenty minutes habituation period to minimize exploratory activity. The test began with a 2 g filament, which was applied to the base of the tail on the ventral surface for a maximum of six seconds, with sufficient force to buckle it slightly (Figure 3.2d). A positive response was considered to have

occurred when the rats respond to the applied filament by flinching, licking, withdrawing or shaking the base of the tail.

This process was repeated five times for the 2 g filament, giving a withdrawal frequency out of five for the tail tested. If a response was obtained with the 2 g filament, it was tested with lower weight filaments until a 0/5 or 0% response was obtained. The test was continued with ascending filament numbers until a 5/5 or

100% response was obtained for two consecutive filaments. The individual percentage response from each time-point was further analysed using non-linear regression to generate exponential decay. The first output measurement was calculated as percentage (%) withdrawal response. This was calculated for test at each filament weight as follows:

$$\frac{\text{Number of positive responses}}{\text{Number of applications (5)}} \times 100$$

The second output measurement was the 50% withdrawal threshold. This was defined as the filament weight (or filament number) at which a 50% withdrawal response was obtained. The filament weight and the % response each day were tabulated for each individual animal. In XY data table of Graphpad Prism, filaments was tabulated in ascending order in the X column, and % response to each filament in each day was tabulated in separate Y column. A non-linear regression curve was ploted (sigmoidal dose-response, variable slope, set bottom and top constraints as 0 & 100 respectively) and the log EC_{50} was obtained from the results sheet. A log EC_{50} for each animal on each day was entered into a separate table (days in the X column and groups in separate Y columns, with each rat as a separate replicate). An average for each group was computed and plotted as von Frey filament weight eliciting a 50% response vs. time (days).

3.2.4.2 Hargreaves Test

The test was performed on days −3, 2, 7, 14 and 29 (relative to surgery). Rats were placed in six-compartment of rat enclosure (arena) on top of a glass plate (IITC, USA), to habituate for twenty minutes. Heat was introduced with a radiant light source, and latency to the response was recorded. Responses included withdrawal, flinching, licking, biting and shaking the base of the tail. The analgesic meter test head was positioned under the base of the tail, with the beam approximately focused

on the ventral surface of the tail, which was opposite to the site of injury (Figure 3.2b). The test head was set to 50% of the maximum output. When the rat responded, the light source was set to 'idle' intensity, and the heat source was deactivated. A cut-off of twenty seconds was set, to prevent tissue damage. If no response occurred in this time, the heat source was automatically returned to idle intensity. On each test day, each rat received four trials, with a minimum interval time of three minutes. Withdrawal latency for each rat was calculated as the average of the four measurements.

3.2.4.3 Tail Flick Test

The tail-flick test was performed on days −2, 3, 8, 15 and 28. On each day, the test for each rat involved four consecutive measurements. Each rat was removed from its home cage and habituated on a towel for ten minutes, then placed on the glass apparatus with its body covered with the towel as a restraint, such that its tail projected out. A radiant light source was focused 5 cm from the distal end on the ventral region of the tail to introduce heat, and the latency to tail flick was recorded (Figure 3.2c). A cut-off point of twenty seconds was assigned, to prevent tissue damage. A period of at least fifteen seconds between each test was observed to avoid sensitization of the tail. Tail-flick latency for each rat was calculated as the average of four consecutive measurements.

3.2.5 Morphine Treatment

For validation of the model, pain was inhibited with morphine. Low-dose morphine (2 mg/kg), high-dose morphine (10 mg/kg) or vehicle (saline) was administered by subcutaneous injection, and behavioral responses were assessed 30 min after injection (Figure 3.1a, ii).

3.3 Post-mortem Analysis

After a 29-day period post-surgery, live rats were decapitated with a guillotine, and trunk blood was collected in EDTA tubes during the procedure. Discs, AF and NP tissues, spinal cords and brains were extracted for further tissue analysis.

a) i.

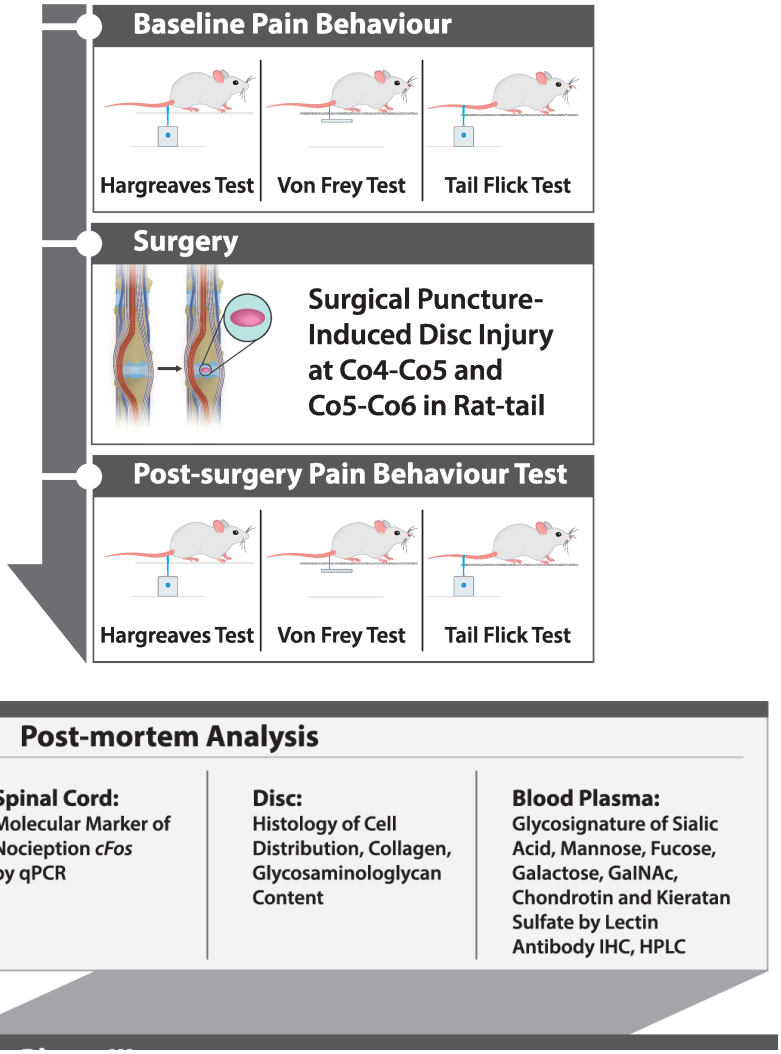

ii.

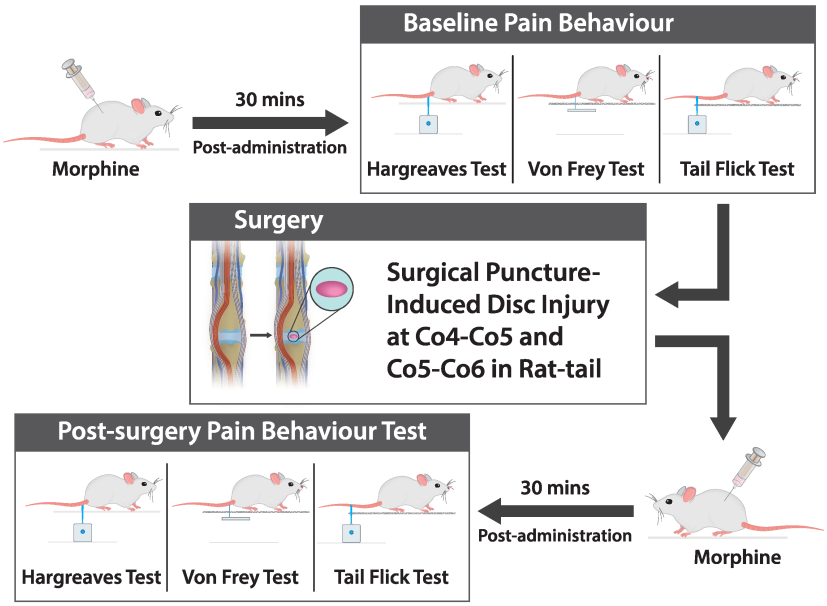

Continued

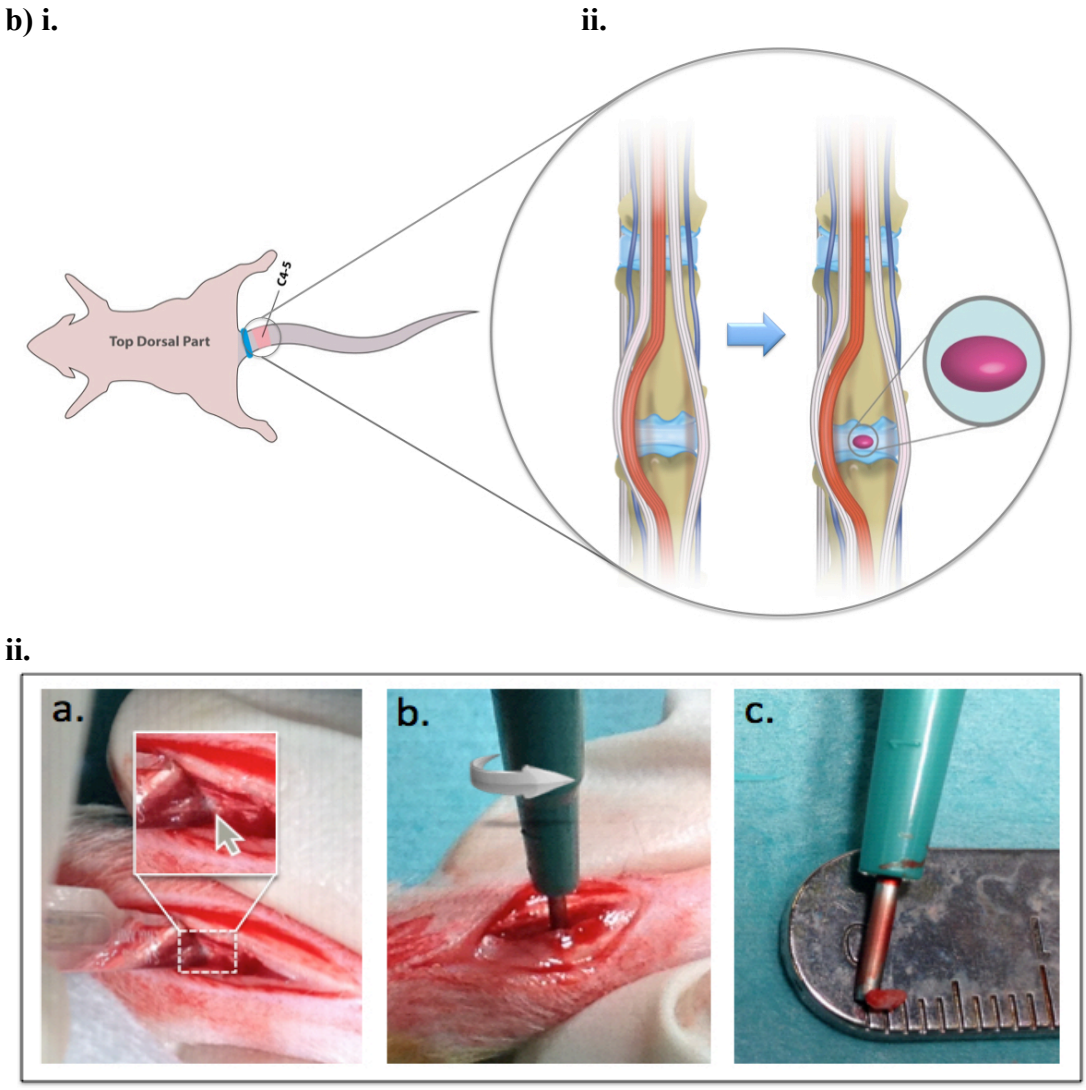

Figure 3.1 Schematic representations of the experimental design and procedures. (a) Experimental design. (i-ii) The study was designed as: Phase I - Development and characterisation of an intervertebral disc (IVD) pain model; Phase II - Validation of the model using morphine. (b) Surgical procedure. (i) Identification of the coccygeal IVD at the Co4–Co5 level. A rubber band (marked in blue) was applied at the base of the tail. Discs were treated by injury alone or injury with implantation of HA hydrogel (marked in purple). (ii) Steps of the surgical procedure. A disc was dissected by pushing aside connective tissue and tendons until the ivory matter of the annulus fibrosus (AF) tissue (gray arrow) was reached. The defect was created by puncturing nucleus pulposus (NP) tissue through AF tissue at a diameter of 1 mm and a depth of up to 2 mm.

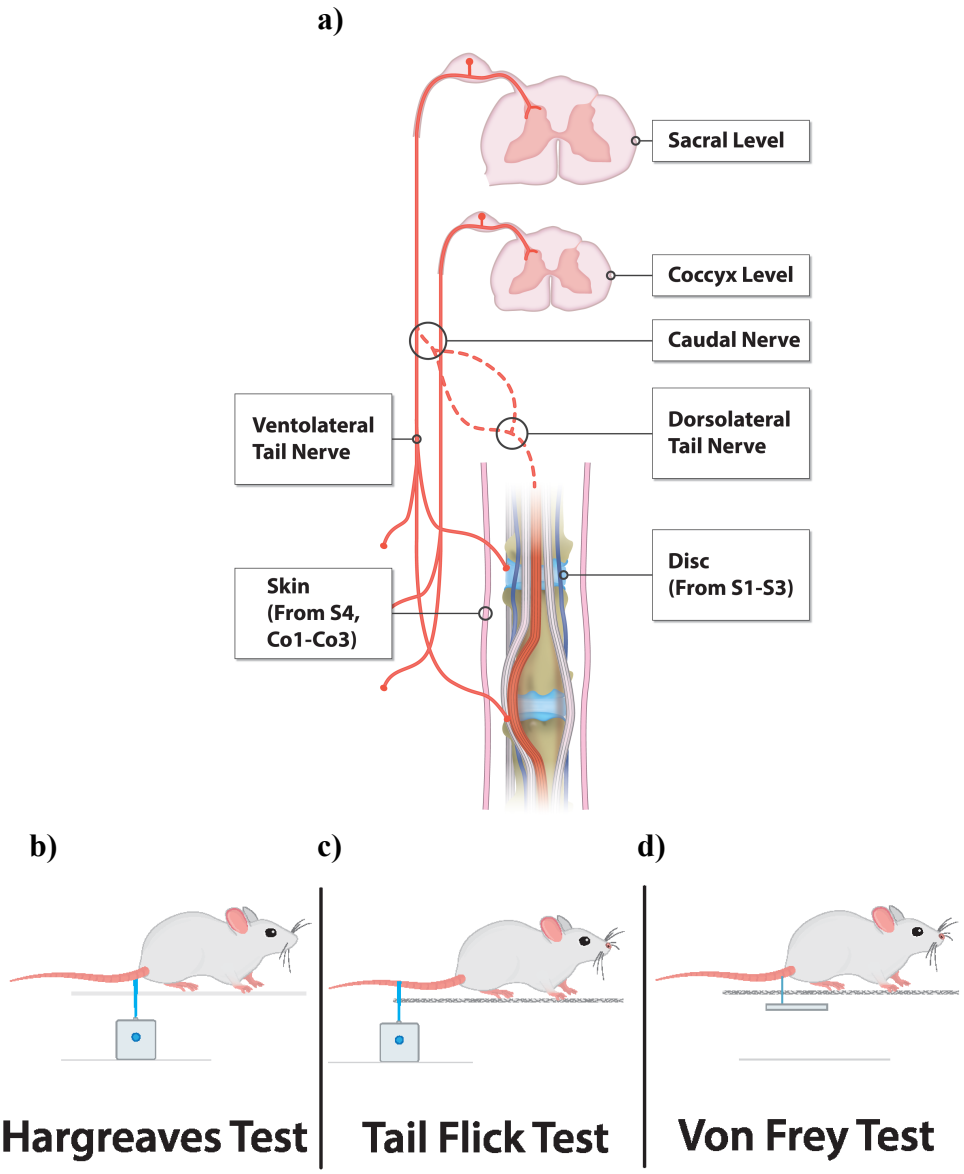

Figure 3.2 Pain behaviour assessment in the rat tail. (a) Neuroanatomy of the rat tail to define the receptive fields of the stimuli used for the pain-behavior tests. (b) Hargreaves' test was adopted to measure thermal hyperalgesia in the rats by applying a radiant heat source to the ventral part proximal of tail. (c) The tail flick test was used to measure thermal pain response in the rats by applying a radiant heat source to the ventral distal part of the tail. (d) The von Frey test was utilised to determine mechanical allodynia by applying von Frey filaments to the ventral part proximal of the tail.

Table 3.1 Sample size with a total 50 of rats used in intervertebral disc pre-clinical study of pain. (a) Number of 20 rats was grouped into four for the development of pain following IVD injury. (b) 30 rats were allocated to study morphine in validation of IVD pain model.

a)

Group	N	Time-point (days)
NP Injury (Co4-Co5)	5	29
NP Injury (Co4-Co5 and Co5-Co6)	5	29
Sham (Incision)	5	29
Sham (Isoflurane)	5	29
Total	**20**	

b)

Group	N	Time-point (days)
Sham + saline	5	29
Sham + morphine low dose (2 mg/kg)	5	29
Sham + morphine high dose (10 mg/kg)	5	29
Injury + saline	5	29
Injury + morphine low dose (2 mg/kg)	5	29
Injury + morphine high dose (10 mg/kg)	5	29
Total	**30**	

3.3.1 Spinal Nociception Marker by RT-qPCR

Left and right dorsal horns of the sacral segment of the spinal cord were dissected within 30 minutes after euthanasia, snap frozen and immediately placed at −80°C until further analysis. The dorsal horn of the spinal cord at the sacral and coccyx levels was homogenized in 1 mL of Trizol® reagent per 50–100 mg of tissue sample using TissueLyser (Qiagen). The samples were shaken at high speed in 2 mL round bottomed microcentrifuge tubes with stainless-steel beads for fifteen minutes at room temperature. Following homogenization, the samples were centrifuged at 1,200 g for five minutes at 4°C, and the fatty layer was discarded. The cleared supernatant was transferred to a new microcentrifuge tube (Qiagen). For phase preparation, 200 µL of chloroform was added per 1 mL of Trizol® reagent, mixed for fifteen seconds and incubated for two minutes at room temperature. The mixture was then centrifuged at 13,300 rpm for fifteen minutes at 4°C. The colorless upper aqueous phase containing RNA was transferred to a fresh tube and mixed with 600 µL of 70% molecular grade ethanol. The mixture was transferred to a Qiagen RNeasy Mini column and centrifuged at 10,000 rpm for fifteen seconds, and flowthrough was discarded. RNA bound to the column was washed with 700 µL of RW1 buffer and centrifugation at 10,000 rpm for fifteen seconds. Next, 500 µL of RPE buffer was added to the column, followed by centrifugation at 10,000 rpm for fifteen seconds, then a further 500 µL of RPE buffer and centrifugation for two minutes. RNase-free water (30 µL) was added, and the mixture was centrifuged at 10,000 rpm for one minute to collect RNA in a new collection tube. The RNA concentration was determined with a NanoDrop spectrophotometer (Thermo Scientific) from the ratio of absorbance at 260 nm and 280 nm, and the quality of the product was determined using a bioanalyzer (Agilent, Santa Clara, CA, USA). Total 5 µL of RNA (100 ng/µL) was reverse transcribed with random primers and reverse transcriptase in a 20 µL reaction mixture consisting of 4.4 µL 5× reaction buffer, 2.64 µL 25 mM $MgCl_2$, 1.1 µL dNTPs, 1.L µL RNasin ribonuclease inhibitor and 1.1 µL ImProm-II TM reverse transcriptase, with the PTC DNA Engine System (PTC-200, Peltier Thermal Cycler, MJ Research, Watertown, MA, USA). cDNA products were amplified with TaqMan gene-expression assays and specific primers for *c-Fos* and *Gapdh*. A multiplex PCR reaction was performed with TaqMan Universal PCR Master Mix, no AmpErase® UNG (Applied Biosystems) and standard thermal

conditions (ten minutes at 95°C for polymerase activation, followed by 40 cycles of 95°C for fifteen seconds and 60°C for 60 seconds) in triplicate using the StepOnePlus Real-Time PCR System (Applied Biosystems). The results were analyzed by the $2^{-\Delta\Delta Ct}$ method, normalized to the endogenous *Gapdh* control and the sham control rats.

3.3.2 Lectin Binding

Post mortem, discs were fixed in 4% (w/v) paraformaldehyde for 48 h, and vertebral bones were decalcified for two weeks in Kristensen's decalcifying solution containing 18% (v/v) formic acid and 3.5% (w/v) sodium formate at 4°C. All tissues were then washed under running tap water overnight, and soaked in 20% (w/v) sucrose until they sank at 4°C. Tissues were embedded in optimal cutting temperature compound and snap-frozen in an isopentane bath with liquid nitrogen, then kept at −80°C until sectioning on a cryostat (CM1850, Leica, Wetzlar, Germany). Tissue sections (10-µm) were collected on Superfrost™® Plus slides (Fisher Scientific, Dublin, Ireland) and stored at −20°C until use. Staining was performed at room temperature, and all washes were performed three times for five minutes each time between incubations, unless otherwise stated. Three slides (one each from three different rats) were used for each lectin incubation.

For lectin histochemistry, slides were washed with Tris-buffered saline supplemented with Ca^{2+} and Mg^{2+} (TBS; 20 mM Tris-HCl, 100 mM NaCl, 1 mM $CaCl_2$, 1 mM $MgCl_2$, pH 7.2) and 0.05% (v/v) Triton X-100 (TBS-T), then blocked with 2% (w/v) periodate-treated BSA (Sigma-Aldrich) in TBS for one hour. Inhibitory controls were carried out in parallel to verify that the lectin binding was glycan-mediated by co-incubating the lectins with 100 mM of the appropriate haptenic sugar in TBS (Table 3.2). Sections were washed, then incubated with eight different FITC-conjugated or TRITC-conjugated lectins (SNA-I, MAA, WGA, Con A, UEA-I, WFA, GS-IB4 and PNA (EY Labs)) in TBS for one hour (Table 3.2). After five washes with TBS-T, the sections were counterstained with a 1:1,000 dilution of DAPI for five minutes. The slides were washed in TBS-T before coverslip mounting with ProLong® Gold Antifade Mountant (Life Technologies). Inhibition by the appropriate haptenic sugar was observed for all lectins used (data not shown). Sections were washed with PBS-T and coverslip-mounted as described

above. All slides were cured at 4°C in the dark for one day before imaging with a laser confocal microscope (Olympus Fluoview 1000, Olympus America, Center Valley, PA, USA).

3.3.3 Lectin Image Analysis and Stereology Quantification

Stereology quantification was adopted to calculate the percentage volume fraction of detectable lectin binding to specific glycans. The confocal microphotographs were obtained from at least five microscopic views of each slide with three technical and three biological replicates using ImageJ software version 1.48 (NIH, Bethesda, MD, USA). Confocal microphotographs were converted to binary mode (8 bit) and adjusted to the optimal threshold of positive staining and total area. Volume fraction (Vv) was calculated by quantifying the area fraction of the positively-stained matrix component divided by the total area and converting into a percentage (%) as below:

$$\text{Percentage volume fraction (\%Vv)} = \frac{\text{Area Fraction x 100}}{\text{Total Area}}$$

3.3.4 Histology

Discs were post-fixed with 4% (w/v) paraformaldehyde for 48 hours and decalcified in Kristensen's decalcifying solution for two weeks, and then washed for 24 hours under running tap water and paraffin-embedded. Discs were cut into transverse 5-µm sections on a microtome (Leica). Tissue sections were collected on Superfrost™ Plus slides and stored at room temperature until use. Staining was performed at room temperature. Sections were de-waxed in xylene in the fume hood and rehydrated through 95%, 70% and 50% ethanol washes for two minutes each.

For hematoxylin and eosin (H&E) staining, sections were stained in Mayer's hematoxylin for six minutes and washed under running tap water before staining in eosin for two minutes. After a quick rinse in tap water, the sections were dehydrated with 50% ethanol for ten seconds, 70% ethanol for ten seconds, 90% ethanol for two minutes (twice) and absolute ethanol for two minutes (twice).

For Alcian blue staining, sections were stained in Alcian blue (pH 2.5) for 30 minutes and washed under running tap water, then counterstained with nuclear fast red for ten minutes. After washing under running tap water, sections were dehydrated with 50% ethanol for ten seconds, 70% ethanol for ten seconds, 90% ethanol for two minutes (twice) and absolute ethanol for two minutes (twice).

For Masson's Trichrome staining, sections were oxidized in 0.5% (w/v) $KMnO_4$, 0.5% (v/v) H_2SO_4 for two minutes and washed in tap water before bleaching with 2% (w/v) $Na_2S_2O_5$ for two minutes. Sections were washed with water and 70% ethanol, then stained with Gomori's aldehyde fuchsin for one minute. After quick rinses in water and 95% ethanol, sections were stained with Celestine blue for four minutes, washed, then stained with Mayer's hemalum stain for four minutes. Sections were washed with water, differentiated in acid alcohol for twenty seconds and washed with water again before staining with Masson's cytoplasmic stain for one minutes. Sections were quickly washed in water and differentiated in 1% (w/v) dodeca-molybdophosphoric acid ($H_3PO_412\ MoO_324H_2O$), then counterstained with Fast Green FCF or Light Green SF, differentiated in 1% (v/v) acetic acid, and dehydrated through 50%, 70%, 95% and absolute ethanol washes for one minute each. All sections were cleared in two changes of xylene and covered with DPX mounting medium and a coverslip. The sections were placed in an oven to enable the mounting medium to solidify before imaging under a light microscope (Leica, Germany).

3.3.5 Histological Classification of Disc Degeneration

Stained slides were graded with a validated histological grading system [11], as described previously [12]. Major anatomical structures of the AF and NP were included in this classification, resulting in four subcategories. Each item was graded as zero, one or two on the H&E and Alcian blue sections, with zero representing non-degenerative characteristics, one representing mild degenerative characteristics and two representing severe characteristics of degeneration (Figure 5b, iv). The total score was the sum of the four different scoring items, resulting in a minimum score of zero, corresponding to a healthy disc, and a maximum score of eight, corresponding to an entirely degenerated disc.

3.3.6 HPLC Analysis of HA and Chondroitin Sulfate

AF and NP tissues were separated from the discs after euthanasia. Tissues were snap frozen and immediately kept at −80°C. The samples were digested with proteinase K (0.5 mg/mL) overnight at 56°C and stored at −20°C until further analyses. HPLC was performed as described previously [13]. For data analysis, the disaccharide content of each sample was identified by comparison with appropriate

Table 3.2 Binding specificity and haptenic sugars of lectins for profiling of tissue glycosylation.

Lectin	**Binding specificity**	**Haptenic sugar (100 mM)**
SNA-I (*Sambucus nigra* agglutinin I)	Sialic acid-α-(2,6)–GalNAc–R	Lactose
MAA (*Maackia amurensis* agglutinin)	Sialic acid-α-(2,3)–GalNAc–R	Lactose
WGA (Wheat germ agglutinin)	Sialic acid, GlcNAc	GlcNAc
PNA (Peanut agglutinin)	Gal-β-(1,3)–GalNAc (T-antigen), > GalNAc > lactose > Gal, terminal β-Gal, non-sialylated	Gal
GS-I-B4 (*Griffonia simplicifolia* isolectin)	Terminal α-linked Gal	Gal
Con A (Concanavalin A)	α-linked mannose, glucosamine and GlcNAc	Mannose
UEA-I (*Ulex europaeus* agglutinin I)	α-(1,2)-linked fucose	Fucose
WFA (*Wisteria floribunda* agglutinin)	GalNAc and chondroitin sulfate	GalNAc

A haptenic sugar is a monosaccharide or disaccharide that can inhibit binding of a lectin. Abbreviations: Gal, galactose; GalNAc, N-acetylgalactosamine; GlcNAc, N-acetyl glucosamine.

chromatograph standards under the same HPLC conditions as the sample, with quantification by comparison with appropriate standard curves generated by the injection of known concentrations of standards.

3.4 Statistical Analysis

Statistical differences were analyzed by GraphPad Software (La Jolla, CA, USA) using repeated measure ANOVA or one-way ANOVA for analyses of the Hargreaves, von Frey and tail-flick tests; one-way ANOVA for the PCR and HPLC. Student's t-test for the lectin analysis in the validation of the injury model. All ANOVAs were further evaluated with Bonferroni *post-hoc* analysis, and $p < 0.05$ was deemed statistically significant. All error bars indicate standard error of the mean (S.E.M).

3.5 Results

3.5.1 Establishment of Painful Intervertebral Disc Degeneration Model

Rat coccygeal IVDs were surgically punctured at levels Co5–Co6 and/or Co4–Co5 (Figure 3.1b, i-iii) to induce robust pain-related behavior. Treated rats demonstrated persistent mechanical allodynia and thermal hyperalgesia, along with changes in molecular marker expression and glycosylation, and structural disc degeneration.

3.5.1.1 Pain Phenotype

Pain phenotyping was conducted by quantitative sensory testing after surgical-puncture-induced IVD injury in the rat tail.

3.5.1.1.1 Thermal Hyperalgesia

The Hargreaves test was performed to study thermal hyperalgesia, by applying a noxious thermal stimulus to the ventral base of the tail. At baseline (prior to any procedure), no significant difference was seen between the four experimental groups (rats receiving only isoflurane (sham–isoflurane), rats receiving a skin incision but no injury to the disc tissues (sham–incision), rats with Co4–Co5 injury and rats with Co4–Co5 + Co5–Co6 injury). Rats in the two sham groups had withdrawal latency comparable to baseline when evaluated on days 2, 7, 14 and 29. However, withdrawal latency was significantly shorter in both the injury groups post-treatment compared with baseline or with the sham groups at each time point. No significant

difference was seen between the Co4–Co5 and Co4–Co5 + Co5–Co6 injury groups, indicating that single-level and adjacent-level injuries produce comparable levels of thermal hyperalgesia in this model. Thus, puncture-induced disc injury evoked thermal hyperalgesia in the rat tail, evident on post-operative days 2, 7, 14 and 29 (tested by one-way and repeated measures ANOVA, n = 5 rats per group, p <0.05; Figure 3.3a).

3.5.1.1.2 Mechanical Allodynia

von Frey filaments were applied to the same receptive field as that in the Hargreaves test, to analyze mechanical allodynia. No differences between the four groups were observed at baseline. The 50% withdrawal threshold was significantly lower in the sham–incision group than in the sham–isoflurane group, and in the Co4–Co5 + Co5–Co6 injury group compared with both sham groups, however no significant different was observed between sham-incision group and Co4–Co5 injury group at day 2. No differences were observed between the injury groups. These results suggest that puncture-induced disc injury elicits mechanical allodynia in the rat tail until at least 29 days post-operation (tested by one-way and repeated measures ANOVA, n = 5 rats per group, p <0.05; Figure 3.3b).

3.5.1.1.3 Thermal Hypoalgesia

Tail-flick testing was conducted by applying a radiant heat stimulus to the ventral middle part of the tail. No differences in withdrawal latency were observed at baseline. No differences from baseline were observed in the sham control groups up to day 28. On days 3, 8 and 15, latency time in the injury groups was higher than at baseline, and significantly higher than in the sham groups on the same days, suggesting hypoalgesia to a stimulus applied distal to the site of injury (tested by one-way and repeated measures ANOVA, n = 5 rats per group, p <0.05; Figure 3.3c).

3.5.1.1.4 Up-regulation of c-Fos Gene

Afferent sensory neurons were activated by applying both thermal stimulus to the distal rat tail, and dissected the sacral dorsal horn in the spinal cord within 30 minutes following stimulation. This approach was used because transcription of the *c-Fos* mRNA occurs rapidly, within minutes of stimulation, and its expression is transient [14]. In our experimental groups, significant upregulation of *c-Fos* mRNA

expression occurred in the left (but not the right) dorsal horn in both injury groups compared to the control groups (fold change versus sham–isoflurane was 5.7 ± 1.7 for Co4–Co5 and 6.2 ± 1.2 for Co4–Co5 + Co5–Co6 injury), however no significant different between sham-incision (3.775 ± 0.7563) with both injury groups (tested by one-way ANOVA, n = 5 rats per group, p <0.05; Figure 3.4). These data suggested IVD-injury induces activation of afferent neurons after noxious stimulation which allows pain processing in the central nervous system by expressing of the immediate-early gene *c-Fos* increases in the second-order pain-transmission neurons of the spinal cord dorsal horn.

3.5.1.2 Injured Discs Show Microstructural Disc Degeneration

In the injured disc tissues at post-surgery day 29, hematoxylin and eosin (H&E) staining revealed annular rupture, mixed clustering of NP cells and the presence of chondroid nests in the NP tissue, whereas uninjured discs had well-organized AF tissue, normal NP cellularity and no cell clusters (Figure 3.5a). Masson's trichrome staining of injured discs showed loose collagen fibers in AF tissue, with fibrinous components dominating both AF and NP tissues (Figure 3.5b). Compared with uninjured discs, reduced Alcian blue staining in the NP matrix in injured discs indicated reductions in proteoglycans and HA in the ECM. The tissue sections were graded according to the main subcategories of histological classification (Figure 3.5c), recording scores of zero for uninjured discs, and higher scores in all categories for injured discs. The mean total score of seven for the injured discs, according to a validated histological grading system [11], corresponded to a Thompson grade of III [12] (Figure 3.5d). These findings indicate that IVD-injury induced anatomical disruption in the disc tissue for at least a month post-injury.

3.5.1.3 Injured Discs Have a Unique Glycosignature

At the cellular and ECM levels, IVDs have been shown to have distinct glycoprofiles, as well as compositions of chondroitin sulfate and sulfation patterns that vary from immaturity to maturity, suggesting a role for sugar moieties in modulation of age-associated disc degeneration. To investigate this role, the glycoprofiles were determined in injured and healthy IVDs with a library of lectins and carbohydrate-specific antibodies that were chosen on the basis of typical

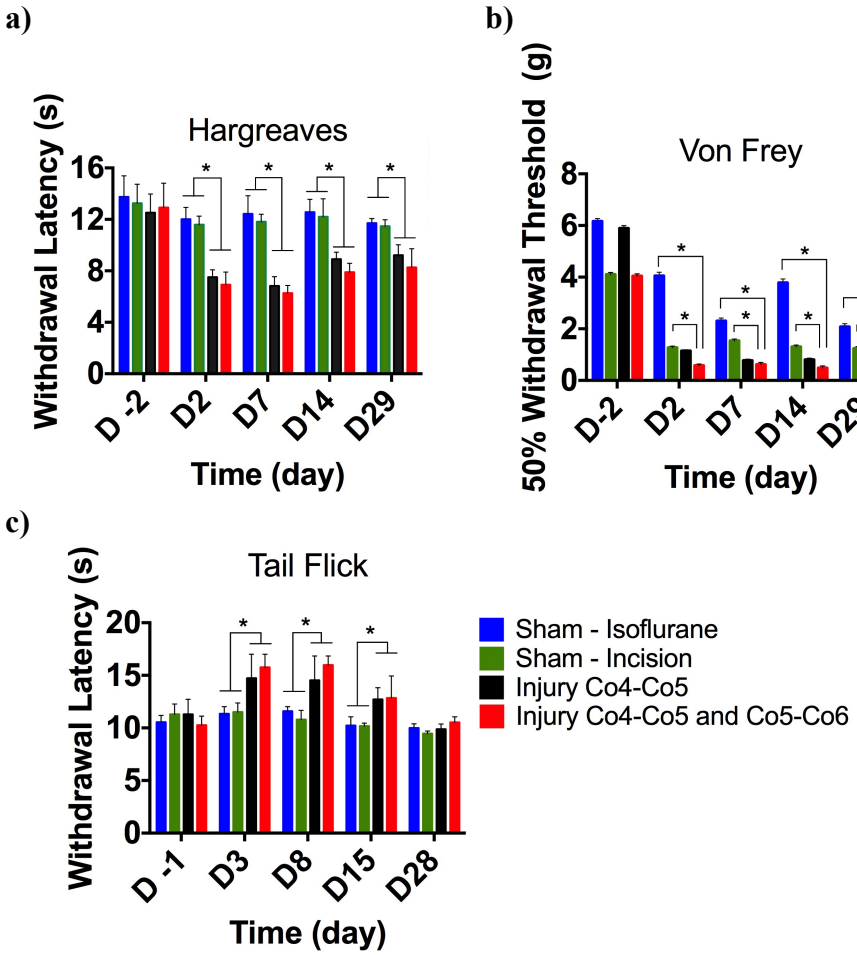

Figure 3.3 Tests of pain sensitivity. (a) The Hargreaves test of sensitivity to a thermal stimulus close to the site of injury demonstrated thermal hyperalgesia, with significantly lower latency times in both single-disc and double-disc injury groups than in both sham control groups, at all post-injury time points. (b) The von Frey test of sensitivity to a mechanical stimulus close to the site of injury demonstrated mechanical allodynia, with significantly lower 50% withdrawal threshold in the double-disc injury group than in either control group, at all post-injury time points. (c) The tail-flick test of sensitivity to a thermal stimulus away from the site of injury demonstrated hypoalgesia, with significantly higher withdrawal latency times in both single-disc and double-disc injury groups than in both sham control groups, on days 3, 8 and 15 post-injury. n = 5 rats per group. *Significant difference between groups by one-way ANOVA (p <0.05). Data are presented as the means ± standard error of the mean.

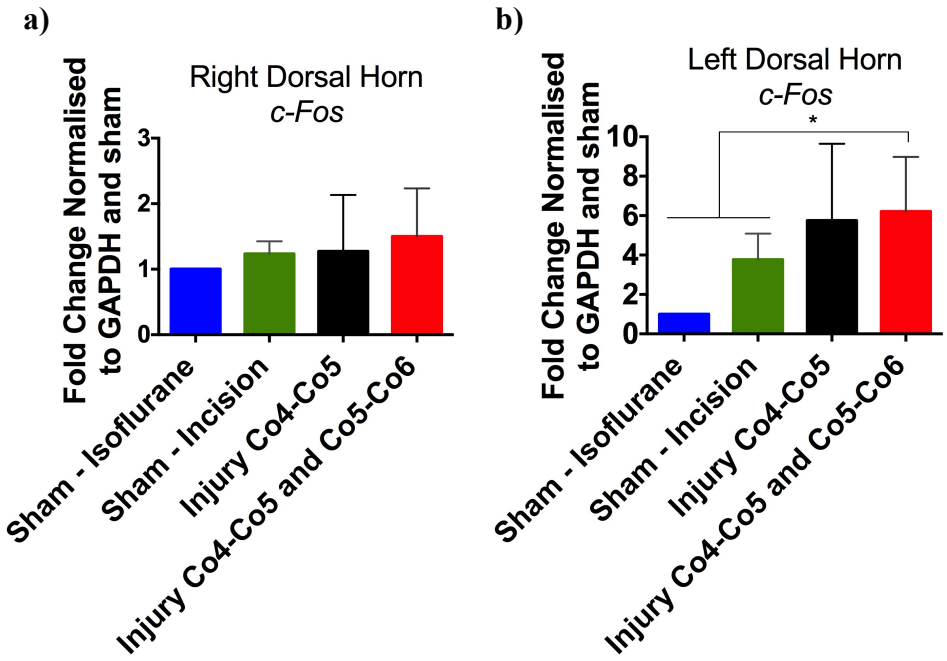

Figure 3.4 Tests of pain sensitivity and their effects on gene expression. Fold change of the immediate-early gene *c-Fos* in the left dorsal horn (b) of the spinal cord was significantly higher after double-disc injury than in either control group with rats euthanized within 30 minutes of thermal stimulation at proximal rat tail at day 29. *n* = 5 rats per group. *Significant difference between groups by one-way ANOVA ($p < 0.05$). Data are presented as the means ± standard error of the mean.

a)

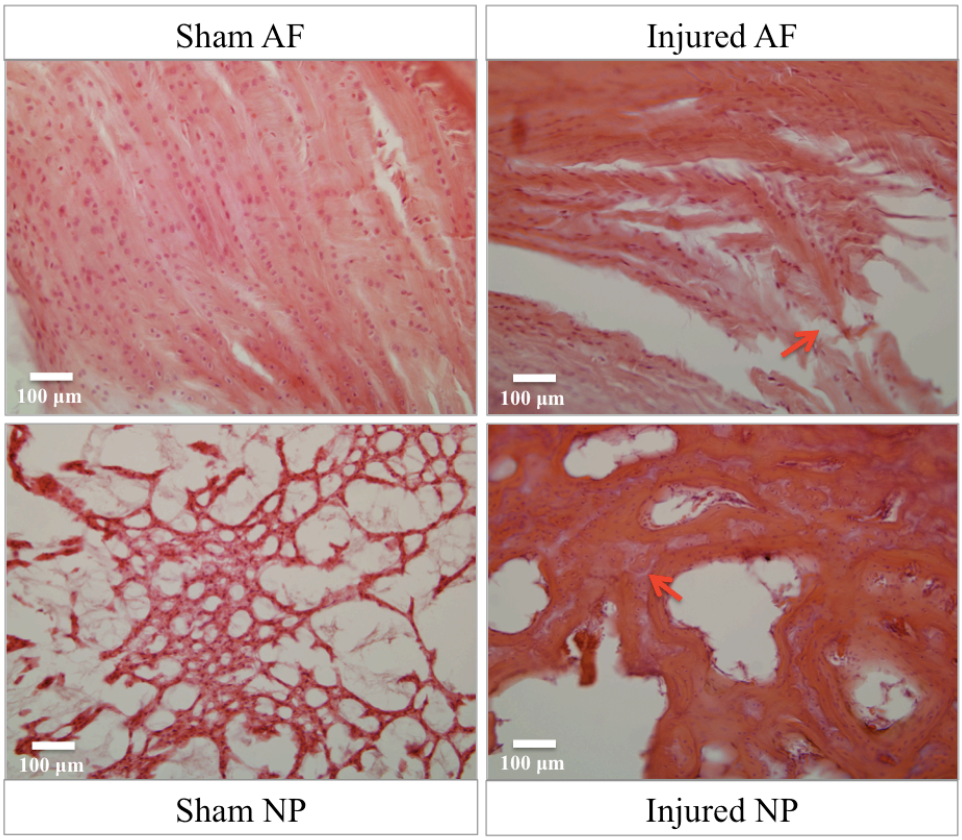

b)

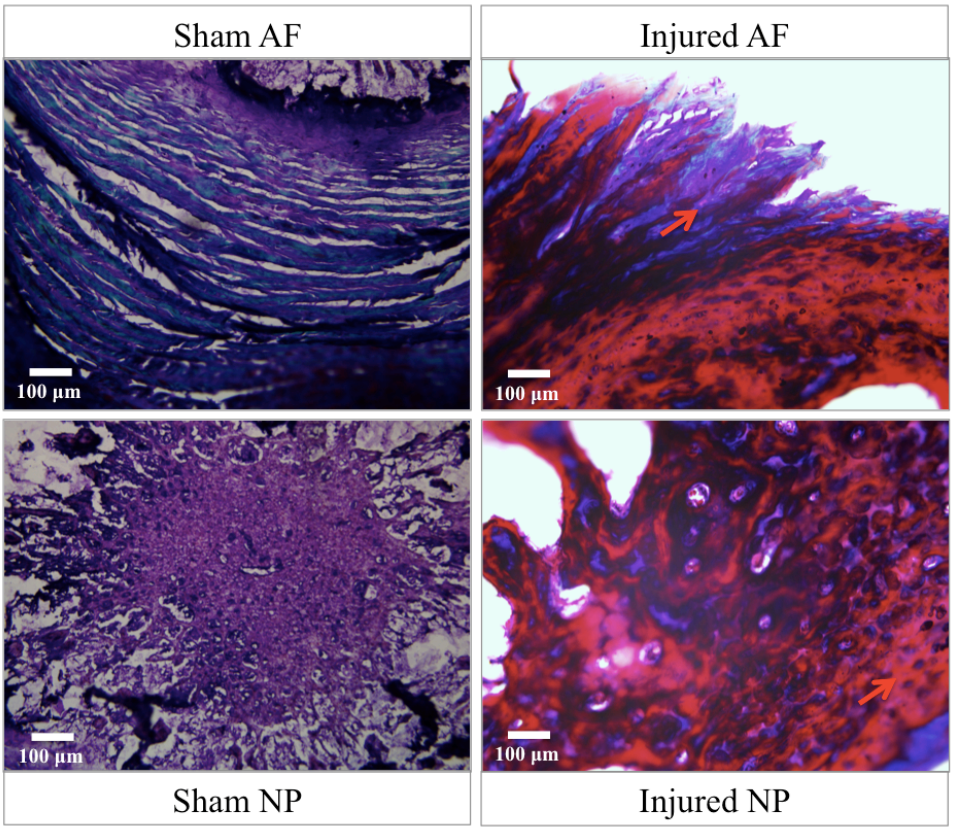

Continued

c)

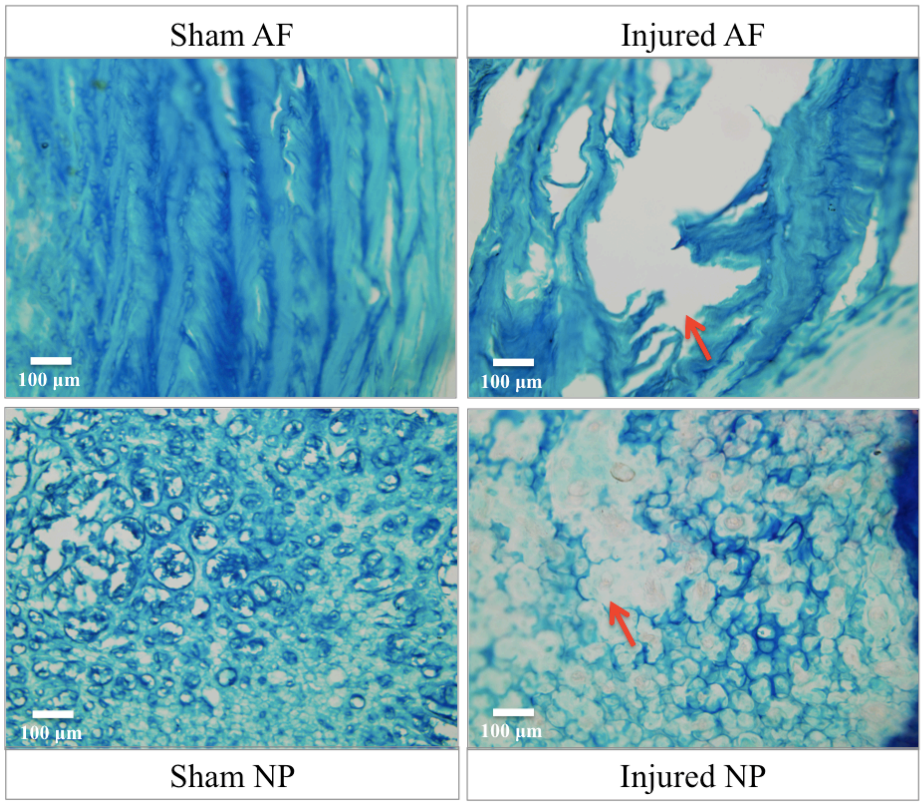
Sham AF
Injured AF
100 µm
100 µm
100 µm
100 µm
Sham NP
Injured NP

Continued

d)

Category	Score	Histological features	Observed score	
			Normal disc	**Injured disc**
AF morphology	0	Well-organized AF, half-ring-shaped structure, collagen lamellae	0	
	1	Partly ruptured AF; loss of half-ring-shaped structure		1
	2	Completely ruptured AF; no intact half-ring-shaped collagen lamellae		
NP cellularity	0	Normal cellularity; no cell clusters	0	
	1	Mixed cellularity; normal pattern with some cell clusters		
	2	Mainly clustered cellularity; chondroid nests present		2
NP matrix	0	Intense staining; blue staining dominates	0	
	1	Reduce staining; mixture of blue and slight red staining		
	2	Faint blue staining; increased red staining		2
Boundary between AF and NP	0	Clear boundary between AF and NP tissues	0	
	1	Boundary less clear; loss of annular–nuclear demarcation		
	2	No distinguishable boundary between AF and NP tissues		2
		Total score	**0**	**7**

Figure 3.5 Histological assessment of healthy and injured IVDs. (a) On post-mortem histology of day 29, hematoxylin and eosin staining showed annular rupture, mixed clustering of nucleus pulposus (NP) cells and the presence of chondroid nests in NP tissue after disc injury. (b) Masson's trichrome staining showed loose collagen fibers in annulus fibrosus (AF) tissue. (c) Alcian blue staining showed reduced levels of proteoglycans in the NP matrix. (d) Histological grading based on all staining showed microstructural disc degeneration after injury, which was clinically classified as being grade III. n = 5 rats per group. Scale bar = 100 μm.

mammalian glycosylation and N-glycan expressions in ovine IVD based on previous results [13].

3.5.1.3.1 Sialylation

SNA-I lectin binds to α-(2,6)-linked sialic acid, MAA binds to α-(2,3)-linked sialic acid and WGA binds to sialic acid and GlcNAc (Table 3.2). In tissues taken on day 29, significantly higher levels of binding of SNA-I and MAA were observed in NP tissue in injured IVDs than in uninjured IVDs (Figure 3.6a-b). However, only slightly higher level of binding SNA-I and MAA in injured AF tissue than in uninjured tissue. No significant difference was found in WGA binding in both AF and NP (Figure 3.6c). Overall, level of SNA-I, MAA and WGA binding in each tissue (AF and NP) was higher in injured discs than in uninjured discs (t-test, $p < 0.05$, $n = 3$; Figure 3.6a-c). These data suggested that increase of sialylation during inflammation and also responsible to induce hyper-polarization of the nerve action potentials.

3.5.1.3.2 High Mannose Type Glycosylation

Con A lectin binds to high-mannose glycans (Table 3.2). An increase in the expression of high-mannose structures is typically observed under cellular stress, and undifferentiated stem cells also express greater quantities of high-mannose structures than differentiated cells. In both NP and AF tissues, significantly higher levels of binding of Con A was detected in the injury groups than in the control groups (t-test, $p < 0.05$, $n = 3$; Figure 3.7a), which may indicate an increase in cellular stress.

3.5.1.3.3 Fucosylation

UEA-I lectin binds to α-(1,2)-linked fucose (Table 3.2). In both NP and AF tissues, significantly higher levels (93.34±2.2% and 94.26±0.52%, respectively) of binding of UEA-I were detected in the injury groups than in the control groups (t-test, $p < 0.05$, $n = 3$; Figure 3.7b), suggesting glycan modification associated with inflammation.

3.5.1.3.4 Galactosylation

GS-I-B4 and PNA lectins bind to terminal α-linked galactose (Gal) residues and Gal-β-(1,3)-GalNAc (T antigen), respectively (T-antigen), respectively (Table 3.2). In both NP and AF tissues, significantly higher levels of binding of GS-I-B4 and PNA

were detected in the injury groups than in the control groups (t-test, $p < 0.05$, $n = 3$; Figure 3.8a-b). GS-I-B4 binding was intracellular, whereas PNA binding was seen in the ECM. WFA lectin binds to either α-linked or β-linked terminal *N*-acetylgalactosamine (GalNAc), including that in chondroitin sulfate (Table 3.2). In both AF and NP tissues, binding of WFA was observed only in the ECM. In NP ECM, significantly lower levels of WFA binding occurred in the injury groups than in the control groups (t-test, $p < 0.05$, $n = 3$; Figure 3.8c).

3.5.1.3.5 Chondroitin Sulfate and HA Composition

The proportions of the HA and chondroitin sulfate (C0S, C4S and C6S) disaccharides were assessed by HPLC in the control and injury groups. A similar trend was seen for NP tissue with a decrease of C6S and an increase of C4S, but was not significant upon injury. HPLC results did not differentiate between HA and C0S because of their peaks had a similar retention time. Although, in both NP and AF tissues, the proportion of C4S seemed to be higher in the injury groups than in the control groups, no significant differences were observed in disaccharide composition ($p < 0.05$). The C6S composition was lower (but not significant) in the injury groups compared to control groups of AF and NP tissue (Figure 3.9a-b). Overall, these findings indicated IVD-injury induced loss of matrix composition and alter sulfation pattern in the injured tissues.

3.5.2 Validation of IVD Pain Model by Morphine Treatment

To inhibit pain in this model, high (10 mg/kg) and low (2 mg/kg) doses of morphine were injected 30 minutes prior to each nociceptive behavioral test on pre-operative and post-operative days, as described in the Methods section (Figure 3.1a, ii).

3.5.2.1 Morphine Reduces Thermal Hyperalgesia

The Hargreaves test demonstrated significantly higher withdrawal latency times in both control and injury groups with low-dose morphine compared with the saline-treated injury group (one-way ANOVA, $n = 5$, $p < 0.05$; Figure 3.10a), indicating that morphine reduced thermal hyperalgesia in the rat tail, and that this effect persisted in the presence of injury when the thermal stimulus was close to the injury site. High-dose morphine induced a state of catalepsy, resulting in withdrawal latency times at or above the maximum for the assay (20 seconds).

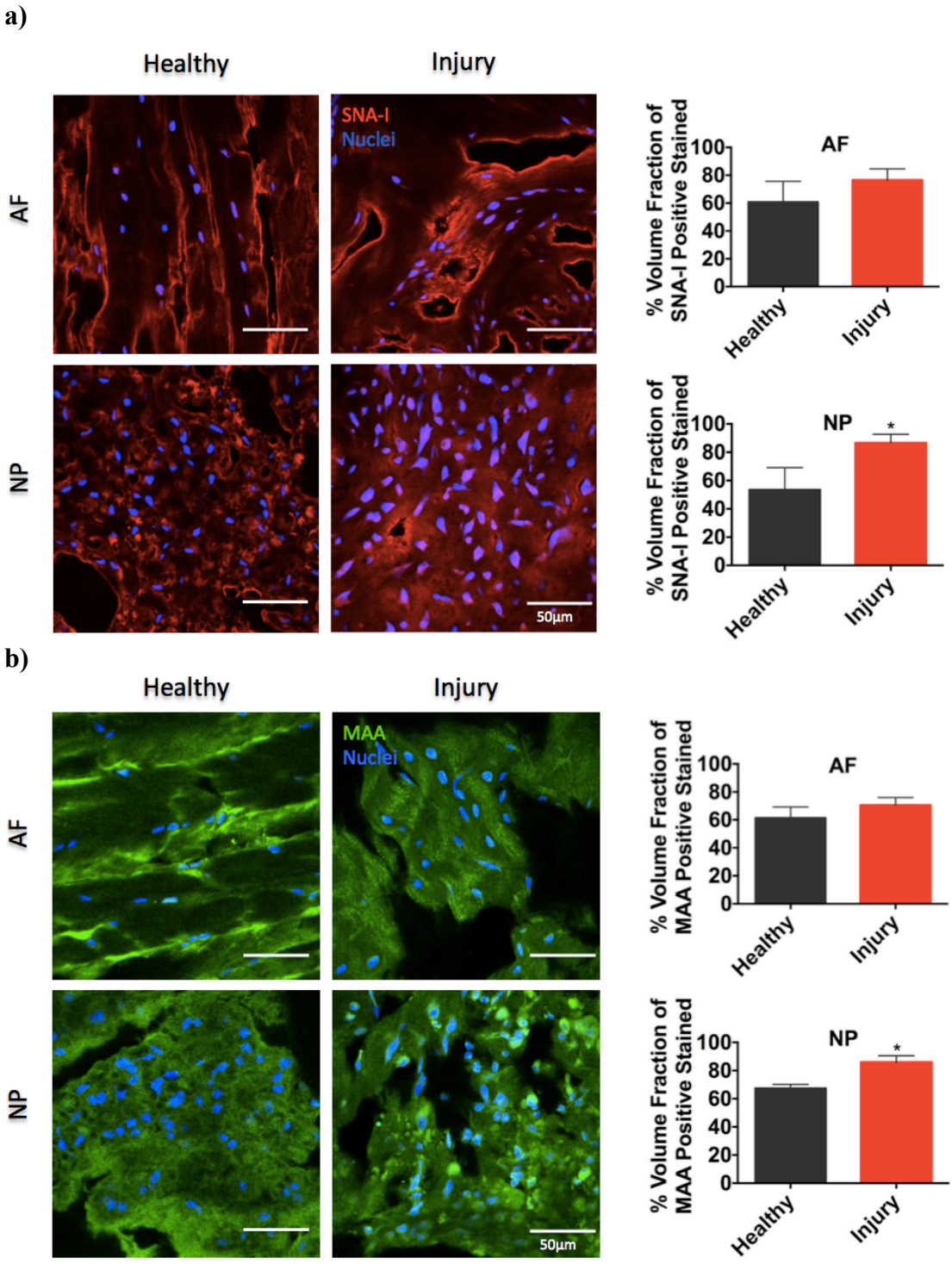
a)
Healthy
Injury
AF
NP
SNA-I
Nuclei
50µm
% Volume Fraction of SNA-I Positive Stained
AF
NP
*
Healthy
Injury
b)
MAA
Nuclei
% Volume Fraction of MAA Positive Stained

Continued

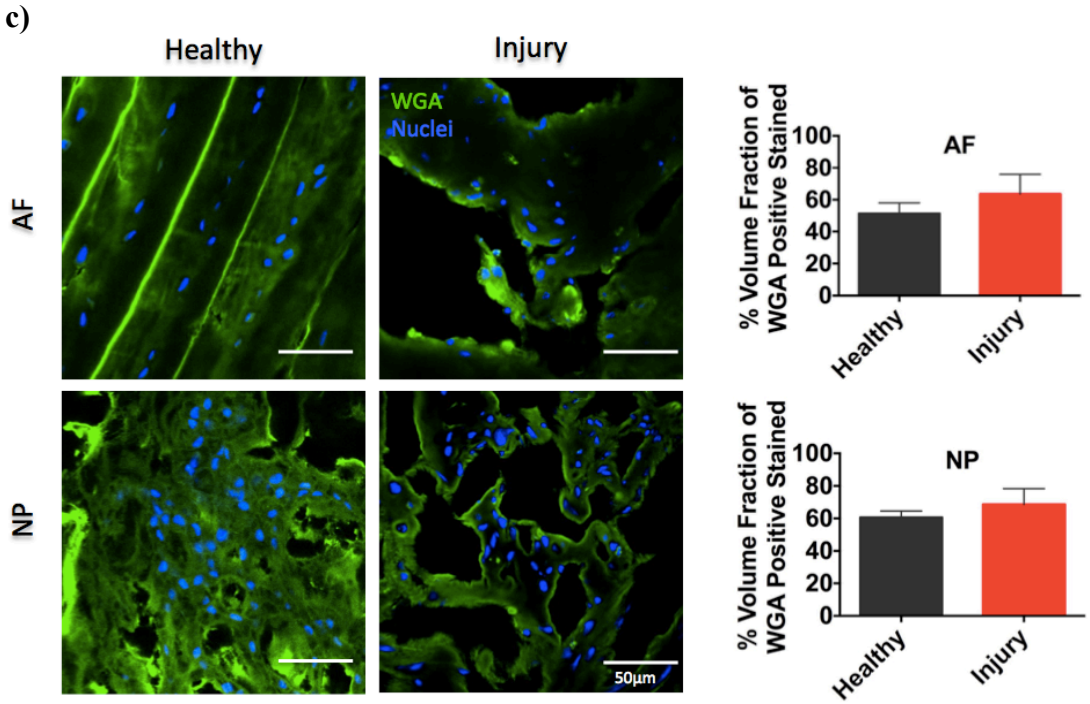

Figure 3.6 Glycosignatures (sialylation) in response to intervertebral disc injury. (a-c) Detection and quantification of sialylated motifs. SNA-I lectin binds α-(2,6)-linked sialic acid, MAA binds α-(2,3) linked sialic acid, and WGA binds N-acetyl-D-glucosamine (GlcNAc) and sialic acid. Binding of SNA-I and MAA was significantly higher in nucleus pulposus (NP) tissue in injured than in uninjured rats. n = 3 rats per group. *Significant differences between groups, by t-test (p <0.05). Area fraction data were normalized to the total area and are presented as the mean ± standard error of the mean. Scale bar = 50 µm.

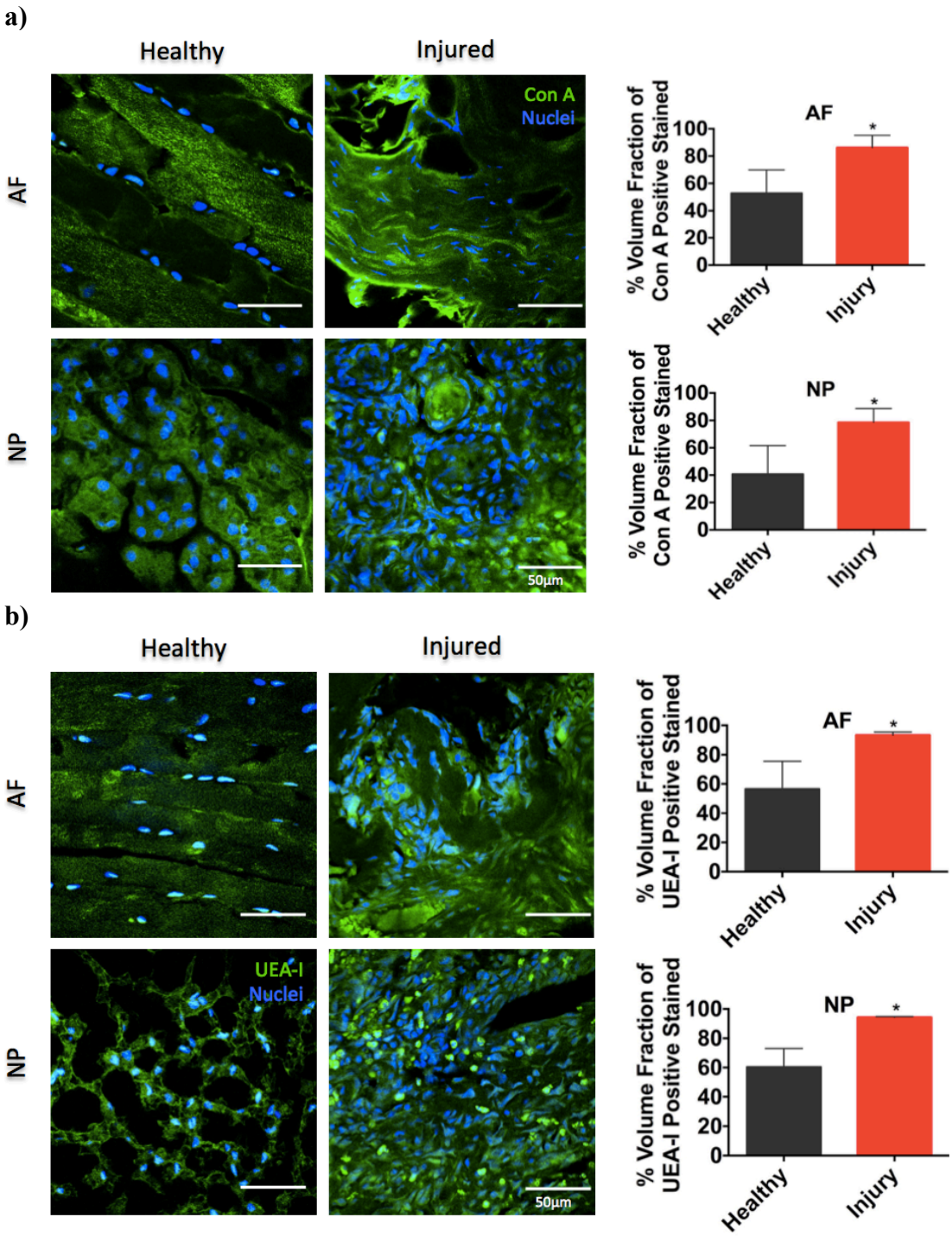

Figure 3.7 Glycosignatures in response to intervertebral disc injury. (a) Binding of Con A lectin (indicating mannose) was higher in annulus fibrosus (AF) and NP tissues in injured than in uninjured rats. (b) Binding of UEA-I (which binds to α-(1,2)-linked fucose) was higher in AF and NP tissues in injured than in uninjured rats. n = 3 rats per group. *Significant differences between groups, by t-test (p <0.05). Area fraction data were normalized to the total area and are presented as the mean ± standard error of the mean. Scale bar = 50 µm.

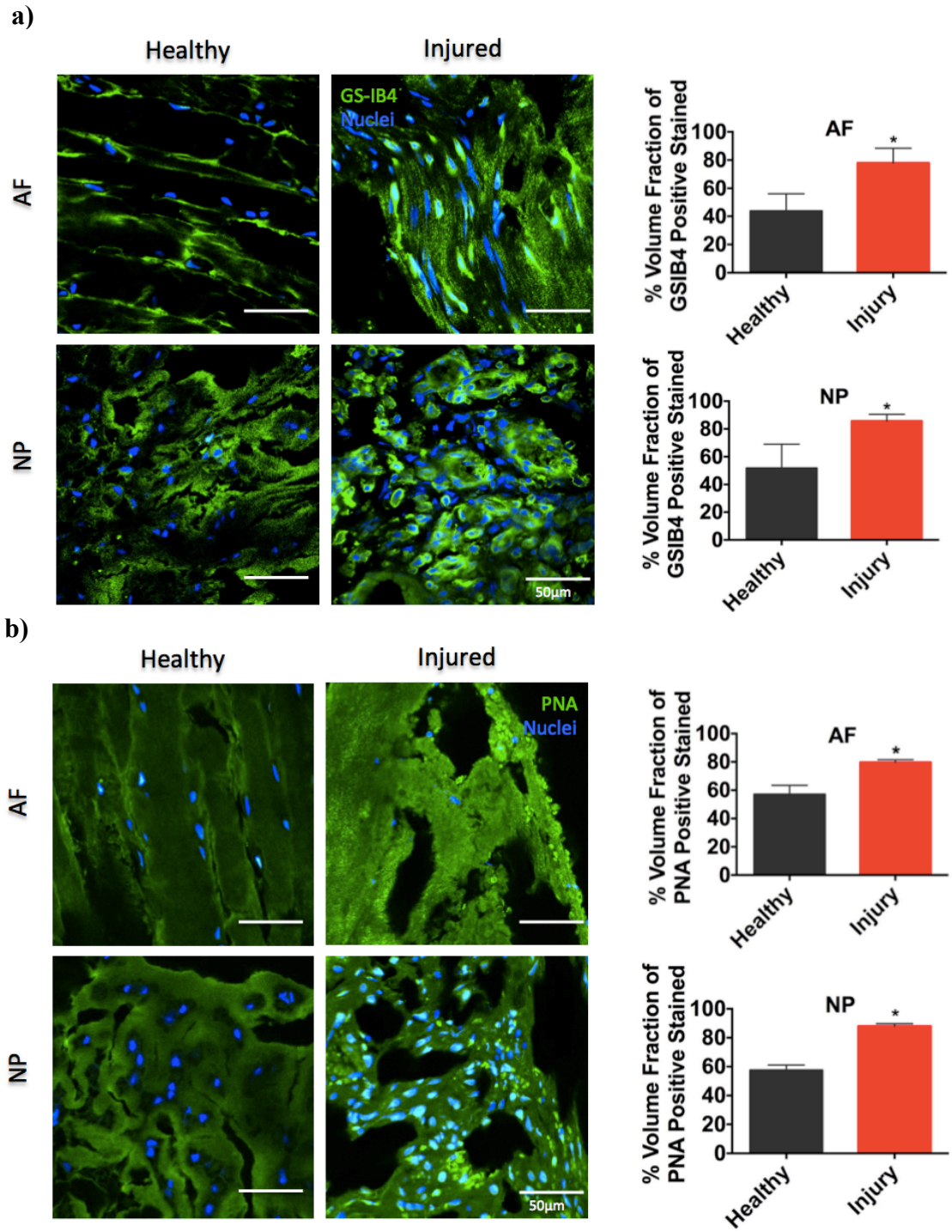
a)
Healthy
Injured
AF
NP
GS-IB4
Nuclei
50µm
% Volume Fraction of GSIB4 Positive Stained
AF
NP
Healthy
Injury
b)
PNA
Nuclei
% Volume Fraction of PNA Positive Stained

Continued

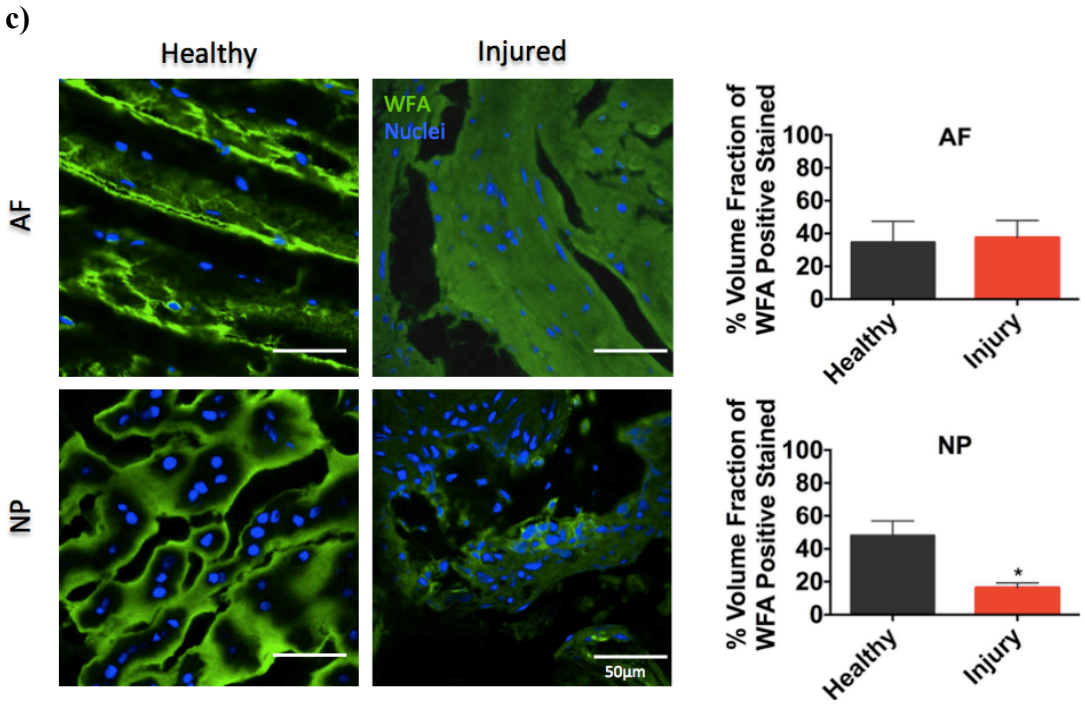

Figure 3.8 Glycosignatures in response to intervertebral disc injury. (a-b) PNA binds to non-sialylated Gal-β-(1,3)-GalNAc, and GS-I-B4 binds to terminal α-galactose. Binding of PNA and GS-I-B4 was higher in AF and NP tissues in injured than in uninjured rats. (c) WFA binds to either α-linked or β-linked terminal GalNAc, including that in chondroitin sulfate. Binding of WFA was lower in NP tissues in injured than in uninjured rats. n = 3 rats per group. *Significant differences between groups, by t-test (p <0.05). Area fraction data were normalized to the total area and are presented as the mean ± standard error of the mean. Scale bar = 50 µm.

a)

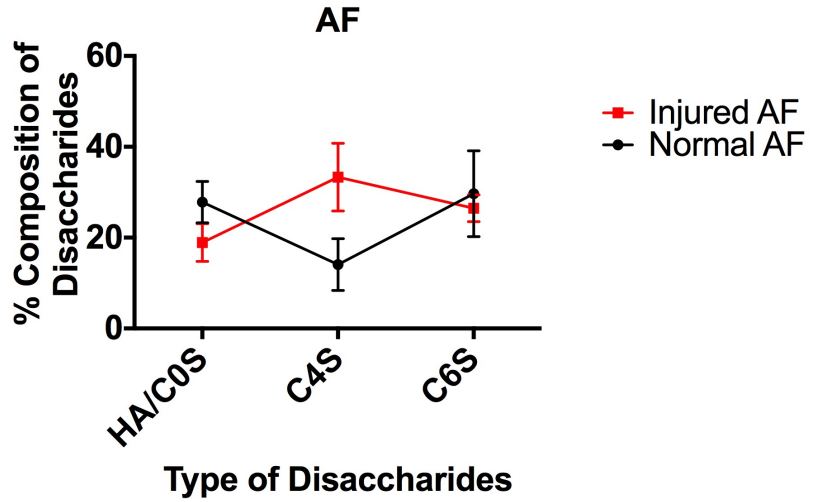

b)

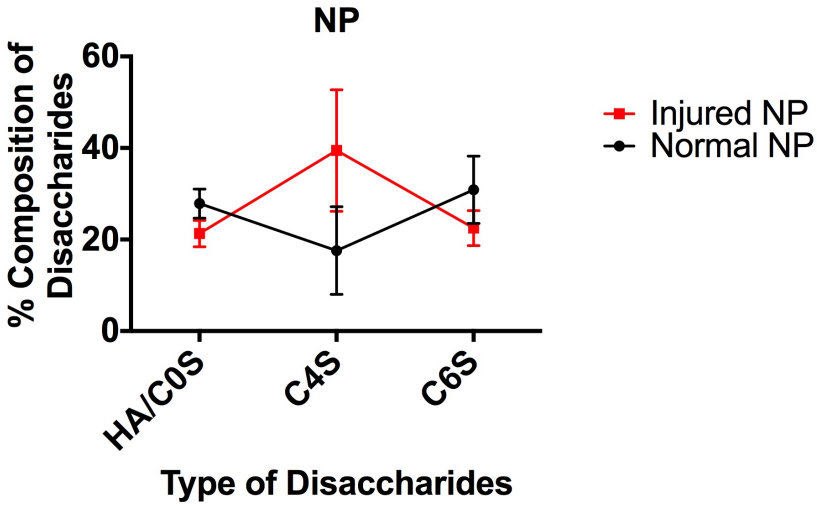

Figure 3.9 Sulfation patterns in response to intervertebral disc injury. Quantification of hyaluronic acid (HA) and the variously sulfated chondroitin sulfate disaccharides (C0S, C4S and C6S) by HPLC in (a) AF and (b) NP tissues. n = 3 rats per group. *Significant differences between groups, by one-way ANOVA (p <0.05).

a)

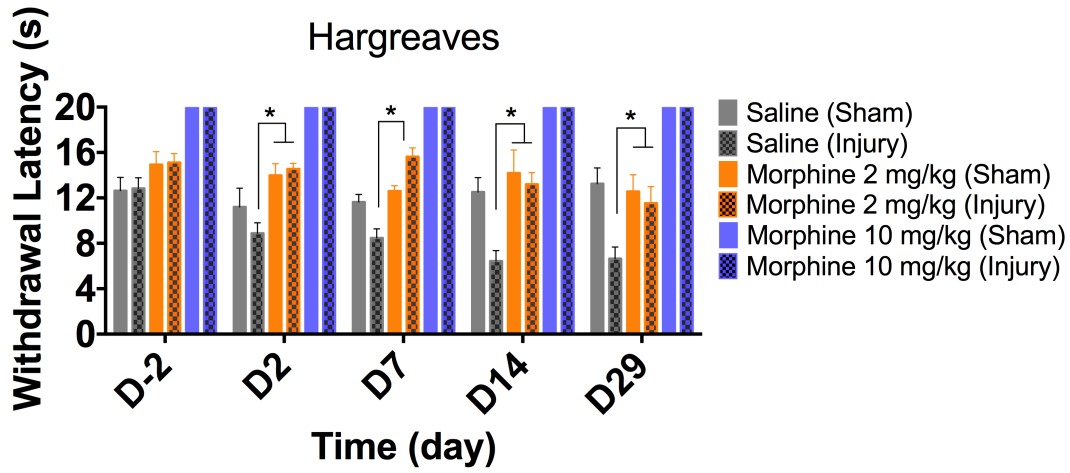

b)

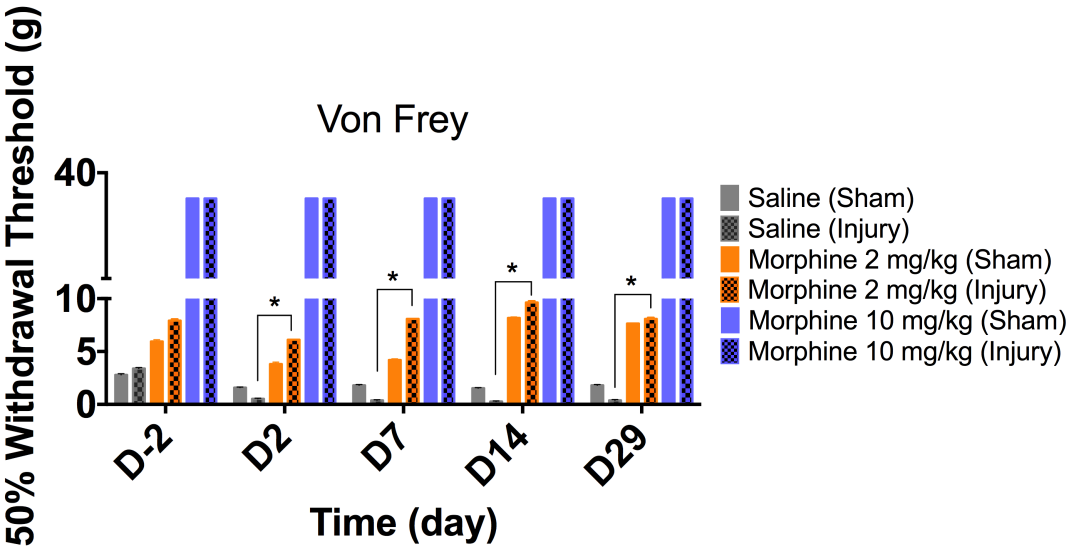

Continued

c)

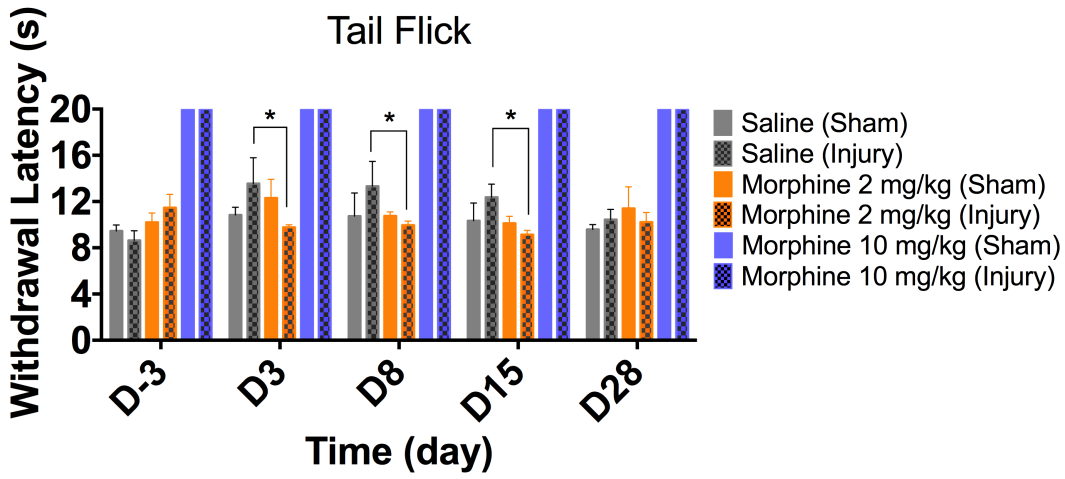

Figure 3.10 Alleviation of the injury-induced pain phenotype by morphine treatment. (a) Low-dose (2 mg/kg) morphine injection 30 min prior to the Hargreaves test of thermal sensitivity resulted in significantly higher withdrawal latency times than in injured rats without morphine. No test response was observed in rats with high-dose (10 mg/kg) morphine. (b) Low-dose morphine injection prior to the von Frey test of mechanical sensitivity resulted in significantly higher 50% withdrawal thresholds than in injured rats without morphine. No test response was observed in rats with high-dose morphine. (c) Low-dose morphine injection prior to the tail-flick test of thermal sensitivity resulted in significantly lower withdrawal latency times than in injured rats without morphine. No test response was observed in rats with high-dose morphine. n = 5 rats per group. *Significant difference between groups, by one-way ANOVA (p <0.05).

3.5.2.2 Morphine Alleviates Mechanical Hyperalgesia

von Frey testing demonstrated that, on days 2, 7 and 14, the 50% withdrawal threshold was significantly higher in the injury group with low-dose morphine than in the injury group with saline treatment (one-way ANOVA, $n = 5$, $p < 0.05$; Figure 3.10b), indicating that morphine alleviated mechanical allodynia in the rat tail close to the site of injury. Rats that received a high dose of morphine exhibited the maximum withdrawal threshold.

3.5.2.3 Morphine Reverses Thermal Hypoalgesia

In the tail-flick test on days 3, 8 and 15, withdrawal latency was significantly lower in the injury groups with low-dose morphine than with saline treatment (one-way ANOVA, $n = 5$, $p < 0.05$; Figure 3.10c), suggesting that morphine alleviated thermal hypoalgesia in the rat tail when the thermal stimulus was not close to the injury site. Rats that received a high dose of morphine were cataleptic, and did not respond to the stimulus within the timeframe of the test.

3.6 Discussion

So far this is the first study to establish a model of painful or symptomatic disc degeneration in the rat tail. A surgical-puncture-induced disc injury was performed at the coccygeal/caudal level to obtain robust pain behavior in rats, which persisted for at least one month, as shown by quantitative sensory testing [15]. Post-mortem, spinal molecular markers of nociception, structural disc degeneration and glycosylation changes were observed in the disc in this model.

The dermatomes (skin regions) and IVD involved in the study are innervated by dorsolateral and ventrolateral caudal nerves that arise from the sacral (S1–S4) and coccygeal (Co1–Co3) segments of the spinal cord [16-18-] (Figure 3.2a). Thermal and mechanical stimuli were applied to the ventral surface of the proximal tail in the Hargreaves and von Frey tests. The Hargreaves and tail-flick tests measure thermal nociception processing, and can assess heat-related hyperalgesia, which is the increased sensitivity to a noxious, high-intensity thermal stimulus, suggesting activation of Aδ and C fibers of primary sensory neurons [10][19]. The Hargreaves test identified thermal hyperalgesia close to the site of injury in the rat tail, with a significantly reduced latency in the injured condition as compared to that of the sham condition.

A von Frey test, with application of different fibers, each of which produced a particular, constant force [10][20] identified mechanical allodynia in the injured rat tail. Previously published results have also demonstrated that annular puncture in lumbar discs evokes mechanical and thermal hyperalgesia in rats [21]. The tail-flick test identified thermal hypoalgesia with stimulus of a region of the rat tail distal to the site of injury, suggesting that the DNIC phenomenon occurred when nociceptive or noxious stimulation was applied outside of the receptive field corresponding to the injury. DNIC is supraspinally mediated, and can inhibit multi-receptive wide-dynamic-range neurons in the dorsal horn of the spinal cord, leading to situations in which pain inhibits pain [22]. Therefore, altered endogenous descending pain modulation by DNIC has been suggested as a mechanism underlying chronic pain [22] that could explain hypoalgesia phenomenon in the proximal rat tail of this model.

Previously, physiological stimulation of afferent sensory neurons in rats has been shown to cause *c-Fos*-like immunoreactivity in the nuclei of dorsal-horn post-synaptic neurons, indicating that *c-Fos* is induced by neuropeptides known to be present in small-diameter sensory neurons [24]. Here, we observed significant upregulation of *c-Fos* mRNA in the left spinal cord dorsal horn at the sacral segment in disc injuries involving the Co4–Co5 and Co4–Co5 + Co5–Co6 groups, suggesting that thermal stimulation on proximal rat tail activates nociceptive sensory neurons during the injury, thereby induces central sensitisation in the dorsal horn of spinal cord.

Histological analysis in rats with IVD injury revealed structural disc degeneration, with annular rupture, reduction in the number of collagen fibers in AF tissue, clustered NP cells, chondroid nests in NP cells, reduction in GAG content in the ECM, and formation of fibrotic tissue in both AF and NP tissues. These anatomical disruptions caused by IVD injury which represent pathological events during disc degeneration.

Glycosylation has important roles in biological processes including angiogenesis, inflammation, adhesion, differentiation, homing and trafficking, signaling, cell–cell and cell–ECM interactions [25]. Here, higher levels of sialylation in injured disc was observed, which is in line with a previous demonstration of high levels of sialylation in inflamed or degenerated human chondrocytes [26-27]. Fully

sialylated β_1 subunits of voltage-gated sodium channels are known to induce uniform, hyperpolarizing shifts in channel gating, thereby being responsible for the initiation and propagation of neuronal action potentials [28]. The results show that surgical-puncture-induced IVD injury is associated with altered glycosylation and degenerative changes in the disc, including neurotransmission, inflammation and an imbalance of catabolic and anabolic processes. Disc degeneration may involve the interaction of altered ECM and cell-surface glycoconjugates with endogenous lectins (such as sialic acid-binding immunoglobulin-type lectins, integrins or CD44) [26].

Alteration of fucosylation is one of most common modifications associated with oligosaccharides on glycoproteins during tumorigenesis and inflammation [29]. In mice, cell-surface fucosylation is regulated via phospholipase Cγ by neural cell adhesion molecule L1 to modulate neurite outgrowth, cell survival and migration [30], and epithelial fucosylation is highly upregulated in intestinal inflammation [31]. In this model, UEA-I binding in NP and AF tissues was significantly higher in injured than in uninjured rats (Figure 3.7b), as was binding of Con A, which indicates the presence of high-mannose-type glycosylation (Figure 3.7a), and of both GS-I-B4 and PNA, which indicate galactosylation (Figure 3.8a-b). Previously, PNA binding was demonstrated in severely degenerated human cartilage [27] and levels of PNA binding to rat pheochromocytoma-derived PC12 cells increased from baseline four days after injury was induced *in vitro* [32]. GS-I-B4 has been used as a marker for neurons sensitive to glial-cell-derived neurotrophic factor, which have been identified in lumbar DRGs, where they were associated with the axonal growth potential of the innervating disc under inflammatory insult [33]. In the development of vertebrae, GalNAc has a key role in differentiation of MSCs into chondroblasts [34]. Here, WFA binding to GalNAc was observed only in the ECM of AF and NP tissues, and this binding was significantly lower in NP tissue (but not in AF tissue) after injury was induced, compared with uninjured tissues (Figure 3.8c). This observation is consistent with previous results that showed a loss of GalNAc in neuronal degenerative disease [35].

To validate this model, pain was inhibited with morphine at low and high doses prior to testing pain behavior (Figure 3.1a, ii). Morphine is an opioid drug that targets the central and peripheral nervous systems, with an affinity for the μ-opioid receptor that is apparently coupled via G-proteins to K^+ channels and voltage-

sensitive Ca^{2+} channels. Morphine reduces Ca^{2+} influx or increases K^{+} efflux, thereby decreasing repolarization time and the duration of the action potential, and inhibiting the release of neurotransmitters (including noradrenaline, acetylcholine and substance P) at presynaptic neurons, to produce an analgesic effect [36]. An inhibitory effect of low-dose morphine was observed on injury-induced thermal hyperalgesia and mechanical allodynia in response to stimuli applied to the tail close to the injury site (Figure 3.10a-b). By contrast, high-dose morphine prevented observation of responses to these stimuli. Low-dose morphine also inhibited injury-induced thermal hypoalgesia to a stimulus applied to the tail distal to the injury site (Figure 3.10c), suggesting inhibition of the DNIC phenomenon. Systemic morphine administration has previously been shown to inhibit supraspinal inhibitory control of dorsal-horn convergent neurons when noxious stimuli are applied [37]. No tail-flick response was observed in the rats treated with high-dose morphine, because high doses of morphine induce a state of catalepsy, which is clinically manifested by muscle rigidity, akinesia, a lack of spontaneous activity and failure to correct an externally imposed posture [38].

In summary, an IVD-injury model for study of pain associated with disc degeneration has been demonstrated. Although this model is restricted to inflammatory pain (not radicular pain) and lack of biomechanical elements as it is adopted in non-load bearing animal, however it can provides a relatively simple platform for investigation of potential IVD interventions.

3.7 Conclusions

The development of pain, anatomical degeneration and distinct glycosylation in a rat tail model of disc degeneration was established in this study. Current analgesic treatment (morphine) reverses pain phenotype that validates this model.

3.8. References

[1] B. G. Peng, “Pathophysiology, diagnosis, and treatment of discogenic low back pain,” *World J. Orthop.*, vol. 4, no. 2, pp. 42–52, 2013.

[2] L. Quero, M. Klawitter, A. Schmaus, M. Rothley, J. Sleeman, A. N. Tiaden, J. Klasen, N. Boos, M. O. Hottiger, K. Wuertz, and P. J. Richards, “Hyaluronic acid fragments enhance the inflammatory and catabolic response in human intervertebral disc cells through modulation of toll-like receptor 2 signalling

pathways," *Arthritis Res. Ther.*, vol. 15, no. 4, p. R94, Jan. 2013.

[3] J. M. Lee, J. Y. Song, M. Baek, H. Y. Jung, H. Kang, I. B. Han, Y. Do Kwon, and D. E. Shin, "Interleukin-1β induces angiogenesis and innervation in human intervertebral disc degeneration," *J. Orthop. Res.*, vol. 29, no. 2, pp. 265–9, Mar. 2011.

[4] A. J. Freemont, A. Watkins, C. Le Maitre, P. Baird, M. Jeziorska, M. T. N. Knight, E. R. S. Ross, J. P. O'Brien, and J. A. Hoyland, "Nerve growth factor expression and innervation of the painful intervertebral disc," *J. Pathol.*, vol. 197, no. 3, pp. 286–92, Jul. 2002.

[5] S. M. Richardson, D. Purmessur, P. Baird, B. Probyn, A. J. Freemont, and J. A. Hoyland, "Degenerate human nucleus pulposus cells promote neurite outgrowth in neural cells," *PLoS One*, vol. 7, no. 10, p. e47735, Jan. 2012.

[6] A. J. Freemont, T. E. Peacock, P. Goupille, J. A. Hoyland, J. O. Brien, and M. I. V Jayson, "Early report nerve ingrowth into diseased intervertebral disc in chronic back pain," *Lancet*, vol. 350, pp. 178–181, 1997.

[7] J. García-Cosamalón, M. E. del Valle, M. G. Calavia, O. García-Suárez, A. López-Muñiz, J. Otero, and J. A. Vega, "Intervertebral disc, sensory nerves and neurotrophins: who is who in discogenic pain?," *J. Anat.*, vol. 217, no. 1, pp. 1–15, Jul. 2010.

[8] X. Zhang, J. Huang, and P. A. McNaughton, "NGF rapidly increases membrane expression of TRPV1 heat-gated ion channels.," *EMBO J.*, vol. 24, no. 24, pp. 4211–23, Dec. 2005.

[9] M. Alini, S. M. Eisenstein, K. Ito, C. Little, A. A. Kettler, K. Masuda, J. Melrose, J. Ralphs, I. Stokes, and H. J. Wilke, "Are animal models useful for studying human disc disorders/degeneration?," *Eur. Spine J.*, vol. 17, no. 1, pp. 2–19, Jan. 2008.

[10] D. Le Bars, M. Gozariu, and S. W. Cadden, "Animal models of nociception," *Pharmacol. Rev.*, vol. 53, no. 4, pp. 597–652, 2001.

[11] J. P. H. J. Rutges, R. A. Duit, J. A. Kummer, J. E. J. Bekkers, F. C. Oner, R. M. Castelein, W. J. A. Dhert, and L. B. Creemers, "A validated new

histological classification for intervertebral disc degeneration.," *Osteoarthritis Cartilage*, vol. 21, no. 12, pp. 2039–47, Dec. 2013.

[12] J. P. Thompson, R. H. Pearce, M. T. Schechter, M. E. Adams, I. K. Tsang, and P. B. Bishop, "Preliminary evaluation of a scheme for grading the gross morphology of the human intervertebral disc," *Spine (Phila. Pa. 1976).*, vol. 15, no. 5, pp. 411–415, 1990.

[13] E. C. Collin, M. Kilcoyne, S. J. White, S. Grad, M. Alini, L. Joshi, and A. Pandit, "Unique glycosignature for intervertebral disc and articular cartilage cells and tissues in immaturity and maturity," *Sci. Rep.*, vol. 6, no. October 2015, p. 23062, 2016.

[14] A. H. Ahmad and Z. Ismail, "*c-Fos* and its consequences in pain," *Malaysian J. Med. Sci.*, vol. 9, no. 1, pp. 3–8, 2002.

[15] M. Mücke, H. Cuhls, L. Radbruch, R. Baron, C. Maier, T. Tölle, R. D. Treede, and R. Rolke, "Quantitative sensory testing (QST)," *Der Schmerz*, DOI: 10.1007/s00482-015-0093-2, pp. 1–8, 2016.

[16] I. M. Jou, "The experimental study of the investigagtion of the pathogenesis and electrodiagnostic significance of radicupathy," 1991.

[17] H. H. Schaumburg, E. Zotova, C. S. Raine, M. Tar, and J. Arezzo, "The rat caudal nerves: A model for experimental neuropathies.," *J. Peripher. Nerv. Syst.*, vol. 15, no. 2, pp. 128–39, 2010.

[18] S. Orita, S. Ohtori, and A. Taniguchi, "Direct evidence for sensory innervation of the dorsal portion of the Co5/6 coccygeal intervertebral disc in rats," *Spine (Phila. Pa. 1976).*, vol. 35, no. 14, pp. 1346–1352, 2010.

[19] J. W. Allen and T. L. Yaksh, "Assessment of acute thermal nociception in laboratory animals," *Methods Mol. Med.*, vol. 99, no. 1, pp. 11–23, 2004.

[20] H. Fruhstorfer, W. Gross, and O. Selbmann, "Von Frey hairs: New materials for a new design," *Eur. J. Pain*, vol. 5, no. 3, pp. 341–342, 2001.

[21] A. Lai, A. Moon, D. Purmessur, B. Skovrlj, B. A. Winkelstein, S. K. Cho, A. C. Hecht, and J. C. Iatridis, "Assessment of functional and behavioral changes sensitive to painful disc degeneration," *J Orthop Res*, vol. 33, no. 5, pp. 755–

764, 2015.

[22] G. van Wijk and D. S. Veldhuijzen, "Perspective on diffuse noxious inhibitory controls as a model of endogenous pain modulation in clinical pain syndromes," *J. Pain*, vol. 11, no. 5, pp. 408–419, 2010.

[23] M. M. Morgan and P. K. Whitney, "Behavioral analysis of diffuse noxious inhibitory controls (DNIC): Antinociception and escape reactions," *Pain*, vol. 66, no. 2–3, pp. 307–312, 1996.

[24] S. P. Hunt, A. Pini, and G. Evan, "Induction of *c-Fos*-like protein in spinal cord neurons following sensory stimulation," *Nature*, vol. 328, no. 6131, pp. 632–634, 1987.

[25] R. S. Haltiwanger and J. B. Lowe, "Role of glycosylation in development," *Annu. Rev. Neurosci.*, vol. 73, pp. 491–537, 2004.

[26] M. Pabst, S. Q. Wu, J. Grass, A. Kolb, C. Chiari, H. Viernstein, F. M. Unger, F. Altmann, and S. Toegel, "IL-1β and TNF-α alter the glycophenotype of primary human chondrocytes *in vitro*," *Carbohydr. Res.*, vol. 345, no. 10, pp. 1389–1393, 2010.

[27] S. Toegel, D. Bieder, S. André, F. Altmann, S. M. Walzer, H. Kaltner, J. G. Hofstaetter, R. Windhager, and H. J. Gabius, "Glycophenotyping of osteoarthritic cartilage and chondrocytes by RT-qPCR, mass spectrometry, histochemistry with plant/human lectins and lectin localization with a glycoprotein," *Arthritis Res. Ther.*, vol. 15, p. R147, 2013.

[28] D. Johnson, M. L. Montpetit, P. J. Stocker, and E. S. Bennett, "The sialic acid component of the β1 subunit modulates voltage-gated sodium channel function," *J. Biol. Chem.*, vol. 279, no. 43, pp. 44303–44310, 2004.

[29] J. Li, H. C. Hsu, Y. Ding, H. Li, Q. Wu, P. Yang, B. Luo, A. L. Rowse, D. M. Spalding, S. L. Bridges, and J. D. Mountz, "Inhibition of fucosylation reshapes inflammatory macrophages and suppresses type II collagen-induced arthritis," *Arthritis Rheum*, vol. 66, no. 9, pp. 2368–2379, 2014.

[30] Y. L. Li, G. Z. Wu, G. S. Dawe, L. Zeng, S. Sen Cui, G. Loers, T. Tilling, L. Sun, M. Schachner, and Z. C. Xiao, "Cell surface sialylation and fucosylation

are regulated by L1 via phospholipase Cγ and cooperate to modulate neurite outgrowth, cell survival and migration," *PLoS One*, vol. 3, no. 12, 2008.

[31] Y. Goto, A. Lamichhane, M. Kamioka, S. Sato, K. Honda, J. Kunisawa, and H. Kiyono, "IL-10-producing CD4+ T cells negatively regulate fucosylation of epithelial cells in the gut," *Sci. Rep.*, vol. 5, p. 15918, 2015.

[32] M. Kilcoyne, S. Sharma, N. McDevitt, C. O'Leary, L. Joshi, and S. S. McMahon, "Neuronal glycosylation differentials in normal, injured and chondroitinase-treated environments," *Biochem. Biophys. Res. Commun.*, vol. 420, no. 3, pp. 616–622, 2012.

[33] Y. Aoki, H. S. An, K. Takahashi, K. Miyamoto, M. E. Lenz, H. Moriya, and K. Masuda, "Axonal growth potential of lumbar dorsal root ganglion neurons in an organ culture system: response of nerve growth factor-sensitive neurons to neuronal injury and an inflammatory cytokine," *Spine (Phila. Pa. 1976).*, vol. 32, no. 8, pp. 857–63, Apr. 2007.

[34] M. M. H. Taheri, A. R. E. Bideskan, and M. R. Miri, "Regulatory changes of n-acetylgalactosamine terminal sugar in early mouse embryonic paraxial mesenchyme," *Cell J.*, vol. 14, no. 2, pp. 130–141, 2012.

[35] S. Baig, G. K. Wilcock, and S. Love, "Loss of perineuronal net N-acetylgalactosamine in Alzheimer's disease," *Acta Neuropathol.*, vol. 110, no. 4, pp. 393–401, 2005.

[36] L. A. Chahl, "Experimental and clinical pharmacology: Opioids - mechanisms of action," *Aust. Prescr.*, vol. 19, no. 3, pp. 63–65, 1996.

[37] D. Le Bars, D. Chitour, E. Kraus, A. M. Clot, A. H. Dickenson, and J. M. Besson, "The effect of systemic morphine upon diffuse noxious inhibitory controls (DNIC) in the rat: evidence for a lifting of certain descending inhibitory controls of dorsal horn convergent neurones," *Brain Res.*, vol. 215, no. 1–2, pp. 257–274, 1981.

[38] E. A. Afify, T. T. Daabees, B. H. Gabra, and M. S. Abou Zeit-Har, "Role of nitric oxide in catalepsy and hyperthermia in morphine-dependent rats," *Pharmacol. Res.*, vol. 44, no. 6, pp. 533–539, 2001.

Chapter 4

The Efficacy of Hyaluronic Acid Hydrogel in a Painful Intervertebral Disc Degeneration Model

Sections of this chapter are in preparation for submission:

Isa I. L. M., Abbah S. A., Kilcoyne M., Sakai D., Dockery P., Finn D. P., Pandit A. Implantation of hyaluronic acid hydrogel prevents the pain phenotype in a rat model with intervertebral disc injury, to be submitted to

4.1 Introduction

Hyaluronic acid (HA), or hyaluronan, is a ubiquitously expressed glycosaminoglycan (GAG) molecule that is located in the extracellular matrix (ECM) and the intracellular environment, and on the cell surface [1]. In physiological conditions, HA typically presents as a high-molecular-weight molecule of $\leq 2 \times 10^4$ kDa, containing around 10,000 alternating units of glucuronic acid and N-acetyl glucosamine (GlcNAc), with β-(1,3) and β-(1,4) linkages [2]. HA is synthesized in the cellular plasma membrane by HA synthases [3], and secreted into the pericellular space via a multidrug-resistance transporter [4]. HA interacts with specific proteins, including aggrecan, versican, lymphatic vessel endothelial HA receptor 1, tumor necrosis factor-inducible gene 6 protein and thrombospondin, as well as membrane receptors, such as CD44, hyaluronan mediated motility receptor and Toll-like receptor 4/2. These interactions are vital for multiple biological processes, including morphogenesis, cell migration, cell survival, apoptosis, inflammation and tumorigenesis [1]. In intervertebral discs (IVDs), the HA chain is aggregated with proteoglycans, such as aggrecan. Proteoglycans consist of core proteins that are modified extensively with anionic sulfated GAGs, such as chondroitin sulfate and keratan sulfate. Proteoglycans enable the generation of osmotic swelling pressure during the maintenance of tissue hydration [5].

The use of HA in tissue engineering to target multiple signaling pathways underlying painful disc degeneration is a potential therapeutic strategy for disc repair. Several different formulations of HA–poly(ethylene glycol) (PEG) hydrogels have been shown to increase formation of multi-cell clusters on seeding with NP or annulus fibrosus (AF) cells, compared with gelatin substrates [6]. In a nucleotomized-organ-culture model, treatment with biomimetic fibrin–HA hydrogel can maintain NP-cell viability at >90%, increase production of GAGs and type II collagen and restore compressive stiffness and disc height, compared with fibrin gels [7]. Furthermore, a type II collagen–HA hydrogel can preserve the viability of mesenchymal stem cells (MSCs) and their differentiation into a chondrogenic lineage *in vitro* [8]. Previously, a hydrogel comprising type II collagen was fabricated and crosslinked to PEG ether tetrasuccinimidyl glutarate (4S-StarPEG) enriched with HA, and this hydrogel increased NP-cell viability and maintained collagen expression in all groups with various molar ratio of HA–collagen [9]. It was

demonstrated that type II collagen–4S-StarPEG–HA microgels resulted in differentiation of adipose-derived stem cells towards an NP-like phenotype [10]. These findings suggest that HA shows potential use as a reservoir system for intervertebral disc regeneration.

Therapeutic applications of high-molecular-weight HA have been shown to facilitate long-term functional improvements by attenuating inflammation and pain in a number of clinical conditions, including osteoarthritis (OA), post-ophthalmic surgery, seborrheic dermatitis and neoplasmic-resection surgery [11-14]. The pre-clinical studies have demonstrated reduction of movement-evoked impulse activities of inflamed knee joints via a blockade of nociceptive sensory–afferent activity after treatment with a high-elastoviscosity HA formulation [15]. Compared with control solutions, HA solutions decrease transient receptor potential cation channel subfamily V member 1 (TRPV1)-mediated impulse firing and channel sensitization in DRG cultures and reduced both heat-induced and capsaicin-induced nocifensive responses in rodents, and intra-articular injections of HA decrease capsaicin responsiveness of joint nociceptor fibers [16]. Topical application of HA decreased expression levels of IL-1β in the epidural space and IL-6 around the nerve root, and ameliorates scar formation in a lumbar post-laminectomy disc model in rats [17]. In case of IVD degeneration, the therapeutic effects of a cross-linked HA–PEG hydrogel have been reported in attenuating inflammation and expression of neurotrophic factors by binding to CD44 in inflamed NP cells [18]. Nonetheless, the mechanisms by which HA targets inflammatory pain in disc degeneration are not currently established.

Herein, the therapeutic efficacy of HA hydrogel was determined in a validated pre-clinical model of pain associated with symptomatic disc degeneration in the rat tail. It was hypothesized that HA hydrogel treatment would subsequently alleviate nociceptive behavior, inhibit sensory hyper-innervation and expression of peripheral pro-nociceptive receptors TRPV1 and high affinity nerve growth factor receptor (Trk-A) *in vivo*, down-regulate mRNA expression of the spinal nociception markers *c-Fos* and *Tac1* (which encodes substance P), and regulate the glycomic signature and proteomic expression to modulate inflammatory and protein-regulatory pathways in both NP and AF tissues.

4.2 Materials and Methods

4.2.1 Materials and Reagents

Sodium hyaluronate (MW 1.19 × 10^6 Da) was purchased from Lifecore Biomedical (Chaska, MN, USA). 4-arm PEG-amine (MW 2,000 Da) was purchased from JenKem Technology (Plano, TX, USA). Teflon tape, Superfrost™ Plus slides, 3 kDa centrifugal filters and scalpel handle number three were purchased from Fisher Scientific (Dublin, Ireland). The RNeasy Mini kit was purchased from Qiagen (Hilden, Germany). Carprofen was purchased from Pfizer (Sandwich, UK). Isoflurane was purchased from Chanelle Group (Loughrea, Ireland). Saline (0.9% (w/v) sodium chloride) was purchased from B. Braun Medical (Dublin, Ireland). Bone-cutting forceps, teeth forceps and iris scissors were purchased from Fine Science Tools (Heidelberg, Germany). A 1-mm biopsy puncher with a plunger, artery forceps and a needle holder were purchase from Medguard (Ashbourne, Ireland). von Frey filaments was purchased from North Coast Medical Inc. (Gilroy, CA, USA). An analgesic meter and six-compartment of rat enclosure (arena) were purchased from IITC Life Science (Woodland Hills, CA, USA). Random primers, reverse transcriptase, 5× Reaction Buffer, 25 mM $MgCl_2$, dNTP mix and recombinant RNasin ribonuclease were purchased from Bioline (Dublin, Ireland). TaqMan® FAM™-labelled preprotachykinin (Substance P Precursor; *Tac1*) primers (Rn01500392_m1) and *c-Fos* primers (Rn00487426_g1) were purchased from Life Technologies (Dublin, Ireland). TaqMan VIC™-labeled rodent glyceraldehyde-3-phosphate dehydrogenase (*Gapdh*) primer and Universal PCR Master Mix were purchased from Applied Biosystems (Dublin, Ireland). Lectins conjugated with fluorescein isothiocyanate (FITC) or tetramethylrhodamine isothiocyanate (TRITC) were purchased from EY Laboratories (San Mateo, CA, USA). Rabbit polyclonal anti-GAP43 (ab12274), mouse monoclonal anti-CGRP (ab81887), donkey anti-rabbit IgG (Alexa Fluor® 555 conjugate; ab150074), rabbit monoclonal anti-Trk-A (Alexa Fluor 647 conjugate; ab194322), rabbit polyclonal anti-fibronectin (ab2413), mouse monoclonal anti-TGF-β1 (ab64715) and donkey anti-goat IgG (Alexa Fluor 488; ab150129) antibodies were purchased from Abcam (UK). Goat polyclonal anti-TRPV1 (AF3066) and rabbit polyclonal anti-keratan-sulfate (NBP1-62542) antibodies were purchased from Novus Biologicals (Littleton, CO, USA). Mouse monoclonal anti-chondroitin-sulfate antibody (C8035) was purchased from Sigma-

Aldrich (Arklow, Ireland). Goat anti-mouse IgG (Cy®5 conjugate; A10524) antibody was purchased from Thermo Fisher Scientific (Dublin, Ireland). FITC-conjugated rabbit polyclonal anti-COL1A1 (orb15412) and FITC-conjugated rabbit polyclonal anti-aggrecan (orb15073) antibodies were purchased from Biorbyt (Cambridge, UK). Rabbit polyclonal phospho-p38 MAPK (Thr180/Tyr182; Cat. 9211) and rabbit monoclonal phospho-NF-κB p65 (Ser536; Cat. 93H1) antibodies were purchased from Cell Signaling Technology (Danvers, MA, USA). 4,6-diamidino-2-phenylindole (DAPI) was purchased from Life Technologies. Multiplex ELISA pro-inflammatory panel 2 was purchased from Meso Scale Discovery (Rockville, Maryland, USA). Other materials and reagents were purchased from Sigma-Aldrich.

4.2.2 Animals

All animal-related protocols were performed in accordance with national guidelines and approved by the Animal Care Research Ethic Committee (ACREC) at the National University of Ireland, Galway and the Health Product Regulatory Authority (HPRA) Ireland. Experiments involved 69 adult (12-week-old) female Sprague–Dawley rats, which were housed two to three per cage in individually ventilated cages, with wood-chip bedding, enriched with a wooden stick. Food and centralized tap water were available *ad libitum*, lights were turned on at 06:00 h, the temperature was maintained at 21 ± 2°C, and the husbandry was provided by female staff. Rats were purchased from Charles River (Margate, UK), and acclimated to the vivarium for at least 7 days prior to testing. For the *in vivo* implantation of HA hydrogel, sample sizes were n = 10 for each group (sham isoflurane; Co4–Co5 + Co5–Co6 NP injury; and Co4–Co5 + Co5–Co6 NP injury with implanted HA hydrogel (4 μL (0.03 mg/ml)) with time-point day 7 (n = 10) and 29 (n = 10) (Figure 4.1a; Table 4.1a). For the *in vivo* injection of fluorescence-labeled HA hydrogel, sample sizes were n = 3 for each group (sham isoflurane; Co4–Co5 + Co5–Co6 NP injury; and Co4–Co5 + Co5–Co6 NP injury with injectable fluorescence-labeled HA hydrogel (5 μL (0.038 mg/mL)) with time-point day 2 (Table 4.1b).

4.2.3 Synthesis of Cross-linked Hyaluronic Acid Hydrogel

HA hydrogel was fabricated by mixing 0.75% (w/v) sodium hyaluronate (1.19×10^6 Da) in 1 mL of distilled water with 75 mM 4-arm PEG-amine, 15% (w/v) N-hydroxysuccinimide and 9% (w/v) 1-ethyl-3-(3-dimethylaminopropyl)carbodiimide.

Spherical hydrogel was obtained by pipetting 4 μL of mixed hydrogel solution (0.03 mg/mL) onto a hydrophobically modified glass slide (Figure 4.1b). The hydrogel was then washed with PBS and sterilized under ultraviolet light for 60 minutes, prior to implantation.

4.2.4 Quantitative Behavioural Nociception Assays

Rats were habituated to the arena test environment for twenty minutes, 24 hours prior to the commencement of testing, which minimized locomotor activity and stress-induced analgesia during testing. The same investigator performed the scoring in all behavioral tests, and was blinded to the experimental groups. The rats were assessed by the Hargreaves, von Frey and tail-flick tests.

4.2.4.1 von Frey Test

The von Frey test was carried out on days −3, 2, 7, 14 and 29. The rats were individually placed into six-compartment of rat enclosure (arena) with wire-mesh floors and lids with air holes for a twenty minutes habituation period to minimize exploratory activity. The test began with a 2 g filament, which was applied to the base of the tail on the ventral surface for a maximum of six seconds, with sufficient force to buckle it slightly. A positive response was considered to have occurred when the rats responded to the applied filament by flinching, licking, withdrawing or shaking base of the tail within the six seconds or immediately after the filament was removed. A negative response was recorded if the animal showed no response to the application of the filament. This process was repeated five times for the 2 g filament, giving a withdrawal frequency out of five for the tail tested. If a response was obtained with the 2g filament, it was tested with lower weight filaments until a 0/5 or 0% response was obtained. The test was continued with ascending filament numbers until a 5/5 or 100% response was obtained for two consecutive filaments. The individual percentage response from each time-point was further analysed using non-linear regression to generate exponential decay. The first output measurement was calculated as percentage (%) withdrawal response. This was calculated for test at each filament weight as follows:

$$\frac{\text{Number of positive responses}}{\text{Number of applications (5)}} \times 100$$

The second output measurement was the 50% withdrawal threshold. This was defined as the filament weight (or filament number) at which a 50% withdrawal response was obtained. The filament weight and the % response each day were tabulated for each individual animal. In XY data table of Graphpad Prism, filaments was tabulated in ascending order in the X column, and % response to each filament in each day was tabulated in separate Y column. A non-linear regression curve was ploted (sigmoidal dose-response, variable slope, set bottom and top constraints as 0 & 100 respectively) and the log EC_{50} was obtained from the results sheet. A log EC_{50} for each animal on each day was entered into a separate table (days in the X column and groups in separate Y columns, with each rat as a separate replicate). An average for each group was computed and plotted as von Frey filament weight eliciting a 50% response vs. time (days).

4.2.4.2 Hargreaves Test

The test was performed on days −3, 2, 7, 14 and 29 (relative to surgery). Rats were placed in six-compartment of rat enclosure (arena) on top of a glass plate (IITC, USA), to habituate for twenty minutes. Heat was introduced with a radiant light source, and latency to the response was recorded. Responses included withdrawal, flinching, licking, biting and shaking the base of the tail. The analgesic meter test head was positioned under the base of the tail, with the beam approximately focused on the ventral surface of the tail, which was opposite to the site of injury. The test head was set to 50% of the maximum output. When the rat responded, the light source was set to 'idle' intensity, and the heat source was deactivated. A cut-off of twenty seconds was set, to prevent tissue damage. If no response occurred in this time, the heat source was automatically returned to idle intensity. On each test day, each rat received four trials, with a minimum interval time of three minutes. Withdrawal latency for each rat was calculated as the average of the four measurements.

4.2.4.3 Tail Flick Test

The tail-flick test was performed on days −2, 3, 8, 15 and 28. On each day, the test for each rat involved four consecutive measurements. Each rat was removed from its home cage and habituated on a towel for ten minutes, then placed on the glass apparatus with its body covered with the towel as a restraint, such that its tail

a)

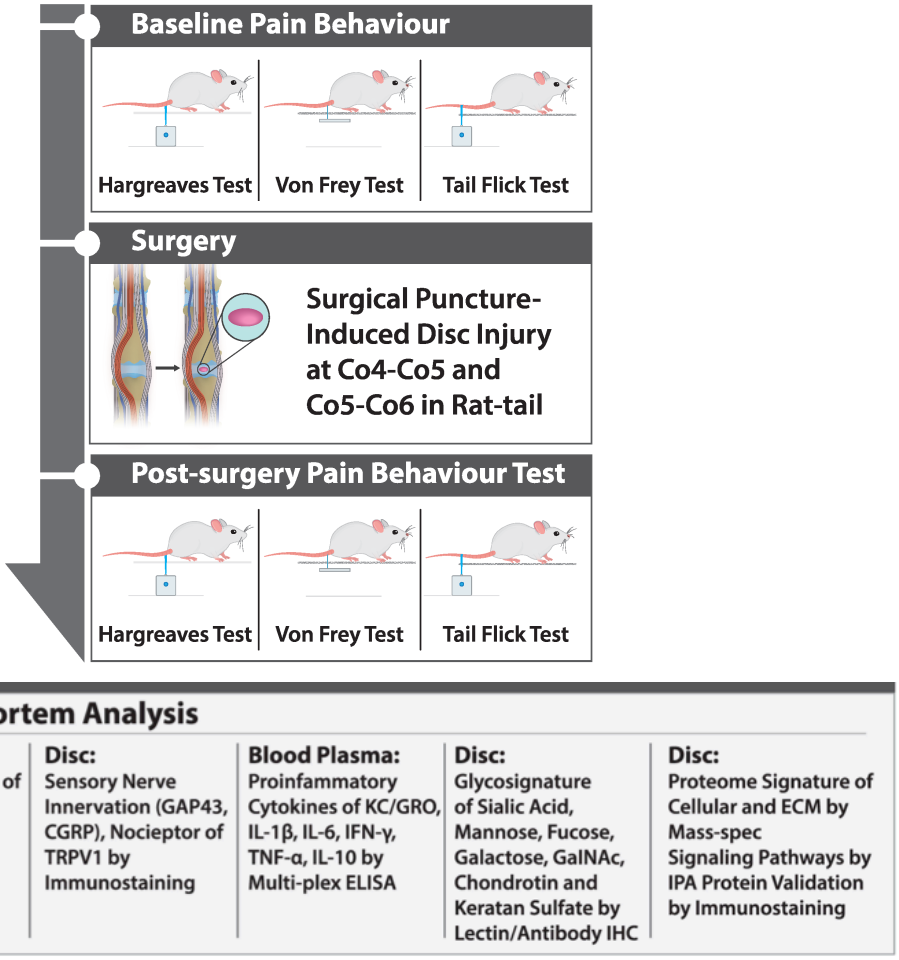
Baseline Pain Behaviour
Hargreaves Test
Von Frey Test
Tail Flick Test
Surgery
Surgical Puncture-Induced Disc Injury at Co4-Co5 and Co5-Co6 in Rat-tail
Post-surgery Pain Behaviour Test
Hargreaves Test
Von Frey Test
Tail Flick Test
Post-mortem Analysis
Spinal Cord: Molecular Marker of Nocieption cFos and Substance P by qPCR
Disc: Sensory Nerve Innervation (GAP43, CGRP), Nocieptor of TRPV1 by Immunostaining
Blood Plasma: Proinfammatory Cytokines of KC/GRO, IL-1β, IL-6, IFN-γ, TNF-α, IL-10 by Multi-plex ELISA
Disc: Glycosignature of Sialic Acid, Mannose, Fucose, Galactose, GalNAc, Chondrotin and Keratan Sulfate by Lectin/Antibody IHC
Disc: Proteome Signature of Cellular and ECM by Mass-spec Signaling Pathways by IPA Protein Validation by Immunostaining

Continued

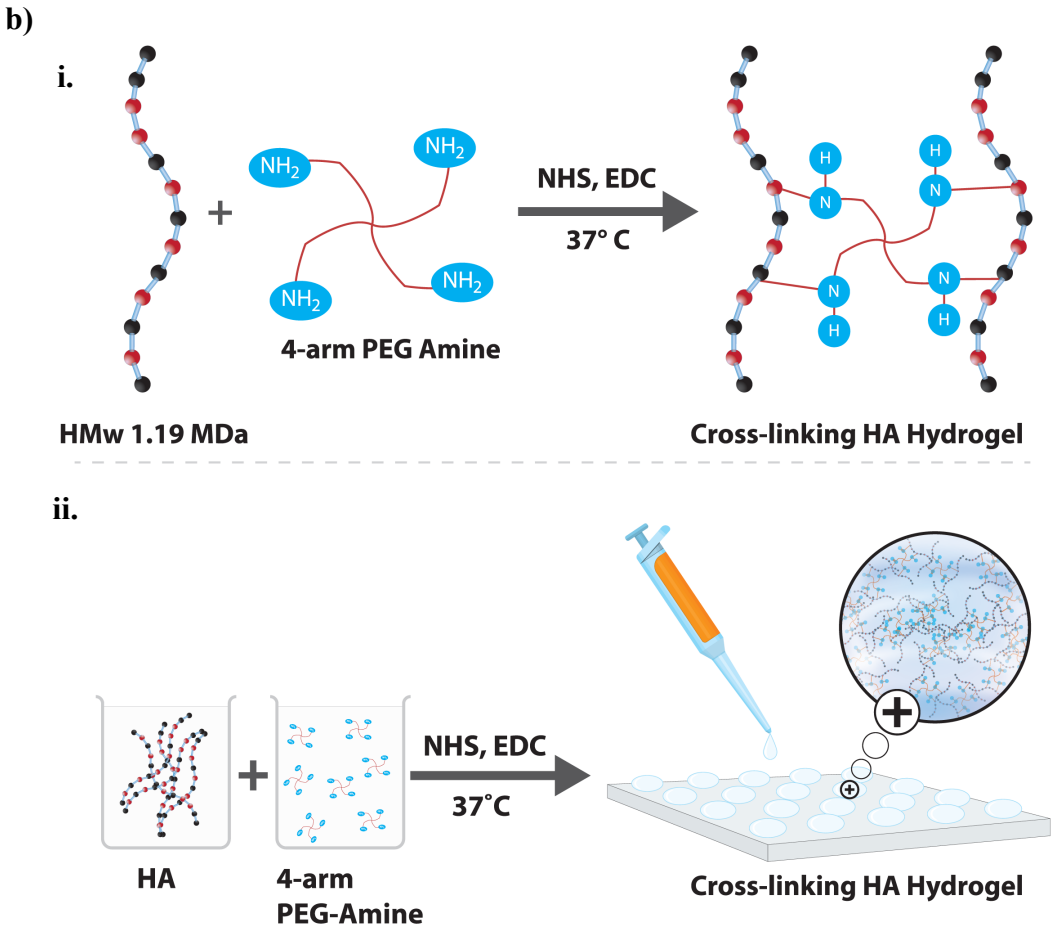

Figure 4.1 Schematic representations of the experimental design and procedures. (a) Phase III - Therapeutic efficacy of implanted hyaluronic acid (HA) hydrogel following IVD injury. Experimental design of therapeutic efficacy of implantation HA hydrogel following intervertebral disc injury. (b) Crosslinking of high-molecular weight HA and 4-arm poly(ethylene glycol) PEG amine. (i) After functionalization with N-hydroxysuccinimide (NHS) and 1-ethyl-3-(3-dimethylaminopropyl)carbodiimide (EDC), the amine groups of HA molecules react with the succinimidyl groups of PEG amine. (ii) Hydrogel for implantation were fabricated by pipetting 4 µL of a mixture of HA, PEG amine, NHS and EDC onto a hydrophobic surface, followed by incubation at 37°C for one hour to complete cross-linking.

Table 4.1 Sample size with a total of 69 rats were used for *in vivo* implantation (a) and injection of fluorescence-labeled HA hydrogel (b) in the intervertebral disc pre-clinical study of pain.

a)

Group	N	Time-point (days)
NP Injury (Co4-Co5 and Co5-Co6)	10	7, 29
NP Injury (Co4-Co5 and Co5-Co6) + Implantation HA Hydrogel 4 μL (0.03 mg/mL)	10	7, 29
Sham	10	7, 29
Total	**60**	

b)

Group	N	Time-point (days)
NP Injury (Co4-Co5 and Co5-Co6)	3	2
NP Injury (Co4-Co5 and Co5-Co6) + Injectable fluorescence-labeled HA Hydrogel 5 μL (0.038 mg/mL)	3	2
Sham	3	2
Total	**9**	

Table 4.2 Binding specificity and haptenic sugars of lectins for profiling of tissue glycosylation.

Lectin	**Binding specificity**	**Haptenic sugar (100 mM)**
SNA-I (*Sambucus nigra* agglutinin I)	Sialic acid-α-(2,6)–GalNAc–R	Lactose
MAA (*Maackia amurensis* agglutinin)	Sialic acid-α-(2,3)–GalNAc–R	Lactose
WGA (Wheat germ agglutinin)	Sialic acid, GlcNAc	GlcNAc
GS-I-B4 (*Griffonia simplicifolia* isolectin)	Terminal α-linked Gal	Gal
WFA (*Wisteria floribunda* agglutinin)	GalNAc and chondroitin sulfate	GalNAc

A haptenic sugar is a monosaccharide or disaccharide that can inhibit binding of a lectin. Abbreviations: Gal, galactose; GalNAc, N-acetylgalactosamine; GlcNAc, N-acetyl glucosamine.

projected out. A radiant light source was focused 5 cm from the distal end on the recorded. A cut-off point of twenty seconds was assigned, to prevent tissue damage. A period of at least fifteen seconds between each test was observed to avoid sensitisation of the tail. Tail-flick latency for each rat was calculated as the average of four consecutive measurements.

4.2.5 Implantation HA Hydrogel Following Surgical-puncture-induced IVD Injury

On day 0, general health measurements, including body weight and temperature, were recorded prior to surgery. A single administration of the non-steroidal anti-inflammatory drug carprofen (5 mg/kg subcutaneous) was given to the rats fifteen minutes before surgery, to manage post-operative pain in the early recovery phase. The rats were briefly anesthetized with inhalation of isoflurane (5% for induction and 1.8–2% for maintenance). The depth of anesthesia was determined by the loss of the pedal withdrawal (toe pinch) reflex. Moisturizer was dropped into the eyes if they remained open. The surgical site of the dorsal rat tail was washed with a betadine solution with gauze. The coccygeal discs Co4–Co5 and Co5–Co6 were identified by anatomical surface markings between two vertebral bones through the tail skin. The first disc between these two vertebral bodies counting from the base of the tail is Co4–Co5, followed by Co5–Co6. A rubber band was applied at the base of the tail not later than 30 minutes after identification of the discs. Surgery began with dissection with the aid of a binocular surgical loupe, and all surgical instruments were handled using aseptic technique. A longitudinal incision was introduced in the skin and at the connective tissue of the dorsal side of the tail covering the discs. The tendons were pushed aside until the AF tissue (ivory matter) was reached. The injury was performed by punching defective NP tissue through the AF tissue at a diameter of 1 mm and a depth of 2 mm using a biopsy needle puncture. After injury, the discs were either left alone or implanted with HA hydrogel. The tendons were layer sutured to close the injury site, thereby covering the discs, and the animals were marked to show that the procedure had been performed. The wound was closed by suturing the skin with nylon suture using the interrupted horizontal mattress suturing method, and the rubber band was then removed from the tail to enable recovery of blood flow. For post-operative care, the rats were closely monitored until they were

completely recovered from anesthesia, then placed singly in individually ventilated cages until the wounds healed satisfactorily, which took approximately one week. Then, the rats were housed two to three per cage in individually ventilated cages for the recovery until day 29. Wounds were examined for signs of inflammation or infection, such as redness, swelling and/or purulent or serous discharge. General health-assessment details, such as tail-skin complications, body weight and body temperature, along with distress scores, were recorded on days 2, 7, 14 and 28 after the operation. The temperature and humidity of the housing environment were monitored, and appropriate bedding materials were provided during the studies.

4.3 Post-mortem Analysis

After a 29-day period post-surgery, live rats were decapitated with a guillotine, and trunk blood was collected in EDTA tubes during the procedure. Discs, AF and NP tissues, spinal cords and brains were extracted for further tissue analysis.

4.3.1 RT-qPCR

Left and right dorsal horns of the sacral segment of the spinal cord were dissected within 30 minutes after euthanasia, snap frozen and immediately placed at −80°C until further analysis. The dorsal horn of the spinal cord at the sacral and coccyx levels was homogenized in 1 mL of Trizol® reagent per 50–100 mg of tissue sample using TissueLyser (Qiagen). The samples were shaken at high speed in 2 ml round-bottomed microcentrifuge tubes with stainless-steel beads for fifteen minutes at room temperature. Following homogenization, the samples were centrifuged at 1,200 g for five minutes at 4°C, and the fatty layer was discarded. The cleared supernatant was transferred to a new microcentrifuge tube (Qiagen). For phase preparation, 200 µl of chloroform was added per 1 mL of Trizol® reagent, mixed for fifteen seconds and incubated for two minutes at room temperature. The mixture was then centrifuged at 13,300 rpm for fifteen minutes at 4°C. The colorless upper aqueous phase containing RNA was transferred to a fresh tube and mixed with 600 µL of 70% (v/v) molecular grade ethanol. The mixture was transferred to a Qiagen RNeasy Mini column and centrifuged at 10,000 rpm for fifteen seconds, and flowthrough was discarded. RNA bound to the column was washed with 700 µL of RW1 buffer and centrifugation at 10,000 rpm for fifteen seconds. Next, 500 µL of RPE buffer was added to the column, followed by centrifugation at 10,000 rpm for fifteen seconds, then a further

500 µL of RPE buffer and centrifugation for two minutes. RNase-free water (30 µL) was added, and the mixture was centrifuged at 10,000 rpm for one minute to collect RNA in a new collection tube. The RNA concentration was determined with a NanoDrop spectrophotometer (Thermo Scientific) from the ratio of absorbance at 260 nm and 280 nm, and the quality of the product was determined using a bioanalyzer (Agilent, Santa Clara, CA, USA). Total 5 µL of RNA (100 ng/µL) was reverse transcribed with random primers and reverse transcriptase in a 20 µl reaction mixture consisting of 4.4 µL 5× reaction buffer, 2.64 µL 25 mM $MgCl_2$, 1.1 µL dNTPs, 1.1 µL RNasin ribonuclease inhibitor and 1.1 µL ImProm-II TM reverse transcriptase, with the PTC DNA Engine System (PTC-200, Peltier Thermal Cycler, MJ Research, Watertown, MA, USA). cDNA products were amplified with TaqMan gene-expression assays and specific primers for *Tac1*, *c-Fos* and *Gapdh*. A multiplex PCR reaction was performed with TaqMan Universal PCR Master Mix, no AmpErase® UNG (Applied Biosystems) and standard thermal conditions (ten minutes at 95°C for polymerase activation, followed by 40 cycles of 95°C for fifteen seconds and 60°C for 60 seconds) in triplicate using the StepOnePlus Real-Time PCR System (Applied Biosystems). The results were analyzed by the $2^{-\Delta\Delta Ct}$ method, normalized to the endogenous *Gapdh* control and the sham control rats.

4.3.2 Lectin and Immuno-histochemistry

Post mortem, discs were fixed in 4% (w/v) paraformaldehyde for 48 hours, and vertebral bones were decalcified for two weeks in Kristensen's decalcifying solution containing 18% (v/v) formic acid and 3.5% (w/v) sodium formate at 4°C. All tissues were then washed under running tap water overnight, and soaked in 20% (w/v) sucrose until they sank at 4°C. Tissues were embedded in optimal cutting temperature compound and snap-frozen in an isopentane bath with liquid nitrogen, then kept at −80°C until sectioning on a cryostat (CM1850, Leica, Wetzlar, Germany). Tissue sections (10-µm) were collected on Superfrost™ Plus slides (Fisher Scientific, Dublin, Ireland) and stored at −20°C until use. Staining was performed at room temperature, and all washes were performed three times for five minutes each time between incubations, unless otherwise stated. Three slides (one each from four different rats) were used for each lectin or antibody incubation.

For lectin histochemistry, slides were washed with Tris-buffered saline supplemented with Ca^{2+} and Mg^{2+} (TBS; 20 mM Tris-HCl, 100 mM NaCl, 1 mM $CaCl_2$, 1 mM $MgCl_2$, pH 7.2) and 0.05% (v/v) Triton X-100 (TBS-T), then blocked with 2% (w/v) periodate-treated BSA (Sigma-Aldrich) in TBS for one hour. Inhibitory controls were carried out in parallel to verify that the lectin binding was glycan-mediated by co-incubating the lectins with 100 mM of the appropriate haptenic sugar in TBS (Table 4.2). Sections were washed, then incubated with eight different FITC-conjugated or TRITC-conjugated lectins (SNA-I, MAA, WGA, Con A, UEA-I, WFA, GS-IB4 and PNA (EY Labs)) in TBS for one hour (Table 4.2). After five washes with TBS-T, the sections were counterstained with a 1:1,000 dilution of DAPI for five minutes. The slides were washed in TBS-T before coverslip mounting with ProLong® Gold Antifade Mountant (Life Technologies). Inhibition by the appropriate haptenic sugar was observed for all lectins used (data not shown).

For immunohistochemistry, sections were incubated with proteinase K for fifteen minutes at 37°C, followed by 2% (w/v) BSA for 30 minutes at room temperature before overnight incubation at 4°C with primary antibodies. Negative-control sections were incubated with PBS and washed in PBS with 0.05% (v/v) Tween 20 (PBS-T). Triple staining was performed with three selected primary antibodies (1:100 anti-GAP43, 1:100 anti-TRPV1 and anti-CGRP) per section. Double staining was carried out with 1:100 anti-chondroitin-sulfate and 1:100 anti-keratan-sulfate, 1:50 anti-TGF-β1 and 1:50 anti-COL1A, or 1:50 anti-fibronectin and 1:50 anti-aggrecan antibodies. Single staining was performed with 1:50 phospho-p38 MAPK (Thr180/Tyr182), 1:50 phospho-NF-κB p65 (Ser536) and 1:50 anti-Trk-A antibodies. Sections were incubated with donkey anti-rabbit, donkey anti-goat and/or goat anti-mouse secondary antibodies at 1:200 dilution in PBS for two hours, then washed with PBS-T before counterstaining with DAPI (1:1,000 in PBS) for five minutes. Sections were washed with PBS-T and coverslip-mounted as described above. All slides were cured at 4°C in the dark for one day before imaging with a laser confocal microscope (Olympus Fluoview 1000, Olympus America, Center Valley, PA, USA).

4.3.3 Histochemical Image Analysis and Stereology Quantification

Stereology quantification was adopted to calculate the percentage volume fraction of detectable lectin binding and antibody staining. Immunohistochemical reactivity to antibody staining and lectin binding to specific glycans were obtained from at least four microscopic views of each slide with three technical and four biological replicates using ImageJ software version 1.48 (NIH, Bethesda, MD, USA). Confocal microphotographs were converted to binary mode (8 bit) and adjusted to the optimal threshold of positive staining and total area. Volume fraction (Vv) was calculated by quantifying the area fraction of the positively-stained matrix component divided by the total area and converting intoa percentage (%) as below:

$$\text{Percentage Volume Fraction (\%Vv)} = \frac{\text{Area Fraction}}{\text{Total Area}} \times 100\%$$

For the clustering analysis, data were normalized to maximal individual lectins or antibody binding across conditions, and the clustering analysis was performed using Hierarchical Clustering Explorer 3.0 (NIH) without additional normalization and with complete linkage, Euclidean distance and Pearson correlation-coefficient determination. The results are represented in heatmap format.

For nuclear stained of antibody staining, relative number estimation was used to quantify positively nuclear stained in a single optical plane of confocal image. The unbiased counting frame was superimposed on fluorescence image obtained from confocal imaging. Positively nuclear stained and total nuclei were counted only in the guard area, without counting nuclei hit forbidden line. Relative number estimation was calculated by quantifying number of positively nuclear stained proportional to total nuclei, and convert to percentage as below:

$$\text{Percentage Relative Number (\%Na)} = \frac{\text{Number of Positive Nuclear Stained}}{\text{Total Number of Nuclei}} \times 100\%$$

4.3.4 Proteomic Analysis by Mass Spectrometry (LC-MS/MS)

NP and AF tissues were extracted from the discs after euthanasia. Tissues were snap frozen and immediately kept at −80°C. To extract ECM proteins, samples were digested with proteinase K (0.5 mg/mL) for <12 hours at 56°C and stored at −20°C before further analyses. To extract both cellular and ECM proteins, tissues were minced with a scalpel, transferred to a microcentrifuge tube and incubated in 6 M

urea, 10 mM dithiothreitol and 50 mM ammonium bicarbonate (NH_4HCO_3) at pH 8.6 for two 2 h at room temperature with gentle agitation. To collect the supernatant, each sample was centrifuged at 3,000 g for three minutes, then the total protein concentration was evaluated. The samples were digested with 2% (w/v) trypsin in 1.5 M NH_4HCO_3 at pH 7.8 for 18 h at 37°C, and the enzymatic reaction was stopped with 2% (v/v) formic acid.

Samples were run on a Thermo Scientific Q Exactive mass spectrometer connected to a Dionex Ultimate 3000 RSLC nano chromatography system. Tryptic peptides were resuspended in 0.1% (v/v) formic acid. Each sample was loaded onto a fused silica emitter (75 µm internal diameter, pulled with a laser puller (Sutter Instruments P2000) and packed with Reprocil Pur C18 (1.9 µm) reverse-phase media), and separated with an increasing acetonitrile gradient over 47 minutes at a flow rate of 250 nl/min. The mass spectrometer was operated in positive-ion mode with a capillary temperature of 320°C and a potential of 2,300 V applied to the frit. All data were acquired with the mass spectrometer operating in the automatic data-dependent switching mode. A high-resolution (70,000) MS scan (300–1,600 m/z) was performed with Q Exactive to select the eight most-intense ions, prior to MS/MS analysis with higher-energy collisional dissociation. For protein identification, the raw data were searched against the *Rattus norvegicus* subset of the UniProt Swiss-Prot database, using the search engine PEAKS Studio 7 (Bioinformatics Solutions, Waterloo, ON, USA) for peptides with unspecified enzymatic cleavage. Each peptide used for protein identification met specific PEAKS parameters: only peptide scores that corresponded to a false discovery rate (FDR) of ≤1% were accepted from the PEAKS PTM database search.

4.3.5 Protein Quantification and Pathway Analysis

To quantify the identified proteins, raw MS data were analyzed with MaxQuant [19] software based on specified peptides with unspecified enzymatic cleavage for proteinase K-digested samples and semi-specific trypsin cleavage with fixed modification of carboxymethylation for tryptic samples. Each peptide used for protein identification and quantification met specific Maxquant parameters: only peptide scores that corresponded to an FDR of ≤1% were accepted from the Maxquant database search. Maxquant data were further analyzed using Perseus

software [20] for comprehensive analysis of proteomics data, including label-free quantification of the identified proteins. The list of differentially expressed proteins with a label-free quantification intensity and fold change relative to sham rats >2 or <−2 that had a *p* value <0.01 were uploaded into Ingenuity Pathway Analysis (IPA®, QIAGEN, Redwood City, USA) for assessment. The protein expression comparison between the injury and HA-hydrogel groups of AF and NP tissues was conducted using an empirical test based on fold-change value as counts, causal networks (such as connective tissue, inflammation, neurotransmission, extracellular matrix and muskuloskeletal) and species accordingly.

4.3.6 Inflammatory Cytokine Profiles by ELISA

After euthanasia (on the same day), the collected blood was transferred to a 2 mL Eppendorf tube and centrifuged at 1,200 g for fifteen minutes to collect blood plasma. For AF and NP proteins, tissues were minced with a scalpel and incubated in 6 M urea, 10 mM dithiothreitol and 50 mM NH_4HCO_3 (pH 8.6) for two hours at room temperature with gentle agitation. The supernatant was centrifuged at 3,000 g for three minutes, then the total protein was collected for analysis. Plasma, AF and NP samples were analyzed with the multiplex ELISA pro-inflammatory panel 2 (rat) for cytokines (IL-6, IL-1β, TNF, IFN-Y, CXCL1, IL-4, IL-5, IL-13 and IL-10). The sample and reagent were prepared according to the manufacturer's protocol. Blood plasma and AF and NP samples were diluted (four-fold) in diluent. Blocker H (150 µL) was added to each well of the ELISA plate and incubated at room temperature with fast shaking for one hour. The plate was then washed three times with ≥150 µL of PBS-T. A 50 µL sample volume, including the calibrators, was added to each well and further incubated at room temperature with shaking for two hours. After three washes with PBS-T, 25 µL of 1× detection-antibody solution was added to each well and incubated at room temperature with shaking for two hours. The plate was washed three times and an additional 150 µL of 2× read buffer T was added to each well before plate reading detection based on electrochemiluminescence using MESO QuickPlex SQ 120 (Meso Scale Discovery (Rockville, Maryland, USA).

4.4. Pharmacokinetic of an Injectable HA Hydrogel in the Punctured Rat Tail

The pharmacokinetic effect of HA hydrogel was observed in the punctured rat tail via injection of fluoresence-label HA hydrogel up to post-injury day 2 using an IVIS® spectrum imaging (fluorescence pre-clinical imaging).

4.4.1 Preparation of Fluorescence-labeled HA Hydrogel

Sterile sodium hyaluronate 0.75% (w/v) was reconstituted with 600 μL of filtered distilled water in 7 mL glass vial for 30 minutes at room temperature. The solution was then mixed with sterile EDC 8.9% (w/v) and NHS 15% (w/v). After 30 minutes of reaction, the mixed solution was incubated with 15 μL of fluorescence dye e.g. secondary antibody Alexa Fluor® 594 (stock 1 mg/mL) for 30 minutes at room temperature for the labeling. For crosslinker preparation, sterile 4 arm PEG amine 15% (w/v) was dissolved in 400 μL of filtered distilled water in the other glass vial. The fluorescence-labeled HA and PEG solutions were loaded in duploject syringe system (Baxter), cured from the light and kept overnight at 4^{o}C. The evidence of fluorescence-labeled HA hydrogel was confirmed by IVIS® spectrum imaging system (PerkinElmer, USA).

4.4.2 Injection of Fluorescence-labeled HA Hydrogel Following Surgically Puncture-induced IVD Injury

The rats underwent surgeries and post-operative care as described in **section 4.2.5**. The hydrogel injection was given at the end of the surgery procedure, which was just after suturing the tendon to close the injury site. The small volume of fluoresence-label HA hydrogel (prepared in duploject syringe system) was injected onto the sterile container for mixing and then immediately loaded in the Hamilton syringe (250 μL scale). Using Hamilton syringe attached to 27G needle, the volume of 5 μL of mixed fluoresence-label HA hydrogel was percutaneously (intradiscal) injected into the injury site of the disc rat tail within 30 minutes after mixing of hydrogel solution. The rats were kept recovery until post-operation day 2 and euthanised to determine the stability of HA hydrogel injection in the punctured rat tail via IVIS® spectrum *in vivo* imaging system.

4.4.3. IVIS® Imaging

To minimize auto-fluoresence from animal tissues during *in vivo* fluoresence imaging, the skin from the rat tail was removed. The rat tails from each group were placed in an anterolateral position on the imaging stage, closest to the detector of the imaging chamber. The instrument was controlled using Living Image® software. In this software, the correct acquisition parameters were set to fluoresence imaging, a quicker exposure time, a larger Fstop, the depth of signal, and specific emission and excitation filter coresponds to the fluorophore used. A sequence of images was captured on rat tails of sham (naïve control), untreated injured discs, and treated injured discs with fluoresence-labeled HA hydrogel. For the *in vitro* control, the images of HA solution alone and fluoresence-labeled HA hydrogel were captured on the glass slide.

4.5 Statistical Analysis

Statistical differences were analyzed by GraphPad Software (La Jolla, CA, USA) using repeated measure ANOVA or one-way ANOVA for analyses of the Hargreaves, von Frey and tail-flick tests; one-way ANOVA for the PCR, HPLC, and lectin and antibody staining, and two-way ANOVA for the ELISA in experiments involving HA hydrogel; and Student's t-test for the lectin analysis in the validation of the injury model. All ANOVAs were further evaluated with Bonferroni *post-hoc* analysis, and $p < 0.05$ was deemed statistically significant. All error bars indicate standard error of the mean (S.E.M).

4.6 Results

4.6.1 HA Hydrogel Exhibits Anti-hyperalgesic and Anti-allodynic Effects

The results of disc-pain model **(Chapter 3)** indicated that the rat tail injury model produced a persistent-pain phenotype, which enable for investigation the effects of HA hydrogel in modulation of pain under physiological conditions. Using this model, quantitative sensory testing was performed to observe therapeutic efficacy of HA hydrogel in alleviation of nociceptive behavior.

In injured rats that were implanted with HA hydrogel (and in sham control rats), the withdrawal latency in the Hargreaves test was significantly higher than in injured rats without HA hydrogel, at each time point over a 29-day period (one-way

ANOVA, $n = 10$, $p < 0.05$; Figure 4.2a). Similarly, significant increases in the 50% withdrawal threshold in the von Frey test were observed in the HA-hydrogel-treated injury group (and in the sham control group) compared with the untreated injury group (one-way ANOVA, $n = 10$, $p < 0.05$; Figure 4.2b). These results suggest that HA hydrogel alleviated thermal hyperalgesia and mechanical allodynia in the rat tail around the injury site. In the tail-flick test, injured rats receiving HA-hydrogel treatment (and sham control rats) had significantly shorter withdrawal latency than injured rats without treatment (one-way ANOVA, $n = 10$, $p < 0.05$; Figure 4.2c), suggesting that HA-hydrogel treatment suppresses thermal hypoalgesia in response to a stimulus applied distal to the site of injury in the rat tail. This result indicates that the HA hydrogel inhibits the diffuse noxious inhibitory control (DNIC) pathway.

4.6.2 HA Hydrogel Suppresses *c-Fos* and *Tac1* Expression at the Spinal Level

The observation that the HA hydrogel modulates pain behavior leads to investigate mRNA expression of the immediate-early gene *c-Fos* and *Tac1*, which encodes protachykinin-1 (a precursor protein that is cleaved into peptides including substance P), in the pain-processing neurons of the left spinal cord dorsal horn. At day 29, the dorsal horn was dissected within 30 min of application of thermal stimulus to the proximal tail. A significantly lower *c-Fos* expression was found in the HA-hydrogel-implanted injury group (and in the sham control group) compared with the untreated injury group. A similar result was obtained for *Tac1* (for both *c-Fos* and *Tac1*: one-way ANOVAs, $n = 4$, $p < 0.05$; Figure 4.2d). These results suggested that the HA hydrogel suppressed nociceptive transmission by attenuating injury-induced *c-Fos* and *Tac1* expression in dorsal-horn neurons.

4.6.3 HA Hydrogel Inhibits Injury-induced Peripheral Sensory Hyper-innervation and Expression of the Pro-nociceptive Receptors TRPV1 and Trk-A

With confocal fluorescence microscopy, co-localization of the GAP43 protein (which is expressed during nerve ingrowth), the sensory neuropeptide CGRP, the pro-nociceptive ion channel TRPV1 and NGF receptor Trk-A were examined in the AF and NP tissues 29 days post-operation. GAP43, CGRP and TRPV1 co-localized in AF tissue post-injury (Figure 4.3a-b). It was also observed a projection of sensory

nerve innervation with neuropeptides (GAP43 and CGRP), TRPV1 and Trk-A in NP tissue (Figure 4.3a-b). Less GAP43, CGRP and TRPV1 immunoreactivity was determined in AF and NP tissues from control rats and from injured rats implanted with HA hydrogels than in tissues from untreated injured rats. In both AF and NP tissues, the percentage volume fractions of immunostained GAP43, CGRP, TRPV1 and Trk-A were all significantly higher in the untreated injury group than in either the HA-hydrogel-treated injury group or the untreated sham control group (one-way ANOVA, $n = 4$ with 5 microscopic views of each slide with three technical and four biological replicates, $p < 0.05$; Figure 4.3a-c). Overall, these findings confirmed that HA-hydrogel implantation inhibited injury-induced peripheral sensory innervation and pro-nociceptive TRPV1 and Trk-A expression in AF and NP tissues.

4.6.4 HA Hydrogel Modulates Sialylation, Galactosylation and Glycosaminoglycan Content

Sialylation has been shown to affect disease progression in degenerative joint diseases [21]. A lower levels of SNA-I binding was observed in AF and NP tissues of rats in the HA-hydrogel-treated injury group than in the untreated injury group (one-way ANOVA, $n = 4$, $p < 0.05$; Figure 4.4a). MAA binding showed a similar pattern (one-way ANOVA, $n = 4$, $p < 0.05$; Figure 4.4b). No significant difference in WGA expression was observed in either AF or NP tissues of rats in the untreated injury group compared with rats in the HA-hydrogel-treated injury group (one-way ANOVA, $n = 4$, $p < 0.05$; Figure 4.4c).

For determination of galactosylation, intracellular GS-I-B4 binding was significantly lower in both AF and NP tissues in the HA-hydrogel-treated injury group than in the untreated injury group (one-way ANOVA, $n = 4$, $p < 0.05$; Figure 4.5a). WFA binding in the ECM of NP tissue was significantly higher in the HA-hydrogel-treated injury group than in the untreated injury group (one-way ANOVA, $n = 4$, $p < 0.05$; Figure 4.5b), but not significantly different in AF tissue.

Content of chondroitin sulfate and keratan sulfate was determined by antibody staining. Chondroitin sulfate localized in the ECM, whereas keratan sulfate localized intracellularly (Figure 4.6a). Chondroitin sulfate expression was significantly higher in the untreated injury group than in the sham control group in both AF and NP tissues (one-way ANOVA, $n = 4$, $p < 0.05$; Figure 4.6b, i-ii) and did

a)

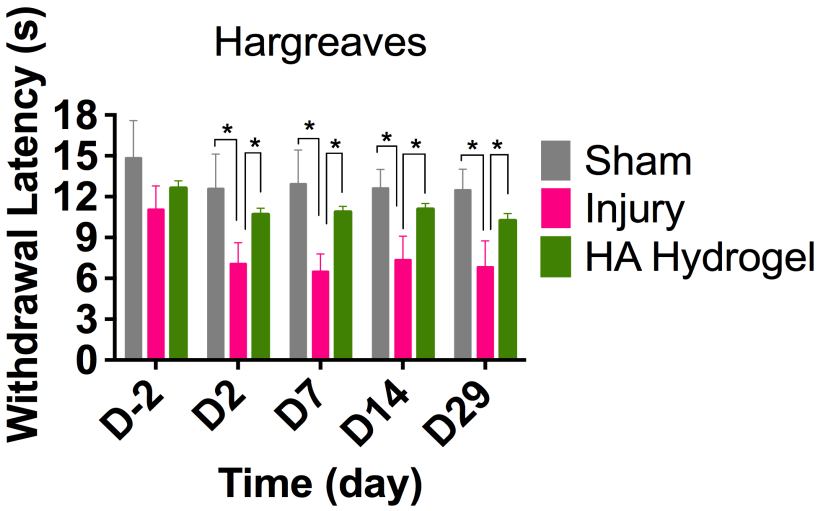

b)

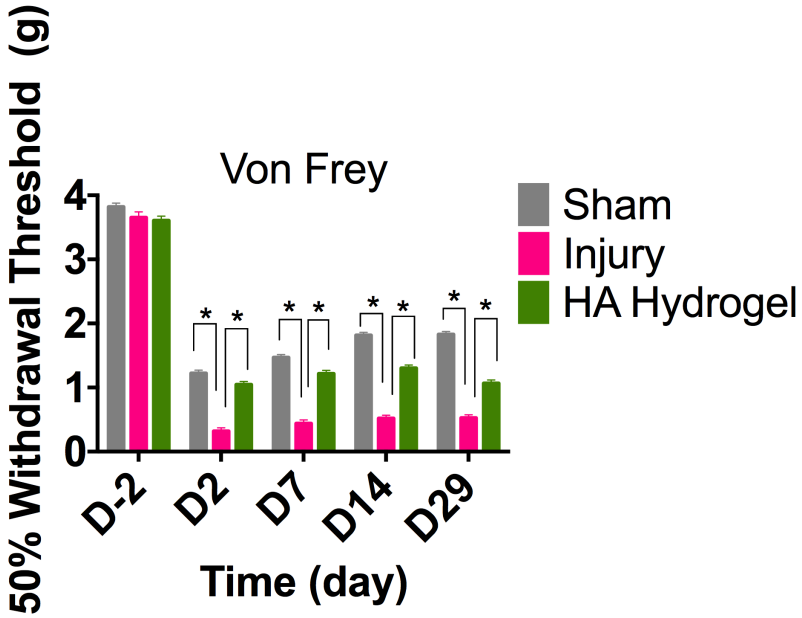

Continued

c)

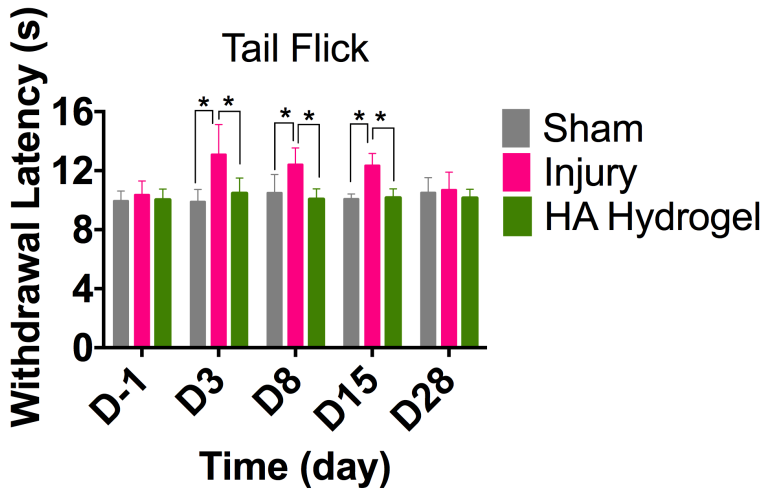

d)

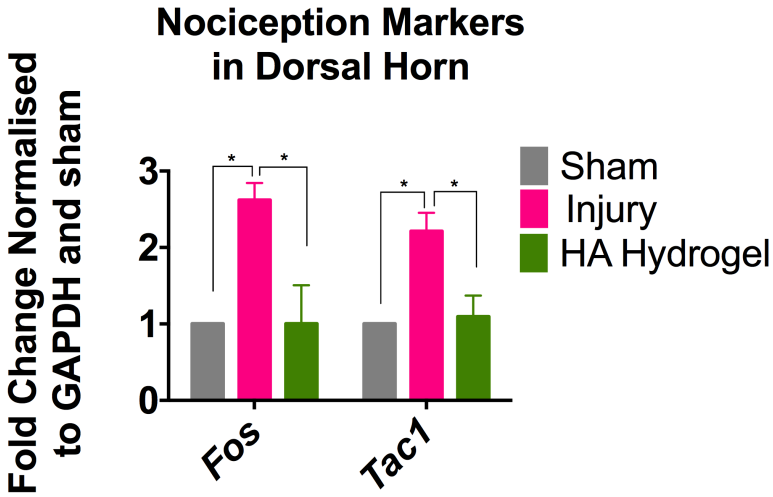

Figure 4.2 Alleviation of the injury-induced pain phenotype by HA-hydrogel implantation. (a) In the Hargreaves test, withdrawal latency times were significantly higher in the HA-hydrogel-treated injury group (and the control group) than in the untreated injury group. (b) In the von Frey test, 50% withdrawal thresholds were significantly higher in the HA-hydrogel-treated injury group (and the control group) than in the untreated injury group. (c) In the tail-flick test, withdrawal latency times were significantly lower in the HA-hydrogel-treated injury group (and the control group) than in the untreated injury group (days 3, 8 and 15). (d) Expression of genes encoding molecular markers of nociception substance P (*Tac1*) and *c-Fos* (measured post-mortem) was significantly lower in the HA-hydrogel-treated injury group (and the control group) than in the untreated injury group. *Significant difference between groups, by repeated measure one-way ANOVA (n = 10 for a-c, n = 4 for d, p <0.05). Data are presented as the mean ± standard error the mean.

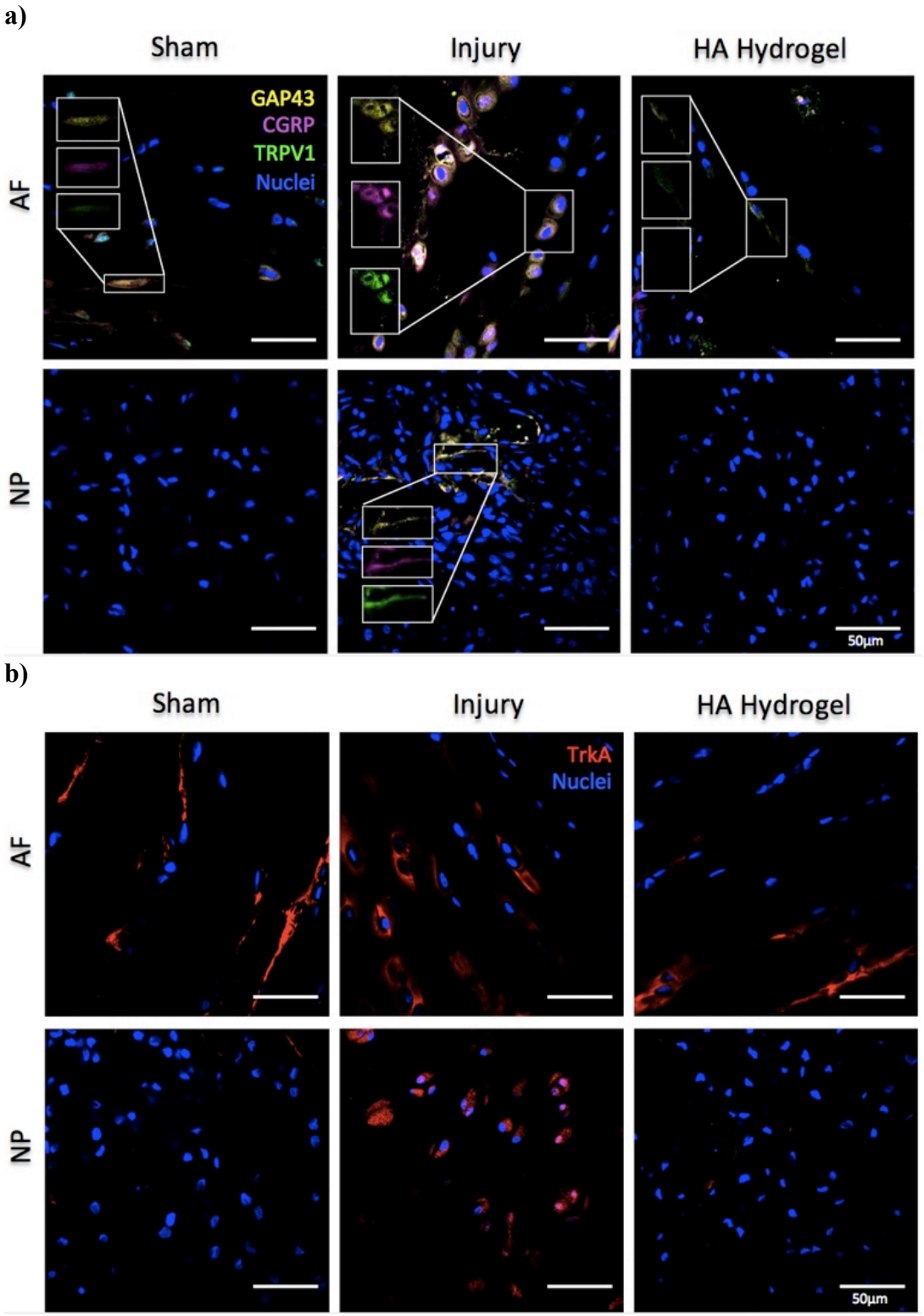
a)
Sham
Injury
HA Hydrogel
GAP43
CGRP
TRPV1
Nuclei
AF
NP
50µm
b)
Sham
Injury
HA Hydrogel
TrkA
Nuclei
AF
NP
50µm

Continued

c) i.

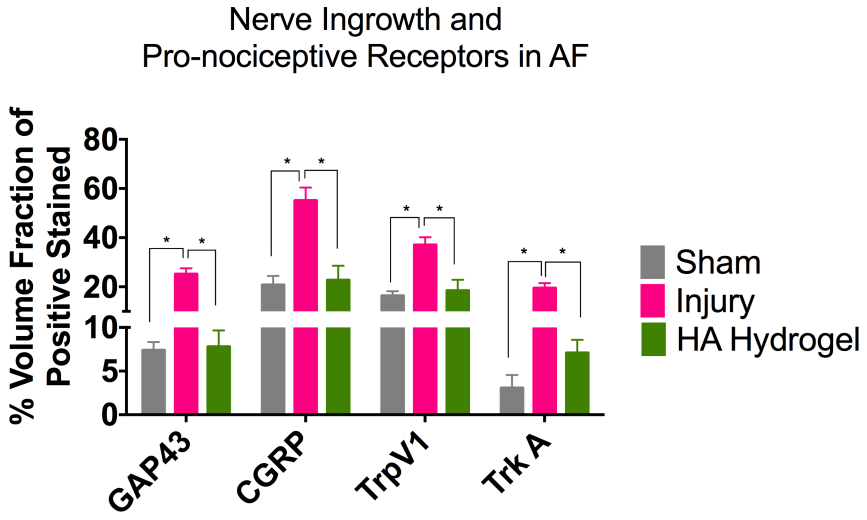

ii.

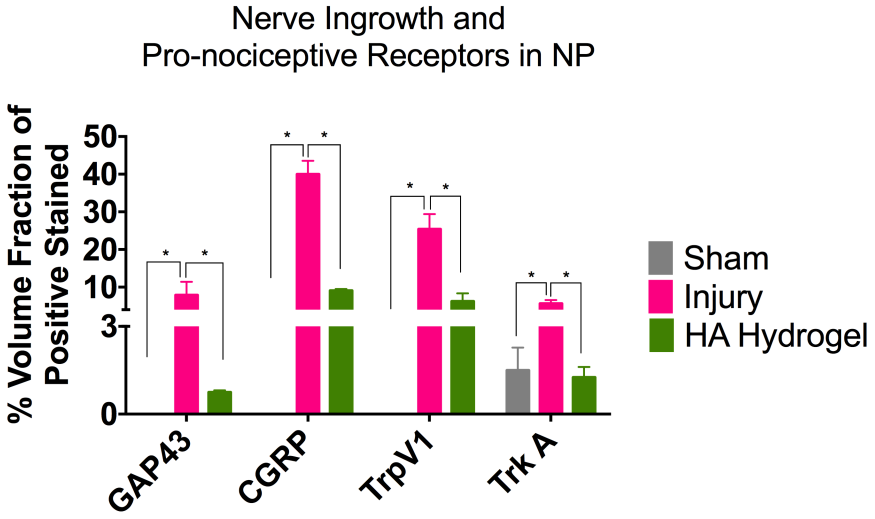

Figure 4.3 Alleviation of the injury-induced pain phenotype by HA-hydrogel implantation. (a) Confocal microscopy demonstrated the presence in annulus fibrosus (AF) and nucleus pulposus (NP) tissues, particularly in the untreated injury group, of the nociception marker GAP43 (yellow label), the sensory neuropeptide calcitonin gene-related peptide (CGRP) (purple label) and the transient receptor potential cation channel subfamily V member 1 (TRPV1) (green label). **(b)** The nerve growth factor receptor Trk-A (red label) was evident in AF and NP tissues **(c)** The quantified percentage volume fractions of GAP43, CGRP, TRPV1 and Trk-A were significantly higher in the untreated injury group than in the sham control group or the HA-hydrogel-treated injury group, in both AF (i) and NP (ii) tissues. *Significant difference between groups, by one-way ANOVA ($n = 4$, $p < 0.05$). Data are presented as the mean ± standard error the mean. Area fraction data were normalized to the total area. Scale bar = 50 μm.

not significantly differ between the untreated injury group and the HA-hydrogel-treated injury group. Keratan sulfate expression was significantly higher in NP cells in the untreated injury group than in the sham control group, and was significantly lower in both AF and NP cells in the HA-hydrogel-treated injury group than in the untreated injury group (one-way ANOVA, $n = 4$, $p < 0.05$; Figure 4.6b, i-ii).

4.6.5 Correlation of Glycosylation, Innervation and Markers of Nociception

Associations between levels of binding of markers of glycosylation and innervation by nociceptive nerves in AF and NP tissues were analyzed by a clustering analysis on the basis of Pearson-correlation-coefficient distances (Figure 4.7a-b). Levels of sialylation (measured by binding of SNA-I, MAA and WGA), galactosylation (GS-I-B4), keratan sulfate and chondroitin sulfate correlated with each other and with sensory innervation (GAP43 and CGRP) and TRPV1 in AF and NP tissues. Additionally, a relationship between WGA and, GS-I-B4 binding, and keratan sulfate and chondroitin sulfate with the GAP43, CGRP and TRPV1 were observed in NP tissue (Figure 4.7b).

4.6.6 Injury and Treatment Modulate the Proteomic Signature at the Cellular and Extracellular Levels

Protein expression in the rat tail injury model was analyzed by liquid chromatography coupled to tandem mass spectrometry (LC-MS/MS). Tryptic digests of AF and NP tissues contained higher numbers of proteins than the ECM-specific proteinase K digests. The proteinase K digestion method identified 532 and 766 proteins specifically in the ECM of AF and NP tissues, respectively (Figure 4.8a, i). Tryptic digestion identified 2,126 and 1,084 cellular and extracellular proteins in AF and NP tissues, respectively (Figure 4.8a, ii). Heatmaps show the relative (log_2-transformed) expression levels of differentially expressed proteins (fold change >2 or <−2 for log_2 expression values, $p < 0.01$) in the AF and NP tissues in the sham control, untreated injury and HA-hydrogel-treated injury groups (Figure 4.8b, i-ii).

For Ingenuity Pathway Analysis (IPA), the –log(*p* value) threshold to 1.3 was set, to determine dysregulated signaling pathways from the dataset of 389 differentially expressed proteins. The main dysregulated cellular functions, including inflammatory response, innervation, neurotransmission, connective tissue and

a)

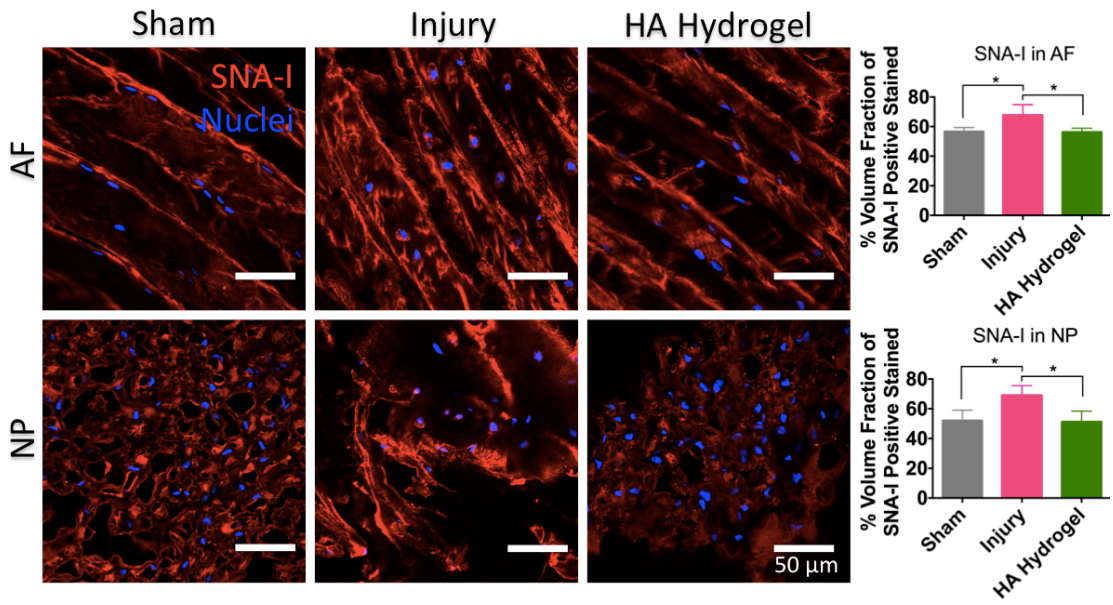

b)

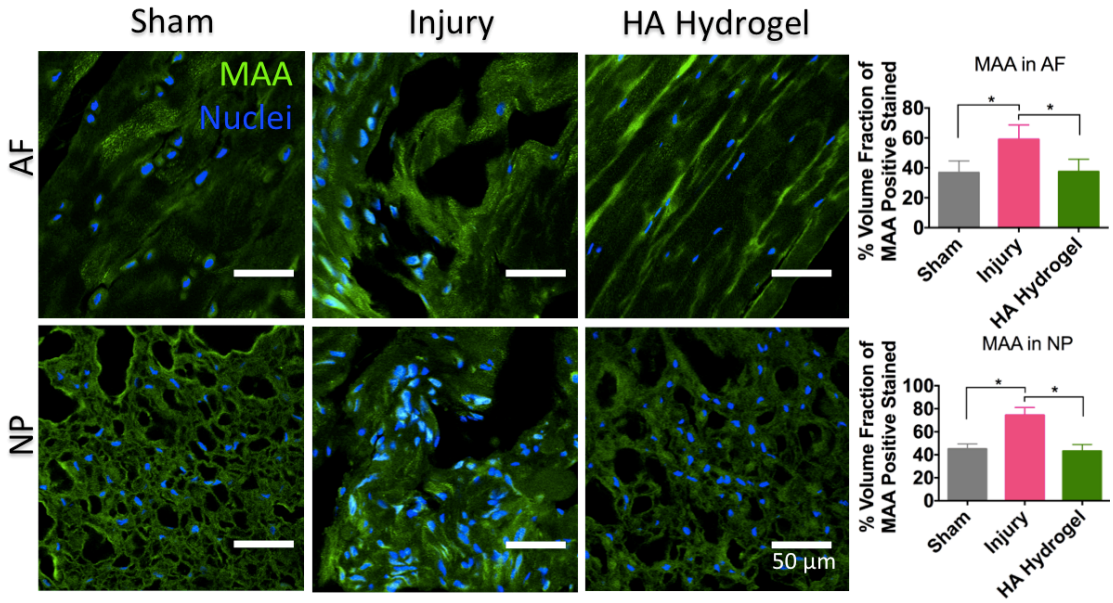

Continued

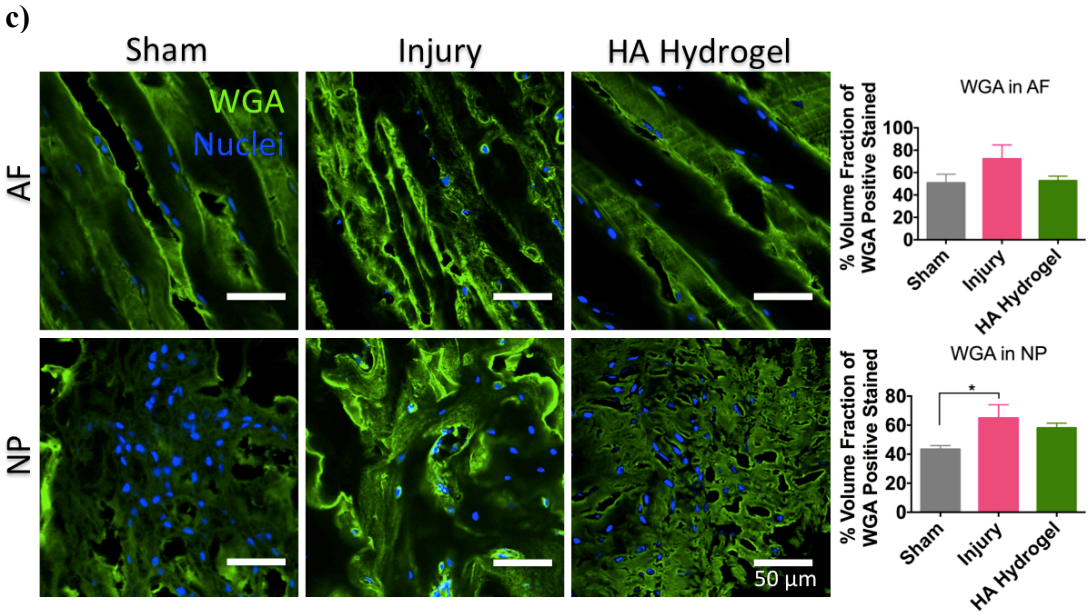

Figure 4.4 Effects of HA-hydrogel implantation on glycosylation in the injury-induced pain model. Assessment of sialylation on day 29 after injury through quantification of lectin binding. (a) SNA-I binding to α-(2,6)-linked sialic acid was significantly higher in the untreated injury group than in the sham control or HA-hydrogel-treated injury groups, in annulus fibrosus (AF) and nucleus pulposus (NP) tissues. (b) MAA binding to α-(2,3)-sialylated galactose was significantly higher in the untreated injury group than in the sham control or HA-hydrogel-treated injury groups, in AF and NP tissues. (c) Binding of WGA to N-acetyl-D-glucosamine or sialic acid was not significantly affected by HA-hydrogel implantation. *Significant differences between groups, by one-way ANOVA (n = 4, p <0.05). Area fraction data were normalized to the total area and are presented as the mean ± standard error of the mean. Scale bar = 50 µm.

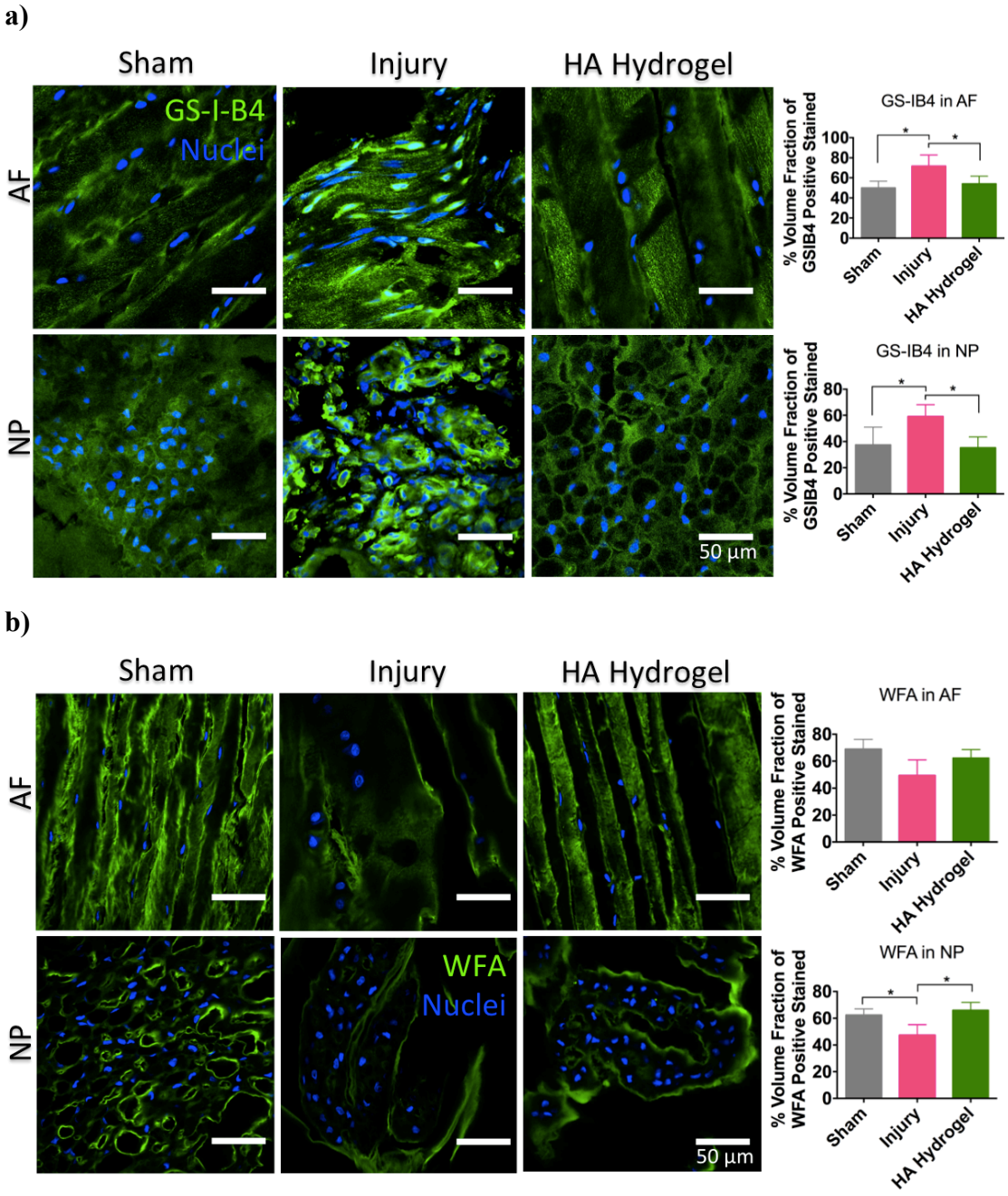

Figure 4.5 Effects of HA-hydrogel implantation on glycosylation in the injury-induced pain model. Assessment of galactosylation on day 29 after injury through quantification of lectin binding. (a) An iterative increase of GS-IB4 binding to α-galactose was observed upon injury and this decreased in response to HA hydrogel. (b) Terminal GalNAc motifs detected extracellularly by WFA lectin staining in AF and NP tissues. *Significant differences were noted between the different groups (n = 4, one-way ANOVA, $p < 0.05$). Data of area fraction was normalised to total area and represented as mean ± standard error of the mean. Scale bar = 50µm.

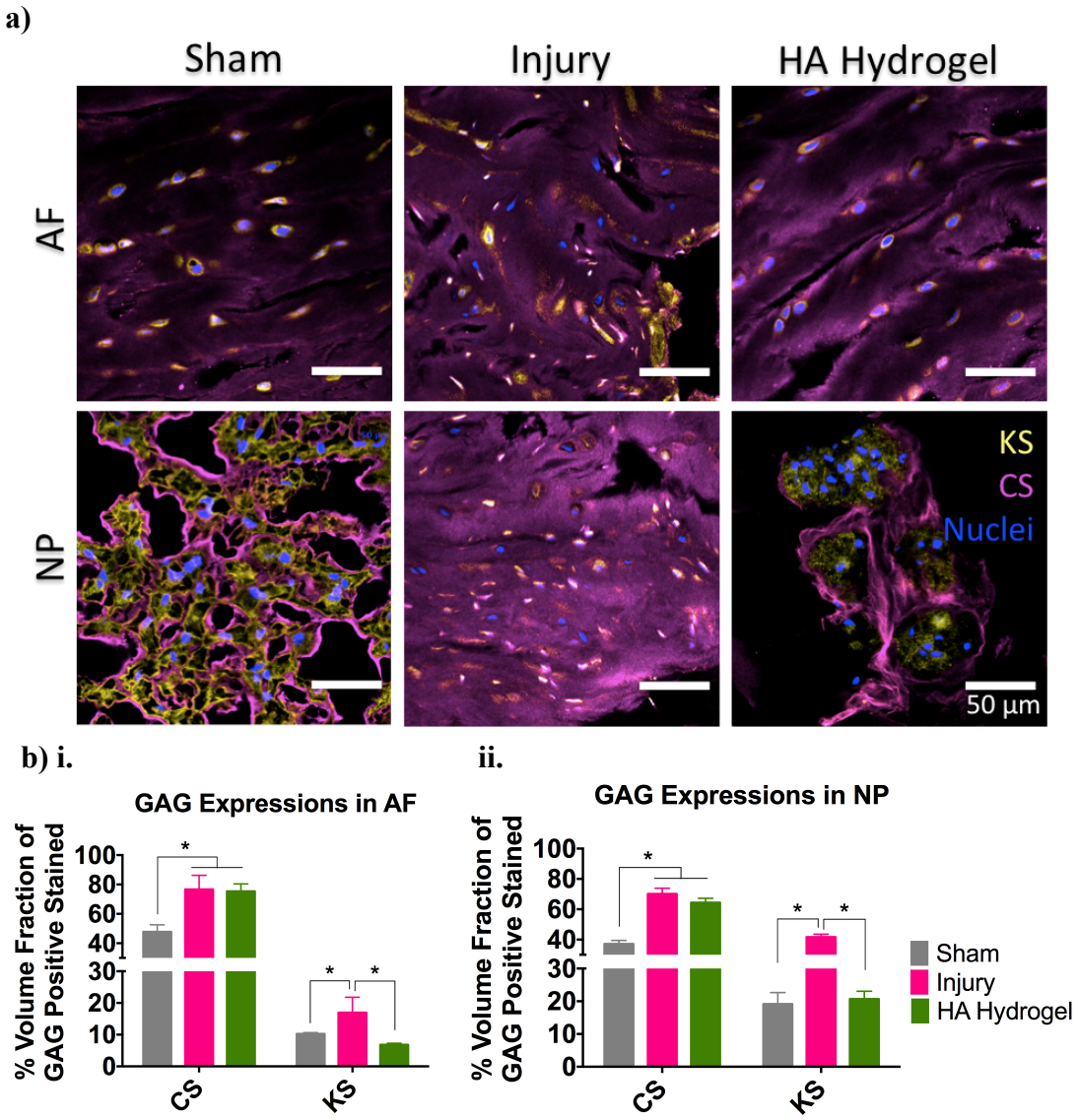

Figure 4.6 Effects of HA-hydrogel implantation on glycosylation in the injury-induced pain model. (a) Assessment of glycosaminoglycan on day 29 after injury through quantification of antibody binding. (b) Levels of chondroitin sulfate (purple label) were significantly higher in the untreated injury group than in the sham control group, but there was no difference between levels in the untreated injury group and the HA-hydrogel-treated injury group, in AF (i) and NP (ii) tissues. Levels of keratan sulfate (yellow label) were significantly higher in the untreated injury group than in the sham control group in NP tissues, or the HA-hydrogel-treated injury groups, in AF (i) and NP (ii) tissues. *Significant differences between groups, by one-way ANOVA (n = 4, p <0.05). Area fraction data were normalized to the total area and are presented as the mean ± standard error of the mean. Scale bar = 50 µm.

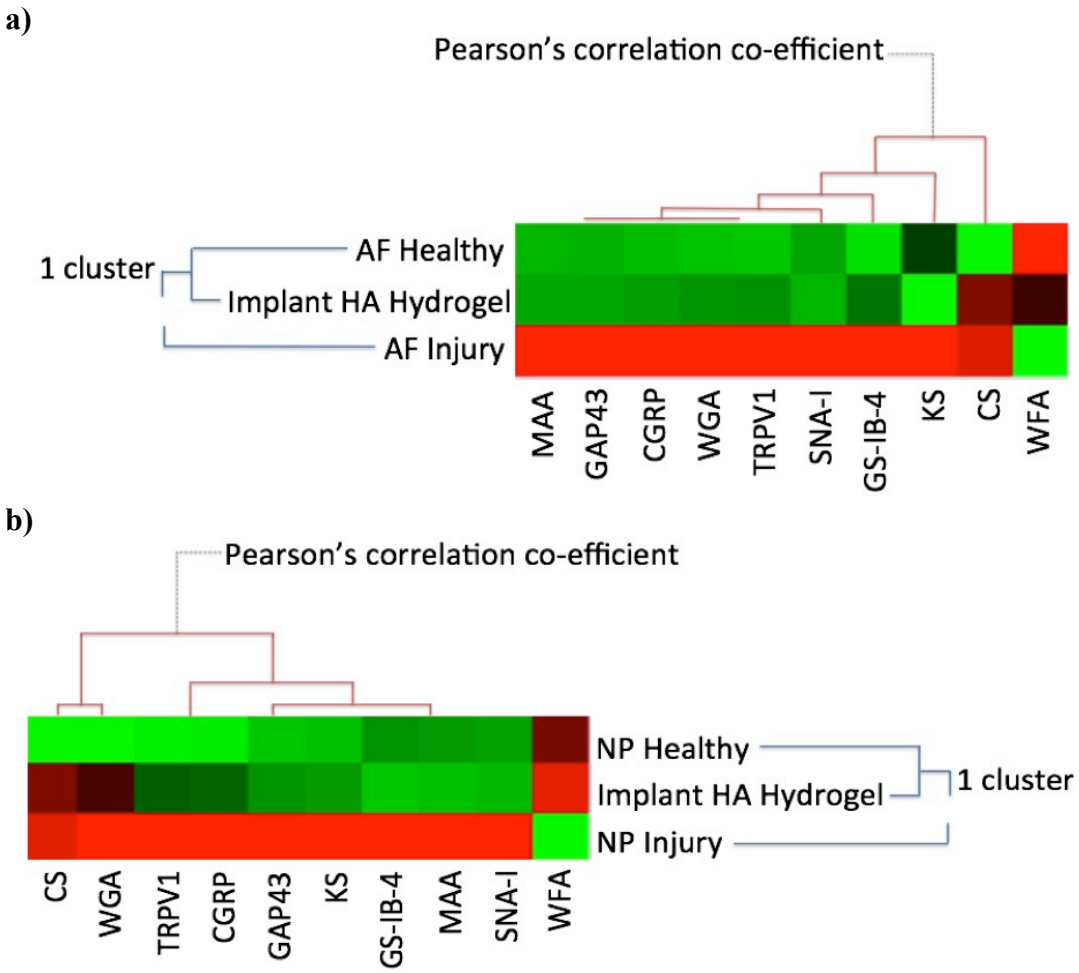

Figure 4.7 Correlation between glycoprofiles and nociception markers. Clustering analysis was carried out on the quantification profiles from confocal fluorescence microscopy of glycosylation and sensory hyper-innervation and nociceptive markers in AF (a) and NP (b) tissues for the sham control, untreated injury and HA-hydrogel-treated injury groups. (n = 4, Pearson correlation CC > 0.5).

neuromuscular disorder and ECM regulation, were analyzed in more detail with IPA, as these functions are key determinants in disc degeneration [22] (Figure 4.9). It was found that pathways involving eukaryotic initiation factor 2, serine/threonine-protein kinase mTOR, the unfolded-protein response, the acute-phase response andendothelial nitric oxide synthase were represented by the differentially expressed proteins (Figure 4.9a). Acute-phase-response signaling involves IL-1β, IL-6, TNF-α and the glucocorticoid receptor (among many other factors), and can modulate inflammation and catabolic responses in AF and NP tissues (Figure 4.10). Among the upstream regulators of the cellular functions that were modified in the rat tail model, transforming growth factor β1 (TGF-β1), proto-oncogene *c-Fos*, SMAD family member 3 (Smad3), p38 MAPK and nuclear factor kappa-light-chain-enhancer of activated B cells (NF-κB) were activated in AF and NP tissues in untreated and HA-hydrogel-treated injury groups, compared with sham controls (Figure 4.9b; Figure 4.13). Finally, protein synthesis, cell death and survival, connective tissue disorder, inflammatory response and skeletal and muscular disorder were the key diseases and biological functions that had significantly higher representation in the experimental groups (Figure 4.9c).

4.6.7 HA Hydrogel Attenuates Injury-induced Expression of IL-6 and IL-1β

To investigate inflammatory signaling in this model, the levels of IL-6, IL-1β, TNF, IFN-γ, CXCL1, IL-10 and IL-13 were determined in blood plasma and disc tissues by the multiplex ELISA method. In AF and NP tissues and plasma, levels of pro-inflammatory cytokines were significantly higher (and anti-inflammatory IL-10 was lower) in the injury group than in the sham control or HA-hydrogel-treated injury groups (two-way ANOVA, $n = 5$ for AF or NP tissues for each group, $n = 10$ for blood plasma for each group, $p < 0.05$; Figure 4.12a-c), suggesting that the effect of local inflammation on systemic inflammation. Furthermore, the levels of cytokines were measured in the plasma after pain inhibition by systemic morphine injections. Plasma levels of CXCL1 and IL-1β were higher in the saline-treated injury group than in the saline-treated sham group or the morphine-treated sham and injury groups (two-way ANOVA, $n = 5$ for each group, $p < 0.05$; Figure 4.12d). These results suggest that acute-response signaling was involved in the dysregulation of IL-6 and IL-1β in response to IVD injury, and that HA-hydrogel treatment targeted these

canonical pathways by downregulating pro-inflammatory cytokines in both AF and NP tissues. Here, upstream regulators of *c-Fos*, p-p38 MAPK and p-NF-κB have been validated as evident in the confocal photomicrographs (Figure 4.13a-e), which may involves in the inflammatory pathways linked to pain signaling.

4.6.8 HA Hydrogel Potentially Regulates ECM Deposition via Smad3–TGF-β1 Signaling

Inflammation has a critical role in modulation of the catabolic process during IVD degeneration (Figure 4.14). The results of pathway analysis suggest that the Smad3 protein family was a candidate for mediation of ECM deposition via Smad3–TGF-β1 signaling during regeneration after HA-hydrogel treatment. Protein analysis demonstrated higher levels of type I collagen, type II collagen, fibronectin, fibromodulin and biglycan in NP tissue in the injury group than in the sham group or the HA-hydrogel-treated injury group. In AF tissue, compared with the sham group, levels of type II collagen and fibronectin were higher and fibromodulin and biglycan were lower in the injury group. HA-hydrogel treatment resulted in a lower level of type II collagen and higher level of fibromodulin compared with injury alone, but did not affect the levels of fibronectin or biglycan. Nuclear expression of Smad3 was observed in AF and NP tissues (Figure 4.13c). Furthermore, ECM proteins for type I collagen, TGF-β1, aggrecan and fibronectin have been seen in both AF and NP tissues (Figure 4.15a-b).

4.6.9 Stability of Injectable HA Hydrogel in the Punctured Rat Tail

Epi-fluorescence mapping of the optical image of fluorescence-labeled HA hydrogel overlaid with photograph of hydrogel was displayed by IVIS® imaging. The radiant efficiency of region of interest was calculated by adopting fractional ratio of fluorescent emitted photons per incident excitation photon [23], which was greater in the fluorescence-labeled HA hydrogel than in HA solution alone (Figure 4.16a). This data indicates the successful of fluoresence-labeled (Alexa Fluor® 594) in the HA hydrogel system *in vitro*.

The stability of HA hydrogel injection in the injured discs of rat tail was seen in the fluorescent optical image overlaid with photograph of the rat tail at post-

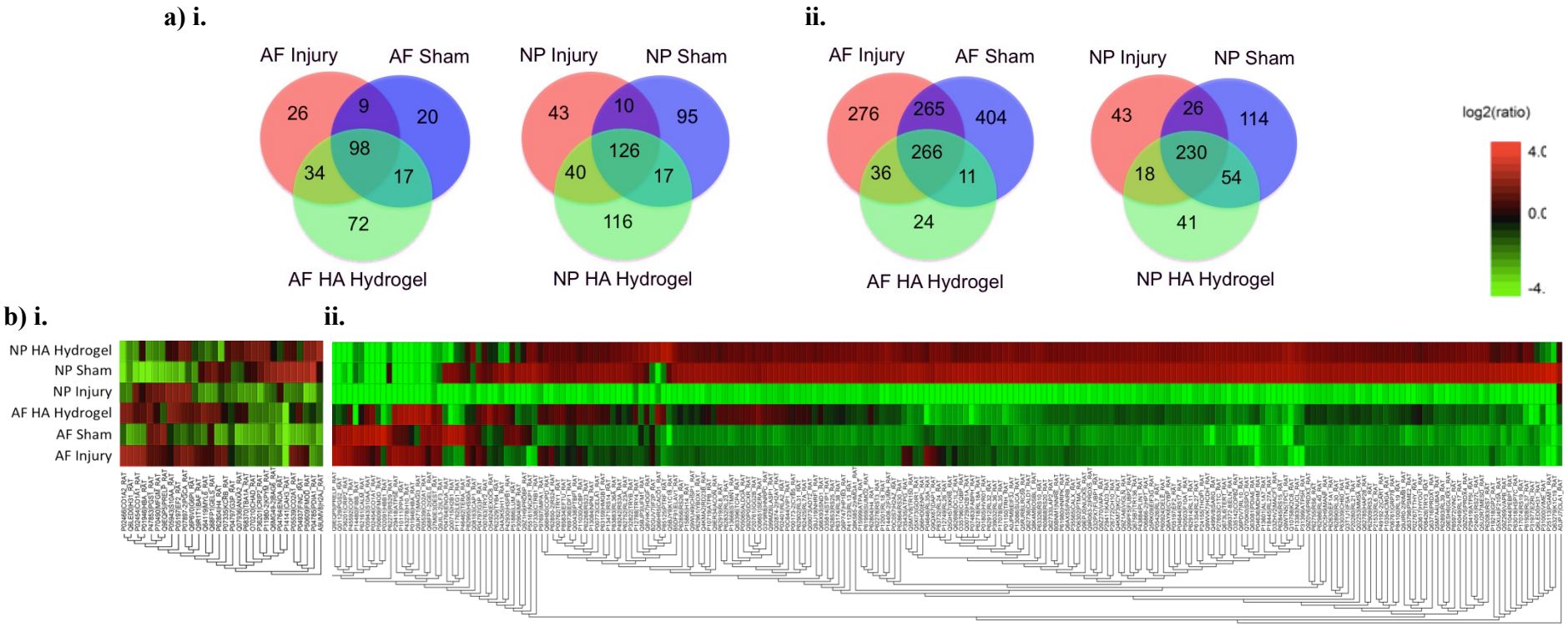

Figure 4.8 Proteomic analysis of intervertebral discs. (a) Venn diagrams showing the numbers of proteins extracted with (a, i) proteinase K digestion (of extracellular matrix) and (a, ii) trypsin digestion of cells and extracellular matrix, in annulus fibrosus (AF) and nucleus pulposus (NP) tissues of the sham control, intervertebral disc injury and HA-hydrogel-treated injury groups. (b) Proteins were isolated from the extracellular matrix (ECM) by proteinase K digestion (b, i), and from cells and ECM by trypsin digestion (b, ii). Differentially expressed proteins are shown in heatmaps of $\log_2$-transformed abundance generated by Peak Studio, with red for high expression and green for low.

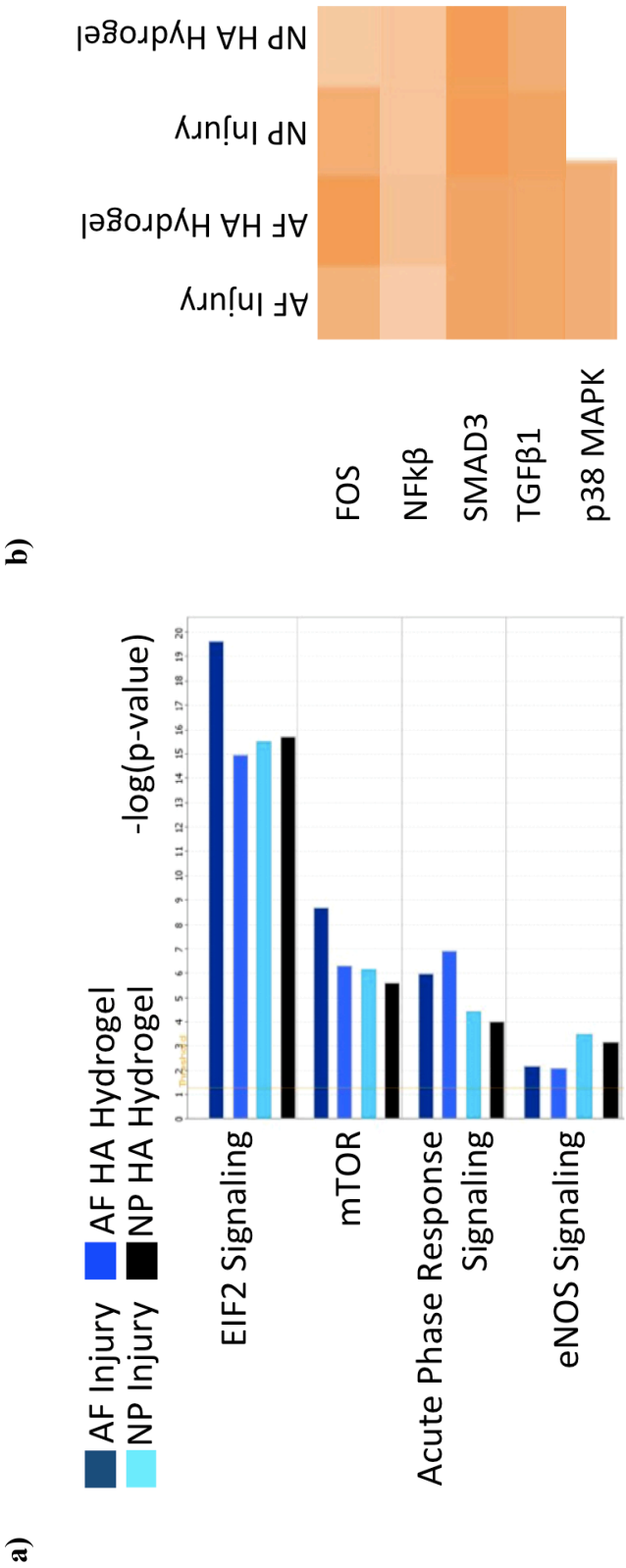
a)
AF Injury
NP Injury
AF HA Hydrogel
NP HA Hydrogel
-log(p-value)
EIF2 Signaling
mTOR
Acute Phase Response Signaling
eNOS Signaling
b)
AF Injury
AF HA Hydrogel
NP Injury
NP HA Hydrogel
FOS
NFkβ
SMAD3
TGFβ1
p38 MAPK

Continued

c)

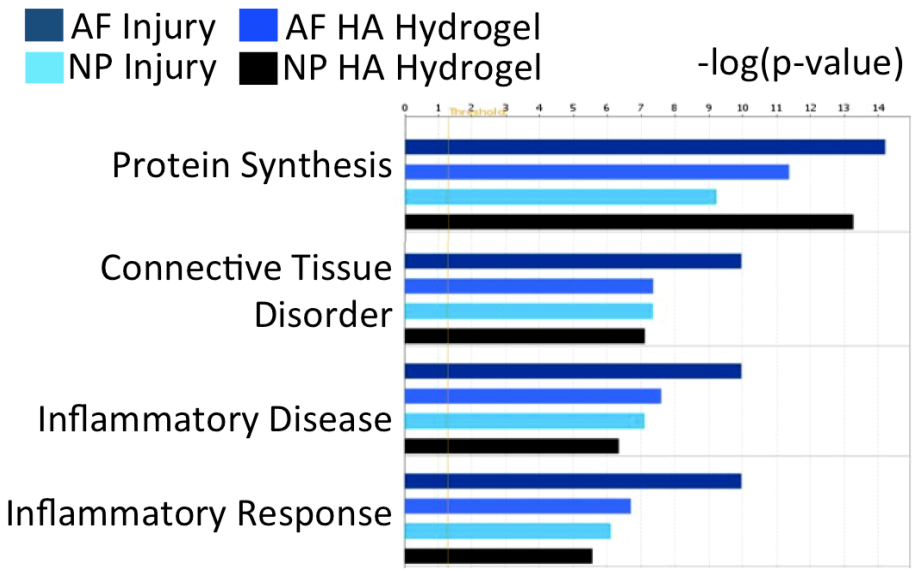

Figure 4.9 Ingenuity Pathway Analysis (IPA) of the protein dataset from MaxQuant analysis. **(a)** IPA identified canonical pathways that were likely to be involved in the response to disc injury and to hyaluronic acid (HA)-hydrogel implantation in annulus fibrosus (AF) and nucleus pulposus (NP) tissues. **(b)** Heatmap of the top upstream regulators involved in modulated cellular functions with a Z score >1.5. **(c)** Disease-related and function-related pathways identified by IPA.

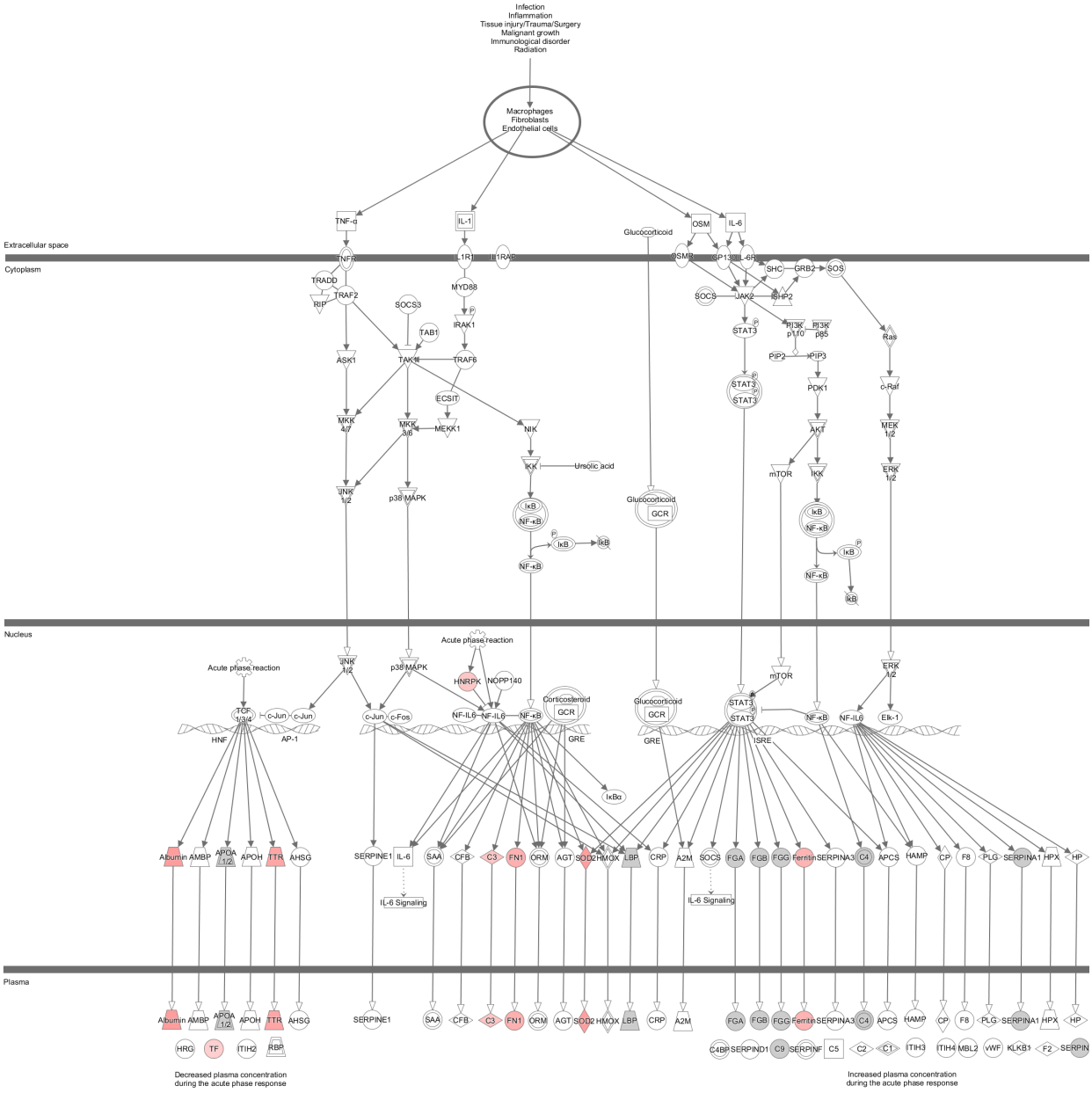

Figure 4.10 Ingenuity Pathway Analysis (IPA) revealed canonical 'acute-phase signaling' in annulus fibrosus (AF) and nucleus pulposus (NP) tissues from the dataset of differentially expressed proteins in the experimental groups. Red symbols indicated activation of acute phase proteins from injured tissue that were presented in the signaling pathways associated with inflammation, pain and dysregulation of matrix.

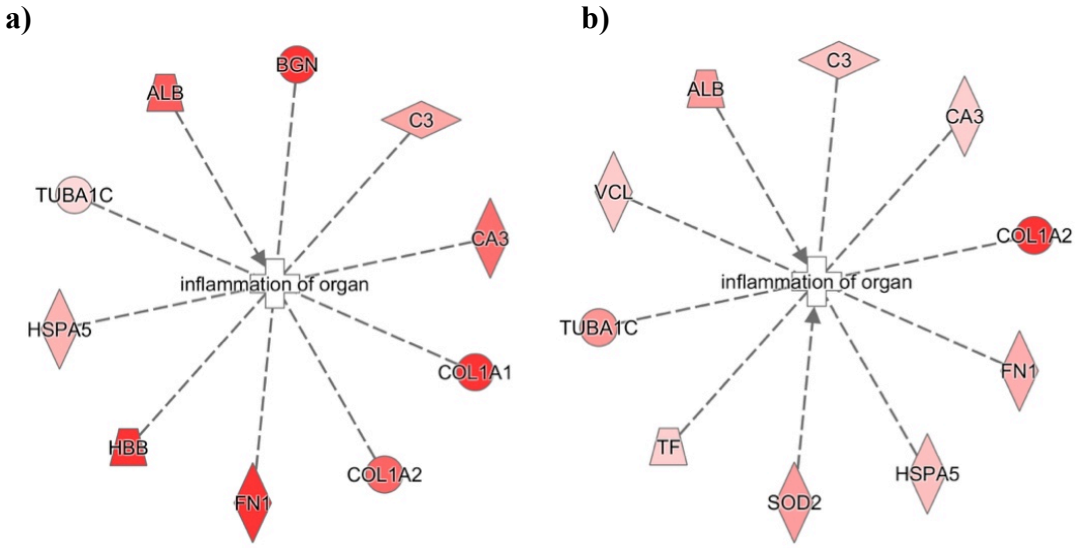

Figure 4.11 Inflammation networks in the injured (a) annulus fibrosus (AF) and (b) nucleus pulposus (NP) tissues, determined by Ingenuity Pathway Analysis (IPA) of the dataset of differentially expressed proteins in the experimental groups. Red symbols from light to intense colour indicated activation of acute phase proteins associated with inflammation in the injured discs.

a)

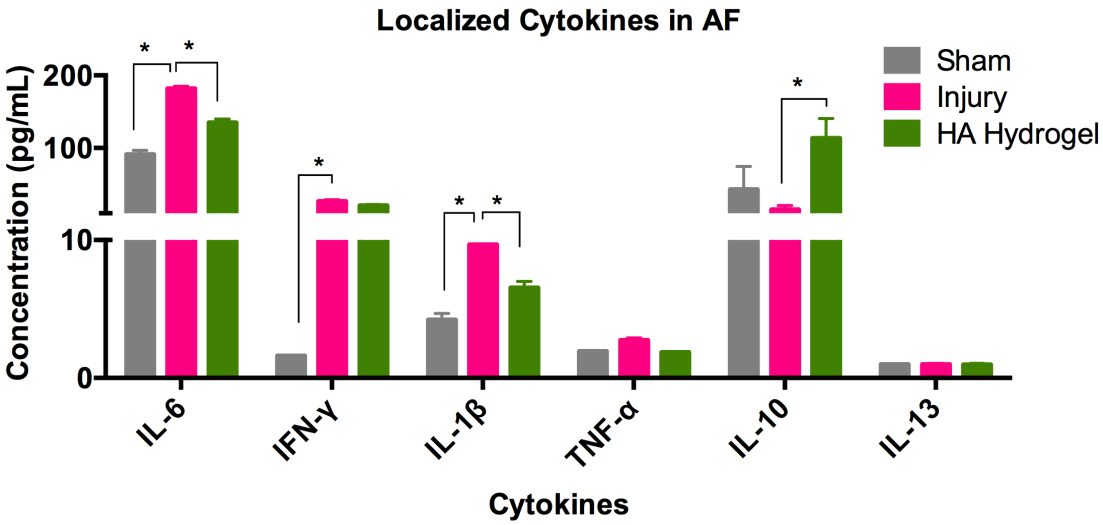

b)

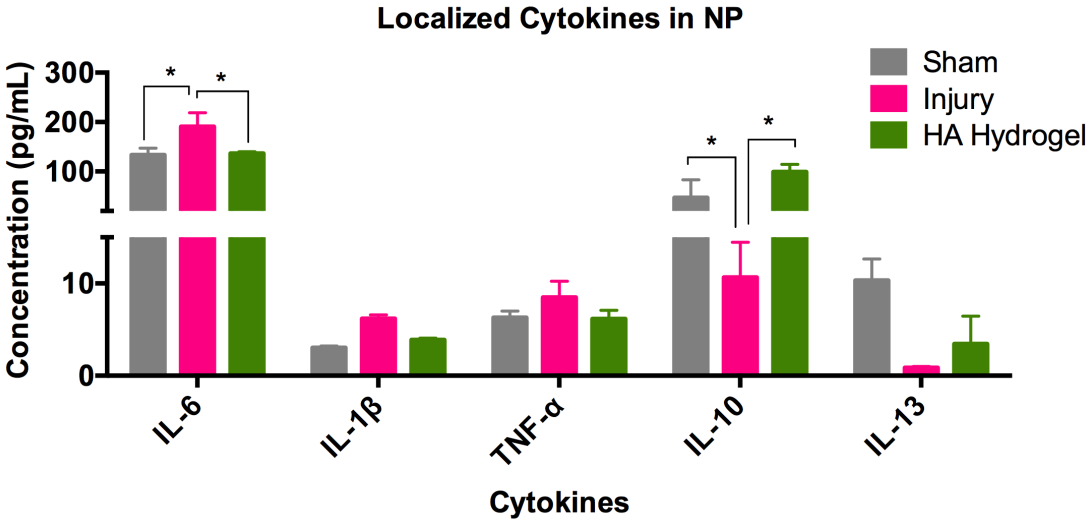

c)

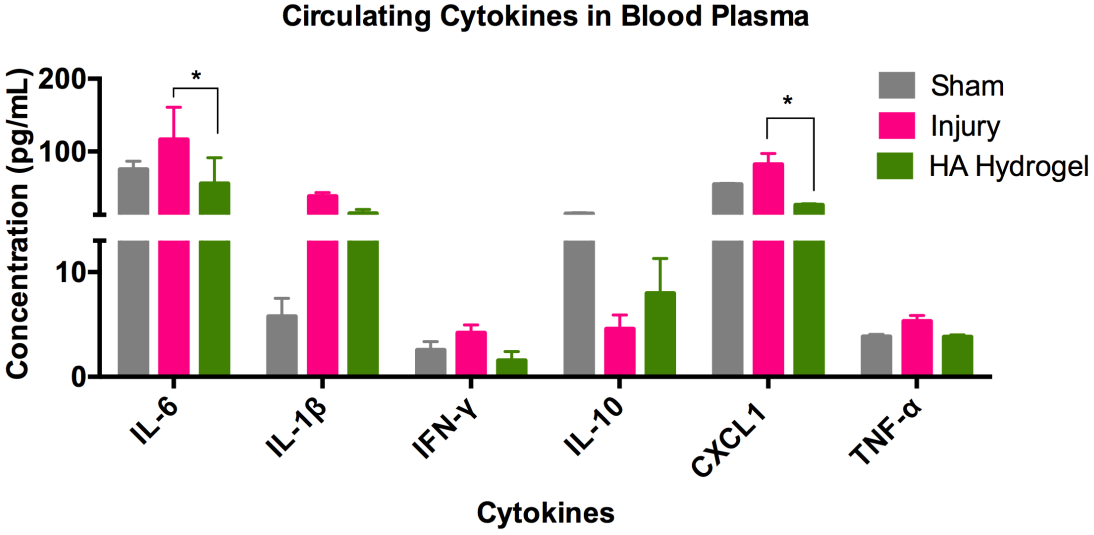

Continued

d)

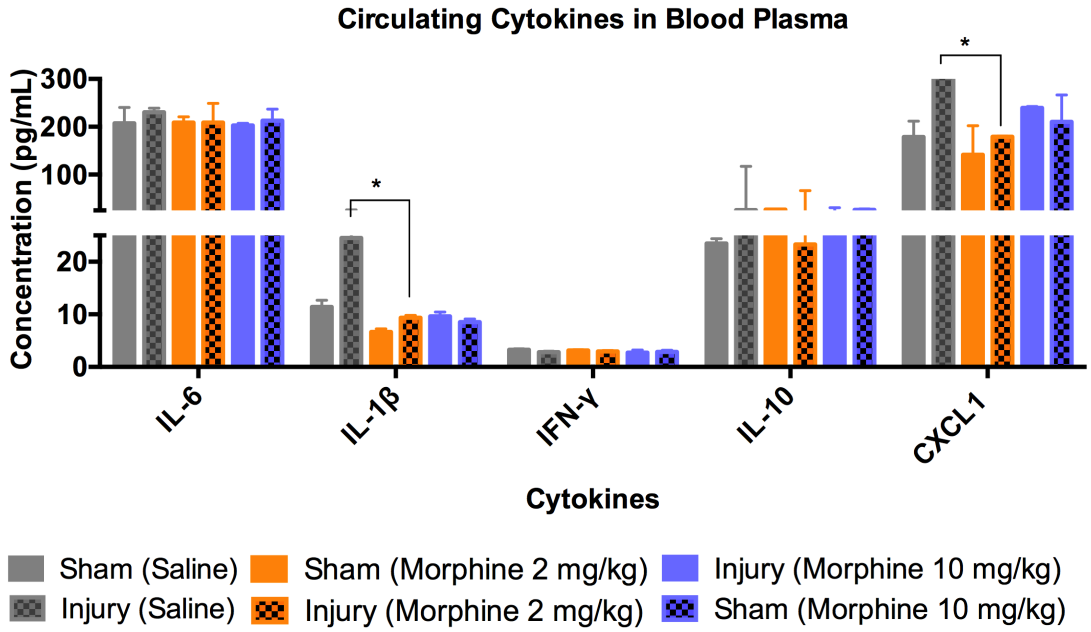

Figure 4.12 Cytokine profiling. (a-b) In AF and NP tissues, the localized levels of inflammatory cytokines IL-6, and IL-1β (and IFN-γ in AF) were significantly higher (and IL-10 was lower) in the untreated injury group than in the sham control or HA-hydrogel-treated injury groups. (c) In blood plasma, the levels of IL-6, CXCL1 and IL-1β were significantly higher in the untreated injury group than in the sham control or HA-hydrogel-treated injury groups (d) Levels of IL-6, CXCL1 and IL-1β varied between saline-treated and morphine-treated groups (n = 10 for d, n = 5 for a-c, two-way ANOVA; p <0.05). Data are presented as the mean ± standard error of the mean.

a)

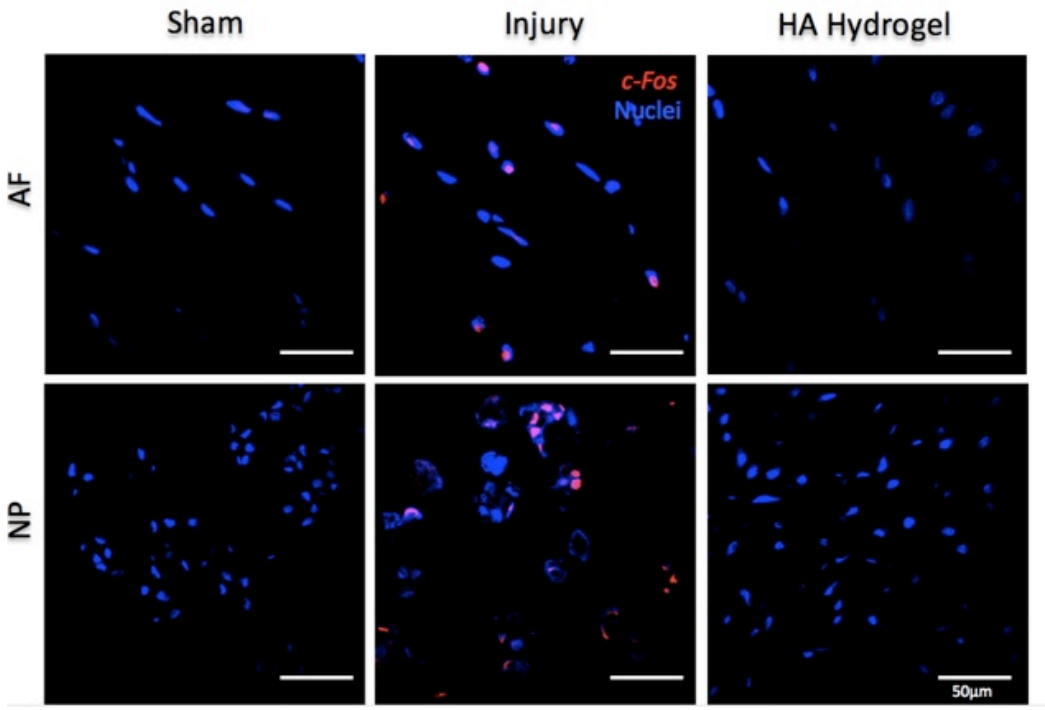

b)

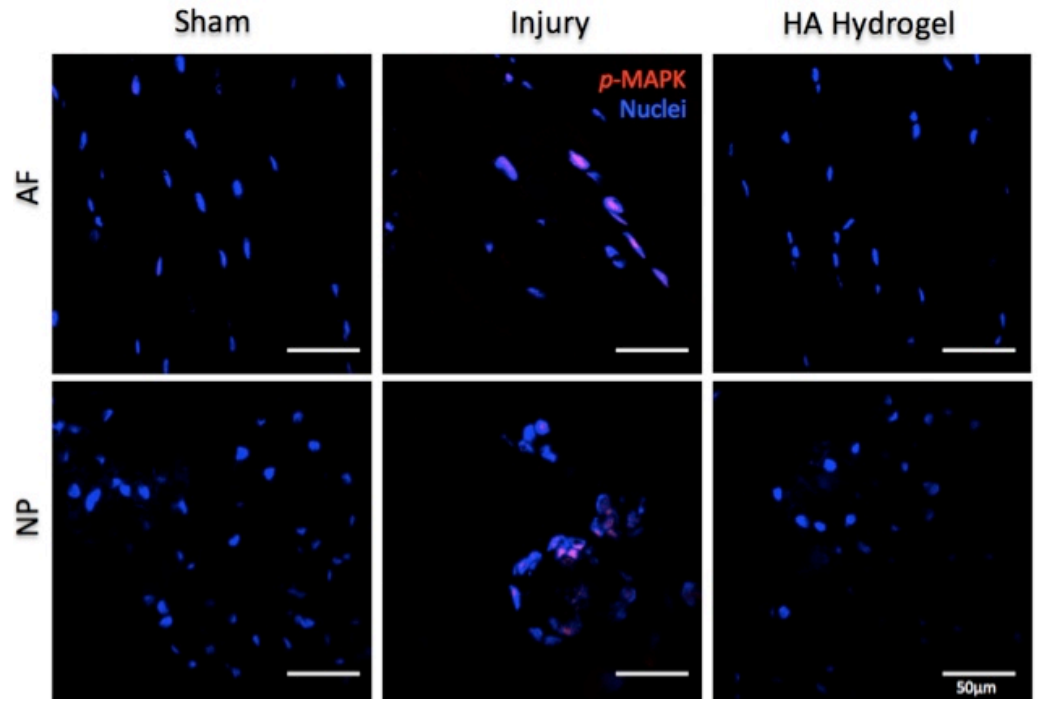

Continued

c)

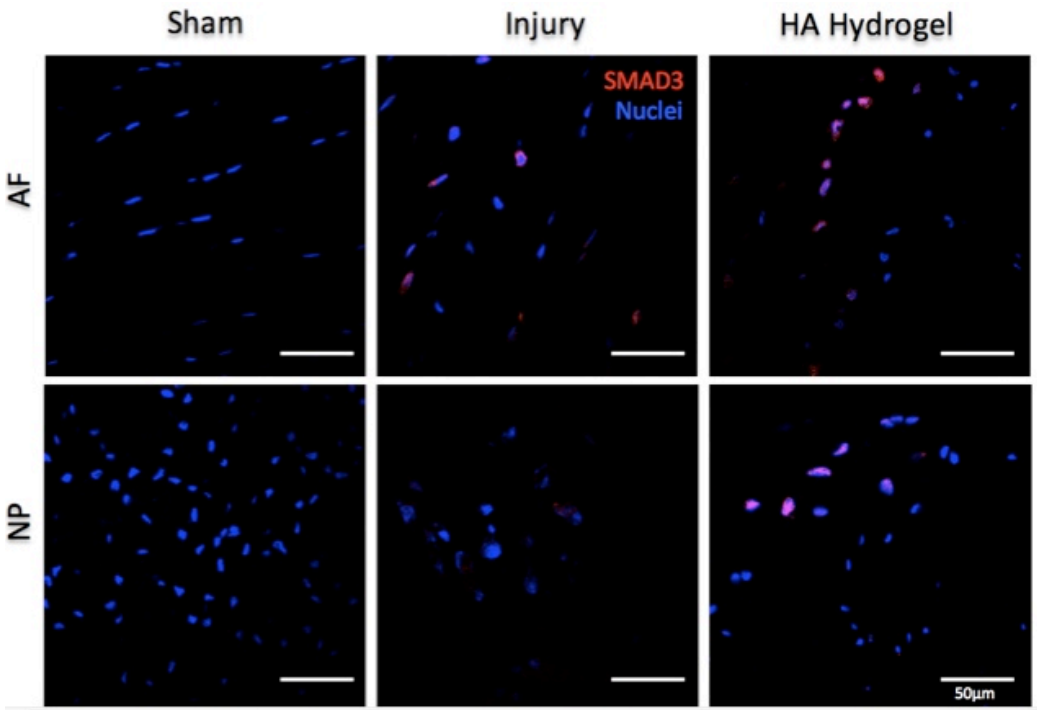

d)

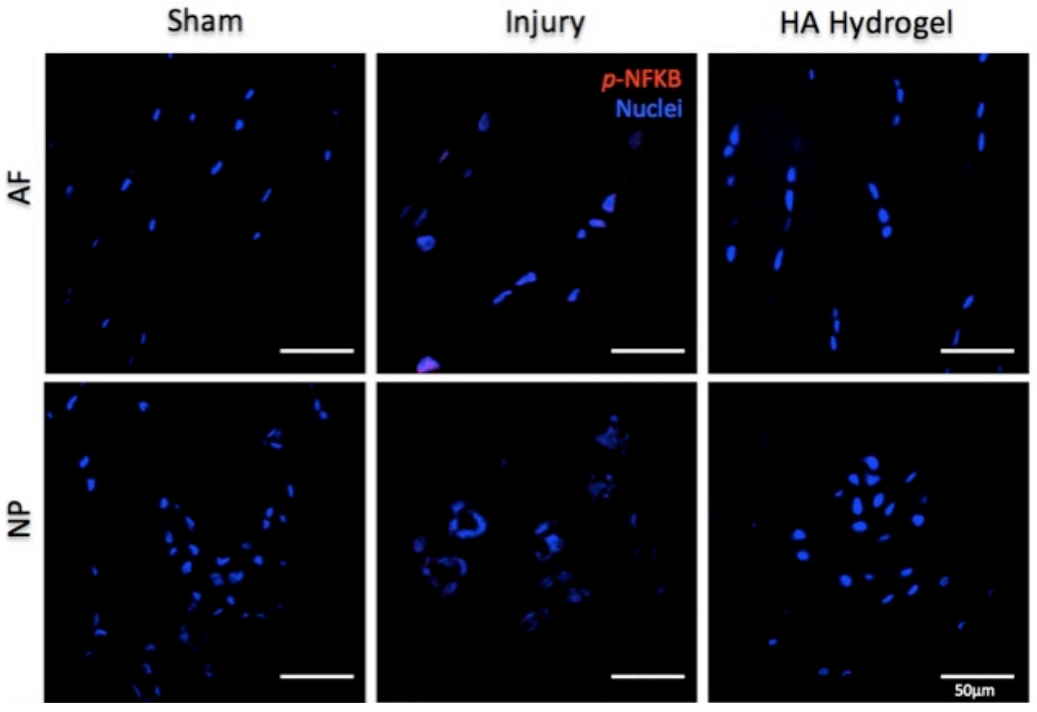

Continued

e) i.

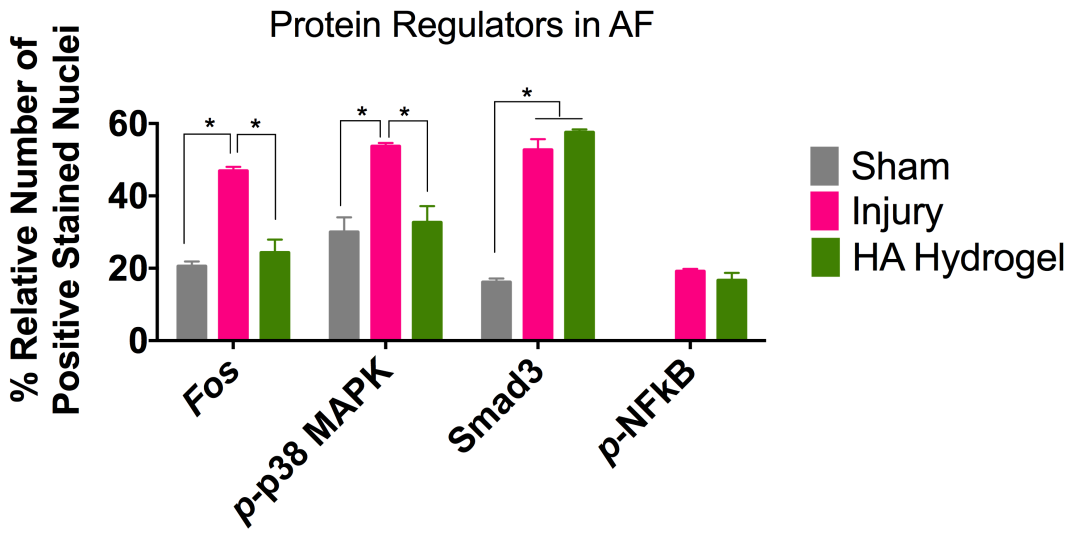

ii.

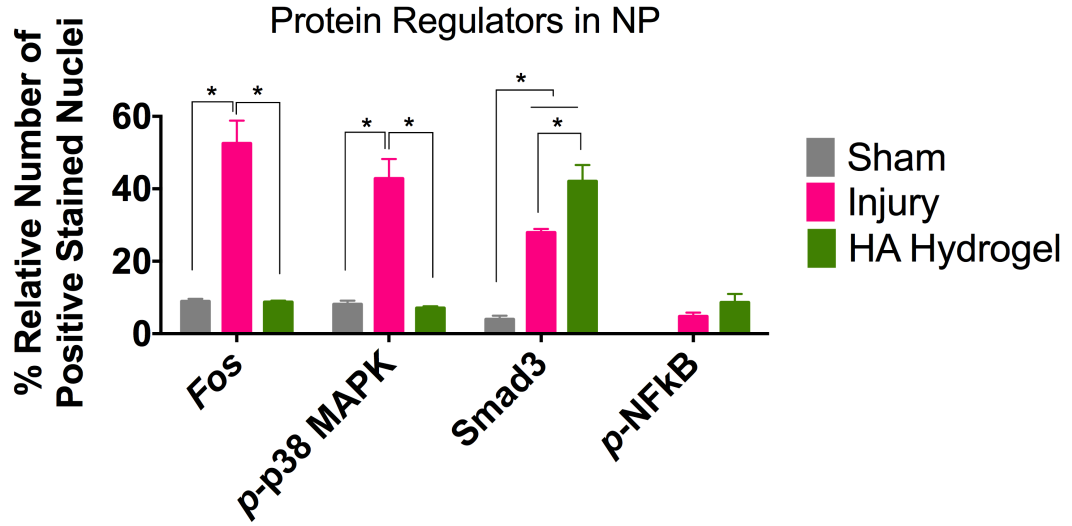

Figure 4.13 Expression of the regulator proteins: **(a)** *c-Fos*; **(b)** phosphorylated p38 MAPK; **(c)** phosphorylated NF-κB; **(d)** Smad3. **(e)** Stereology quantification of positively stained of regulator proteins in AF (i) and NP (ii) tissues. *Significant differences were noted between the different groups (n = 3, one-way ANOVA, $p < 0.05$). Data are presented as the mean ± standard error of the mean. Scale bar = 50μm.

a)

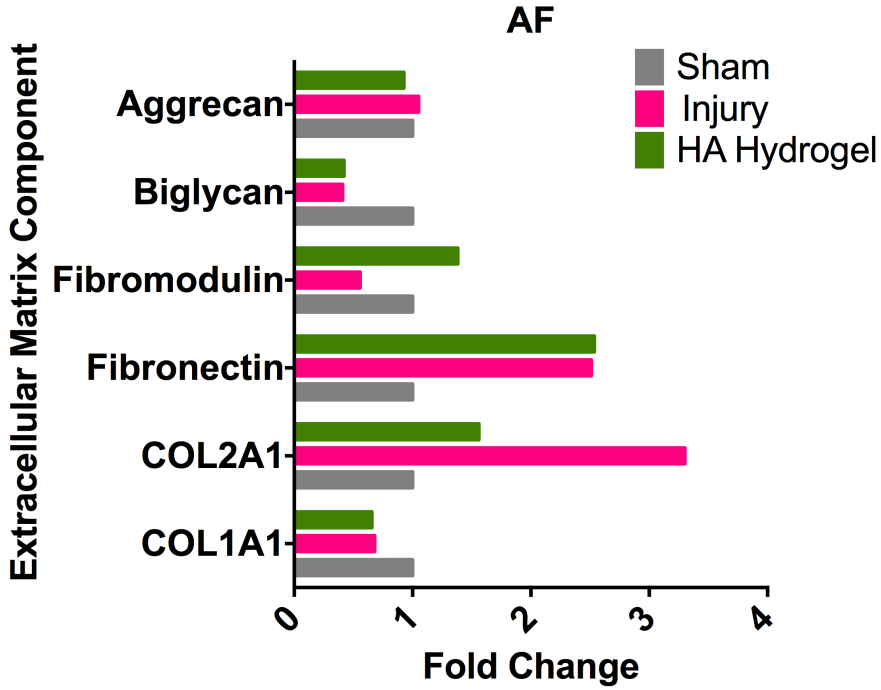

b)

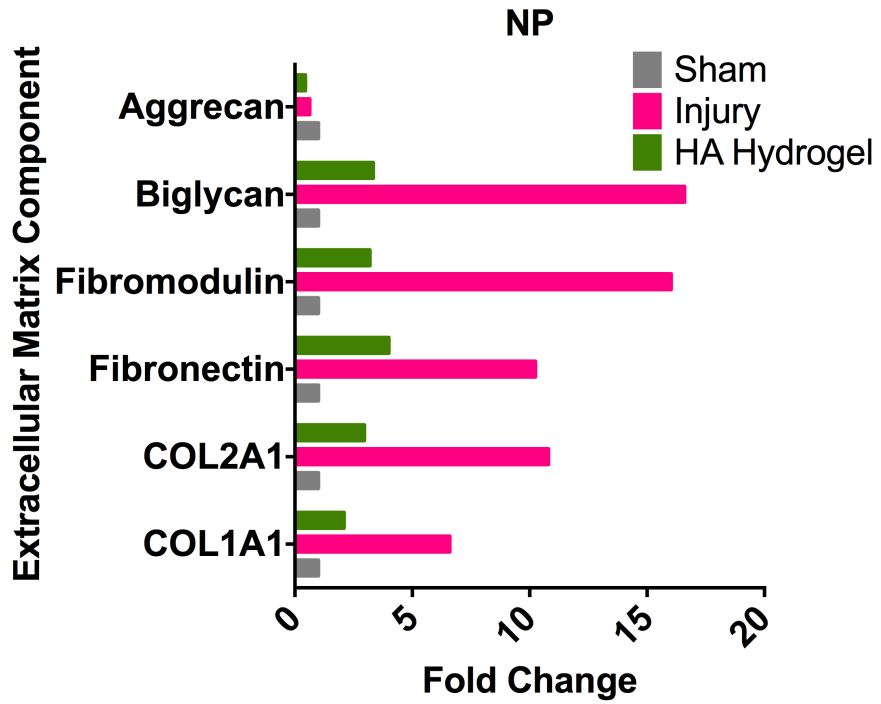

Figure 4.14 Dysregulation of ECM proteins in sham control, intervertebral disc injury and HA-hydrogel-treated injury groups in (a) annulus fibrosus (AF) and (b) nucleus pulposus (NP) tissues on post-operation day 29. Abbreviations: COL1A1, α1 type I collagen; COL2A1, α1 type II collagen.

a)

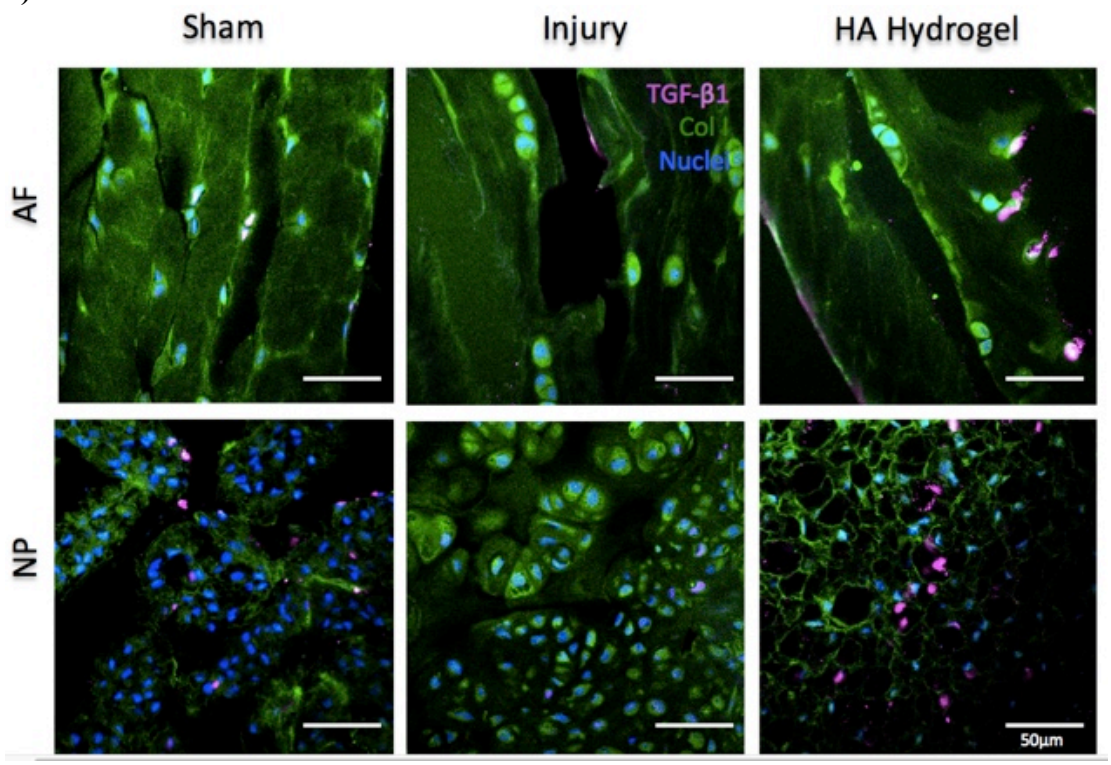

b)

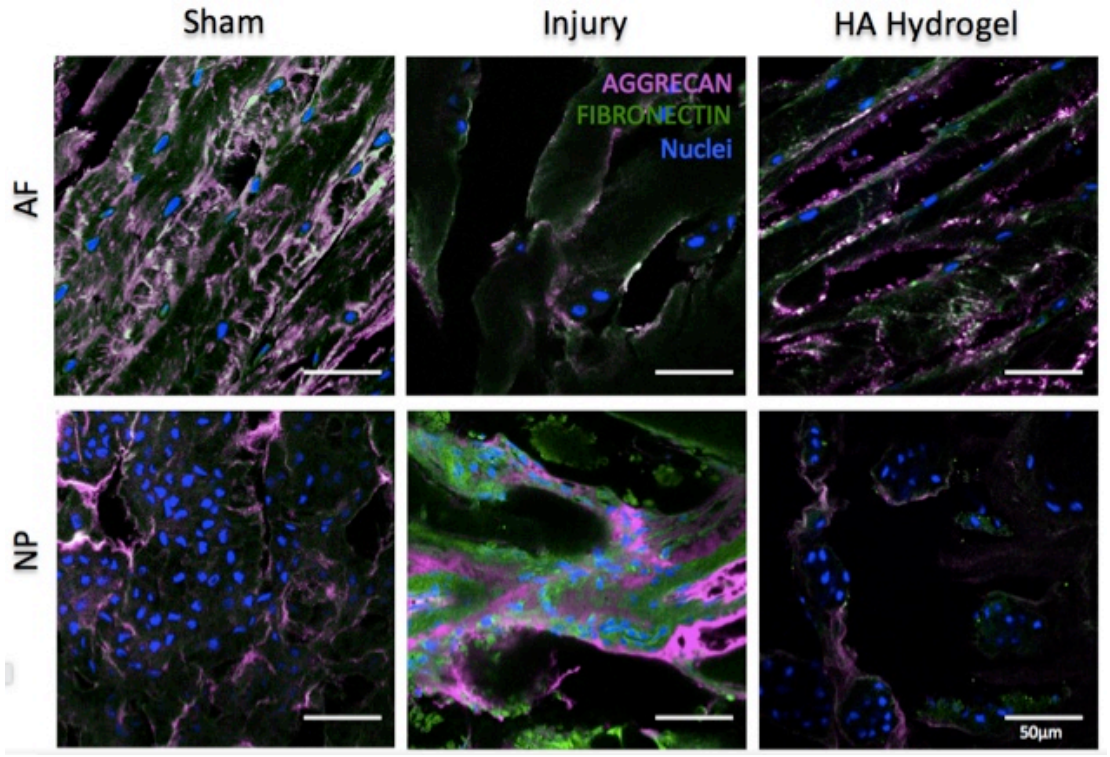

Continued

c) i.

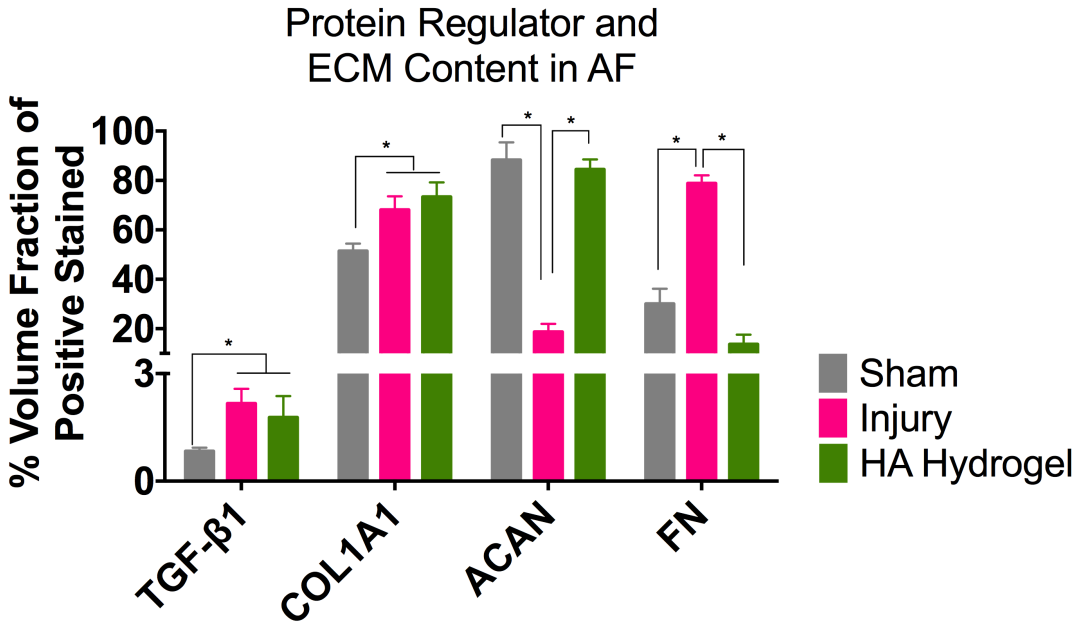

ii.

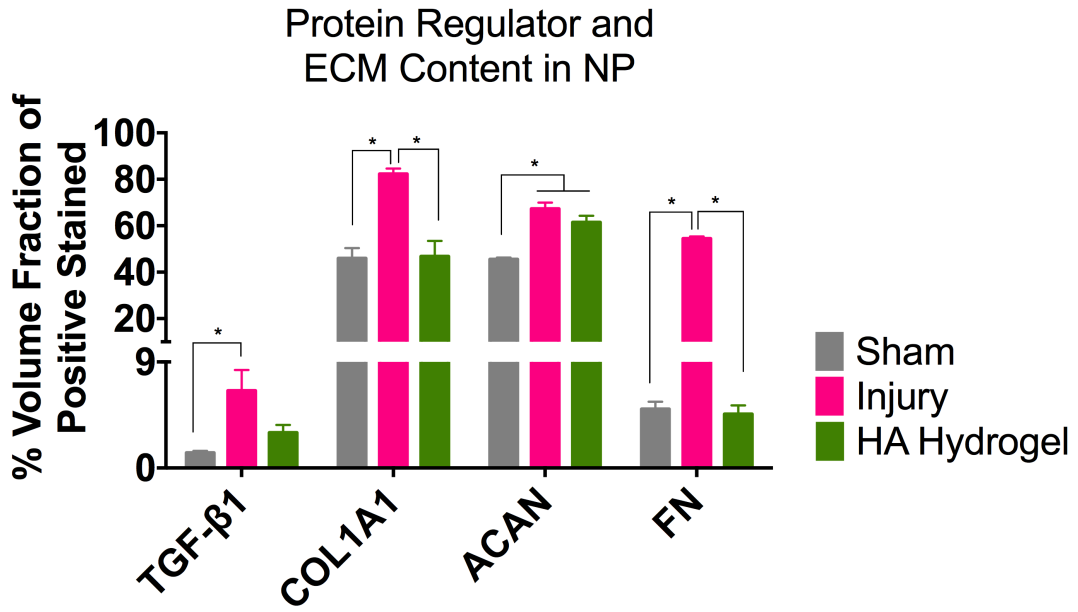

Figure 4.15 Expression of the ECM contents **(a)** TGF-β1 and type I collagen; **(b)** aggrecan and fibronectin. **(c)** Stereological quantification of regulator protein and ECM contents in AF (i) and NP (ii) tissues. *Significant differences were noted between the different groups (n = 3, one-way ANOVA, $p < 0.05$). Data are presented as the mean ± standard error of the mean. Scale bar = 50μm.

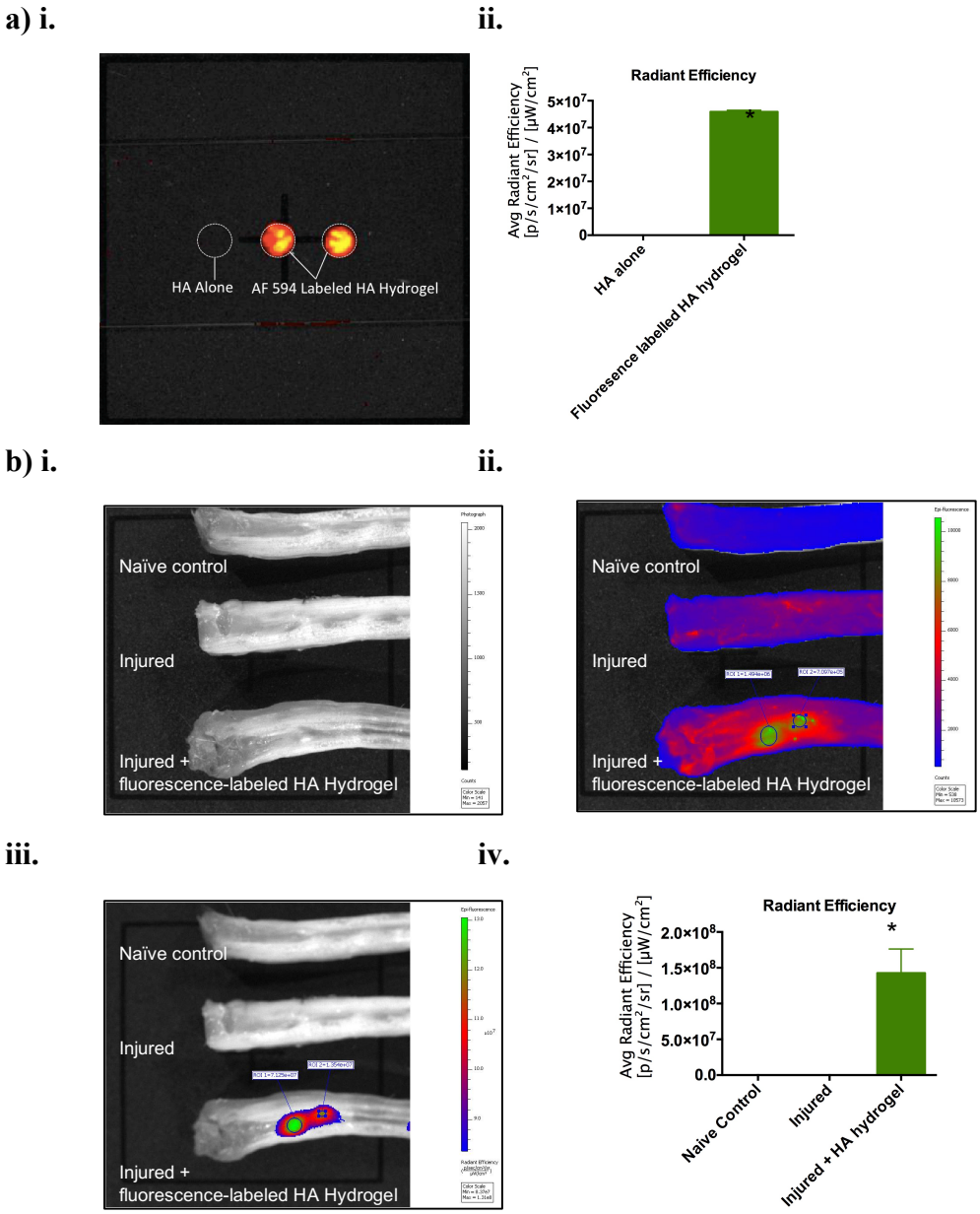

Figure 4.16 Pharmacokinetic effect of an injectable HA hydrogel in the punctured rat tail at post-injury day 2 by IVIS® imaging. (a, i) Control of hydrogel *in vitro*. Overlay of fluorescent image and photograph of fluorescence-labeled HA hydrogel and HA solution alone was observed. (a, ii) An average radiant efficiency of region of interest in the fluorescence-labeled HA hydrogel was higher than in HA hydrogel alone. (b, i) Photograph of the rat tails. (b, ii) The composite fluorescent image of total tissue overlay with photograph of the rat tails. Fluorescence-labeled HA hydrogel indicated by green colour. (b, iii) Localisation of HA hydrogel (mapped in green colour) in the rat tail. *Significant differences were noted between the groups. (n = 2, Student t-test for a; n = 3, one-way ANOVA for b, $p < 0.05$). Data presented as the mean ± standard deviation.

operation day 2. The fluoresence-labeled HA hydrogel was indicated by green epi-fluorescence (Figure 4.16b, i-iii). The localization of HA hydrogel (green epi-fluorescence) was confirmed in the rat tail after subtracting the background of fluorescence relative to the naïve control (Figure 4.16b, iii). A significant higher of radiant efficiency of fluoresence in the rats injected with fluoresence-labeled HA hydrogel (Figure 4.16b, iv), suggesting that HA hydrogel was maintain in the injury site over time (post-injury day 2).

4.7 Discussion

At the time of surgery, HA hydrogel was implanted in one group of rats, to investigate the pharmacodynamic effects in physiological conditions. Rats implanted with HA hydrogel had lower levels of thermal hyperalgesia than those with injury alone (Figure 4.2a), which corresponds to a previous observation that an HA solution reduces behavioral nocifensive responses to noxious heat in a mouse model [16]. A reduction in mechanical allodynia was also observed with HA-hydrogel treatment (Figure 4.2b). The tail-flick test showed that HA-hydrogel-treated rats exhibited diminished thermal hypoalgesia, to a level that was similar to that of the sham group (Figure 4.2c), suggesting inhibition of the DNIC phenomenon, as seen with low doses of morphine. Overall, these data support the hypothesis that HA hydrogels reduce nociceptive behavioral responses to noxious or innocuous stimuli in an IVD-injury pain model of the rat tail.

Hyperalgesia resulting from tissue injury and inflammation contributes to central sensitization because of the continuous activation of spinal-cord excitatoryneurotransmitters or neuropeptides [24]. A significantly higher level of *c-Fos* mRNA expression was observed in the untreated injury group than in the sham group or in the HA-hydrogel injury group (Figure 4.2d), which agrees with previously observed induction of *c-Fos* with the development of pain hypersensitivity [25]. Central sensitization also increases the activity of C fibers, enhancing the excitability of post-synaptic neurons by the release of glutamate and substance P [26]. Mechanistically, substance P binds to its receptor and enhances glutamate–NMDA activity, enabling sustained influx of Ca^{2+} into post-synaptic neurons, promoting impulse transmission [27]. A significantly higher level of *Tac1*

mRNA expression was observed in the untreated injury group than in the sham group or in the HA-hydrogel injury group (Figure 4.2d). This is inline with other IVD-injury model, combining annular puncture with an injection of TNF showed evidence of substance P in DRG neurons [28]. Injury-induced inflammation in peripheral tissues might shift Aβ fibers to a nociceptive phenotype like that of C fibers, in which substance P is expressed, post-synaptic transmission is elevated and the central response to innocuous stimuli is exaggerated [26]. HA-hydrogel treatment suppresses injury-induced expression of markers of central nociception in the dorsal horn of the spinal cord, thereby interfering with nociceptive processing in a higher region of the CNS.

Nociceptors are free nerve endings of fiber types Aδ or C of afferent sensory nerves that terminate in the dorsal horn of the spinal cord. Neurogenic mediators are released during hyperalgesia after tissue injury, and can sensitize nociceptors, initiating nociceptive nerve transmission to the spinal cord [29]. An inhibitory effect of HA hydrogel was demonstrated on injury-induced expression of GAP43 (which is expressed during nerve ingrowth), the sensory neuropeptide CGRP and the pro-nociceptive ion channel TRPV1 and Trk-A in AF and NP tissues (Figure 4.3). Previously, growth of small, unmyelinated sensory nerve fibers into the inner third of the AF and into the NP has been identified in association with chronic low-back pain; these fibers expressed GAP43 and substance P [30]. The levels of expression of CGRP and Trk-A in sensory nerve fibers innervating the outer AF define these nociceptive DRG neurons as being NGF-sensitive neurons, which are small C fibers that convey a dull pain [31-35]. Trk-A activation leads to neuronal transduction in the adult nervous system, and NGF has been linked to mechanically-evoked pain in OA [36-37]. These results demonstrated the inhibitory effect of HA hydrogels on innervation and on pro-nociceptive receptors. HA has previously been shown to lower the excitability of the TRPV1 channel, reducing impulse activity in peripheral nociceptor endings underlying pain in cultured DRG neurons and *in vivo* in mice [16].

Injury-induced degenerative changes influence glycosylation in AF and NP tissues. Upregulation of glycosyltransferase mRNA and expression of α-(2,3)/α-(2,6)-sialylated *N*-glycans have been observed in severely degenerated human cartilage, as indicated by the presence of GalNAcβ1–4GlcNAc-terminated structures

and Core 2 O-glycans, as well as the binding of several lectins [21]. It was found that HA-hydrogel implantation eliminated the injury-induced elevation of binding in AF and NP tissues of SNA-I, MAA and WGA (which indicate sialylation) and GS-I-B4 (which indicates galactosylation). GS-I-B4 can be used to trace non-peptide-containing sensory neurons in cervical discs [38], and elevation of GS-I-B4 binding and the number of sensory nerve terminals were observed in the coccygeal disc after injury, suggesting that sensory hyper-innervation in the injury model mimics the processes involved in discogenic pain. This innervation seems to be inhibited by HA-hydrogel implantation

Chondroitin sulfate is composed of repeating units of GalNAc and glucuronic acid, and GalNAc may be sulfated at the 4-position or the 6-position, which produces a high degree of structural heterogeneity [39]. It was found that, compared with uninjured controls, chondroitin sulfate expression was significantly higher in the ECM of AF and NP tissues in injured rats, and was not affected by implantation of HA hydrogel. Synthesis of sulfated GAGs may promote disc tissue restoration, as chondroitin sulfate has been shown to increase ECM production via the integrin–WNT5A pathway [40]. Notably, chondroitin sulfate from IVD-derived notochordal cells has also been shown to inhibit neurite growth *in vitro* [41]. Here, it was observed chondroitin sulfate was correlated (CC > 0.5) with peripheral sensory innervation and nociceptive TRPV1, which may indicate that recruitment of chondroitin sulfate deposition is needed not only for tissue recovery, but also to modulate hyper-innervation and peripheral nociception in AF and NP tissues.

Fibromodulin is an ECM protein of cartilage which is linked to keratan sulfate (KS) and N-linked oligosaccharides that has a key role for maintenance of collagen architecture. KS structures control of collagen fibrils diameter and interfibrillar spacing. KS is modified with sulfated Gal and GlcNAc, α-(2,3)- and α-(2,6)-linked sialic acid and α-(1,3)-linked fucose upon maturity [42]. Here, upregulation of KS expression was indicated in injured AF and NP than in control and HA-hydrogel-treated groups. Similar trends were observed in this study with an increase binding of α-(2,3)- and α-(2,6)-linked sialic acid in the injured tissues than in control and HA-hydrogel-treated injury discs, which may be related to tissue reorganization during injury and remodeling over the treatment.

To elucidate the therapeutic effect of HA hydrogel in targeting signaling pathways underlying disc degeneration and pain, proteins were identified, quantified and mapped their interactions using pathway analysis. Pathway analysis revealed that 'acute-phase-response signaling' involving IL-6, IL-1β and the glucocorticoid receptor is one of the pathways that contributes to the downstream signaling cascade that activates NF-κB, p38 mitogen-activated protein kinase (MAPK) and *c-Fos*, which encode pro-inflammatory, catabolic and acute-phase proteins that act during disc degeneration (Figure 4.9a; Figure 4.10; Figure 4.11; Figure 4.13). High local levels of pro-inflammatory cytokines IL-1β, IL-6, IL-8 and TNF have been shown to have an essential role in the development of pain during disc degeneration [43]. Higher levels of pro-inflammatory cytokines, including IL-6 and IL-1β (and lower levels of IL-10) were observed in AF and NP tissues and blood plasma in the untreated injury group than in the sham control group or in the HA-hydrogel-treated injury group (Figure 4.12a-c), which is consistent with the previous observation that HA hydrogels target the IL-1β pathway in inflamed NP cells [18]. These data suggest that HA hydrogel reduces injury-induced inflammation not only in AF and NP tissues, but also systemically. The level of circulatory cytokines was measured after pain inhibition by systemic morphine administration in which levels of IL-6, CXCL1 and IL-1β were higher in the saline-treated injury group than in the low-dose morphine-treated injury group (Figure 4.12d). These findings indicate that both localized and systemic pro-inflammatory cytokines are important in the acute response following disc injury. The implication of this finding can provide a diagnostic platform for screening degenerative disc event (such as inflammation) at systemic level. Thus, systemic levels of IL-6 have previously been shown to be elevated in patients with low-back pain diagnosed with disc diseases [44].

Degenerative change commences in the ECM of NP tissue, with reductions in levels of proteoglycans, type II collagen and water content, leading to poor hydrodynamic transfer of axial stress to the AF [45-47]. The higher levels of type I collagen, type II collagen, fibronectin, fibromodulin and biglycan were observed in NP tissue, and type II collagen in AF tissue in the untreated injury group, compared with the sham and HA-hydrogel-treated injury groups (Figure 4.14; Figure 4.15). In the later stages of IVD degeneration, dysregulated ECM synthesis has been observed, with type I collagen forming strong fibrils predominantly within the NP

and inner AF, type II collagen in the outer AF, downregulation of aggrecan, and upregulation of fibronectin, versican, biglycan and decorin, leading to the loss of weight-bearing capacity and disc height [48-49]. It was found that HA-hydrogel treatment inhibited ECM dysregulation, reducing the development of fibrous tissue formation. Protein pathway analysis suggested that the Smad3 family regulated the ECM content, including aggrecan, type I collagen and fibronectin, via TGF-β1 (Figure 4.13; Figure 4.15), It was previously shown that GlcNAc, a component of HA, promotes ECM deposition through the MAPK and SMAD pathways in *ex vivo* degenerated bovine discs [50].

These findings provide the basis for a model of HA hydrogel action in reducing discogenic pain. HA hydrogel may target inflammation and nociception by attenuation of the key IL-1β and IL-6 inflammatory pathways, thereby inhibiting sensory nerve innervation and suppressing expression of peripheral and central pain markers, and modulating the ECM and cellular composition (Figure 4.17). During disc-injury-induced inflammation, pro-inflammatory cytokines, such as IL-1β, IL-6 and IFN-γ, are produced by NP and AF cells as well as by invading macrophages. IL-1β binds to its receptor IL-1R and recruits myeloid differentiation primary response protein MyD88 and IL-1R-associated kinase 4 (Irak4) to phosphorylate Irak1, enabling transient recruitment of TNF receptor-associated factor 6, dissociation of Irak1 from the receptor and activation of TGF-beta-activated kinase 1 (Tak1) [51]. Activated Tak1 (Tab1 in rats) phosphorylates the IκB kinase complex and MAPKs to further activate and translocate *c-Jun*, *c-Fos*, CCAAT/enhancer-binding protein β and NF-κβ into the nucleus, resulting in the transcription of genes encoding acute-phase-response proteins, cytokines and degradative enzymes [51]. Binding of IL-6 to IL-6R facilitates IL-6R subunit β (gp130) trans-phosphorylation and Janus-kinase activation, which mediates recruitment of Stat3. Dimerization of phosphorylated Stat3 results in nuclear translocation and transcriptional activation of genes including those encoding acute-phase-response proteins [52] (Figure 4.17b, i).

In the peripheral region of healthy IVDs, afferent nerves terminate in the outer regions of the AF tissue, but in degenerated discs they project into the inner layer of AF and NP tissues [30]. After induced disc injury, noxious stimuli and the release of neurogenic mediators (such as pro-inflammatory cytokines) and neurotrophic factors promote hyper-innervation of the sensory nerve. Activation of

afferent unmyelinated C fibers or thinly myelinated Aδ fibers occurs by sensitization of nociceptors, such as the ion channel TRPV1, through post-translational phosphorylation upon activation of G-protein-coupled receptors or tyrosine kinase receptors (such as Trk-A). This process results in the influx of sodium and calcium ions, which eventually induces membrane-potential excitability and generation of the nociceptive impulse (Figure 4.17c, i) [53]. The nociceptive input is transmitted from the injury site to the dorsal horn of the spinal cord and is terminated in lamina II in C fibers and lamina I and laminal V in Aδ fibers. The upregulation of pre-synaptic neurotransmitters, such as the amino acids aspartate and glutamate, leads to an increase in neurotransmitter release at post-synaptic neurons, which is enhanced by substance P. Synaptic impulse transmission to second-order neurons occurs [29][54] and subsequently activates expression of the immediate-early gene *c-Fos*, thereby conveying nociceptive input to higher centers in the brain (Figure 4.17c, iii) [25]. Here, afferent neurons connect with second-order neurons and cross over anterolaterally. The projections of these neurons relay pain signals along the spinothalamic tract to the thalamus and along the spinoreticulothalamic tract to the brainstem. From these locations, the signals can be propagated to different areas of the brain, including the cerebral cortex area containing the primary and secondary somatosensory cortexes (SI and SII) and cingulate gyrus. The descending inhibitory pathways release noradrenaline and serotonin into the spinal cord to inhibit pain (Figure 4.17a) [25].

This raises the possibility that mechanism of action of HA hydrogel involves interference in the binding of IL-1β and IL-6 to their receptors, and inhibition of transcription of genes that encode pro-inflammatory cytokines and acute-phase proteins. Additionally, glucocorticoid receptor signaling is involved in suppressing inflammation. HA hydrogel, possibly via the Smad3 family and TGF-β1 promotes regulation of ECM proteins (Figure 4.17b, ii) [29]. A high level of chondroitin sulfate in the ECM and downregulation of neurotrophic factors, such as NGF, mediate the inhibition of neurite outgrowth of sensory nerves in discs. Evidence for this process is provided by the suppression of GAP43, which is important for axonal growth, along with inhibition of sensory neuropeptides in AF and NP tissues. The inhibition of NGF binding to its receptor, Trk-A, also interferes with post-translational phosphorylation and can inactivate the ion channel TRPV1, reducing

a)

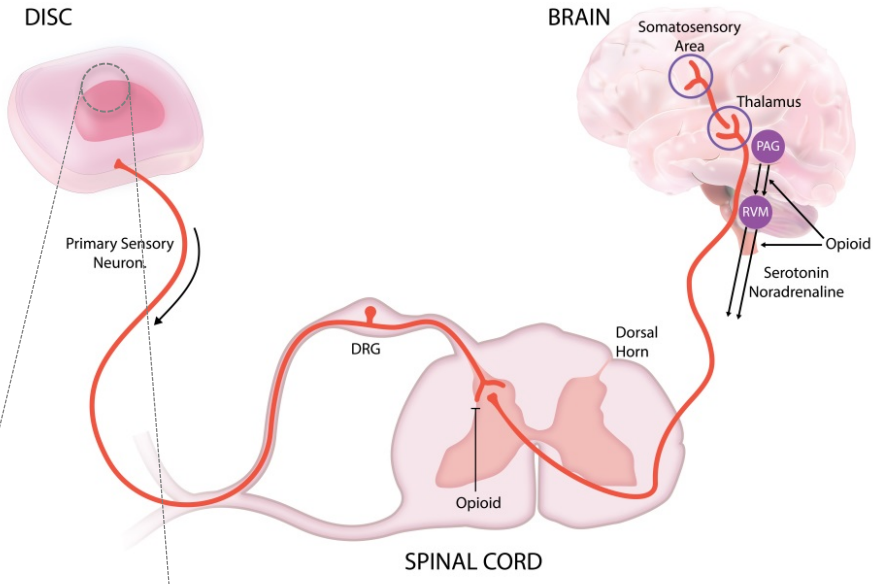

b)

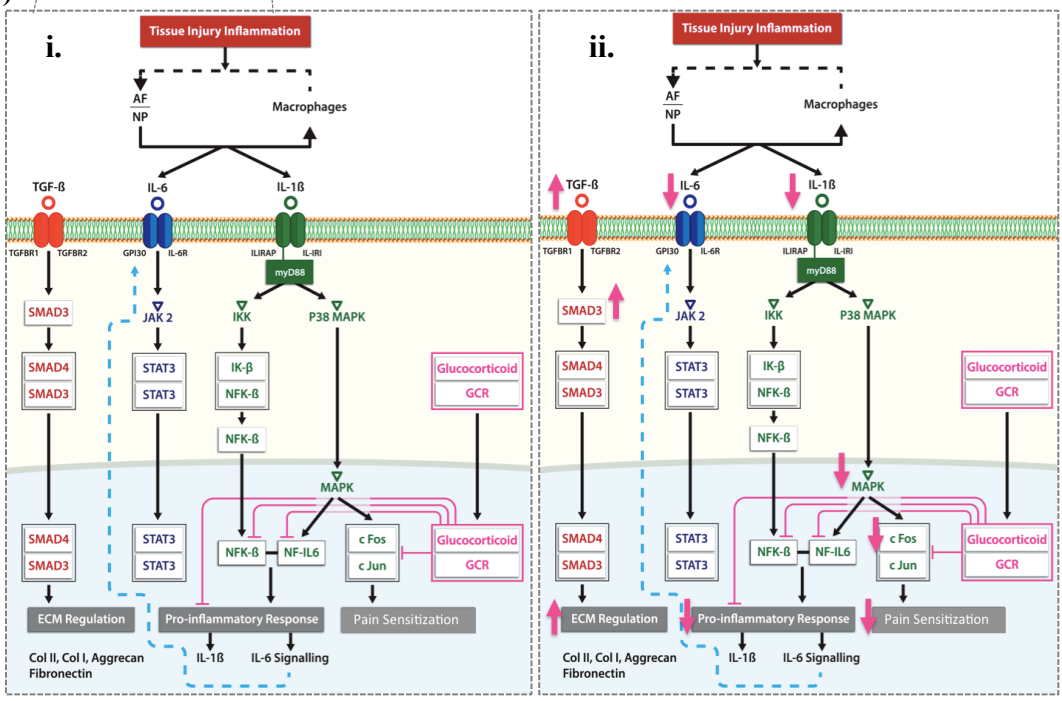

Continued

c) i. **ii.**

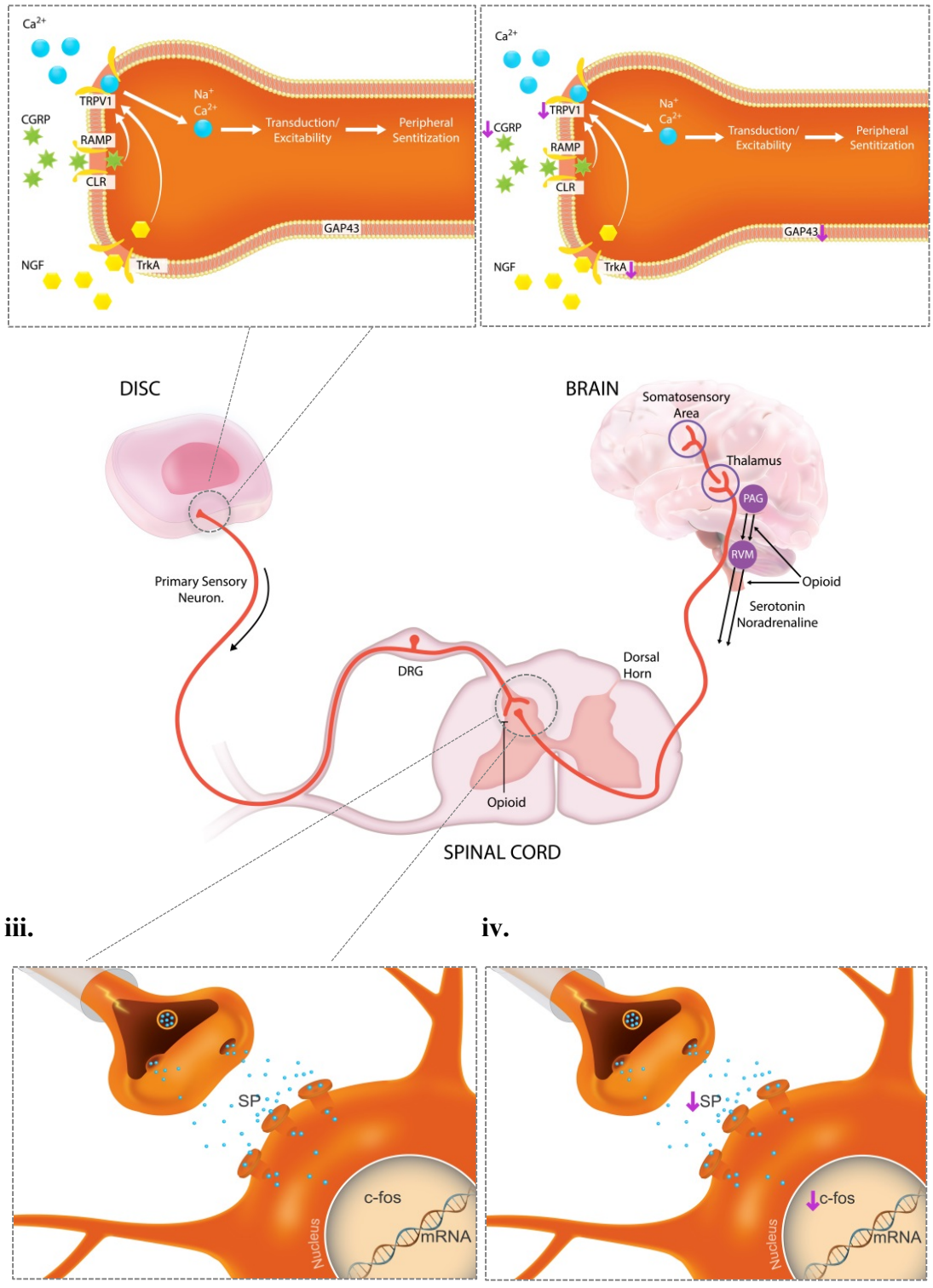

Continued

Figure 4.17 Possible mechanism of action of HA hydrogel in the injury-induced model of disc pain. (a) Pain signaling from the intervertebral discs (IVDs) via the dorsal horn of the spinal cord to the brain for pain processing. Descending pathways inhibit pain transmission by releasing noradrenaline and serotonin into the spinal cord. (b, i) In injured IVDs, annulus fibrosus (AF) and nucleus pulposus (NP) cells (and macrophages) produce IL-1β, IL-6 and IFN-γ. IL-1β binds to IL-1R and recruits the myD88 complex to phosphorylate IL-1R-associated kinase 1 (Irak1) and activate TGF-beta-activated kinase 1 (Tak1) (Tab1 in rats). Tak1 phosphorylates IκB kinase (IKK) complex and p38 mitogen-activated protein kinase (MAPK), inducing nuclear translocation of *c-Jun*/*c-Fos*, CCAAT/enhancer-binding protein β (NF-IL6) and nuclear factor kappa-light-chain-enhancer of activated B cells (NF-κB), for transcription of genes encoding cytokines and catabolic and acute-phase-response proteins. IL-6 binds to IL-6R to facilitate IL-6R subunit β (gp130) trans-phosphorylation and Janus kinase 2 (JAK-2) activation, facilitating nuclear translocation of signal transducer and activator of transcription 3 (Stat3), and transcription of acute-phase-response genes. (b, ii) Implanted HA downregulates IL-1β and IL-6 and interferes with receptor binding, inhibiting downstream cascades and gene transcription. HA hydrogel also upregulates SMAD family member 3 (Smad3) via TGF-β signaling, promoting extracellular matrix synthesis. (c, i) In injured IVDs, sensory nerves terminate in aneural AF and NP tissues. Neurogenic mediators (cytokines and neurotrophins) are released to promote nerve ingrowth, and the presence of noxious stimuli can activate nociceptive fibers by sensitizing transient receptor potential cation channel subfamily V member 1 (TRPV1), enabling influx of sodium and calcium, inducing membrane-potential excitability. (c, ii) With implanted HA hydrogel, IVD expression of calcitonin gene-related peptide (CGRP) and nerve growth factor receptor (Trk-A) is reduced compared with untreated injury, preventing hyper-innervation in discs, and inhibiting pain sensitization. (c, iii-iv) In the dorsal horn, HA hydrogel may suppress nociceptive transmission by attenuating injury-induced expression of *c-Fos* and substance P (*Tac1*).

.

excitability of nociceptive nerve transmission and reducing ion-channel responsiveness to noxious stimuli (Figure 4.17c, ii). At the spinal level, HA hydrogel suppresses substance P in the dorsal horn and reduces *c-Fos* expression, thereby inhibiting nociceptive processing up to the supra-spinal region of the brain to exhibit analgesic effect (Figure 4.17c, iv).

Finally, pharmacokinetic of *in vivo* study revealed the stability of HA hydrogel injection in the punctured discs of the rat tail model atleast at post-injury day 2. Here, Alexa Fluor® 594 was used to label HA hydrogel because the near infrared fluorescence dye is known to be the best choice for the IVIS spectrum imaging especially for living organism. The HA hydrogel was percutaneously (intradiscal) injected in the injury site and it was observed to maintain over time without leaking to the serounding tissues. These obervations indicate the potential application of HA hydrogel in an injectable form.

Overall, the pharmacodynamic effects of HA hydrogel have been seen in alleviation of pain phenotype in IVD injury pain model, and the pharmacokinetic finding may implies the next generation of the HA hydrogel in an injectable system, that could be translated clinically in patients with discogenic back pain due to degenerated disc.

4.8 Conclusions

It was demonstrated the anti-allodynic and anti-hyperalgesic properties of HA-hydrogel treatment of disc injury pain model. The HA hydrogel acts through reduction of nociception, and inhibition of hyper-innervation and expression of nociceptive markers via alteration of glycosylation, attenuation of key inflammatory signaling molecules and modulation of protein regulatory pathways. These results suggest that HA hydrogel has a potential therapeutic application for the treatment of back pain associated with disc degeneration.

4.9 References

[1] K. T. Dicker, L. A. Gurski, S. Pradhan-Bhatt, R. L. Witt, M. C. Farach-Carson, and X. Jia, “Hyaluronan: A simple polysaccharide with diverse biological functions,” *Acta Biomater.*, vol. 10, no. 4, pp. 1558–1570, 2014.

[2] A. J. Day and J. K. Sheehan, “Hyaluronan: polysaccharide chaos to protein organisation,” *Curr. Opin. Struct. Biol.*, vol. 11, no. 5, pp. 617–622, Sep.

2001.

[3] P. Prehm, "Hyaluronate is synthesized at plasma membranes," *J. Biomech.*, vol. 220, pp. 597–600, 1984.

[4] P. Prehm and U. Schumacher, "Inhibition of hyaluronan export from human fibroblasts by inhibitors of multidrug resistance transporters," *Biochem. Pharmacol.*, vol. 68, no. 7, pp. 1401–10, Oct. 2004.

[5] L. J. Smith, N. L. Nerurkar, K. S. Choi, B. D. Harfe, and D. M. Elliott, "Degeneration and regeneration of the intervertebral disc: Lessons from development," *Dis. Model. Mech.*, vol. 4, no. 1, pp. 31–41, 2011.

[6] C. G. Jeong, A. T. Francisco, Z. Niu, R. L. Mancino, S. L. Craig, and L. A. Setton, "Screening of hyaluronic acid-poly(ethylene glycol) composite hydrogels to support intervertebral disc cell biosynthesis using artificial neural network analysis," *Acta Biomater.*, vol. 10, no. 8, pp. 3421–3430, 2014.

[7] Z. Li, K. M. Kaplan, M. Peroglio, B. Amit, M. Alini, S. Grad, and A. Yayon, "Biomimetic fibrin–hyaluronan hydrogels for nucleus pulposus regeneration," *Regen. Med.*, vol. 9, pp. 309–326, 2014.

[8] L. Calderon, E. Collin, D. Velasco-Bayon, M. Murphy, D. O'Halloran, and A. Pandit, "Type II collagen-hyaluronan hydrogel - A step towards a scaffold for intervertebral disc tissue engineering," *Eur. Cells Mater.*, vol. 20, pp. 134–148, 2010.

[9] E. C. Collin, S. Grad, D. I. Zeugolis, C. S. Vinatier, J. R. Clouet, J. J. Guicheux, P. Weiss, M. Alini, and A. Pandit, "An injectable vehicle for nucleus pulposus cell-based therapy," *Biomaterials*, vol. 32, no. 11, pp. 2862–70, Apr. 2011.

[10] G. Fontana, D. Thomas, E. Collin, and A. Pandit, "Microgel microenvironment primes adipose-derived stem cells towards an NP cells-like phenotype," *Adv. Healthc. Mater.*, vol. 3, no. 12, pp. 2012–2022, 2014.

[11] M. Dougados, M. Nguyen, V. Listrat, and B. Amor, "High molecular weight sodium hyaluronate (hyalectin) in osteoarthritis of the knee: A 1 year placebo-controlled trial," *Osteoarthritis Cartilage*, vol. 1, pp. 97–103, 1993.

[12] X. Chevalier, J. Jerosch, P. Goupille, N. van Dijk, F. P. Luyten, D. L. Scott, F. Bailleul, and K. Pavelka, "Single, intra-articular treatment with 6 ml hylan G-F 20 in patients with symptomatic primary osteoarthritis of the knee: a randomised, multicentre, double-blind, placebo controlled trial," *Ann. Rheum.*

Dis., vol. 69, no. 1, pp. 113–9, 2010.

[13] J. M. Bert and D. D. Waddell, "Viscosupplementation with hylan G-F 20 in patients with osteoarthrosis of the knee," *Ther. Adv. Musculoskelet. Dis.*, vol. 2, no. 3, pp. 127–132, 2010.

[14] I. F. I. Radaeva and G. A. Kostina, "Use of hyaluronic acid for the treatment of various pathologic states," *Pharm. Chem. J.*, vol. 32, no. 9, pp. 492–494, 1999.

[15] A. Gomis, A. Miralles, R. F. Schmidt, and C. Belmonte, "Intra-articular injections of hyaluronan solutions of different elastoviscosity reduce nociceptive nerve activity in a model of osteoarthritic knee joint of the guinea pig," *Osteoarthr. Cartil.*, vol. 17, no. 6, pp. 798–804, Jun. 2009.

[16] R. Caires, E. Luis, F. J. Taberner, G. Fernandez-Ballester, A. Ferrer-Montiel, E. A. Balazs, A. Gomis, C. Belmonte, and E. de la Peña, "Hyaluronan modulates TRPV1 channel opening, reducing peripheral nociceptor activity and pain," *Nat. Commun.*, vol. 6, p. 8095, 2015.

[17] J. B. Massie, A. L. Schimizzi, B. Huang, C. W. Kim, S. R. Garfin, and W. H. Akeson, "Topical high molecular weight hyaluronan reduces radicular pain post laminectomy in a rat model," *Spine J.*, vol. 5, no. 5, pp. 494–502, 2005.

[18] I. L. M. Isa, A. Srivastava, D. Tiernan, P. Owens, P. Rooney, P. Dockery, and A. Pandit, "Hyaluronic acid based hydrogels attenuate inflammatory receptors and neurotrophins in interleukin-1β induced inflammation model of nucleus pulposus cells," *Biomacromolecules*, vol. 16, no. 6, pp. 1714–1725, 2015.

[19] J. Cox and M. Mann, "MaxQuant enables high peptide identification rates, individualized p.p.b.-range mass accuracies and proteome-wide protein quantification," *Nat. Biotechnol.*, vol. 26, no. 12, pp. 1367–72, 2008.

[20] S. Tyanova, T. Temu, P. Sinitcyn, A. Carlson, M. Y. Hein, T. Geiger, M. Mann, and J. Cox, "The Perseus computational platform for comprehensive analysis of (prote)omics data," *Nat. Methods*, vol. 13, no. 9, pp. 731–40, 2016.

[21] S. Toegel, D. Bieder, S. André, F. Altmann, S. M. Walzer, H. Kaltner, J. G. Hofstaetter, R. Windhager, and H. J. Gabius, "Glycophenotyping of osteoarthritic cartilage and chondrocytes by RT-qPCR, mass spectrometry, histochemistry with plant/human lectins and lectin localization with a glycoprotein," *Arthritis Res. Ther.*, vol. 15, p. R147, 2013.

[22] M. H. Walker and D. G. Anderson, "Molecular basis of intervertebral disc

degeneration.," *Spine J.*, vol. 4, no. 6 Suppl, p. 158S–166S, 2004.

[23] T. Troy, D. Jekic-McMullen, L. Sambucetti, and B. Rice, "Quantitative comparison of the sensitivity of detection of fluorescent and bioluminescent reporters in animal models," *Mol. Imaging*, vol. 3, no. 1, pp. 9–23, 2004.

[24] D. J. Mayer, J. Mao, J. Holt, and D. D. Price, "Cellular mechanisms of neuropathic pain, morphine tolerance, and their interactions," *Proc. Natl. Acad. Sci.*, vol. 96, pp. 7731–7736, 1999.

[25] Y. J. Gao and R. R. Ji, "*c-Fos* and pERK, which is a better marker for neuronal activation and central sensitization after noxious stimulation and tissue injury?," *Open Pain*, no. 617, pp. 11–17, 2009.

[26] S. Neumann, T. P. Doubell, T. Leslie, and C. J. Woolf, "Inflammatory pain hypersensitivity mediated by phenotypic switch in myelinated primary sensory neurons," *Nature*, vol. 384, no. 6607, pp. 360–364, 1996.

[27] B. L. Kidd and L. A. Urban, "Mechanisms of inflammatory pain," *Br. J. Anaesth.*, vol. 87, no. 1, 2001.

[28] A. Lai, A. Moon, D. Purmessur, B. Skovrlj, D. M. Laudier, B. A. Winkelstein, S. K. Cho, A. C. Hecht, and J. C. Iatridis, "Annular puncture with tumor necrosis factor-alpha injection enhances painful behavior with disc degeneration *in-vivo*," *Spine J.*, pp. 1–12, 2015.

[29] Y. Sadovsky, L. Myatt, and G. Burton, "The anatomy and physiology of pain," *Basic Sci.*, vol. 36, no. 4, pp. 473, 2015.

[30] A. J. Freemont, T. E. Peacock, P. Goupille, J. A. Hoyland, J. O. Brien, and M. I. V Jayson, "Early report nerve ingrowth into diseased intervertebral disc in chronic back pain," *Lancet*, vol. 350, pp. 178–181, 1997.

[31] Y. Aoki, H. S. An, K. Takahashi, K. Miyamoto, M. E. Lenz, H. Moriya, and K. Masuda, "Axonal growth potential of lumbar dorsal root ganglion neurons in an organ culture system: response of nerve growth factor-sensitive neurons to neuronal injury and an inflammatory cytokine," *Spine (Phila. Pa. 1976).*, vol. 32, no. 8, pp. 857–63, Apr. 2007.

[32] A. J. Freemont, A. Watkins, C. Le Maitre, P. Baird, M. Jeziorska, M. T. N. Knight, E. R. S. Ross, J. P. O'Brien, and J. A. Hoyland, "Nerve growth factor expression and innervation of the painful intervertebral disc," *J. Pathol.*, vol. 197, no. 3, pp. 286–92, Jul. 2002.

[33] P. W. McCarthy, B. Carruthers, D. Martin, and P. Petts,

"Immunohistochemical demonstration of sensory nerve fibers and endings in lumbar intervertebral discs of the rat," *Spine*, vol. 16, no. 6. pp. 653–5, 1991.

[34] Y. Aoki, S. Ohtori, K. Takahashi, H. Ino, Y. Takahashi, T. Chiba, and H. Moriya, "Innervation of the lumbar intervertebral disc by nerve growth factor-dependent neurons related to inflammatory pain," *Spine (Phila. Pa. 1976).*, vol. 29, no. 10, pp. 1077–81, May 2004.

[35] A. I. Basbaum, D. M. Bautista, G. Scherrer, and D. Julius, "Cellular and molecular mechanisms of pain," *Cell*, vol. 139, no. 2, pp. 267–284, 2010.

[36] E. J. Huang and L. F. Reichardt, "Trk receptors: Roles in neuronal signal transduction.," *Annu. Rev. Biochem.*, vol. 72, pp. 609–42, Jan. 2003.

[37] N. E. Lane, T. J. Schnitzer, C. A. Birbara, M. Mokhtarani, D. L. Shelton, M. D. Smith, and M. T. Brown, "Tanezumab for the treatment of pain from osteoarthritis of the knee," *N.Engl.J.Med.*, vol. 363, no. 1533–4406 (Electronic), pp. 1521–1531, 2010.

[38] K. Fujimoto, M. Miyagi, T. Ishikawa, G. Inoue, Y. Eguchi, H. Kamoda, G. Arai, M. Suzuki, S. Orita, G. Kubota, Y. Sakuma, Y. Oikawa, K. Kuniyoshi, N. Ochiai, S. Kishida, J. Nakamura, Y. Aoki, T. Toyone, K. Takahashi, and S. Ohtori, "Sensory and autonomic innervation of the cervical intervertebral disc in rats: the pathomechanics of chronic discogenic neck pain," *Spine (Phila. Pa. 1976).*, vol. 37, no. 16, pp. 1357–62, Jul. 2012.

[39] A. J. Hayes, D. Tudor, M. A. Nowell, B. Caterson, and C. E. Hughes, "Chondroitin sulfate sulfation motifs as putative biomarkers for isolation of articular cartilage progenitor cells," *J. Histochem. Cytochem.*, vol. 56, no. 2, pp. 125–138, 2008.

[40] M. Bhattacharjee, S. Chawla, S. Chameettachal, S. Murab, N. S. Bhavesh, and S. Ghosh, "Role of chondroitin sulphate tethered silk scaffold in cartilaginous disc tissue regeneration.," *Biomed. Mater.*, vol. 11, no. 2, pp. 25014, 2016.

[41] D. Purmessur, M. C. Cornejo, S. K. Cho, P. J. Roughley, R. J. Linhardt, A. C. Hecht, and J. C. Iatridis, "Intact glycosaminoglycans from intervertebral disc-derived notochordal cell conditioned media inhibits neurite growth while maintaining neuronal cell viability," *Spine J.*, vol. 15, no. 5, pp. 1060–1069, 2015.

[42] R. M. Lauder, T. N. Huckerby, and I. A. Nieduszynski, "Lectin affinity chromatography of articular cartilage fibromodulin: Some molecules have

keratan sulphate chains exclusively capped by (2-3)-linked sialic acid," *Glycoconj. J.*, vol. 28, no. 7, pp. 453–461, 2011.

[43] K. Wuertz and L. Haglund, "Inflammatory mediators in intervertebral disk degeneration and discogenic pain.," *Glob. Spine J.*, vol. 3, no. 3, pp. 175–84, Jun. 2013.

[44] K. T. Weber, D. O. Alipui, C. P. Sison, O. Bloom, S. Quraishi, M. C. Overby, M. Levine, and N. O. Chahine, "Serum levels of the proinflammatory cytokine interleukin-6 vary based on diagnoses in individuals with lumbar intervertebral disc diseases," *Arthritis Res. Ther.*, vol. 18, no. 1, pp. 3, 2016.

[45] B. G. Peng, "Pathophysiology, diagnosis, and treatment of discogenic low back pain.," *World J. Orthop.*, vol. 4, no. 2, pp. 42–52, 2013.

[46] J. H. Adler, M. Schoenbaum, and R. Silberberg, "Early onset of disk degeneration and spondylosis in sand rats (Psammomys obesus)," *Vet. Pathol.*, vol. 20, no. 1, pp. 13–22, 1983.

[47] K. Singh, K. Masuda, E. J. M. Thonar, H. S. An, and G. Cs-Szabo, "Age-related changes in the extracellular matrix of nucleus pulposus and anulus fibrosus of human intervertebral disc," *Spine (Phila Pa 1976)*, vol. 34, no. 1, pp. 10–16, 2010.

[48] G. Cs-Szabo, D. Ragasa-San Juan, V. Turumella, K. Masuda, E. J. M. A. Thonar, and H. S. An, "Changes in mRNA and protein levels of proteoglycans of the anulus fibrosus and nucleus pulposus during intervertebral disc degeneration," *Spine (Phila. Pa. 1976).*, vol. 27, no. 20, pp. 2212–2219, 2002.

[49] C. Le Maitre, A. Pockert, D. J. Buttle, A. J. Freemont, and J. A. Hoyland, "Matrix synthesis and degradation in human intervertebral disc degeneration," *Biochem. Soc. Trans.*, vol. 35, no. Part 4, pp. 652–5, Aug. 2007.

[50] S. Murab, J. Samal, A. Shrivastava, A. R. Ray, A. Pandit, and S. Ghosh, "Glucosamine loaded injectable silk-in-silk integrated system modulate mechanical properties in bovine ex-vivo degenerated intervertebral disc model," *Biomaterials*, vol. 55, pp. 64–83, 2015.

[51] M. Braddock and A. Quinn, "Targeting IL-1 in inflammatory disease: new opportunities for therapeutic intervention," *Nat. Rev. Drug Discov.*, vol. 3, no. 4, pp. 330–9, Apr. 2004.

[52] N. Nishimoto and T. Kishimoto, "Interleukin 6: from bench to bedside," *Nat Clin Pr. Rheum*, vol. 2, no. 11, pp. 619–626, Nov. 2006.

[53] X. Zhang, J. Huang, and P. A. McNaughton, "NGF rapidly increases membrane expression of TRPV1 heat-gated ion channels," *EMBO J.*, vol. 24, no. 24, pp. 4211–23, Dec. 2005.

[54] G. Baranauskas and A. Nistri, "Sensitization of pain pathways in the spinal cord: Cellular mechanisms," *Prog. Neurobiol.*, vol. 54, no. 3, pp. 349–365, 1998.

Chapter 5

Summary and Future Directions

5.1 Introduction

Low back pain (LBP) has become a common health problem with a lifetime prevalence of 54-80% in the world population [1-5]. The most common etiology of LBP is strongly associated with intervertebral disc (IVD) degeneration for approximately 26%-42% of the patients who experience discogenic low back pain [6-8]. The onset of discogenic back pain is characterised by the presence of sensory nerve ingrowth or innervation into the inner third of the AF and deep into the NP, which initiates the development of nociception [9]. Additionally, neurogenic mediators such as pro-inflammatory cytokines and neurotrophins also induce nerve ingrowth and enhance sensory sensitization in the degenerative disc, leading to discogenic pain [10]. However, little is known on the mechanisms underlying painful disc degeneration. Thus, the development of a pre-clinical discogenic pain model is essential to study the pathogenesis of painful disc degeneration, which also provides a platform from which to study disc regeneration. At tissue and cellular level, a dysregulation of extracellular matrix (ECM) homeostasis has been reported to induce degenerative events in the disc. These events are characterised by loss of proteoglycan, aggrecan and glycosaminoglycan (GAG) content and an increase in other ECM compositions such as fibronectin, versican, biglycan and decorin [11]. Additionally a shift in type II collagen to stronger collagen I fibrils predominantly found within the NP and inner AF is seen. Moreover, a distinct glycosylation in AF and NP tissues has been identified from immature to advanced age in the disc [12], and this phenomena is also seen in the injured disc as the studies in this thesis show. These glycans play a key biological role in the process including cell-cell and cell-ECM interaction, inflammation and neurotransmission [13].

A better knowledge of the disc glycoenvironment in both healthy and injured discs is essential to design biomaterial systems that will provide an optimal regenerative microenvironment. Such an environment will maintain the disc phenotype and promote deposition of new ECM to facilitate regeneration. The overall goal of this project was to develop a regenerative strategy for disc regeneration by using biomaterials that are informed by attenuating inflammation in a relevant *in vitro* model and subsequently modulates the disc glycoenvironment, inflammatory and regulatory signalling pathways, sensory hyper-innervation and nociception in a validated pre-clinical model of pain following disc injury *in vivo*.

5.2 Summary

5.2.1 Phase I – The Development of HA Hydrogel in an Inflammation Milieu

Inflammation plays a key role in mediating a degenerative event in the disc. Thus, the objective of phase I **(Chapter 2)** was to develop a therapeutic biomaterials system by using a high molecular weight (HMW) of HA hydrogel that can modulate the key inflammatory pathway of IL-1β in NP cells. Therefore, the potential of an optimally stabilised HA hydrogel crosslinked with 4-arm PEG amine was investigated in response to inflammation. HA cross-linking was optimized using various concentrations of 4-arm PEG- amine by determination of free carboxyl groups of HA and unreacted free amine groups of PEG-amine. The optimally crosslinked HA hydrogels were characterized for hydrolytic stability, enzymatic degradation and cytotoxicity on NP cells. The therapeutic effect of HA hydrogels was further determined in IL-1β induced inflammation on NP cell cultures and in the mechanism of HA by examining the expression of cell surface receptor of CD44. The hydrogel was optimally crosslinked at 75 mM of 4-arm PEG amine, which exhibited hydrolytic stability, and showed greater than 40% resistance to enzymatic degradation. No marked cytotoxic effect of NP cells was observed in the presence of hydrogels for one, three and seven days. The crosslinked HA hydrogel suppressed IL-1β signalling molecules of IL-1R1 and MyD88 more than the inflamed and un-crosslinked hydrogel treated cells. Additionally, NGF and BDNF mRNA were down regulated after treatment with cross-linked HA hydrogel. The possible protective mechanism of HA is seen by high expression of CD44, a cell surface receptor in NP cells after HA treatment, suggesting that the binding of HA to CD44 receptor shields NP cells from further inflammation (Figure 5.1).

5.2.2 Phase II – The Establishment of a Pre-clinical Model of Pain in Disc Degeneration

A relevant discogenic pain model in a pre-clinical setting is essential to enable an improved understanding of the pathogenesis of painful disc degeneration, and will provide a platform from which to study the efficacy of promising therapies for disc regeneration. The rat tail model has been widely used for the investigation of disc degeneration due to less surrounding tissue damage during surgery and is thus feasible for the intervention [14]. However, no report investigating pain phenotype

following disc or annular defect in the rat tail has yet to be documented. In addition, glycosylation is a key biological process that contributes to cell-cell, cell-ECM interaction and development of the diseased state. At present, little is known of the glycosylation pattern in the disc cells and tissues and their alteration during development.

Therefore, the overall aim of phase II **(Chapter 3)** was to develop a clinically relevant pain model of disc degeneration *in vivo*, determine the disc glycosylation profile in pathologic condition, and validate the model using a current reversible analgesic. Here for the first time, a pre-clinical model of pain associated with painful disc degeneration in the rat tail was developed by adopting a surgical puncture-induced disc injury in the coccygeal discs. The quantitative sensory testing comprised of Hargreaves, von Frey and tail flick tests was used to study the pain phenotye in the rat tail. The Hargreaves's latencies of pain sensitivity indicated injury-evoked thermal hyperalgesia close to the site of injury. The tail flick test demonstrated injury-induced thermal hypoalgesia at a lower level of the rat tail while the von Frey test revealed injury-evoked mechanical allodynia close to site of injury. Thus, up-regulation of the molecular marker of nociception was marked in the left dorsal horn of spinal cord. Histological analysis demonstrated injury-induced microstructural disc degeneration and this was clinically classified as Thompson Grade III. A distinct ECM and cellular glycosylation of NP and AF tissues were identified in healthy and diseased tissues. An increase in sialylation, galactosylation, fucosylation and high mannose and loss of GalNAc was observed on injured AF and NP tissues. In addition, a decrease of the chondroitin sulfation profile (C6S) was demonstrated in the injured AF and NP tissues. For validation of the pain model, low dose morphine significantly alleviated thermal hyperalgesia and mechanical hyperalgesia close to the site of injury; however reversed thermal hypoalgesia occurred at a lower level of rat tail. Overall, these data denote surgically induced disc injury that evokes robust pain phenotype, structural disc degeneration and distinct glycosylation in a rat tail model thereby providing a better understanding of the mechanism underlying painful disc degeneration and a platform from which to study potential intervention for disc regeneration (Figure 5.1).

5.2.3 Phase III – The Efficacy of HA Hydrogel in Painful Disc Degeneration

High molecular weight of HA has been widely used in ophthalmology practice and other pathologic conditions such as osteoarthritic pain. Nevertheless, the effect of HA hydrogel in painful disc degeneration is still unknown. Therefore, the overall objective of phase III **(Chapter 4)** was to further evaluate the therapeutic efficacy of HA hydrogel in modulating inflammatory pain through regulation of glycomic and proteomic signatures for disc repair. To do so, the potential efficacy of HA hydrogel was investigated in a validated IVD pain model *in vivo* which had been established previously and described in **Chapter 3**. A nociceptive assay of Hargreaves' test revealed a significant reduction of thermal hyperalgesia close to the site of injury in the HA treated disc. Similarly, HA hydrogel alleviated injury-evoked mechanical allodynia close to site of injury as demonstrated in the von Frey test. In contrast, HA suppressed injury-induced thermal hypoalgesia in tail flick. At spinal level, HA hydrogel down-regulated nociception markers of *c-Fos* and substance P in the dorsal horn. An inhibition of sensory hyper-innervation was evident in HA treated injured disc, as indicated by both GAP43 and CGRP stained for protein expression during axogenesis and sensory neuropeptide respectively. Similarly, pro-nociceptive receptors of TRPV1 and Trk A were reduced following HA hydrogel treatment. Glycosylation plays an important role in ECM regulation, here for the first time HA hydrogel treatment was seen to alter glycan moieties by reducing sialylation and galactosylation in the injured disc. In contrast, an increase of endogenous GalNAc and chondroitin sulfate was observed in HA-treated injured disc. Further, extensive proteomic analysis indicated that HA hydrogel attenuated key inflammatory pathways of IL-6 and IL-1β, and modulated regulatory signalling proteins of Smad3 via TGF-β1 for ECM depositions. Collectively, HA hydrogel modulates inflammatory pain through alteration in glycomic and protein regulatory pathways, thereby giving a promising new therapeutic candidate for the treatment of degenerative disc related back pain (Figure 5.1).

5.3 Limitations

5.3.1 Phase I – The Development of HA Hydrogel in an Inflammation Milieu

The *in vitro* study of NP was carried out in a two-dimensional (2D) culture, which had an effect on the NP phenotype including cell morphology and distribution.

Live/Dead® assay showed rounded NP morphology; however clustering cell distribution was observed in a basal control. Nevertheless, homogenous cell distribution was demonstrated in the presence of HA hydrogel, which maintains the NP phenotype. On the other hand, elongated cells were observed in all conditions due to the detrimental NP microenvironment of the *in vitro* inflammation study.

Apart from therapeutic efficacy, the reason for introducing the hydrogel system in this study was to assess the phenotypic changes of NP cell with regard to GAG content. The quantification of GAG is usually determined by dye 1,9-dimethylene blue (DMMB) assay, a method fundamentally based on the binding of negatively charged sulfated GAGs to the cationic 1,9-dimethylene blue dye [15]. Any negatively charged molecules including HA that are derived from the hydrogel can interact with the dye, which contribute to the false positive results. Therefore, quantification of GAG was not done in this study. However, the specific GAG composition such as chondroitin sulfate was further determined in the subsequent studies of phase II **(Chapter 3)** and phase III **(Chapter 4)** using HPLC and immunohistochemistry techniques as the reliable alternative to quantifying GAG deposition.

Mechanistically, the possible pharmacodynamic action of HA in attenuating inflammation through binding cell surface receptor CD44, a HA receptor, was proposed in this study. Nevertheless, no inhibitory control of CD44 with blocking antibody or siRNA was confirmed. However, this study was supported by a previous study showing that HA crosslinking provides the protective mechanism at the site of inflammation by promoting cell adhesion to the HA complex through binding to CD44 instead of to the inflammatory receptor, and subsequently interferes with further inflammation insults [16].

5.3.2 Phase II – The Establishment of a Pre-clinical Model of Pain in Disc Degeneration

This study revealed the first demonstration of pain following surgically puncture-induced disc degeneration in the rat tail. Hence, this model was applicable to the study of pain in disc degeneration, which is clinically relevant to discogenic pain.

Nevertheless, the complexity of other spinal pain pathologies such as nerve root compression cannot be investigated in this model. This is because the neuroanatomical features of the discs in the rat tail are innervated by dorsolateral and ventrolateral caudal nerves that arise from sacral (S1-S4) and coccygeal (Co1-Co3) segments of the spinal cord [17-19]. This explains the absence of nerve root from the spinal cord in the surrounding discs and vertebrae of the rat tail, which means the model is restricted to mechanical (inflammatory) pain and not radicular pain. However, this model represented clinical painful disc degeneration in which the source of pain is generated from the disc pathology, thereby allowing investigations of a therapeutic target for disc regeneration that alleviates pain.

In spine research, imaging techniques such as MRI or plain radiography are essential to determine structural deterioration in the degenerated disc. However, such an imaging modality was not available to perform this study due to the lack of an x-ray machine as this study was carried out in a new pre-clinical facility. The old machine could not be transferred to a new pre-clinical facility due to logistical issues. Nonetheless, a similar rat tail study was performed. The study revealed a significant disc height collapse in punctured AF disc, suggesting that punctured AF induces disc height collapse in the rat tail (data not shown) that can support this study.

Disc degeneration is characterised by the loss of biomechanical properties. Thus, static loading with high frequency induced disc collapse in the rat tail [20]. In humans, the discs are exposed to multi-directional loads such as tension, compression, torsion, and bending [21-22]. Therefore, the biomechanics of the spine must be considered in investigating degenerative disc disease. Nevertheless, the biomechanical testing is not performed in this study because it is not feasible to expose predominant axial loading since the rat tail is known to be in the horizontal position. However, the increased torsional range of motion correlated with clinical symptoms of disc degeneration [23]. Therefore, the torsional range of motion with static or cyclic loading from the horizontal approach can determine the biomechanic effect in the rat tail. Since this is a study of pain, no analgesic is given in later post-operative days. This can increase the severity of injury in animals if biomechanical loading is coupled with injury and nociceptive procedures are followed that cause distress to the animals, thereby affecting the general health of the animal. Such a

study will not be ethically permissible. Alternatively, the biomechanics procedure can be done in a separate study.

5.3.3 Phase III – The Efficacy of HA Hydrogel in Painful Disc Degeneration

The scientific breakthroughs of HA hydrogel in this study were shown by its anti-inflammatory and anti-nociceptive effects. Herein, the pharmacodynamic action of HA has been demonstrated by attenuating key inflammatory signalling molecules in the disc. The HA hydrogel was shown to alleviate nociceptive behaviour and nociception markers in both the spinal cord and the disc. The proposed mechanism of action of HA by recruiting endogenous chondroitin sulfate component and inhibiting binding of pro-inflammatory cytokines and neurotrophic factor to their receptors, thereby reducing inflammation, receptor sensitization and innervation. Nevertheless, there is no inhibitory control with knockout animal studies being carried out to confirm this effect. However, the proposed mechanism was supported by previous studies which revealed that a higher chondroitin sulfate composition inhibited neurite out-growth [24] and HA suppressed IL-1β signalling as described in **Chapter 2**.

The disadvantage in using a rodent model even in skeletally mature rats results from the presence of notochordal cells in the disc throughout the animal's entire lifespan. There is a major dissimilarity of the cellular population in human disc compared to that of rodents, since only 5-0% progenitor cells remain after the age of 37 years [25]. In the degenerative rat tail model, one possible mechanism for tissue regeneration is that HA hydrogel provides an optimal microenvironment for resident cells, including progenitor cells that can differentiate towards NP and AF phenotype for disc repair. However, regeneration in degenerated human disc depends only on the remaining NP or AF cells population (not progenitor cells). This may mean that regeneration in the human disc may not be similar as that seen in the rat tail model.

In the study of pain, sensory nerve conduction is one of key elements to determine peripheral sensory sensitisation following HA treatment in local tissue. In future, the pain neurotransmission can be improved by recording sensory nerve action potential (SNAP) of the caudal nerve in the proximal of rat tail, and thereby determine the efficacy of HA in suppressing sensory neurotransmission in the disc.

In addition, the degenerative changes in the disc are characterized by an acidic environment and contain a higher expression of degradative enzymes. Therefore, a time-course of pharmacokinetic study of HA hydrogel is also essential but has not been done in this study. It is important to know how long the HA hydrogel will remain in response to the local tissue environment, in order to determine the effectiveness of HA hydrogel in a time dependent manner. Thus, a kinetic study of injectable HA hydrogel in the rat tail or rabbit model desired.

As stated in the phase II **(Section 5.3.2, Chapter 5)**, disc height or disc hydration by radiology procedure could not be performed in this study. However, a similar implantation of HA hydrogel in the rat tail was investigated in a separate study. The result demonstrated that an increase of disc height occurred in HA-treated punctured AF disc, suggesting that HA hydrogel improves anatomical restoration in the rat tail (data not shown). To avoid a repetitive analysis from the above mentioned study, therefore, a histological procedure following post-implantation of HA hydrogel in this study was not performed. The H&E and Masson Trichrome staining revealed structural repair in HA-treated AF tissue (data not shown). Indeed, disc tissues in this study were allocated for a better immunohistochemistry and mass spectrometry analysis to identify the mechanism of action of HA hydrogel in regulating ECM component in the disc. The results confirmed that regulators of Smad3 family via TGF-β1 to modulate ECM content such as aggrecan, fibronectin and collagen expressions following post-implantation of HA hydrogel in the disc **(Chapter 4)**.

From a biomechanical point of view, the rodent model does not represent the biomechanical characteristics in human, even at the lumbar level. Nonetheless, as mentioned above, an increased torsional range of motion was associated clinically with disc degeneration. In humans, facet joints of the lumbar spine restrict rotation to only around 2° per IVD level in each direction [23]. Herein, the absence of facet joints do not limit torsional range of motion in the rat tail, and thereby provide a high level of multi-directional motion in the tail. This accounts for the fact that implantation of HA hydrogel in the rat tail exposes a higher degree of torsional motion than that at the lumbar level. Nonetheless, testing HA hydrogel in a a bioreactor simulatory environment that mimics the human spine will provide some relevant answers.

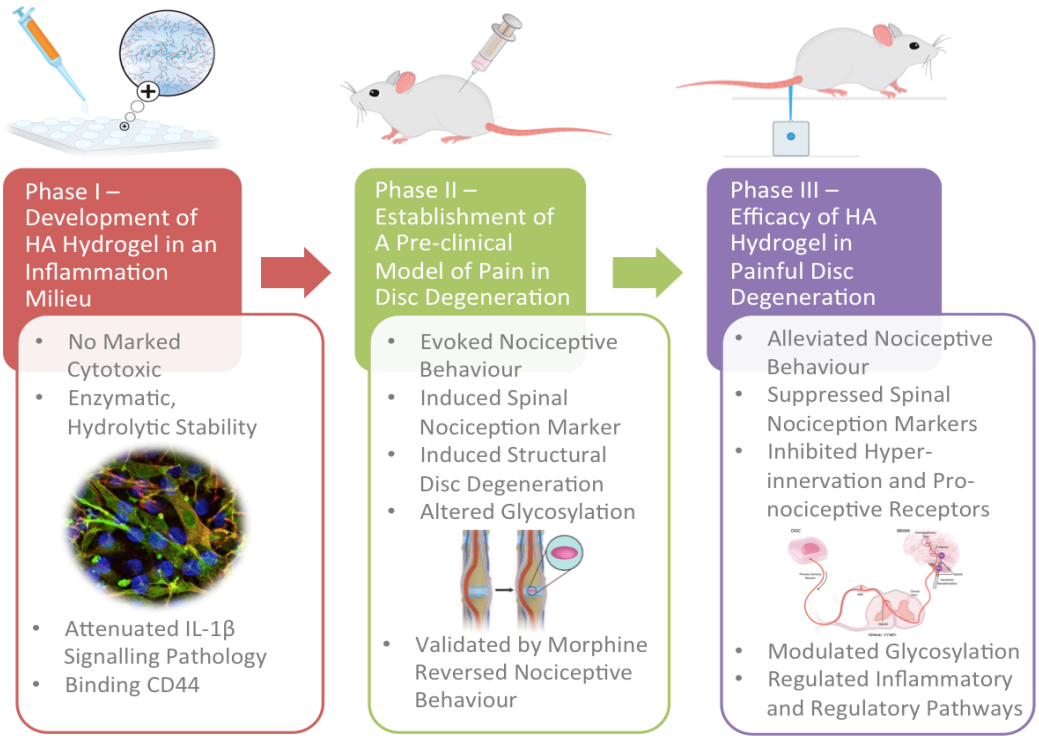

Figure 5.1 Schematic representation of the milestones achieved during the study. Each phase of study is correlated towards the development of HA hydrogel in modulating inflammatory pain for disc repair.

5.4 Future Directions

5.4.1 A Clinically Relevant Injectable HA Hydrogel in a Rabbit Model for Disc Regeneration

Clinically relevant future studies of the potential efficacy of HA hydrogel in degenerative disc for the treatment of back pain were determined via a multiple interview sessions with two clinicians, an orthopedic surgeon and a neurosurgeon. The findings are described in **section AA of Appendices**. Undoubtedly, it is advisable to carry out studies of an injectable HA hydrogel in trials with larger animal before translation to human. It is envisioned that the HA hydrogel will be injected using a duploject easy prep system (Baxter) that is attached to a needle (23G or 25G) (Figure 5.2a). Prior to this, viscoelasticity of HA hydrogel can be determined by dynamic rheological measurements. Shear oscillations can be carried out at a constant stress of 0.5 Pa and a frequency of 1Hz to observe storage modulus (G^0), loss modulus (G^{00}) and gelation time of the hydrogel. (Figure 5.2b).

Finally, the pharmacodynamic effect of injectable HA hydrogel can be determined after a certain period of time of induced disc degeneration in the rabbit model (Figure 5.2b). Surgically puncture-induced disc injury can be adopted using 18-gauge needle to puncture AF to NP tissue at a depth of 5 mm. The HA hydrogel will be injected after one week induced disc injury and will be further investigated at appropriate time-points. The parameters evaluated will be i) pain phenotype by nociceptive behavior (after established pain in the rabbit model), nociception markers (peripheral, spinal and supra-spinal level), sensory neuron tracking and neurotransmission via recording sensory nerve action potential, ii) anatomical restoration by plain radiographs x-ray or MRI imaging for disc height and hydration, and histological/immunohistochemical analysis, iii) inflammation by immunoassay for cytokines at local tissue and systemic level, iv) protein or molecular analysis for signalling pathways to determine a possible mechanism of action of HA hydrogel. The limitation of this study is the absence of relevant markers in the rabbit model.

5.4.2 Human Trials – A Randomised Controlled Trials for Safety and Efficacy of Injectable HA Hydrogel in Subjects with Discogenic Pain

HMW HA has been widely used in various clinical applications such as osteoarthritic pain. Nevertheless, the trials to test the effectiveness of HA in

a)

b)

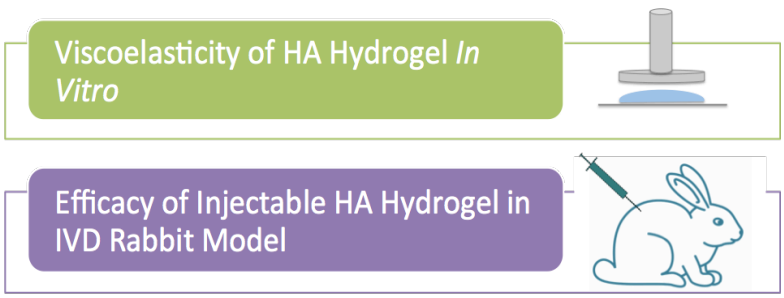

Figure 5.2 The clinically relevant injectable HA hydrogel system. The injection using duploject easy prep system, consists of double syringe clip, 2 mL syringes, joining piece and appropiate needle size. Sodium hyaluronate (HA) is reconstituted in distilled water and filled in 2 mL syringe, while the crosslinker solution is loaded in the other 2 mL syringe. Both solutions will be mixed up via joining piece and directly inject to the tissue of interest (a). The viscoelasticity of HA hydrogel will be determined by rheology. The efficacy of HA hydrogel will be carried out in a larger animal model (b).

degenerative disc patients with back pain have only been carried out recently and are currently awaiting publication outcomes **(Chapter 1)**. The clinical trials are of both NCT01290367 and NCT02412735 used HA as a carrier for cell therapy in treating patients with low back pain caused by degenerative disc disease. However, no clinical report has investigated the pharmacological effect of crosslinked HMW HA hydrogel for discogenic pain. Indeed, the HA hydrogel developed in this study was patented in 2016 (IDF filed Tech-2016-029). Therefore, a future clinical trial of HA hydrogel will be initiated after obtaining pre-clinical findings from a rabbit model (Figure 5.3). In the case of positive results, a randomised controlled trial phase I/II (estimate of 100 subjects) to evaluate safety and pre-liminary efficacy of HA hydrogel in subjects with chronic discogenic low back pain caused by moderate degenerative disc will be planned. The route of administration will be via percutaneous intradiscal injection. A varying volume of HA hydrogel is to be considered. The outcome measurements will be determined primarily through physical examinations, vital signs, treatment emergent adverse events, and clinical biochemistry, hematology and immunology analysis. Second, MRI and x-ray imaging will be performed to evaluate disc hydration and disc height in the HA-treated disc. Success of the treatment in reducing pain will be assessed using Visual Analogue Scale (VAS) and Oswestry Disability Index (ODI) score at baseline and post-treatment [26]. Subject inclusive and exclusive indications are listed in Table 5 [27]. If success is achieved, a randomised double blind with placebo-control of prospective clinical trial phase II/III with subject enrollment of 300, will be further carried out to evaluate the efficacy and safety of HA hydrogel in subjects with degenerative disc for the treatment of chronic discogenic low back pain.

5.4.3 Encapsulation of Progenitor Cells in a HA Hydrogel System for Disc Regeneration

The next generation of HA hydrogel system can be improved by incorporation of progenitor cells. In 2007, skeletal progenitor cell populations in AF and NP cells have been identified in moderate degenerative human disc. Both isolated cells expressed CD105, CD166, CD63, CD49a, CD90, CD73, p75 and CD133/1, the antigen markers for marrow mesenchymal stem cells that can be differentiated

Figure 5.3 Clinical trials for the safety and efficacy of injectable HA hydrogel in subjects experienced discogenic low back pain due to degenerative disc.

Table 5.1 Subject's indications for clinical trials.

	Inclusion criteria	Exclusion criteria
Gender	Both female and male	Pregnant or nursing female
Age	18 years and older	Below 18 years old
Clinical indications	Chronic discogenic low back pain more than 6 months	History of neoplasm
	Failed conservative pain management at least 6 months	Ongoing conservative treatment
	Diagnosed degenerative disc disease	Intact herniated disc
	Moderate radiographic degenerative disc atsinglelevel from L1 to S1 with loss of disc hydration confirmed by MRI	Have nerve root compression due to spinal stenosis or herniated disc
	Disc height loss than 30% compared to a normal adjacent disc indicated by x-ray radiograph	Lumbar spondylitis
	With or without disc protrusion at the index disc	Acute vertebra fracture at treated disc during the study
	Baseline low back pain ≥40 mm on a 100 mm VAS	Underwent surgery at the relevant disc site
	Baseline leg pain ≤20mm in both legs on a 100mm VAS scale	Hypersensitivity to HA
	Baseline ODI score ≥30 on the 100-point questionnaire	

towards mesodermal lineages and reorganization of disc tissue [28]. Later, Henriksson *et. al* reported that less than 5% of AF and NP cell population in degenerated human disc expressed progenitor/stem cell markers including Stro-1 and Ki67 [29]. Recently, progenitor markers such as Tie2 positive (Tie2+) and disialoganglioside 2 positive (GD2+) were identified in the NP cell population derived from humans. Nevertheless, this cell population (0-5%) was remarkably decreased with aging and degeneration in human disc [25]. A comprehensive understanding of the cell population is needed for better understanding of the niche elements or conducive microenvironment that support the progenitor cells to be differentiated into the correct phenotype, and thereby repopulate the native NP or AF populations in degenerated disc for regeneration [30].

Therefore, engineered progenitor cell population within the hydrogel will allow ECM component of the glyco- and/or micro- environment (niche elements) provide stimulatory or inhibitory effects that promote differentiation of progenitor cells toward specific phenotype (Figure 5.4) [31]. In this case, AF and NP phenotype will be maintained in a regenerative environment using a functionalized biomaterials system (specifically a functionalized HA hydrogel). This will repopulate native NP and AF in the tissue and promote secretion of paracrine factors for disc repair. Indeed, this system can be used as a paracrine production factory for such biomolecules [32][33]. In this study (**Chapter 4**), the HA hydrogel has been demonstrated to modulate the intracellular Smad3 family via TGF-β1 to regulate ECM deposition *in vivo*. This finding is supported by previous study in which TGF-β1was supplemented in the scaffold to support MSC differentiation towards NP-like phenotype [34]. Therefore, incorporation of engineered progenitor cells in the hydrogel will possibly stimulate and repopulate AF and NP cells in degenerated disc and continuously secrete essential biomolecules/paracrine factors to restore imbalance ECM homeostasis for disc repair and/or delay degeneration.

5.4.4 Glyco-engineered Hydrogel System – Functionalisation of HA Particles in a HA Hydrogel System for Long-term Efficacy

The therapeutic efficacy of HA can be enhanced by the incorporation of functionalised HA particles within the hydrogel system. HA particles can be formulated with or without any potential inhibitor or drug or therapeutic molecule

using the precipitation method (Figure 5.5). Preliminary attempts in fabrication show that the resulting size of particles are within the ±500 nm range (Figure 5.6a) with a charge of -55 mV, as indicated by dynamic light scattering (DLS) and zeta potential respectively. However, a high polydispersity of particles is observed in the SEM images (Figure 5.6b). The target size of particles can be optimized by a specific centrifugation speed or dialysis method. At high SEM magnification, a coral-like structure was observed on the surface of the particles (Figure 5.6c).

The findings from the phase II study revealed different regulation of glycosylation by an increase of sialylation, high mannose, α-linked Gal residues and Gal-β-(1,3)-GalNAc in AF and NP. Therefore, HA particles can be functionalised with a specific lectin such as SNA-I and Con A that have binding affinity to sialic acid and high mannose respectively. Other lectins include MAA, WGA, GS-IB-4 and PNA. This will target HA particles to a specific tissue region and allow a synergistic effect if incorporated with a drug or molecule, by modulating glycosylation during the degenerative event and the executing mechanism of action of a specific drug/molecule respectively. If targeting ECM regulation, the relevant growth factor can be incorporated.

Nevertheless, the release of functionalised HA particles needs to be controlled. A hydrogel system can control release of any bioactive compound in a time-dependent manner. Herein, the functionalised HA particles can be loaded in HA hydrogel, which enables the slow release of the cargo to the target tissue, thus maintains the effectiveness of HA over a longer period. Indeed, the hydrogel is not only for the optimal glyco- or micro- environment of AF and NP, but also for therapeutic efficacy, which will enhance the tissue regeneration.

5.5 References

[1] L. Manchikanti, V. Singh, S. Datta, S. P. Cohen, and J. A. Hirsch, "Comprehensive review of epidemiology, scope, and impact of spinal pain," *Pain Physician*, vol. 12, pp. 35–70, 2009.

[2] G. B. Andersson, "Epidemiological features of chronic low-back pain," *Lancet*, vol. 354, no. 9178, pp. 581–585, 1999.

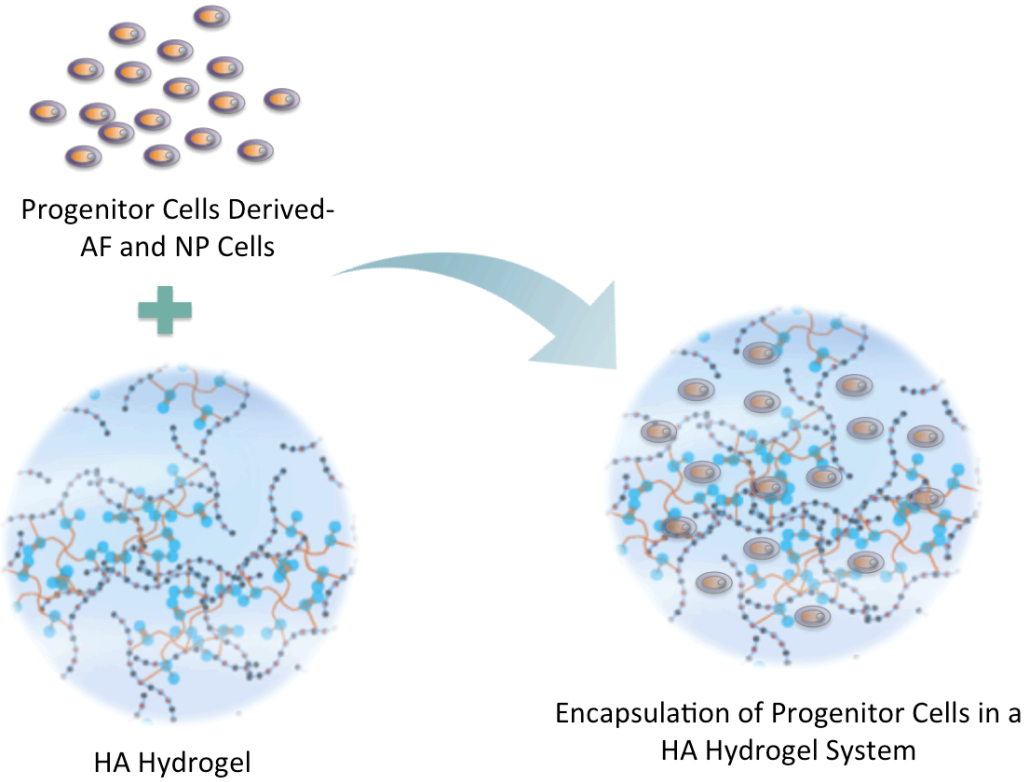

Figure 5.4 Encapsulation of progenitor cells of NP or AF in an injectable HA hydrogel for disc regeneration.

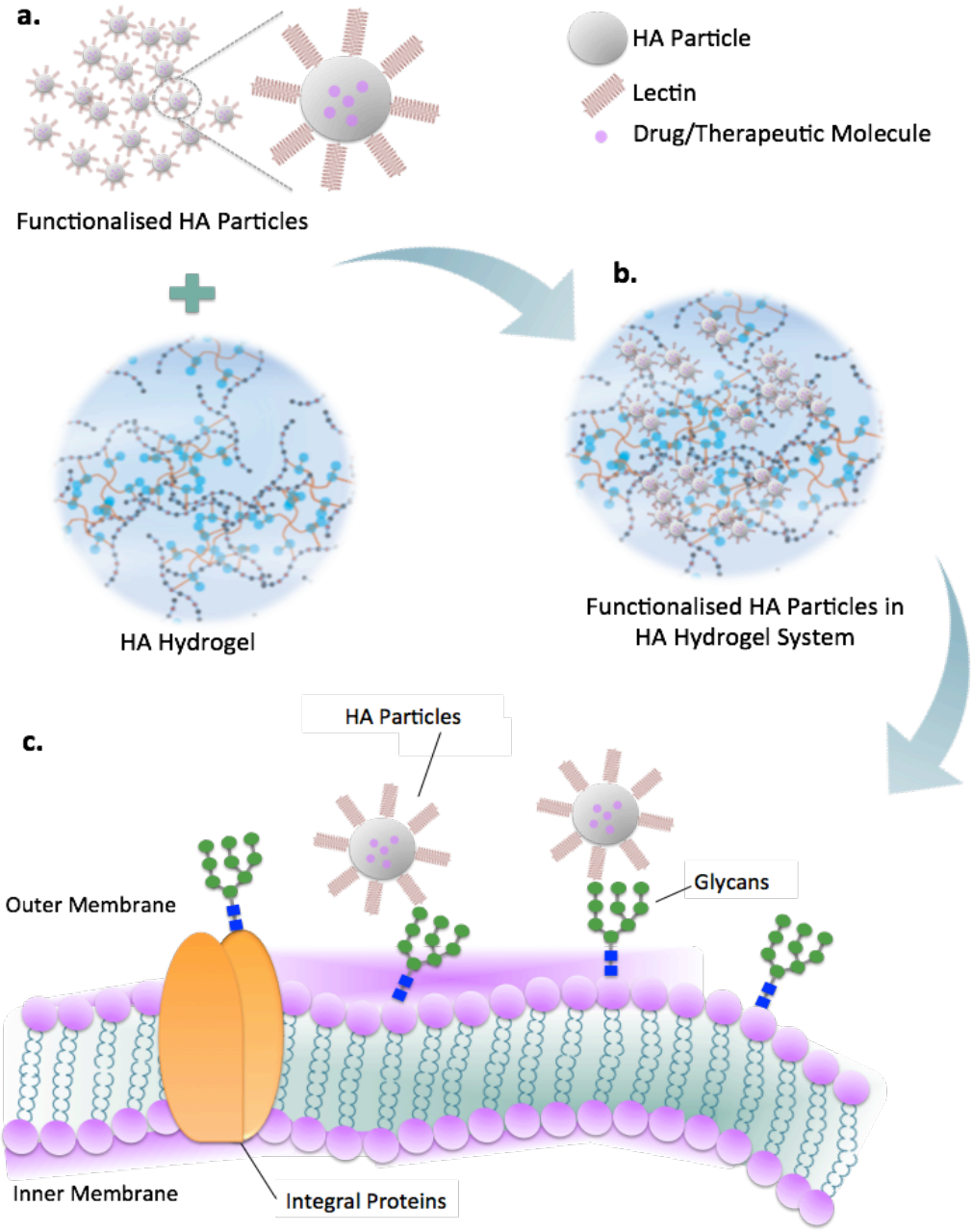

Figure 5.5 Schematic of incorporation of functionalised HA particles in a HA hydrogel system. Drug or inhibitor or therapeutic molecule can be loaded in HA particles and further functionalised with relevant lectins (a). Functionalised HA particles will be subsequently incorporated in a HA hydrogel (b). At cellular level, lectin-functionalised HA particles can be released towards specific glycan that are present on the cell surface or intracellular or ECM, allowing the therapeutic action of drug/inhibitor/therapeutic molecule to take place in response to pathological insults (c).

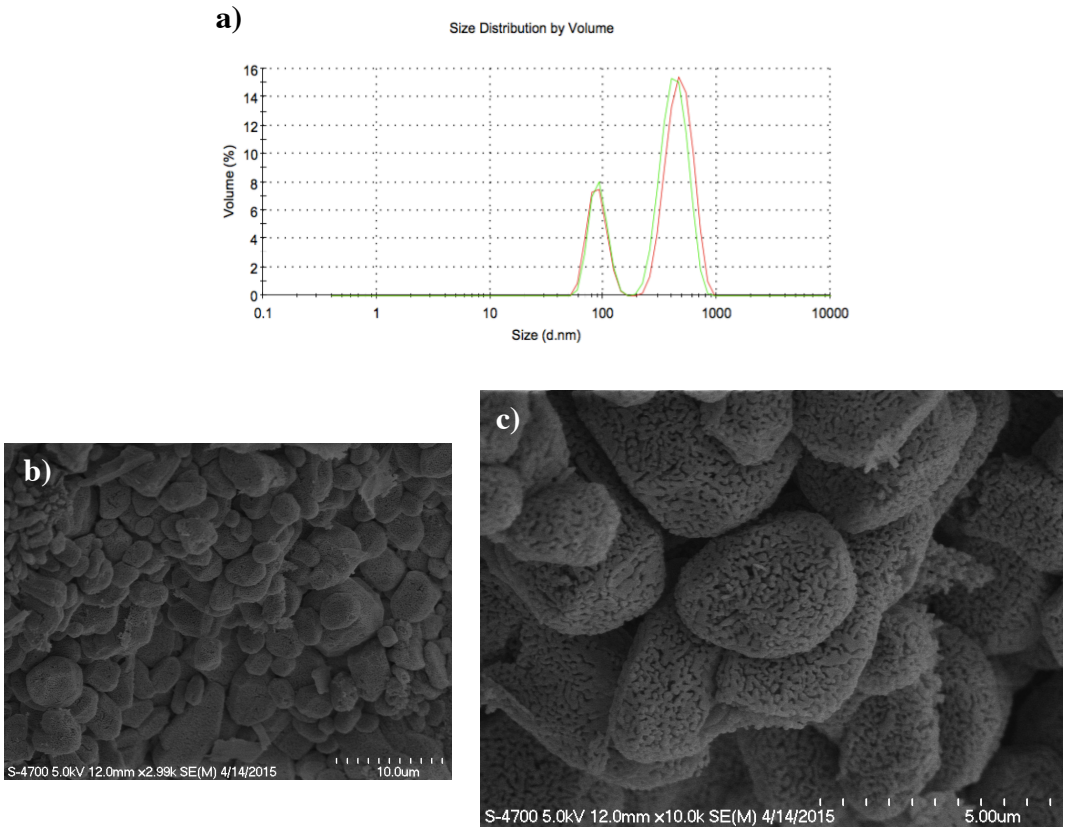

Figure 5.6 Characterisation of HA particles. The size distribution of HA particles (±500 nm) determined by DLS (a). A higher polydispersity of HA particle was observed by SEM images (b). High SEM magnification of HA particles revealed coral-like structure on the surface of particles (c).

[3] M. L. Skovron, "Epidemiology of low back pain," *Baillieres. Clin. Rheumatol.*, vol. 6, no. 3, pp. 559–573, 1992.

[4] A. M. Elliott, B. H. Smith, K. I. Penny, W. C. Smith, and W. A. Chambers, "The epidemiology of chronic pain in the community," *Lancet*, vol. 354, no. 9186, pp. 1248–1252, 1999.

[5] D. Hoy, P. Brooks, F. Blyth, and R. Buchbinder, "The Epidemiology of low back pain," *Best Pract. Res. Clin. Rheumatol.*, vol. 24, no. 6, pp. 769–781, 2010.

[6] K. M. C. Cheung, J. Karppinen, D. Chan, D. W. H. Ho, Y. Q. Song, P. Sham, K. S. E. Cheah, J. C. Y. Leong, and K. D. K. Luk, "Prevalence and pattern of lumbar magnetic resonance imaging changes in a population study of one thousand forty-three individuals," *Spine (Phila. Pa. 1976).*, vol. 34, no. 9, pp. 934–40, 2009.

[7] K. Luoma, H. Riihimäki, R. Luukkonen, R. Raininko, E. Viikari-Juntura, and A. Lamminen, "Low back pain in relation to lumbar disc degeneration," *Spine (Phila. Pa. 1976).*, vol. 25, no. 4, pp. 487–92, Mar. 2000.

[8] C. J. Zheng and J. Chen, "Disc degeneration implies low back pain," *Theor. Biol. Med. Model.*, vol. 12, no. 1, pp. 24, 2015.

[9] A. J. Freemont, T. E. Peacock, P. Goupille, J. A. Hoyland, J. O. Brien, and M. I. V. Jayson, "Early report Nerve ingrowth into diseased intervertebral disc in chronic back pain," *Lancet*, vol. 350, pp. 178–181, 1997.

[10] D. Purmessur, A. J. Freemont, and J. A. Hoyland, "Expression and regulation of neurotrophins in the nondegenerate and degenerate human intervertebral disc," *Arthritis Res. Ther.*, vol. 10, no. 4, p. R99, Jan. 2008.

[11] A. J. Freemont, "The cellular pathobiology of the degenerate intervertebral disc and discogenic back pain," *Rheumatology (Oxford).*, vol. 48, no. 1, pp. 5–10, Jan. 2009.

[12] E. C. Collin, M. Kilcoyne, S. J. White, S. Grad, M. Alini, L. Joshi, and A. Pandit, "Unique glycosignature for intervertebral disc and articular cartilage cells and tissues in immaturity and maturity," *Sci. Rep.*, vol. 6, no. October

2015, p. 23062, 2016.

[13] R. S. Haltiwanger and J. B. Lowe, "Role of glycosylation in development," *Annu. Rev. Neurosci.*, vol. 73, pp. 491–537, 2004.

[14] M. Alini, S. M. Eisenstein, K. Ito, C. Little, A. A. Kettler, K. Masuda, J. Melrose, J. Ralphs, I. Stokes, and H. J. Wilke, "Are animal models useful for studying human disc disorders/degeneration?," *Eur. Spine J.*, vol. 17, no. 1, pp. 2–19, Jan. 2008.

[15] I. Barbosa, S. Garcia, V. Barbier-Chassefière, J. P. Caruelle, I. Martelly, and D. Papy-García, "Improved and simple micro assay for sulfated glycosaminoglycans quantification in biological extracts and its use in skin and muscle tissue studies," *Glycobiology*, vol. 13, no. 9, pp. 647–653, 2003.

[16] A. J. Day and C. A. de La Motte, "Hyaluronan cross-linking: A protective mechanism in inflammation?," *Trends Immunol.*, vol. 26, no. 12, pp. 637–43, Dec. 2005.

[17] I. M. Jou, "The experimental study of the investigagtion of the pathogenesis and electrodiagnostic significance of radicupathy," 1991.

[18] H. H. Schaumburg, E. Zotova, C. S. Raine, M. Tar, and J. Arezzo, "The rat caudal nerves: A model for experimental neuropathies.," *J. Peripher. Nerv. Syst.*, vol. 15, no. 2, pp. 128–39, 2010.

[19] S. Orita, S. Ohtori, and A. Taniguchi, "Direct evidence for sensory innervation of the dorsal portion of the Co5/6 coccygeal intervertebral disc in rats," *Spine (Phila. Pa. 1976).*, vol. 35, no. 14, pp. 1346–1352, 2010.

[20] C. T. S. Ching, D. H. K. Chow, F. Y. D. Yao, and A. D. Holmes, "The effect of cyclic compression on the mechanical properties of the inter-vertebral disc: An *in vivo* study in a rat tail model," *Clin. Biomech.*, vol. 18, no. 3, pp. 182–189, Mar. 2003.

[21] A. Nachemson, "The effect of forward leaning on lumbar intradiscal pressure," *Acta Orthop. Scand.*, vol. 35, no. Nachemson 1960, pp. 314–28, 1965.

[22] H. J. Wilke, P. Neef, M. Caimi, T. Hoogland, and L. E. Claes, "New *in vivo*

measurements of pressures in the intervertebral disc in daily life," *Spine (Phila. Pa. 1976).*, vol. 24, no. 8, pp. 755–62, 1999.

[23] A. Barbir, K. E. Godburn, A. J. Michalek, A. Lai, R. D. Monsey, and J. C. Iatridis, "Effects of torsion on intervertebral disc gene expression and biomechanics, using a rat tail model," *Spine (Phila Pa 1976)*, vol. 36, no. 8, pp. 607–614, 2011.

[24] D. Purmessur, M. C. Cornejo, S. K. Cho, P. J. Roughley, R. J. Linhardt, A. C. Hecht, and J. C. Iatridis, "Intact glycosaminoglycans from intervertebral disc-derived notochordal cell conditioned media inhibits neurite growth while maintaining neuronal cell viability," *Spine J.*, 2015.

[25] D. Sakai, Y. Nakamura, T. Nakai, T. Mishima, S. Kato, S. Grad, M. Alini, M. V. Risbud, D. Chan, K. S. E. Cheah, K. Yamamura, K. Masuda, H. Okano, K. Ando, and J. Mochida, "Exhaustion of nucleus pulposus progenitor cells with ageing and degeneration of the intervertebral disc," *Nat. Commun.*, vol. 3, pp. 1264, 2012.

[26] NCT01290367, "Safety and preliminary efficacy study of mesenchymal precursor cells (MPCs) in subjects with lumbar back pain," *https://clinicaltrials.gov/ct2/show/NCT01290367?term=NCT01290367*, 2016. (29 May 2017).

[27] NCT02412735, "A prospective, multicenter, randomized, double-blind, placebo-controlled study to evaluate the efficacy and safety of a single injection of Rexlemestrocel-L alone or combined with hyaluronic acid (HA) in subjects with chronic low back pain," *https://clinicaltrials.gov/ct2/show/study/NCT02412735?term=NCT02412735,* 2017. (29 May 2017).

[28] M. V. Risbud, A. Guttapalli, T. T. Tsai, J. Y. Lee, K. G. Danielson, A. R. Vaccaro, T. J. Albert, Z. Gazit, D. Gazit, and I. M. Shapiro, "Evidence for skeletal progenitor cells in the degenerate human intervertebral disc," *Spine (Phila. Pa. 1976).*, vol. 32, no. 23, pp. 2537–2544, 2007.

[29] H. Henriksson, M. Thornemo, C. Karlsson, O. Hägg, K. Junevik, A. Lindahl, and H. Brisby, "Identification of cell proliferation zones, progenitor cells and

a potential stem cell niche in the intervertebral disc region: A study in four species," *Spine (Phila. Pa. 1976).*, vol. 34, no. 21, pp. 2278–87, Oct. 2009.

[30] R. Rodrigues-Pinto, S. M. Richardson, and J. A. Hoyland, "An understanding of intervertebral disc development, maturation and cell phenotype provides clues to direct cell-based tissue regeneration therapies for disc degeneration," *Eur. Spine J.*, vol. 23, no. 9, pp. 1803–1814, 2014.

[31] D. T. Scadden, "The stem-cell niche as an entity of action," *Nature*, vol. 441, no. 7097, pp. 1075–9, 2006.

[32] G. Fontana, D. Thomas, E. Collin, and A. Pandit, "Microgel microenvironment primes adipose-derived stem cells towards an NP cells-like phenotype," *Adv. Healthc. Mater.*, vol. 3, no. 12, pp. 2012–2022, 2014.

[33] G. Fontana, A. Srivastava, D. Thomas, P. Lalor, P. Dockery, and A. Pandit, "Three-dimensional microgel platform for the production of cell factories tailored for the nucleus pulposus," *Bioconjug. Chem.*, 2014.

[34] Z. Bian and J. Sun, "Development of a KLD-12 polypeptide/TGF-β1-tissue scaffold promoting the differentiation of mesenchymal stem cell into nucleus pulposus-like cells for treatment of intervertebral disc degeneration," *Int J Clin Exp Pathol*, vol. 8, no. 2, pp. 1093–1103, 2015.

Appendices

I. Protocols

A. List of Components and Reagents

Materials	Supplier
Sodium hyaluronate	Lifecore Biomedical, USA
4-arm PEG-amine MW 2000	JenKem Technology, USA
Teflon™ tape	Fisher Scientific, Ireland
Tween20®	
Phosphate buffer saline (PBS)	
Urea	
Live/Dead® staining kit	Life Technologies, Ireland
AlamarBlue® assay	
Anti-rabbit antibody Alexa Fluor® 488 conjugate	
Anti-rabbit antibody Alexa Fluor® 564 conjugate	
Rhodamine phalloidin	
ProLong® gold antifade	
4,6-diamidino-2-phenylindole (DAPI)	
TaqMan® VIC® labelled GAPDH primer	
TaqMan® Universal PCR Master Mix, no AmpErase® UNG	
Human recombinant IL-1β cytokine	PeproTech, USA
Rabbit anti-IL-1R1 antibody	Novus Biologicals, USA
Goat polyclonal anti-TRPV1 antibody	

Materials	Supplier
Rabbit polyclonal keratan sulfate antibody	Novus Biologicals, USA
Rabbit polyclonal anti-GAP43 antibody	
Rabbit anti-MyD88 antibody	Abcam, UK
Donkey anti-goat antibody Alexa Fluor® 488 conjugate	
Donkey anti-rabbit antibody Alexa Fluor® 555 conjugate	
Donkey anti-rabbit antibody Alexa Fluor® 555 conjugate	
Anti-CD44 antibody FITC conjugate	
Mouse monoclonal anti-TGF-β1antibody	
Rabbit polyclonal anti-fibronectin antibody	
Rabbit monoclonal anti-Trk A antibody Alexa Fluor® 647 conjugate	
Rabbit polyclonal anti-COL1A antibody FITC conjugate	Biorbyt, Cambridgeshire, UK
Rabbit polyclonal anti-aggrecan antibody FITC conjugate	
Rabbit polyclonal phospho-p38 MAPK (Thr180/Tyr182)	Cell Signaling Technology, MA, USA
Rabbit monoclonal phospho-NF-κB p65 (Ser536)	

Materials	Supplier
SYBR® green PCR Master Mix	Qiagen, Germany
miRNeasy mini kit	
OCT embedding medium	Thermofisher Scientific, Ireland
TNBSA (2,4,6-trinitrobenzene sulfonic acid)	
Goat anti-mouse antibody Cy®5 conjugate	
Taqman FAM™ labeled preprotachykinin (Substance P Precusor)	
Taqman FAM™ labelled *c-Fos* primer	
Mouse monoclonal anti-chondroitin sulfate antibody	Sigma-Aldrich, Ireland
Glutaraldehyde (GTA)	
N-hydroxysuccinimide (NHS)	
Lactose	
GlcNAc	
1-ethyl-3-(3-dimethylaminopropyl)carbodiimide (EDC)	
Galactose	
Mannose	
Sucrose	
Dithiothreitol	

Materials	Supplier
Ammonium bicarbonate (NH_4HCO_3)	Sigma-Aldrich, Ireland
Pronase/Protease	
Isopentane	
Sodium formate	
Formic acid	
Molecular grade ethanol	
Molecular grade chloroform	
Trizol® reagent	
Triton™ X-100	
Paraformaldehyde (PFA)	
Penicillin/streptomycin (P/S)	
Fetal bovine serum (FBS)	
Collagenase type IV	
Acetonitrile	
Sodium bicarbonate	
Sodium dodecyl sulfate (SDS)	
Mayer's haematoxylinand eosin	
Alcian blue	
Nuclear fast red	
Basic fuchsin	
Celestine blue	

Materials	Supplier
Proteinase K	Sigma-Aldrich, Ireland
Acetic acid	
Trypsin	
Tris-buffered saline	
NaCl	
$CaCl_2$	
$MgCl_2$	
BSA	
HCl	
Hyaluronidase	
Hanks' balanced salt solution (HBSS)	
High glucose (HG) Dulbecco's modified Eagle's medium (DMEM) - 6429	
Ponceau 2R	
Glacial acetic acid	
Acid fuchsin	
Fastgreen stain	
Xylene	Lennox, Ireland
Ethanol	
$KMnO_4$	Riedel-de Haen, Germany
Sodium metabisulphite ($Na_2S_2O_5$)	

Materials	Supplier
H_2SO_4	Merck, UK
HCL	
Paraldehyde	
D.P.X. mounting medium	
Dodecamolybdophosphoric acid ($H_3PO_412MoO_324H_2O$)	Hopkin& Williams, UK
Random primer	Promega, Ireland Bioline, Ireland
ImProm-II TM reverse transcriptase	
ImProm-II TM reaction buffer 5X	
$MgCl_2$ 25mM	
dNTP mix	
Recombinant riboSafe RNase inhibitor	
NGF primers	Eurofin, Germany
BDNF primers	
18S primers	
SNA-I, MAA, WGA, Con A, UEA-I, WFA, GS-IB4 and PNA lectin FITC/TRITC conjugate	EY Laboratories, USA
Multiplex ELISA pro-inflammatory panel 2 (rat)	Meso Scale Discovery, UK
Betadine (pavidone-iodine) solution	Animalcare Ltd, UK
Vidisic 0.2% w/w eye gel	Bausch & Lomb UK Ltd, UK

Materials	Supplier
Saline chloride	B. Braun Medical Limited, Ireland
Carprofen	Pzifer, UK
Isoflurane	Chanelle Group, Ireland
Morphine sulfate	MercuryPharma Group Limited, UK

B. Hydrogel Preparation

The HA hydrogel fabrication is based on amidation of the HA molecule with carbodiimide and then crosslinked with 4-arm PEG amine. The initiation of the amidation reaction starts with the activation of the HA carboxylic acid by EDC, which forms an O-acyl isourea intermediate. The second step of the reaction is the nucleophilic reaction by the amine on the activated HA which leads to the formation of the amide bond. NHS is used to prevent the formation of the irreversible N-acylurea, to form more hydrolysis-resistant and non-rearrangeable intermediates [1]. Here, the succinimidyl groups of 4-arm PEG amine react with the amine groups on the HA molecules to form crosslinked hydrogel. Hydrogel preparation is based on a previous method [2] by pipetting a channel volume of 4-5 µL onto a hydrophobically modified glass slide prepared by layering Teflon™ tape to obtain spherical-shaped hydrogels. The hydrogels are incubated for one hour at 37°C to allow complete crosslinking (Figure B.1, Chapter 2).

Procedure

1. Reconstitute 7.5 mg sodium hyaluronate with 1 mL distilled water to final concentration of 7.5 mg/mL.
2. Mix HA solution with 4-arm PEG amine accordingly (Table B.1).
3. Dissolve 150 mg NHS (15% (w/v)) with 50 µL distilled water and then mix well with HA/PEG mixture and vortex.
4. Initiate the crosslinking reaction by adding 90 mg EDC (9% (w/v)) into HA/PEG/NHS mixture and vortex.
5. Dispense spherical-shaped droplets by pipetting a channel volume of 4-5 µL gel solution onto a hydrophobically modified glass slide prepared by layering

Teflon™ tape.

6. Incubate the spherical-shaped droplets of the reaction mixture for one hour at 37°C to allow complete crosslinking reaction.

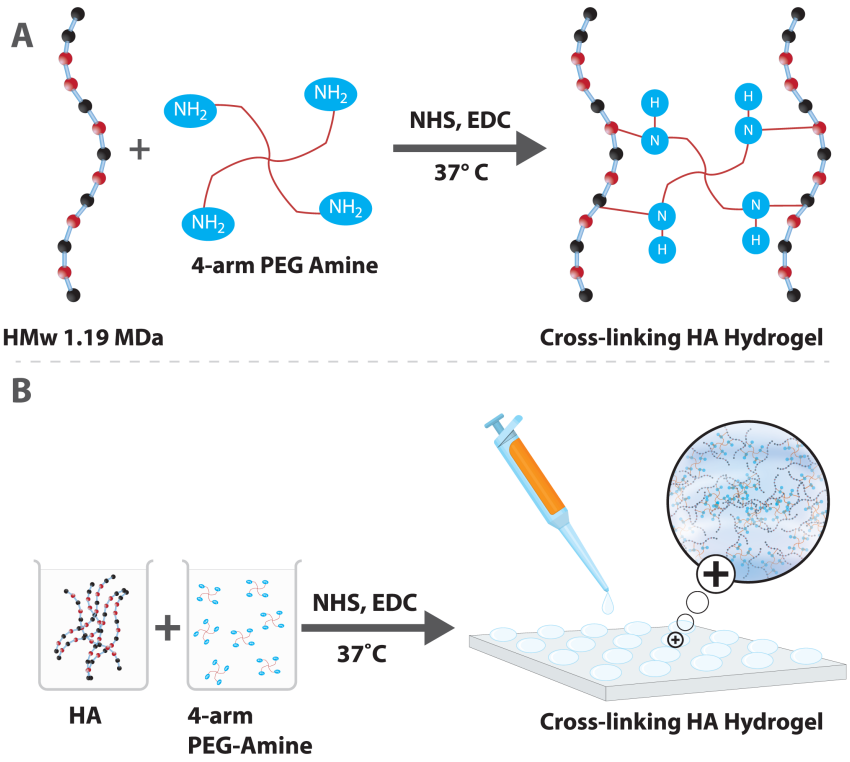

Figure B.1 Hyaluronic acid and 4-arm PEG amine. The succinimidyl groups of PEG react with the amine groups present on the HA molecule.

Table B.1 Preparation of HA hydrogel with various concentration of crosslinker.

Materials	Volume (mL)	Concentration (mg/mL)	Crosslinker	Molarity (mM)
HA	1	7.5	4-arm PEG amine	25
				50
				75
				100
			0.625% GTA	50

Table B.2 Preparation of HA hydrogel for *in vitro* and *in vivo* applications.

Materials	Concentration (mg/mL)	Crosslinker concentration (mM)	One bead of hydrogel	
			Volume (µL)	Concentration (mg/mL)
HA	7.5	75	4	0.030
			5	0.038

C. Isolation of NP Cells

The NP cells from disc T9-S1 spine are isolated from freshly obtained five-month-old bovine tails that are collected directly after sacrifice from a local slaughter house.

i. Tissue Dissection

1. Dissect the disc by eliminating the soft tissues surrounding the disc including muscles, tendons and ligaments (Figure C.1a) using custom dissection tools (be careful not to damage the discs during this process).
2. Isolate the disc with a new scalpel.
3. Cut the disc into mid-sagittal and coronal sections (4 mm wide) (Figure C.1b) and then collect NP and AF from each part into Hanks' balanced salt solution (HBSS).

   Note: It is important to avoid contamination of cells from the intermediate zones (cartilage endplate and bone tissue).

i. Cell Isolation

1. Wash tissues twice with HBSS and once using blank high glucose (HG) Dulbecco's modified Eagle's medium (DMEM).
2. Incubate tissues with 0.19% pronase in blank medium (~76 mg in 40 mL (Sigma P6911)) in incubator at 37°C for one hour.
3. Remove the supernatant.
4. Wash three times with complete medium (DMEM supplemented with 10% FBS and 1% Penicillin/streptomycin (P/S)) to inhibit the enzyme activity.
5. Resuspend with 40 mL of complete medium containing collagenase type IV (32IU/mL ~ 1.78mg in 40 mL).

6. Incubate overnight (~twelve hours) at 37°C in incubator with agitation.
7. Filter the suspension on a 70 µm cell strainer.
8. Centrifuge the cells for eight minutes at 1,200rpm.
9. Wash the pellet with complete media (one time).
10. Centrifuge the cells for eight minutes at 1,200rpm.
11. Resuspend in 10 mL of complete media.
12. Count cells.
13. Seed cells around 1M cells per 10 mL in T75 flask for approximately 10 ten days to growth.

a) **b)**

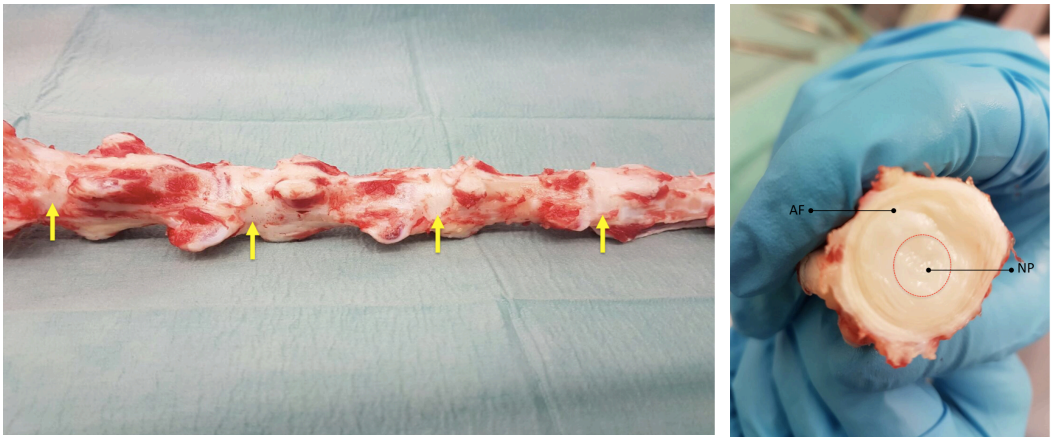

Figure C.1 AF and NP cell isolation from bovine intervertebral disc. (a) Dissection of disc by eliminating soft tissues surrounding disc. Yellow arrow indicated IVD (b) Extraction of AF and NP tissues by cutting mid-sagittal and coronal sections in the disc.

D. Live/Dead® Staining

The cell viability Live/Dead® assay is used to assessed live and dead cells. Live cell is visualised by calcien dye that produces an intense green fluorescence. While, ethidium homodimer (EthD-1) is used to determine dead cells, thereby producing a bright red fluorescence.

Procedure

1. Wash cells in well chambers plate with HBSS (two times).

2. Add 100 µL of 4 µM ethidiumhomodimer (EthD-1) (5 µL from 2 mM EthD-1 stock diluted in 2.5 mL HBSS) and 100µl of 2 µM calcein (1.25 µL from 4mM calcein stock) into each well.
3. Incubate for 30 minutes at room temperature.
4. Image the stained cells under inverted fluoresence microscope with FITC channel (excitation/emission~495 nm/~515 nm) and Texas Red channel (excitation/emission ~495 nm/~635 nm).

E. alamarBlue® Assay

The alamarBlue® assay is used to detect metabolic activity based on fluorometric/colorimetric growth indicator. The growth medium with alamarBlue® changes color from non-fluorescent blue (oxidation) to fluorescent red (reduction) form in response to chemical reduction from cell growth.

Table E.1 Experimental groups for alamarBlue® assay

Groups	Description
Blank	HBSS only
Control	alamarBlue® only
	alamarBlue® with HBSS
	alamarBlue® with un-treated cells
Treatment	alamarBlue® with treated cells (HA 0.75 mg)
	alamarBlue® with treated cells (HA 1.5 mg)

Procedure

1. Prepare 10% of alamarBlue® with DMEM media.
2. Remove media from each well of tissue culture plate.
3. Add 500 µl of prepared alamarBlue® and HBSS into each well accordingly (Table E.1)
4. Incubate tissue culture plate in incubator at 37°C with 5% CO_2 for four hours.
5. Pipette 100 µL supernatant into each well of a clear, flat bottom 96 well plate.
6. Read absorbance at 540 nm wavelength using plate reader (Varioskan Flash, Thermo Fisher Scientific).

F. TNBSA Assay

Procedure

1. Reconstitute the standard, 1 mg of glycine in 1 mL reaction buffer containing 0.1 M sodium bicarbonate pH 8.5 to a final concentration 1 mg/mL.
2. Dilute glycine according to Table F.1.
3. Dissolve onebead hydrogel completely in 1 mL reaction buffer containing 0.1 M sodium bicarbonate at pH 8.5.
4. Mix each 200 µL sample and standard with 100 µL of 0.01% TNBSA.
5. Incubate at 37°C for two hours to allow the reaction.
6. Following incubation, load 100 µL of each sample, standard and blank (reaction buffer) on 96 well clear bottom plate.
7. Add 100 µL 10% solution of SDS and 50 µL of 1 N HCl into each sample.
8. Measure the absorbance at 335 nm wavelength using plate reader (Varioskan Flash, Thermo Fisher Scientific).
9. Generate standard curve to quantify amine concentration in each sample.

Table F.1 Serial dilution of glycine for TNBSA.

Initial glycine concentration (mg/mL)	Dilution factor	Final glycine concentration (mg/mL)
1	3.12	320
	6.25	160
	12.5	80
	25	40
	50	20
	100	10

G. Scanning Electron Microscopy

1. Dehydrate hydrogel in a series of increasing ethanol concentrations in water.
2. Freeze-dry hydrogel overnight.
3. Coat the hydrogel with gold.
4. Image the hydrogel using SEM at 10 kV accelerating voltage (Hitachi S-4700).

H. Hydrolytic and Enzymatic Degradation

1. Record the initial dry weight (W_1) of hydrogels.
2. Incubate hydrogels in 1 mL of PBS and hyaluronidase (5U/mL) respectively at 37°C using a water bath.
3. Replenish the medium with either PBS or a freshly prepared enzyme solution every two days.
4. Recover the hydrogels at one, three, seven, fourteen and 28 days and dry under vacuum.
5. Record the dry weight of hydrogels (W_2) at each time point
6. Calculate the weight-percentage of remaining hydrogels (wt%) using formula:

$$wt\% = \frac{W_1 - W_2}{W_1} \times 100\%$$

I. Immunocytochemistry

1. Wash seeded cells on coverslip-modified tissue culture plate with 1X PBS three times for five minutes each.
2. Fix the cells with 3.7% PFA for fifteen minutes and then wash with 1X PBS three times for five minutes each.
3. Incubate the cells with 0.1% triton X for five minutes and then wash with 1X PBS three times for five minutes each.
4. Incubate the cells with primary antibody (1:100 dilution in PBS) on shaker at 4^oC for overnight and then wash with 1X PBS three times for five minutes each.
5. Incubate the cells with fluoresencely labelled secondary antibody (1:200 dilution in PBS) on shaker at room temperature for two hours and then wash with 1X PBS three times for five minutes each.
6. If stained for double staining, continue with another primary and secondary antibodies staining (step four-five).
7. If stained for rhodamine phalloidin, incubate the cells with rhodamine phalloidin (1:200 dilution in PBS) at room temperature for two hours and then wash with 1X PBS three times for five minutes each.
8. Incubate cells with DAPI (1:1000 dilution in PBS) for two minutes and then wash with 1X PBS three times for five minutes each.
9. Place a drop of mounting medium ProLong® gold antifade on glass slide.
10. Gently transfer and turn over the cover slip seeded with cells towards glass slide

using forcep.

11. Protect the slide from light and cure the staining at 4°C overnight before fluoresence imaging.

J. Tissue Immuno- and Lectin-Histochemistry

i. Tissue Preparation

1. Post-fix the discs in 4% paraformaldehyde for 48 hours.
2. Decalcify vertebral bones in Kristensen's decalcifying solution contains 18% (v/v) of formic acid and 3.5% (w/v) of sodium formate for two weeks.
3. Wash in running tab water for overnight
4. Infiltrate tissues with 20% sucrose until they sink.
5. Embed tissues in OCT medium and then snap-freeze in isopentane bath with liquid nitrogen.
6. Keep tissue blocks at -80°C until use.
7. Cut tissue blocks to 10μm thick sections on a cryostat (Leica™ CM1850, Germany).
8. Collect the tissue sections on Superfrost™ Plus slides and store at -20°C until use.

ii. Immunohistochemistry Staining

1. Warm tissue cryosection slides from -20°C at room temperature and make circle serounding sections using hydrophobic Dako pen.
2. Incubate sections with proteinase K for fifteen minutes at 37°C and then wash in PBS with 0.05% Tween20® (PBS-T) three times for five minutes each.
3. Incubation with 2% BSA for 30 minutes at room temperature and then wash in PBS-T three times for five minutes each.
4. Incubate sections with each primary antibody (1:100 dilution in PBS-T) and negative control (PBS) at 4°C and then wash in PBS-T three times for five minutes each.
5. From this point onwards, maintain darkness while processing.
6. Incubate sections with each fluoresencely labelled secondary antibody (1:200 dilution in PBS-T) for two hours and then washed with PBS-T three times for five minutes each.
7. If stained for double staining, continue with another primary and secondary

antibody staining (step 5-6).

8. Counterstain with DAPI (1:1000 diluted in PBS) for five minutes and wash the sections with PBS-T three times for five minutes each.
9. Mount with ProLong® gold antifade and apply coverslip on top of sections.
10. Cure slides at 4°C in the dark for one day before imaging with a laser confocal microscope.

iii. Lectin Staining

1. Prepare TBS (Table J1) and adjust pH to 7.2 with adding HCl.
2. Prepare TBS-T by adding 0.05% Triton™ X-100.
3. Warm tissue cryosection slides from -20°C at room temperature.
4. If fresh tissue is processed without preservation, fix sections in 4% PFA for two minutes if necessary.
5. Wash sections with TBS-T three times for three minutes each wash with gentle shaking.
6. Block with 2% BSA (periodate-treated of high grade BSA, made in TBS) for one hour at room temperature.
7. In parallel, carry out haptenic sugar inhibition controls with co-incubation of 100 mM appropriate sugar in TBS-T with the lectin in 15 mL falcon tube.
8. Wash the sections with TBS three times for three minutes each.
9. From this point onwards, maintain darkness while processing.
10. Incubate with fluorescently labelled lectin (Table J.2) for one hour at room temperature (concentration of 5-20 μg/mL prepare in TBS-T, but concentrations should be titrated for specific samples).
11. Wash the sections with TBS three times for three minutes each.
12. If staining with antibody, should be done after lectin incubation.
13. Counterstain with DAPI (1:1000 dilution in TBS) for five minutes.
14. Wash the sections with TBS three times for three minutes each.
15. Apply mounting medium with ProLong® gold antifade and coverslip on top of sections.
16. Leave slides at 4°C to cure in the dark for one day.
17. Image slides within two days after curing.

Table J.1 Preparation of TBS.

Chemicals	Concentration (mM)
Tris-HCl	20
NaCl	100
$CaCl_2$	1
$MgCl_2$	1

Table J.2 List of lectin and inhibitor controls.

Lectin	Binding specificity	Haptanic sugar (100 mM)
SNA-I (*Sambucusnigra* agglutinin I)	Sialic acid-α-(2,6)-Gal(NAc)-R	Lactose
MAA (*Maackiaamurensis* agglutinin)	Sialic acid-α-(2,3)-Gal(NAc)-R	Lactose
WGA (Wheat germ agglutinin)	Sialic acid, GlcNAc	GlcNAc
PNA (Peanut agglutinin)	Gal-β-(1,3)-GalNAc (T-antigen), >GalNAc> Lac > Gal, terminal β-Gal, non-sialylated	Gal
GS-I-B4 (*Griffonia simplicifolia* isolectin)	Terminal α-linked Gal	Gal
Con A (Concanavalin A)	α-linked Man, Glc and GlcNAc	Man
UEA-I (*Ulex europaeus* agglutinin I)	α-(1,2)-linked Fuc	Fuc
WFA (*Wisteria floribunda* agglutinin)	GalNAc and chondroitin sulfate	GalNAc

K. Fluorescence and Stereology Quantification of Confocal Optical Images

i. Fluorescence Intensity Quantification

1. Open the fluorescence (optical) image (.tif) in ImageJ software.

2. Go to menu image > stacks > stack to images, to split the fluorescence channels of the image.
3. Click the assign channel of the image and go to the menu image>adjust>color balance.
4. Press 'auto' to adjust the intensity and press 'apply'.
5. Go to the menu process>subtract background, and keep the rolling ball radius '50' and check on 'disable smoothing' and press 'ok'.
6. Repeat step two and three.
7. Finally go to the 'analyze menu' and select 'histogram', and record the fluorescence reading e.g. mean value and standard deviation of the image.

ii. Stereology Quantification using Volume Fraction Method

1. Use volume fraction methods if matrix components are to be quantified in single optical plane of tissue sections.
1. Open the fluorescence image obtained from confocal imaging (.tif) in Image J software.
2. To split the fluorescence channels of the image, go to menu image > stacks and click stack to images.
3. Click the interested channel of the image for quantification and go to menu image > type and click 8 bit to convert to binary mode.
4. Go to menu image > adjust and click threshold.
5. Adjust the optimal threshold that cover positively stained area of interest.
6. To set analysis measurement, go to analyse > set measurements and tick icon area fraction.
7. Go to analyse and click measure to obtain area fraction value of positively stained interested area.
8. To analyse total area, adjust threshold until it covers the entire area of tissue image as per step four to five and repeat step six and seven.
9. Calculate percentage volume fraction by quantifying area fraction of the positively stained matrix component divided with total area and convert into percentage as below:

   $$\text{Percentage volume fraction (\%Vv)} = \frac{\text{Area fraction}}{\text{Total area}} \times 100\%$$

iii. Stereology Quantification using Relative Number Method

2. Use relative number estimation if quantify for stained nuclei in single optical plane of tissue sections.
3. Superimpose unbiased counting frame on fluorescence image obtained from confocal imaging.
4. Count number of positive stained nuclei and total nuclei only in the guard area.
5. Do not count nuclei hit forbidden line (Figure K.1).
6. Calculate relative number estimation by quantifying number of stained nuclei proportional to total nuclei, and convert to percentage as below:

   Percentage relative number (%Na) = $\frac{\text{Number stained nuclei}}{\text{Total number nuclei}} \times 100\%$

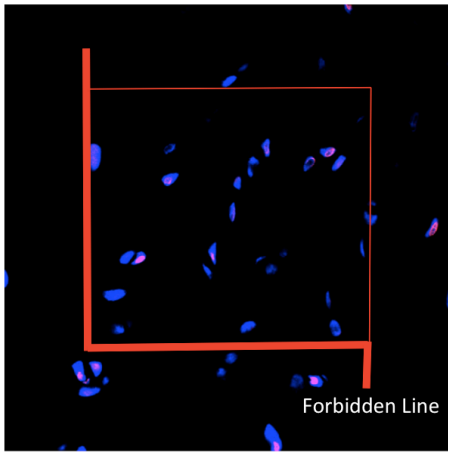

Figure K.1 Stereological methods for number estimation using unbiased counting frame.

L. Histology

i. Tissue Processing

1. Post-fix the discs in 4% paraformaldehyde for 48 h.
2. Decalcify vertebral bones in Kristensen's decalcifying solution contains 18% (v/v) of formic acid and 3.5% (w/v) of sodium formate for two weeks.
3. Wash tissues in running tap water for overnight.
4. Place tissue in labeled cassettes.
5. Place cassettes in metal container provided.
6. Place container in tissue processor.
7. Select routine overnight program from touch screen accordingly Table L.1.

8. When finished, remove container from chamber and select cleaning option from touch screen.
9. Wipe inside of chamber with soft tissue after cleaning cycle finished.

ii. Tissue Embedding with Paraffin Wax

1. Ensure there is enough molten wax in reservoir on top of embedding station.
2. Switch on cold plate beside embedding station.
3. Place small amount of molten wax in embedding mould.
4. Orient specimen in the molten wax using a hot forceps (correct orientation is very important).
5. Place inverted cassette onto the embedding mould and fill with wax.
6. Leave mould on cold plate beside embedding station to solidify.
7. Ensure the trays and general areas are clean when you are finished.

iii. Tissue Sectioning using Microtome

1. Fill floating out bath (water bath) with distilled water.
2. Set temperature to 45° C to 50°C.
3. Cut discs into transverse sections (5µm) on a microtome (Leica™, Germany).
4. Transfer sections onto water bath using forceps.
5. Collect floating sections on Superfrost™ Plus slides and store at room temperature until use.
6. Empty and dry water bath when finished.

Table L.1 Routine program overnight for tissue processor

Reagent	Duration	Temperature	Drain	Delay
Formalin	1:00	-	140	10 min
Ethanol 70%	00:45	-	120	-
Ethanol 90%	00:45	-	120	-
Ethanol 100%	00:45	-	120	-
Ethanol 100%	1:00	-	120	-
Ethanol 100%	1:00	-	140	-
Xylene	00:45	-	120	-

Reagent	Duration	Temperature	Drain	Delay
Xylene	1:00	-	140	-
Xylene	1:15	-	140	-
Paraffin Wax	1:00	62	140	-
Paraffin Wax	1:00	62	140	-
Paraffin Wax	1:00	62	140	-

iv. Haematoxylin and Eosin Staining

1. Dewax sections in xylene; two changes of ten minutes. Each of these is carried out in the fume hood.
2. Remove xylene; two changes of absolute ethanol two minutes each bath.
3. Bring to water through 95%, 70% and 50% ethanol for two minutes each bath.
4. Remove alcohol in running tap water for two minutes.
5. Stain in Mayer's Haematoxylin for six minutes.
6. Blue nuclei in running tap water for four minutes.
7. Examine under microscope and differentiate in acid alcohol if necessary.
8. If acid alcohol used, blue nuclei in running tap water for four minutes.
9. Stain in Eosin for two minutes.
10. Rinse in tap water quickly.
11. Dehydrate through 50% ethanol for ten seconds.
12. Dehydrate through 70% ethanol for ten seconds.
13. Dehydrate through 90% ethanol for two minutes.
14. Dehydrate through absolute ethanol two times for two minutes.
15. Clear in xylene with two changes for ten minutes.
16. Under fume hood, cover sections with D.P.X. mounting medium and apply coverslip.
17. Place slide in oven at 37°C to allow mounting medium to solidify.

v. Masson's Trichrome with Gomori's Aldehyde Fuchsin Staining

1. Dewax sections in xylene; two changes of ten minutes. Each of these is carried out in the fume hood.
2. Remove xylene; two changes of absolute ethanol one minute each bath.
3. Bring to water through 95%, 70% and 50% ethanol for one minute each bath.

4. Remove alcohol in running tap water for two minutes.
5. Oxidise in 0.5% KMnO4 / 0.5% H_2SO_4 (equal parts) for two minutes.
6. Rinse in tap water and bleach in 2% sodium metabisulphite ($Na_2S_2O_5$) for 2 two minutes.
7. Wash in water 30 seconds, followed by 70% ethanol for one minute.
8. Stain in Gomori's aldehyde fuchsin for one minute.
9. Rinse in water (very quickly) then in 95% ethanol ten seconds and followed by water again for ten seconds.
10. Stain in Celestine blue for four minutes.
11. Rinse in water, 30 seconds.
12. Stain in Mayer's Haemalum for four minutes.
13. Quick rinse in water for 20 seconds.
14. Differentiate in acid alcohol for 20 seconds.
15. Blue nuclei in running tap water for four minutes.
16. Stain in Masson's cytoplasmic for one minute.
17. Rinse very quickly in water and differentiate in 1% dodeca-molybdophosphoric acid ($H_3PO_412MoO_324H_2O$) for two minutes.
18. Rinse in water and counterstain in fastgreen or light green for one minute.
19. Differentiate in 1% acetic acid for one minute.
20. Dehydrate through 50%, 70%, 95% and absolute ethanol for one minute each bath.
21. Clear in xylene with two changes for ten minutes each bath.
22. Under fume hood, cover sections with D.P.X. mounting medium and apply coverslip.
23. Place slide in oven 37°C to allow mounting medium to solidify.

vi. Alcian Blue Staining

1. Dewax sections in xylene with two changes of ten minutes each; this is carried out in the fume hood.
2. Remove xylene with two changes of absolute ethanol for two minutes.
3. Bring to water through 95%, 70% and 50% ethanol for two minutes each bath.
4. Remove alcohol in deionized water for two minutes.
5. Stain in Alcian blue solution for 30 minutes.
6. Rinse in running tap water for five minutes.

7. Counterstain in nuclear fast red for ten minutes.
8. Wash in running tap water for one minute.
9. Dehydrate through graded ethanol for two minutes each.
10. Clear in xylene with two changes of ten minutes.
11. Cover sections with D.P.X. mounting medium and apply coverslip.
12. Place slide in oven 37°C to allow mounting medium to solidify.

M. RNA Extraction Using Trizol® Technique Combined With RNeasy® Kit

a. Tissue Homogenisation of Dorsal Horn Spinal Cord

1. For *in vivo* study, dissect left and right dorsal horn of spinal cord from sacral to coccyx level within 30 minutes after euthanasia and immediately kept at -80°C until further analysis.
2. Homogenise spinal cord in 1 mL Trizol® reagent per 50-100 mg of tissue using TissueLyser (Qiagen) through high-speed shaking in 2 mL microcentrifuge round bottom tubes with a bead for fifteen minutes at room temperature.
3. Following homogenisation, centrifuge sample at 1,200 rpm for five minutes at 4°C and discarded the fatty layer. Transfer the cleared supernatant to a new appendorf microcentrifuge tube (Qiagen).

b. Cell Lysis

1. For *in vitro* study, remove media from cells, but do not wash.
2. Add 1 mL of Trizol® reagent for every 10 cm^2 (1 well of 6-well plate) of culture disc area.
3. Use pipette to help lyse the cells in culture dish.
4. Incubate cell lysate at room temperature for five minutes.
5. Remove all the Trizol® and cell lysate mixture into 2 mL appendorf tubes.

i. Phase Separation

1. Add 200 µL of chlorofom without isoamyl alcohol for every 1 mL of Trizol®.
2. Vortex the mixture for fifteen seconds and incubate at room temperature for five minutes.
3. Centrifuge at 13,300 rpm for fifteen minutes at 4°C (do not exceed 8°C which can cause some DNA partition in the aqueous phase).

4. Transfer 600 µL aqueous phase (colourless top layer) to a fresh appendorf tube and mix well with 600 µL of 70% molecular grade ethanol. Store remaining bottom layers for DNA and protein isolation at -20^{o}C.

ii. RNA Isolation

1. Transfer 600 µL of mixture into Rneasy® mini/micro column (Qiagen, Germany) to remove genomic DNA.
2. Centrifuge at 10,000 rpm for fifteen seconds at room temperature and discard flow through.
3. Repeat step two if necessary.
4. Add 700 µL of RW1 to wash and centrifuge at 10,000 rpm for fifteen seconds at room temperature and discard flow through.
5. Add 500 µL of RPE and centrifuge at 10,000 rpm for fifteen seconds at room temperature and discard flow through.
6. Add 500 µL of RPE and centrifuge at 10,000 rpm for two minutes at room temperature and discard flow through.
7. Place column in a new collection tube and add 30 µL RNase free water and centrifuge at 10,000 rpm for one minute at room temperature.
8. Pipette eluted 30 µL into column again and centrifuge at 10,000 rpm for one minute at room temperature.
9. Check RNA concentration by droping 2 µL in NanoDrop™ spectrophotometer (Thermo Fisher Scientific).
10. Keep RNA in -20^{o}C.

iii. RNA Quantification and Purity Determination

1. Calibrate the spectrometer with RNase free water.
2. Measure the absorbance of the RNA at 230nm, 260nm and 280nm.
   1 unit of A260 = 40 µg/mL of RNA
   Concentration of RNA sample = 40 x A260 x dilution factor = x µg/mL
   Quantity of RNA = concentration x volume of sample in mL = x µg
3. The reading at ratio 260/280 close to 2.00 indicates a good grade RNA and the ratio at 230/260 close to 2.00 remarks little protein.
   Note: The ratio at A260/A280 provides an estimation of the purity of RNA with respect to contaminants that absorb in the UV such as protein; and the ratio at

A230/A260 provides an estimation of the purity of RNA with respect to organic contaminant.

N. Synthesis of cDNA by Reverse Transcription

Note 1: For the entire procedure, use filter tips, sterile and nuclease-free tubes pre-chilled on ice.

1. Dilute RNA with RNase free water to a final concentration of 100 ng/µL.
2. For 20 µL reverse transcription reaction, mix 1 µL of RNA with 1 µL random primer, and then RNase free water to a final volume of 5 µL in PCR tube 0.2 mL.
3. Incubate at 70°C for five minutes, for the denaturation of the RNA template and the primers in DNA engine.
4. Quick chill at 4°C for five minutes and hold on ice (or direct in the bath of ice).
   Note 2: Keep on ice during the preparation of the reverse transcription mix.
5. Prepare reverse transcription mix as Table N.1.
6. Dispense 15 µL of the mix into the reaction tubes onto the 5 µL template/primers mix.
7. Mix gently and run the program described in Table N.2 after addition of the tube onto a DNA engine.
8. After this step, keep samples at -20°C until further PCR analysis.

Table N.1 Master mix composition of reverse transcription

Component	Volume per one reaction (µL)	Final concentration
RNAse free water	5.34	-
ImProm-II TM 5X reaction buffer	4.4	1X
$MgCl_2$ 25 mM	2.64	3 mM
dNTP mix (10mM)	1.1	0.5 mM
Recombinant RNasin Ribonuclease inhibitor (20/40U/µl)	1.1	1U/µL
ImProm-II TM reverse transcriptase	1.1	
Final volume for 20 µL reaction	**15**	

Table N.2 Reverse transcription program in DNA engine.

Step	Temperature	Time
Steps temperature time annealing	25°C	5 minutes
Extension heat inactivation	42°C	60 minutes
Reverse transcriptase	70°C	15 minutes

O. RT-qPCR Analysis

a. RT-qPCR Analysis using SYBR® Green Methods

Note: Keep samples on ice during the PCR preparation.

1. Prepare PCR master mix as Table O.1.
2. Add 2 µL of cDNA template into each well of PCR 96-well plate in triplicate.
3. Mix well with 18 µL of master mix to obtain a final volume of 20 µL by pipeting and adding into well containing cDNA.
4. Seal the plate with plastic cover.
5. If any bubbles are seen, centrifuge the plate at 2000 rpm for five minutes.
6. In StepOnePlus™ Real-Time PCR software, configure plate setup and PCR experiment according to program described in Table O.2.
7. Insert PCR plate into StepOnePlus™ Real-Time PCR machine and run the instrument accordingly e.g. fast rpm speed and analysis methods via quantitative comparative CT.

Table O.1 PCR master mix for SYBR® Green

Component	Volume per one reaction (µL)	Final concentration
QuantiFast SYBR®Green PCR kit 2X	10	1.2 mM
Forward primer	0.1	500 nM
Reverse primer	0.1	500 nM
RNAse free water	7.8	
Total volume	18	

Table O.2 qPCR program for NGF, BDNF and 18S primers.

Step	Temperature	Time	Number of cycles
Holding stage			
Initial denaturation	95°C	5 minute	1 Cycle
Cycling stage			
Denaturation	95°C	15 seconds	40 Cycles
annealing	60°C	30 seconds	
Melt curve stage			
Denaturation	95°C	15 seconds	1 Cycle
final extension	60°C	60 seconds	

Table O3. PCR TaqMan master mix for *c-Fos*, *Tac1* and *Gapdh* primers.

Component	Volume per one reaction (µL)
TaqMan reagent master mix 2X	10
TaqMan FAM™ labelled Substance P or *c-Fos*	1
TaqMan VIC® labelled GAPDH	1
RNAse free water	6
Total volume	**18**

Table O.4 qPCR program for *c-Fos*, *Tac1* and *Gapdh* primers.

Step	Temperature	Time	Number of cycles
Holding stage			
Initial step	50°C	2 minutes	1 Cycle
Initial activation step	95°C	10 minutes	
Cycling stage			
Denaturation	95°C	15 seconds	40 Cycles
annealing/ extension	60°C	60 seconds	

b. RT-qPCR Analysis using TaqMan Methods

Note: Keep samples on ice during the PCR preparation.

1. Prepare PCR master mix as Table O.3.
2. Add 2 µL of cDNA template into each well of PCR 96-well plate in triplicate.
8. Mix well with 18 µL of master mix to obtain a final volume of 20 µL by pipeting and adding into well containing cDNA.
9. Seal the plate with plastic cover.
10. If any bubbles are seen, centrifuge the plate at 2000 rpm for five minutes.
11. In StepOnePlus™ Real-Time PCR software, configure plate setup and PCR experiment according to program described in Table O.4.
12. Insert PCR plate into StepOnePlus™ Real-Time PCR machine and run the instrument accordingly e.g. standard rpm speed and analysis methods comparative CT.

P. Surgically Puncture-induced IVD Injury in the Rat Tail

Note: Prepare sterile surgical instruments before surgery as shown in Figure P.1.

1. Needle driver
2. Surgical clamp
3. Iris scissor
4. Teeth forceps
5. Blade holders no. 3
6. Biopsy puncher with plunger
7. Blades no. 15
8. Nylon (non-absorbable) sutures no. 4-0
9. Nylon (non-absorbable) sutures no. 3-0
10. Syringes for administering the analgesics
11. Sterile drape
12. Gauzes
13. Sterile surgery gloves
14. 70% (v/v) ethanol
15. Betadine

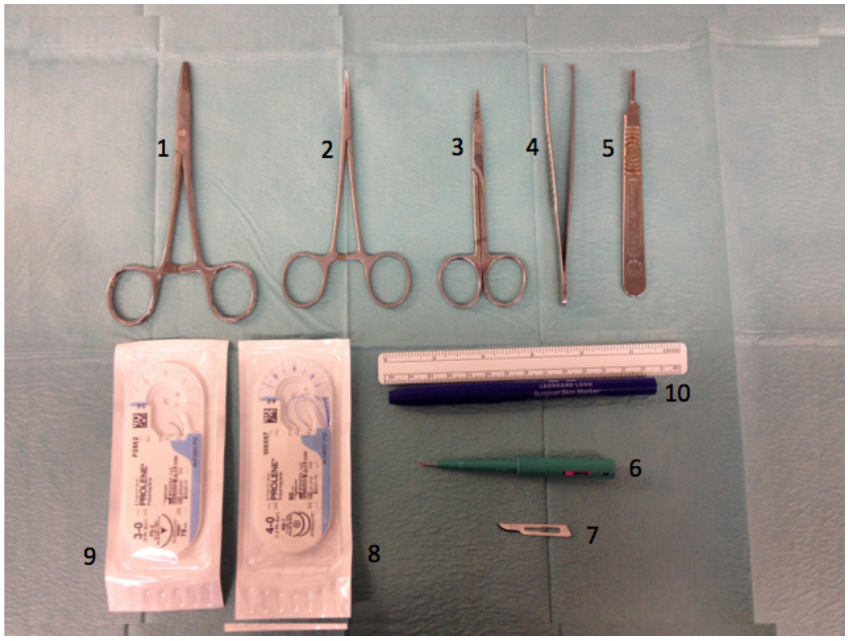

Figure P.1 Surgical instruments for surgery.

Procedure

1. Clean the surgical table with 70% ethanol and cover with sterile drape.
2. Place the sterile surgical instruments onto the drape.
3. Record the weight of the rat in the rat procedure room.
4. Bring the rat's cage into surgical room.
5. Give a single injection of the non-steroidal anti-inflammatory drug carprofen (5 mg/kg, s.c.) fifteen minutes before the surgery to manage operative pain in the early recovery phase.
6. Anesthetize the rat using isoflurane, inhalation anesthesia 5% induction and 1.8-2% for maintenance.
7. Verify the depth of anesthesia by loss of animal's pedal withdrawal (toe pinch) reflex.
8. Add a drop of eye moisturizer onto each rat's eye.
9. Surgeon should be ready to scrub the hand and use sterile gloves for the surgery.
10. Wash the surgical site of rat tail using betadine solution with gauze. Be careful not to wet the animal.
11. Identify coccygeal disc at level Co4-Co5 and/or Co5-Co6 by image intensifier before the surgery procedure or by anatomical surface marking of the vertebral bodies from the surface of the skin tail. The first disc between these two vertebral

bodies counting from the base of the tail is disc Co4-Co5 and the following one is Co5-Co6.

12. Apply a rubber band on the base of the tail not longer than 30 minutes after identifying the IVD and just before the surgery (Figure P.2).
13. Handle surgical instruments with aseptic technique.
14. Begin the surgery with the aid of surgical microscope or binocular loupe under aseptic conditions. Introduce a longitudinal incision in the skin and the connective tissue of the dorsal side of tail covering the IVD level between Co4-Co5 and/or Co5-Co6. Push aside the tendons until the AF tissue (ivory matter) is reached. Perform the injury by puncturing out 1.0 mm (diameter) and up to 2 mm (depth) of NP tissue through AF tissue using biopsy puncture (Figure P.3).
15. After inducing the injury in the NP, leave the IVD as it is or implant with HA hydrogel depending on the experimental group and then layer suture the tendons close to the injury site to show that it was operated.
16. Close the wound by suturing the skin with nylon suture using interrupted horizontal mattress suturing method, thereby covering the IVD.
17. Remove the rubber band.
18. Closely monitor the rat after the procedure until completely recovered from anesthesia.
19. Place the rats in a warm place in a new single cage until the wound healing is satisfactory for approximately one week.

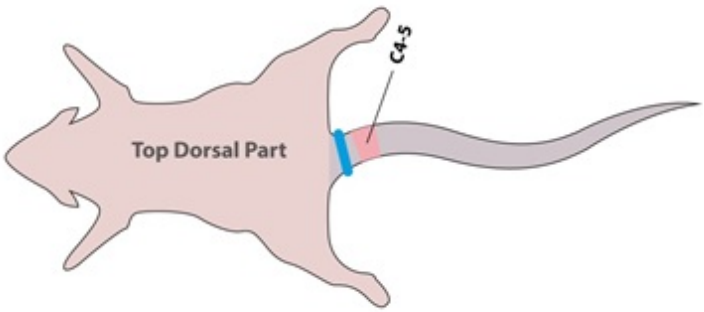

Figure P.2 Identification of coccygeal intervertebral disc Co4-Co5, and rubber band (marked in blue) is applied at the base of the tail.

a) **b)**

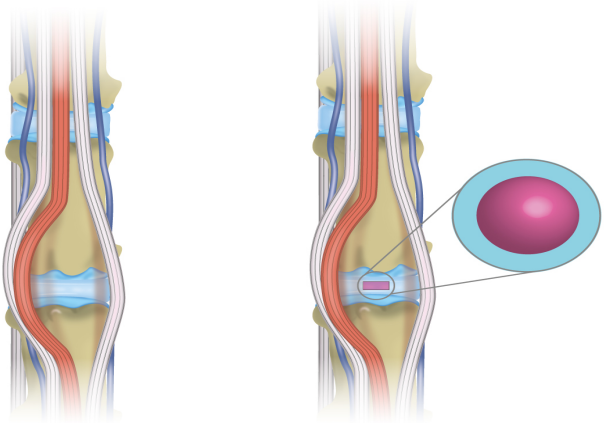

Figure P.3 Dissect the disc by making a longitudinal incision in the skin and the connective tissue of the dorsal side of tail and pushing aside the tendons until the ivory matter of AF tissue (a) is reached. Create injury by puncturing out 1 mm (diameter) and up to 2 mm (depth) of NP tissue through AF tissue. The injured disc will be left as it is or implanted with sphere shape HA hydrogel (b).

Q. Behavioural Nociception Assay

Quantitative sensory testing (QST) is used for pain phenotyping in rodents. QST includes Hargreaves' and tail flick test, both of which are well-established assays to measure thermal nociception and to assess for heat hyperalgesia, an increased sensitivity to a high intensity thermal stimulus, which is noxious. A von Frey test was used to analyse mechanical allodynia or hyperalgesia.

Note: Habituate the rats to the test environment for twenty minutes to the arena 24 hours prior to commencement of testing which may be useful to minimize locomotor activity and stress-induced analgesia during testing. The same investigator who performed the scoring in all of the behavioural tests was blind to the experimental groups.

i. Hargreaves Test

1. Place six-compartment of rat enclosure (arena) on top of Hargreaves' glass apparatus (IITC Life Science, US).
2. Place the individual rats in the arena and allow to habituate for twenty minutes (Figure Q.1).

3. Position the test head of the analgesia meter under the base of the tail with the beam (a radiant light source to introduce heat) focuses approximately on the ventral surface of the tail, which is opposite site to injury.
4. Press the start button on the test head to active intensity at 50% of max output. Once the rat responds, press the button and the light source returns to idle intensity, and then the heat source is deactivated. A cut-off parameter of twenty seconds is set to prevent tissue damage. If no response occurs during this time the heat source automatically returns to idle intensity, and the cut off point is recorded as the latency.
5. Record the time display as latency to the withdrawal response. A response is considered to be withdrawing, flinching, licking, biting and shaking the base of tail.
6. Press the start button again to reset before continuing with testing with four trials in total for each rat tail, with a minimum interval time of three minutes.
7. After complete testing, return rats to their home cages and clean the arena thoroughly with warm soapy water (e.g. dishwasher liquid).

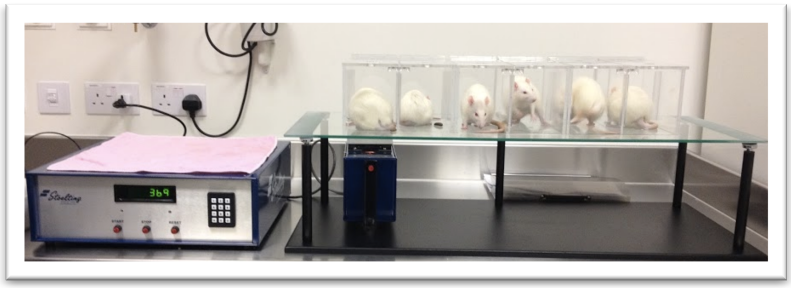

Figure Q.1 Photograph of Hargreaves test. Animals were placed on the rat enclosure (arena) for the thermal hyperalgesia testing.

ii. Tail Flick Test

1. Habituate the rats to the restrainer for a number of days prior to testing to minimize stress-induced analgesia.
2. Remove rats from their home cages and place on the apparatus (IITC Life Science, US) in a towel restraint that allows their tails to project out.
3. Allow animal to habituate for ten minutes prior to testing.
4. Position the test head of the analgesia meter on ventral part of tail with the beam (a radiant light source to introduce heat) focused 2 cm from the distal end of the tail. A cut-off point of twenty seconds is assigned to prevent tissue damage.

5. When the rat flicks away its tail, press the button and the light source returns to idle intensity, and then the heat source is deactivated
6. Record the latency from onset of stimulus to when animal flicks its tail away.
7. A period of at least fifteen seconds between each test is observed to avoid sensitisation of the tail. Re-testing should only be carried out when the temperature of the tail is more than 20^{o}C above initial temperature recorded.
8. Calculate tail-flick latency for each rat as the average of four consecutive measurements.

iii. von Frey Test

1. Place a tissue paper under wire mesh floor.
2. Place the rats individually into six-compartment of rat enclosure (arena) on a wire mesh floor and close with lids with air holes for a 20 minutes habituation period. Exploratory activity should be minimal at this point, without animals being asleep (Figure Q.2).
3. Start the test with 2 g filament (filament number 10) by applying the von Frey filament to the base of the tail on the ventral surface of the tail with such force that it buckles slightly for a maximum of six seconds. Record the positive response when the rats respond to the applied filament by flinching, licking, withdrawing or shaking base of the tail within the six seconds or immediately after the filament is removed. Record the negative response if the animal shows no response to the application of the filament.
4. Repeat this process for five times for the 2 g filament, giving a withdrawal frequency out of five for the tail tested. If obtain a response with the 2 g filament, continue testing with the lower weight filaments until a 0/5 or 0% response is obtained. Continue the testing with ascending filament numbers until a 5/5 or 100% response was obtained for two consecutive filaments.
5. Once testing on all animals is completed, return animals to their homecages.
6. Clean arena with mild detergent and ensure wire mesh is clear of pellets. Remove tissue from under wire mesh.
7. Calculate the first output measure as % withdrawal response. This is calculated for test at each filament weight as follows:

$$\frac{\text{Number of positive responses}}{\text{Number of applications (5)}} \times 100$$

Note: Generally, present results for the lowest filament weight at which a difference between groups of interest is obtained. As the filament weight increases, the force applied to paw increases and at higher filament weights (above ~15 g) will become noxious. Differences between groups at these weights are indicative of mechanical hyperalgesia, not allodynia.

8. The second output measure is the 50% withdrawal threshold. This is defined as the filament weight (or filament number) at which a 50% withdrawal response is obtained and is calculated as follows:
9. For each individual animal, tabulate the filament weight/number and the % response each day. In a Graphpad Prism, tabulate XY data table with filaments in ascending order in the X column, and each day will be a separate Y column containing the % response to each filament.
10. Plot a non-linear regression curve (sigmoidal dose-response, variable slope, set bottom and top constraints as 0 & 100 respectively) and get the log EC_{50} from the results sheet.
11. A log EC_{50} for each animal on each day can then be entered into a separate table (days in the X column and groups in separate Y columns, with each rat as a separate replicate). An average for each group can then be computed and plotted as von Frey filament weight eliciting a 50% response vs. time (days). Groups will appear as separate lines on the final graph.

    Note: If the non linear regression curve fit "does not converge" enter a small value e.g. 1e-3 in place of the last 0 value, this should allow the calculation of regression.

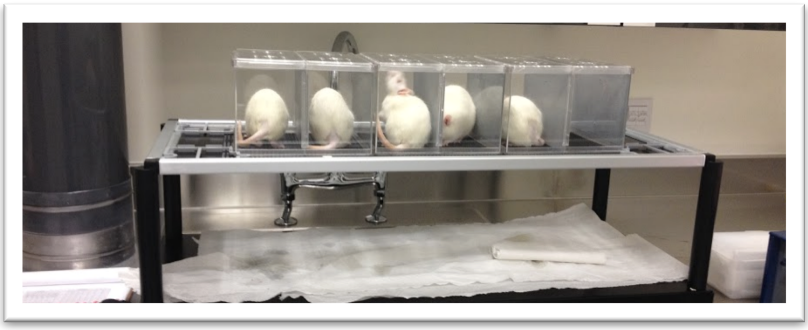

Figure Q2. Photograph of von Frey test. Animals were placed in the rat enclosure (arena) for the von Frey test to determine mechanical allodynia or hyperalgesia.

R. Live Decapitation

1. Ensure the guillotine is clean, free of any blood or anything else that might obstruct its proper functioning. Ensure that the blade is in good and sharp condition.
2. Place guillotine on flat worktop beside sink in necropsy room and place the heavy metal weight on top of the guillotine base to ensure it does not move or slide when it is being used.
3. If right-handed, hold the rat in left hand, ensuring that the fingers remain behind the two forepaws. Cross the rat's forepaws over one another to further reduce chance of head movement during the procedure.
4. While holding the rat in left hand, use right hand to raise the guillotine blade using the handle, then quickly insert the rat's head so that its neck is directly under the guillotine blade and then use right hand to bring the blade down quickly and forcefully through the rat's neck to decapitate it. Speed, force, confidence and conviction are the key elements for a successful and humane decapitation. Always keep hand and fingers behind the blade, with the rat's head and forepaws between your fingers and the blade, and never place hand or fingers under the blade.
5. Try to avoid cutting the forepaws with the blade when performing decapitation. However, it is acknowledged that sometimes cutting of one or both forepaws is an unavoidable consequence of doing a quick, forceful and successful decapitation.
6. If the procedure is done correctly and the blade is sufficiently sharp, then only one drop of the guillotine blade should be necessary to successfully and completely decapitate the rat. However, on occasions the blade may only partially cut through the neck or the skin on the ventral surface of the neck in which case the blade should be quickly lifted and dropped forcefully a second time to fully cut through the neck and skin, completing the decapitation.
7. From start to finish the process of decapitation should take only two to three seconds if done correctly e.g. from time of arrival at the guillotine with rat in hand. It is important to try and minimise the time between collecting the rat from the behavioural arena or home cage and decapitation because the aim is to take a time-sensitive snapshot of brain neurochemistry or molecular biology.

Therefore, walk purposefully from behavioural room or home cage with rat in hand and complete the decapitation immediately, as quickly and humanely as possible.

8. Immediately following decapitation, use left hand to hold the body of the rat firmly over the sink or, if collecting trunk blood, over a pre-labelled (permanent marker) blood collection tube (e.g. heparanised or EDTA tubes) with a clean, dry funnel inserted into the tube to aid blood collection and the tube immersed in ice in a polystyrene box. Hold the base of the tail with right hand to further restrain the muscle spasms and movements of the body to direct the flow of blood into the sink or collection funnel and tube, minimize spattering of blood around the work area.
9. After collection of trunk blood into tube, put the cap on the tube and gently invert it and rotate it for about ten seconds to mix the anti-coagulant with the blood. Then, put the tube back on ice until ready to centrifuge for collection of plasma.
10. Put the carcass into a carcass disposal bag, tie-up at the end of the session and store in -80^{o}C freezer.
11. Always wash and dry the guillotine quickly before using it again for the next rat. It is important that the next rat does not see or smell any blood or tissue on the guillotine or in the surrounding work area before it is killed.

S. AF and NP Protein Extraction

i. ECM Protein Extraction

1. Extract NP and AF tissues separately from the disc, snap frozen with dry ice and keep at -80°C until further analysis.
2. Digest both AF and NP tissues with proteinase K (0.5mg/mL) for less than twelve hours at 56°C and store at -20°C before further analyses.
3. Filter 100 µL of the proteinase K-digested NP and AF (113.5 to 584.1 µg of protein) through a 3 kDa molecular weight cut off centrifugal filter with 100 µL water according to manufacturer's instructions.

   Note: Use HPLC-grade water throughout the procedure.
4. Wash centrifugal filters with water prior to use.

5. Elute the retentate from the filter with 50 µL of water, and 390 µL of digestion buffer (50 mM Tris-HCl, 60mM sodium acetate, pH8.0) and 10 µL of chondroitinase ABC (ChABC, 100 mU).
6. Digest elute at 37 °C for three hours with gentle agitation (300 rpm).
7. Filter the digested mixture using a 3 kDa MWCO spin filter as above and dry the lower molecular weight filtrate in a vacuum centrifuge (~ 2 h).
8. Store the digested dried samples at -20°C until further analysis.

ii. Cellular and ECM Protein Extraction

1. Isolate NP and AF tissues from the disc after euthanasia, snap frozen with dry ice and keep at -80°C until further analysis.
2. To extract both cellular and ECM protein, mince AF and NP tissues with a scalpel and transfer to a microcentrifuge tube and incubate in 6 M urea, 10 mM dithiothreitol and 50 mM NH_4HCO_3 (pH 8.6) for two hours at room temperature with gentle agitation. Collect supernatant by centrifugation at 3,000 g for three minutes.
3. Check protein concentration.
4. Digeste the protein with 2% trypsin in 1.5 M NH_4HCO_3 at pH 7.8 for eighteen hours at 37°C and stop the enzymatic reaction using 2% formic acid.
5. Keep protein samples at -20^{o}C until further analysis.

T. HPLC for Chondroitin Sulfation and Hyaluronic Acid Compositions

1. Dissolve digested samples from ECM protein in 200 µL water.
2. Prepare standard accordingly (Table T.1)
3. Prepare buffer for mobile phase consists of (A) 2 mM aqueous tetrabutyl ammonium bisulfate (TBAB) and (B) 1 or 2 mM TBAB in 2:1 mixture of acetonitrile and water, with starting conditions of 80% A and 20% B. The gradient of 20-65% B is applied over seven minutes, held at 65% B for five minutes and returned to 20% B by twelve and a half minutes.
4. Chromatographic separation is carried out on a Synergi^{TM} column (250 x 4.6mm, 4µm, 80 Å) (Phenomenex Inc., Torrance, CA, USA) at 25°C at a flow rate of 1.1mL/minutes.
5. Inject a volume of 10 µL sample and standard on a Varian 920 HPLC instrument (USA).

6. Monitor the sample at an absorbance of 232 nm on a Varian 920 LC UV-Vis detector.
7. Re-equilibrate the system at 20% B for ten minutes before the next sample injection.
8. Identify the disaccharide content of each sample by comparison with appropriate chromatographed standards under the same HPLC conditions as the sample and quantify by comparison with the appropriate standard curve generated by injection of known concentrations of the standards.

Table T.1 Standard preparation for HPLC.

Carbohydrate	Initial concentration (mg/mL)	Dilution factor	Final concentration (µg/mL)
HA	2	20	0.100
		40	0.050
		200	0.010
D di-0S	1	10	0.100
D di-4S		20	0.050
D di-6S		100	0.010

U. Mass Spectrometry Analysis

1. Run the samples on a Thermo Scientific Q Exactive mass spectrometer connected to a Dionex Ultimate 3000 (RSLC nano) chromatography system.
2. Resuspend tryptic peptides in 0.1% formic acid.
3. Load each sample onto a fused silica emitter (75 µm ID, pulled using a laser puller (Sutter Instruments P2000)), packed with Reprocil Pur C18 (1.9 µm) reverse phase media and separate by an increasing acetonitrile gradient over 47 minutes at a flow rate of 250 nL/min.
4. Operate the mass spectrometer in positive ion mode with a capillary temperature of 320°C, and with a potential of 2300V applied to the frit.
5. All data is acquired with the mass spectrometer operating in automatic data dependent switching mode.

6. Perform a high resolution (70,000) MS scan (300-1600 m/z) using the Q Exactive to select the eight most intense ions prior to MS/MS analysis using HCD.
7. Extract the raw mass spectrometry data.

i. Protein Identification using PEAKS Studio 7 Analysis

1. For protein identification analysis, search the raw data against the *Rattus norvegicus* a subset of the Swiss UniProt database using the search engine PEAKS Studio 7 (Bioinformatics Solutions) for peptides with unspecified enzymatic cleavage.
2. Use only peptide for protein identification that meets specific Peaks parameters, e.g. only accept peptide scores that corresponded to a false discovery rate (FDR) of ≤1% from the Peaks PTM database search.
3. Generate a heatmap of protein distribution.

ii. Protein Identification and Quantification using MaxQuant and Perseus Analysis

1. To identify and quantify protein, analyse the raw mass spec data using MaxQuant [3] search engine based on specification peptides with unspecified enzymatic cleavage for proteinase K digested sample and semi specific trypsin cleavage with fixed modification of carboxymethylation for tryptic digest samples.
2. Use each peptide for protein identification and quantification to meet the specific Maxquant parameters, e.g. only peptide scores that correspond to a false discovery rate (FDR) of ≤1% were accepted from the MaxQuant database search.
3. Extract data from Maxquant analysis.
4. Using Perseus [4] software, perform further computational analysis from Maxquant data to extract analysed proteome data including label free quantification (LFQ) intensity of identified proteins and log 2 value.
5. Extract identified protein with quantification of LFQ and log 2 value from Perseus software, and then calculate for fold change value to continue with protein pathway analysis.

V. Bioinformatics Analysis using Qiagen's Ingenuity Pathway Analysis

1. Upload protein dataset from mass spectometry quantification which have UniProt identifier, LFQ intensity and fold change greater than 2 (two) or less than -2 (minus two) that have a p value < 0.01 into IPA software for pathway analysis.
2. Analyse the dataset with causal networks and species accordingly.
3. Perform comparison analysis between the injury and treatment group of both AF and NP using an empirical test based on fold change value as counts.
4. Extract the data includes diagram, graph, ratio and Z score values from analysis results for canonical signaling pathways, regulators, and disease and functions.

W. ELISA for Inflammatory Cytokines

Protein Extraction

1. Separate the blood plasma from whole blood. **Note:** Perform this procedure on the same day after euthanasia.
1. Transfer, the blood in EDTA tube into 2 mL appendorf tube.
2. Centrifuge for 1,200 rpm at room temperature for fifteen minutes to collect a top layer of blood plasma.
3. Extract cellular and ECM protein from AF and NP tissue as per **protocol S.ii**.

Procedure

1. Use multiplex ELISA pro-inflammatory panel 2 (rat) (Meso Scale Discovery, UK) for analysis of IL-6, IL-1β, TNF-α, IFN-Y, KC/GRO, IL-4, IL-5, IL-13, IL-10.
2. Prepare the sample and reagent according to manufacturer protocol.
3. Dilute blood plasma and protein extracted from AF and NP samples **(section S.ii)** to four fold in diluent.
4. To prepare calibration solutions, reconstitute lyophilised calibrator blend with diluent 42 to a series of four fold dilution steps and zero calibrator.
5. Dilute each detection antibody to 50-fold in diluent 40.
6. Dilute 4X read buffer T to two fold in deionized water.
7. Add 150 µL of blocker H in each well of ELISA plate and incubate at room temperature with fast shaking for one hour.

8. Wash the plate three times with at least 150 µL of wash buffer containing PBS 1X with 0.05% Tween20®.
9. Add a volume of 50 µL of sample including calibrators in each well and further incubate at room temperature with shaking for two hours.
10. Wash the plate for three times with at least 150 µL of wash buffer.
11. Add 25 µL of 1X detection antibody solution in each well and incubate at room temperature with shaking for two hours.
12. Wash the plate for three times with at least 150 µL of wash buffer.
13. Add 150 µL of 2X read buffer T in each well for reading on the plate reader (MESO QuickPlex SQ 120, Meso Scale Diagnostics, USA).

II. Supplementary

X. A Preliminary Study of Innervation in a Rat Tail Model Following HA Hydrogel Treatment

State-of-the-art

Symptomatic intervertebral disc (IVD) degeneration is mediated by an inflammation that induces neurotrophin production which can sensitizes innervation in the disc leading to back pain. High molecular weight hyaluronic acid (HA) hydrogels demonstrate potential as bioactive materials for disc regeneration as they exhibit an anti-inflammatory effect, reduce pain and mimic the microenvironment of the disc. A previous report has documented that small unmyelinated sensory nerve fibers project into the inner AF and NP of degenerated human disc. These expressed GAP43 protein, indicating that the neurons were actively growing into the disc [5]. However, no reports have so far reported on the innervation in disc degeneration following therapy. Therefore, in this study, it was hypothesized that surgical induced AF injury sensitized hyper-innervation in AF and NP tissues and this phenomenon was inhibited following implantation of HA hydrogel in a rat tail model.

Materials and Methods

Synthesis of Cross-linked HA Hydrogel

HA hydrogels were fabricated using 1.19×10^6 Da MW sodium hyaluronate 0.75% (w/v), mixed in 1 ml distilled water with 2000 MW 4-arm PEG-amine 75 mM, N-hydroxysuccinimide (NHS) 15% (w/v) and 1-ethyl-3-(3-dimethylaminopropyl)carbodiimide (EDC) 9% (w/v). The spherical-shaped hydrogels were then obtained by pipetting a channel volume of 4 μL mixed hydrogel solution (0.03 mg/mL) onto a hydrophobically modified glass slide. Hydrogels were then washed in PBS and sterilized under ultra violet light for 60 minutes and were then ready for further *in vivo* implantation.

Implantation HA Hydrogel following Surgically Induced AF Injury in a Rat Tail Model

The adult (12 twelve-week old) female Sprague Dawley rats were purchased from Charles River, UK and eight (n = 8) rats were used in this study. The rats were housed two per cage with wood-chip bedding enriched with a wood stick, *ad libitum* access to food and tap water, with a lights on at 06:00 h and temperature-controlled

(21 ± 2 °C) environment, while the husbandry was provided by female staff. The rats were acclimatised to the vivarium for at least seven days before testing. At day zero, general health including body weight and temperature of the rats was recorded before the surgeries. Single administration of Buprenophrine hydrochloride (0.025 mg/kg, s.c) was given to rats at fifteen minutes before the surgery to manage post-operative pain in the early recovery phase. The rats were briefly anesthetized using isoflurane via inhalation anesthesia 5% induction and 1.8-2% for maintenance. The depth of anesthesia was determined by loss of rat's pedal withdrawal (toe pinch) reflex. The moisturizer was dropped into the eyes if they remained open. The surgical site of the dorsal rat tail was cleaned using betadine solution with gauze. The coccygeal discs Co4-Co5, Co5-Co6 and Co6-Co7 were identified by image intensifier before the surgeries. The first disc between these two vertebral bodies counting from the base of the tail is Co4-Co5 and this is followed by Co5-Co6 and Co6-Co7 which were randomized to defect, defect with implant HA hydrogel and sham (control) respectively. A rubber band was applied on the base of the tail not later than 30 minutes after identification of the disc. The surgery began with the dissection with the aid of surgical microscope and all surgical instruments were handled with an aseptic technique. A longitudinal incision was introduced in the skin and the connective tissue of the dorsal side of tail covering the disc. The tendons were pushed aside until the AF tissue (ivory matter) was reached. The defect was induced by excising a square (1 mm^2) on the dorsal part of the AF the tissue. The discs were left with or without implant HA hydrogel (Figure X.1). The tendons were layer sutured to close the injury site, thereby covering the discs and marked to show that it was operated. The skin was sutured with nylon using the interrupted horizontal mattress to close the wound. The rubber band was then removed from the tail to allow recovery of the blood flow.

For post-operative care, the rats were closely monitored until they completely recovered from anaesthesia and were placed in single housing in an individual cage until the wound healing was satisfactory. This process took approximately one week. The wound was examined for signs of inflammation or infection such as redness, swelling, purulent or serous discharge. General health assessment such as tail skin complications, body weight and temperature, and rats distress scoring was recorded at post-operation day 2, 7, 14, 28 and 56. The temperature and humidity of

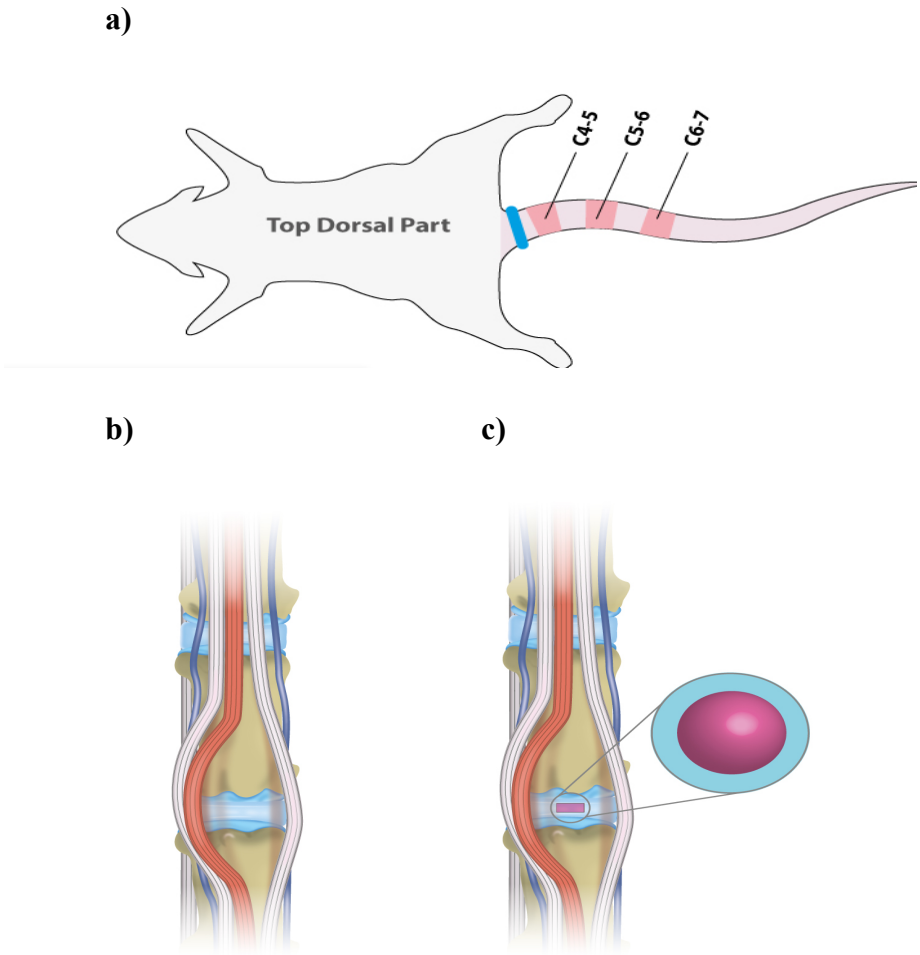

Figure X.1 (a) Rat tail discs identified and rubber band applied at the base. (b) Access of rat tail disc after making an incision in the skin and pushing the tendons aside. (c) Rat tail disc with a rectangle defect created and implanted with spherical-shape HA hydrogel as indicated in pink.

the housing environment were monitored and appropriate bedding materials were provided during the studies. The rats were euthanized at day 56 to harvest the disc for immunohistological analysis.

Immunohistochemistry Analysis

The discs were post-fixed in 4% (w/v) paraformaldehyde for 48 hours and vertebral bones were decalcified in Kristensen's decalcifying solution contains 18% (v/v) of formic acid and 3.5% (w/v) of sodium formate for two weeks. After washing in running tap water overnight, tissues were infiltrated with 20% (w/v) sucrose until they sank. Tissues were OCT embedded and snap-frozen in an isopentane bath with liquid nitrogen, and kept at -80°C until sectioned on a cryostat (Leica™ CM1850, Germany). Tissue sections were collected on Superfrost™ Plus slides (Fisher Scientific Inc., Ireland) and stored at -20°C until use. The staining procedures were performed at room temperature and all washes were done three times for five minutes each between incubation, unless otherwise stated. sections were incubated with proteinase K for fifteen minutes at 37°C, followed by 2% (w/v) BSA for 30 minutes at room temperature before overnight incubation at 4°C with the primary antibody 1:100 mouse polyclonal anti-GAP43 (Abcam, UK) and negative control sections incubated with PBS. Sections were incubated with secondary antibody goat anti-mouse Cy®5 (Thermofisher Scientific, USA) at 1:200 diluted in PBS for two two hours and then washed with PBS-T before counterstaining with DAPI (1:1000 in PBS) for five minutes. All sections were washed with PBS-T before mounting the coverslip. The slides were cured at 4°C in the dark for one day before imaging with a laser confocal microscope (Olympus Fluoview 1000, USA).

Immunohistochemical Image Analysis and Stereology Quantification

Stereological methods for quantification was adopted to calculate the percentage volume fraction of detectable lectin binding to specific glycan. Immunohistochemical reactivity to antibody staining was obtained from at least five microscopic field of views of each slide with three technical and four biological replicates using ImageJ software version 1.48 (National Institutes of Health, USA). Confocal microphotographs were converted to a binary mode (8 bit) and adjusted to the optimal threshold of positive stained and total area. Volume fraction (Vv) was

calculated by quantifying the area fraction of the positively stained nerve divided with total tissue area and converted into percentage as below:

$$\text{Percentage Volume Fraction (\%Vv)} = \frac{\text{Area Fraction}}{\text{Total Area}} \times 100\%$$

Results

HA Hydrogel Inhibited Innervation in the Aneural Disc

Confocal microphotographs indicated substantial evidence of GAP43 expression demonstrated by magenta fluorescence in the outer AF tissue with a projection of nerve innervation towards inner AF tissue following post-injury. However, this marker appeared to show less immune-reactivity in AF tissue implanted with HA hydrogels than that seen in the injury group. The percentage volume fraction of detectable immunoreactive GAP43 was calculated to confirm a significantly reduced expression of nerve-ingrowth (innervation) in AF tissue in the HA hydrogel injury group (10%), than in control injury group (35%) (Figure X.2). Healthy NP tissue (non-operative and sham) exhibited no evidence of GAP43 expression as indicated in confocal images. Nevertheless, a thin nerve outgrowth in NP tissue in injured AF indicated a projection of nerve into aneural NP (Figure X.3). In contrast, no expression of GAP43 in injured AF tissue implanted with HA hydrogel up to day 56 were seen. To confirm this expression trend, the percentage volume fraction of detectable immunoreactive GAP43 was calculated and this was found to be significantly decreased in HA hydrogel group (0%) compared to that in untreated injured AF tissue (6%) (Figure X.2).

Overall, surgically induced AF injury in the disc elicited hyper-innervation in rat tail discs. This is supported by the study which reports the presence of thinly unmyelinated sensory nerve fibers (as indicated by GAP43 expression) growth into the aneural disc in the inner AF and NP tissue in patients who experience discogenic pain [5]. This pathological insult was presumably induced by the release of pro-inflammatory cytokines [6], neurotrophins [7,8] and neuropeptides [5]. Interestingly, in the presence of HA in, an inhibitory effect of nerve innervation in both AF and NP tissues was seen. Nevertheless the mechanism of action of HA in attenuating innervation is still unclear at this stage and further studies have been discussed in **Chapter 4**.

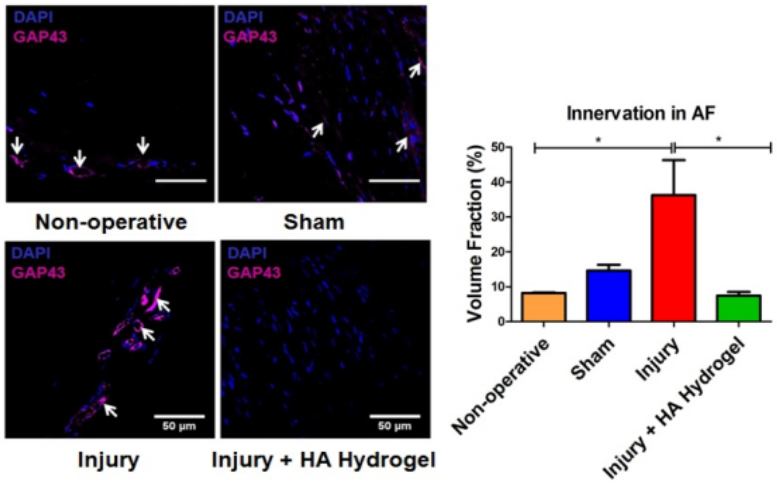

Figure X.2 Confocal micrograph showing expression of GAP43 protein (magenta) (for assessing innervation) increased after induced injury and was fully attenuated in the treatment with implantable HA hydrogel in AF and NP tissue. *Significant differences were noted between the different groups (n = 4, one-way ANOVA, p < 0.05). Data of area fraction was normalised to total area and represented as mean ± S.E.M. Scale bar = 50µm.

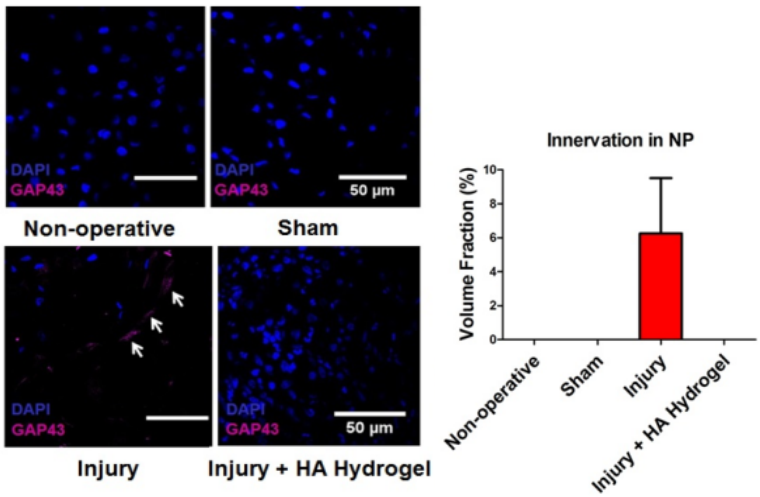

Figure X.3 Confocal images showing expression of GAP43 (for assessing innervation) in NP tissue was increased after induced injury. The GAP43 expression was inhibited in the HA hydrogel group. *Significant differences were noted between the different groups (n = 3, one-way ANOVA, $p < 0.05$). Data of area fraction was normalised to total area and represented as mean ± S.E.M. Scale bar = 50µm.

Y. Optimisation of Lectin Histochemistry

Methods

The healthy discs were processed in accordance with lectin histochemistry procedure. The staining steps were performed at room temperature and all washes were done three times for three minutes each between incubation, unless otherwise stated. Three slides were used for each lectin incubation. The slides were washed with Tris-buffered saline supplemented with Ca^{2+} and Mg^{2+} (TBS; 20 mM Tris-HCl, 100 mM NaCl, 1 mM $CaCl_2$, 1 mM $MgCl_2$, pH 7.2) with 0.05% (v/v) Triton X-100 (TBS-T) and then blocked with 2% (w/v) periodate-treated BSA in TBS for one hour. Inhibitory controls were carried out in parallel to verify that the lectin binding was glycan-mediated by co-incubating lectins in 100 mM of the appropriate haptenic sugar in TBS. Sections were washed and then incubated with eight different fluorescein isothiocyanate (FITC) or tetramethylrhodamineisothiocyanate (TRITC)-conjugated lectins (SNA-I, MAA, WGA, Con A, UEA-I, WFA, GS-IB4 and PNA (EY Labs Inc.)) in TBS for one hour. After five washes with TBS-T, sections were counterstained with 1:1000 DAPI for five minutes. The slides were washed in TBS-T before mounting the coverslip with ProLong® gold antifade (Life Technologies™). All slides were cured at 4°C in the dark for one day before imaging with a laser confocal microscope (Olympus Fluoview 1000, USA).

Results

Sialylation

SNA-I and MAA lectins bind to α-(2,6)-linked sialic acid and α-(2,3)-linked sialic acid respectively. SNA-I binding on AF and NP cells was observed at all concentrations and optimally at 15 µg/µL (Figure Y.1). In NP, MAA lectin showed less binding at 5 – 10 µg/µL, in contrast the staining covered most cellular area at 15 µg/µL. Similarly, optimal MAA binding in AF was observed at 15 µg/µL (Figure Y.2). Overall, SNA-I and MAA binding was eliminated in tissue co-incubated with lactose.

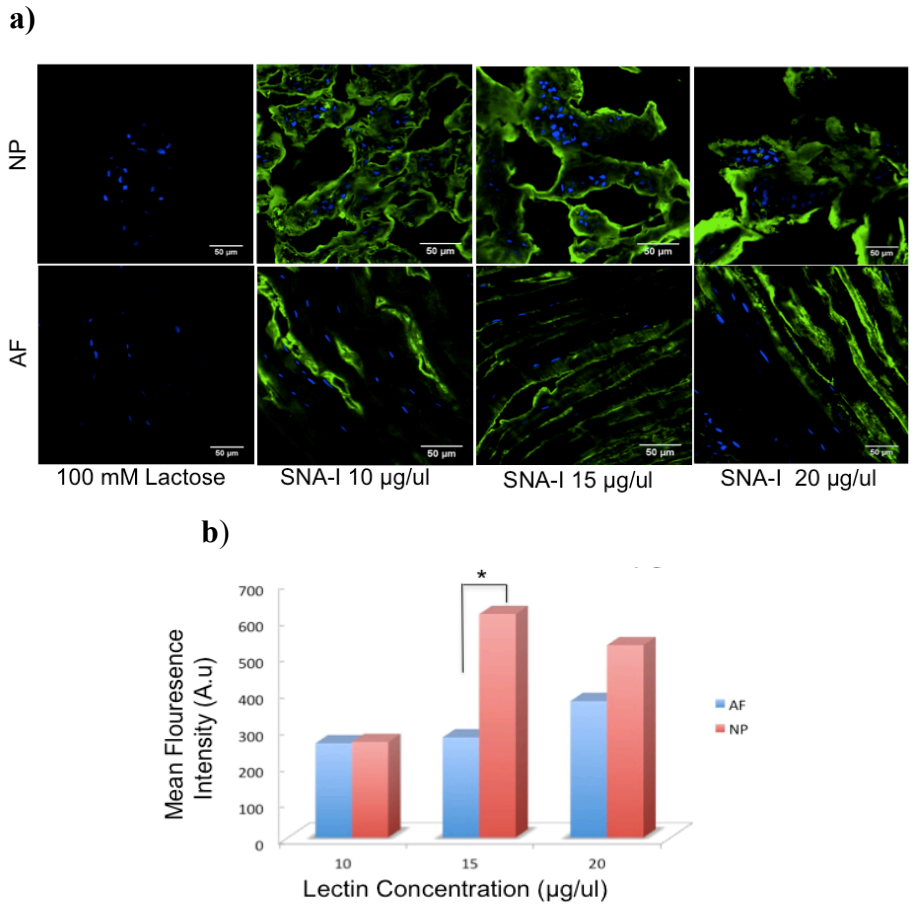

Figure Y.1 Confocal microphotographs showing SNA-I binding to α-(2,6)-linked sialic acid indicated in green fluorescence and the expression was eliminated using inhibitor sugar of lactose. *Significant differences were noted between the different groups (n = 3, one-way ANOVA, $p < 0.05$). Data of area fraction was normalised to total area and represented as mean ± S.E.M. Scale bar = 50µm.

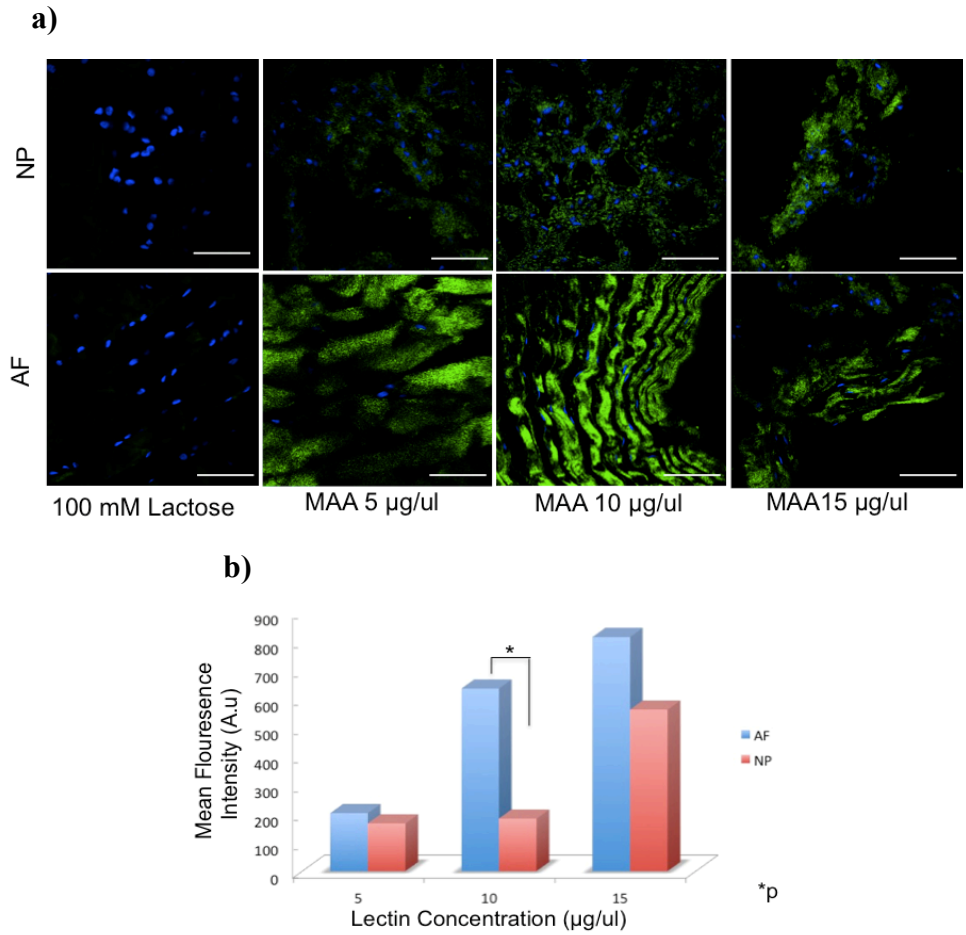

Figure Y.2 α-(2,3)-linked sialic acid was indicated by MAA lectin staining using confocal analysis (in green fluorescence). The binding was diminished using lactose. *Significant differences were noted between the different groups (n = 3, one way ANOVA, $p < 0.05$). Data of area fraction was normalised to total area and represented as mean ± S.E.M. Scale bar = 50µm.

Fucosylation

UEA-I lectin binds to α-(1,2)-linked fucose. The optimal binding was detected on NP cells at 15 μg/μL. Co-incubation of tissue with fucose diminished the lectin binding in cells (Figure Y.3).

High Mannose Type Glycosylation

Con A lectin binds to high mannose type glycosylation. This binding was optimally observed in AF and NP cells at 15 μg/μL (Figure Y.4). Mannose was used to determine specific Con A binding in tissue.

Galactosylation

PNA has binding affinity to Gal-β-(1,3)-GalNAc (T-antigen). The binding was optimally observed in the ECM of AF and NP at 15 μg/μL (Figure Y.5). GS-I-B4 binds to terminal α-linked Gal residues for AF and NP intracellularly at 15-20 μg/μL (Figure Y.6). WFA lectin binds to either α- or β-linked terminal GalNAc and chondroitin sulfate. The binding was only observed in the ECM of AF and NP tissue at 15-20 μg/μL (Figure Y.7). In contrast, PNA, GS-I-B4 and WFA binding was abolished in tissue co-incubated with inhibitor sugar of galactose.

Z. Negative and Positive Control of Immunohistochemistry for Chapter 4

Methods

The injured disc tissue was processed according to immunohistochemistry procedure. For positive control, injured spinal cord tissues from *Xenopus sp*. were used to determine GAP43, TRPV1 and *c-Fos* antibodies stained absolutely in nerve tissues. The staining steps were performed at room temperature and all washes were done three times for three minutes each between incubations, unless otherwise stated. Three slides from three different rats were used for each antibody incubation. Sections were incubated with proteinase K for fifteen minutes at 37°C, followed by 2% (w/v) BSA for 30 minutes at room temperature before overnight incubation at 4°C with the primary antibodies, negative control sections were incubated with PBS and washed in PBS with 0.05% (v/v) Tween20® (PBS-T). Triple staining of three selected primary antibodies 1:100 rabbit polyclonal anti-GAP43 (Cat. ab12274, Abcam, UK), 1:100 goat polyclonal anti-TRPV1 (Cat. AF3066, Novus Biologicals,

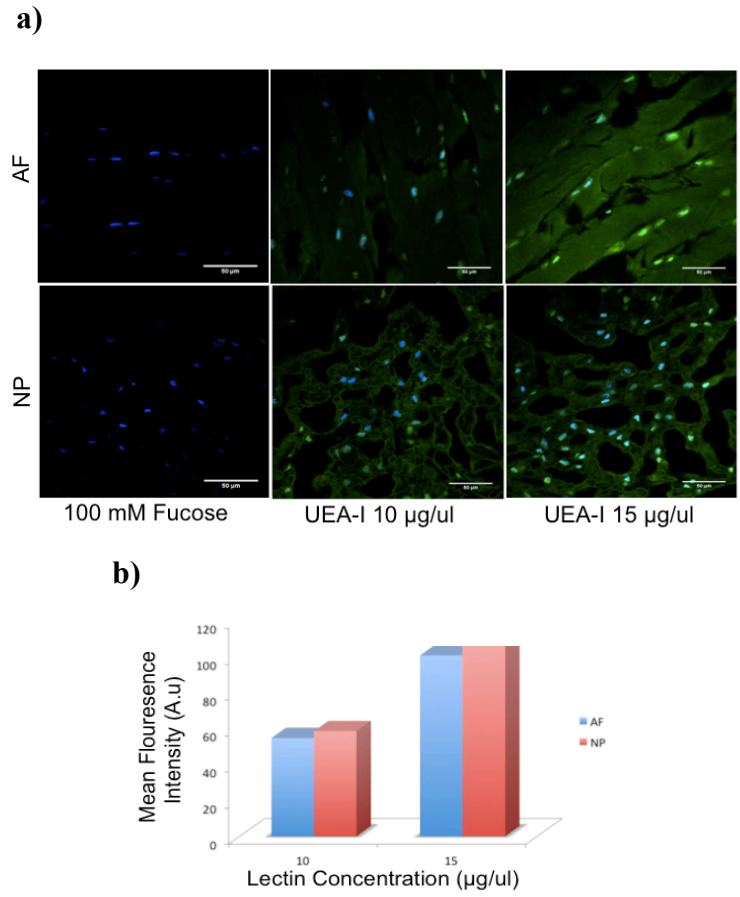

Figure Y.3 Confocal microphotographs showing UEA-I bond to α-(1,2)-linked fucose demonstrated in green fluorescence and the expression was eliminated using inhibitor sugar which is fucose. *Significant differences were noted between the different groups (n = 3, one-way ANOVA, $p < 0.05$). Data of mean fluorescence intensity and represented as mean ± S.E.M. Scale bar = 50µm.

a)

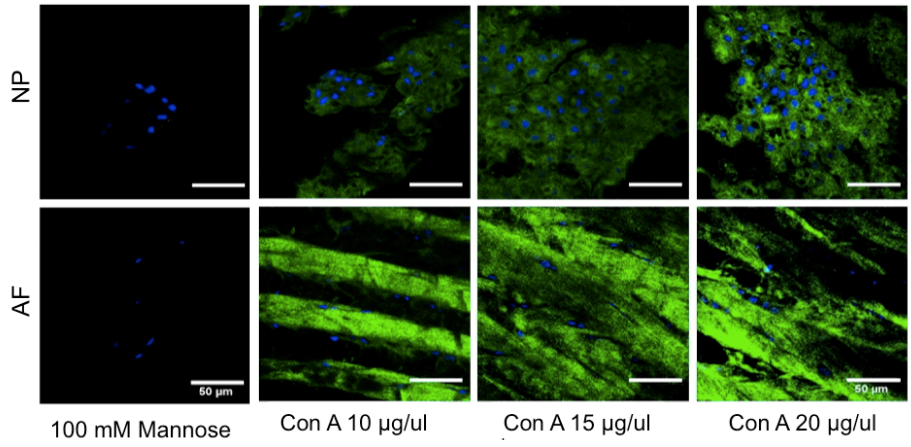

b)

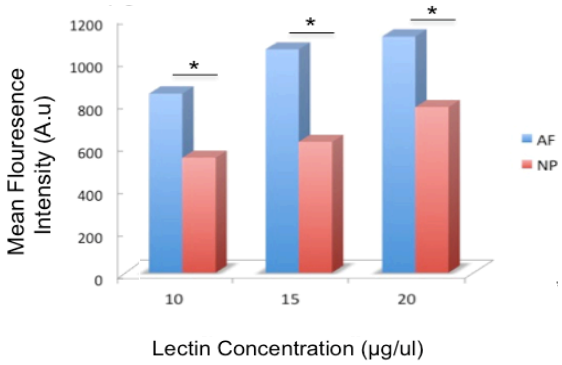

Figure Y.4 Con A stained high mannose type glycosylation which was indicated by confocal analysis (in green fluorescence). The binding was diminished using lactose. *Significant differences were noted between the different groups (n = 3, one-way ANOVA, $p < 0.05$). Data of mean fluorescence intensity and represented as mean ± S.E.M. Scale bar = 50µm.

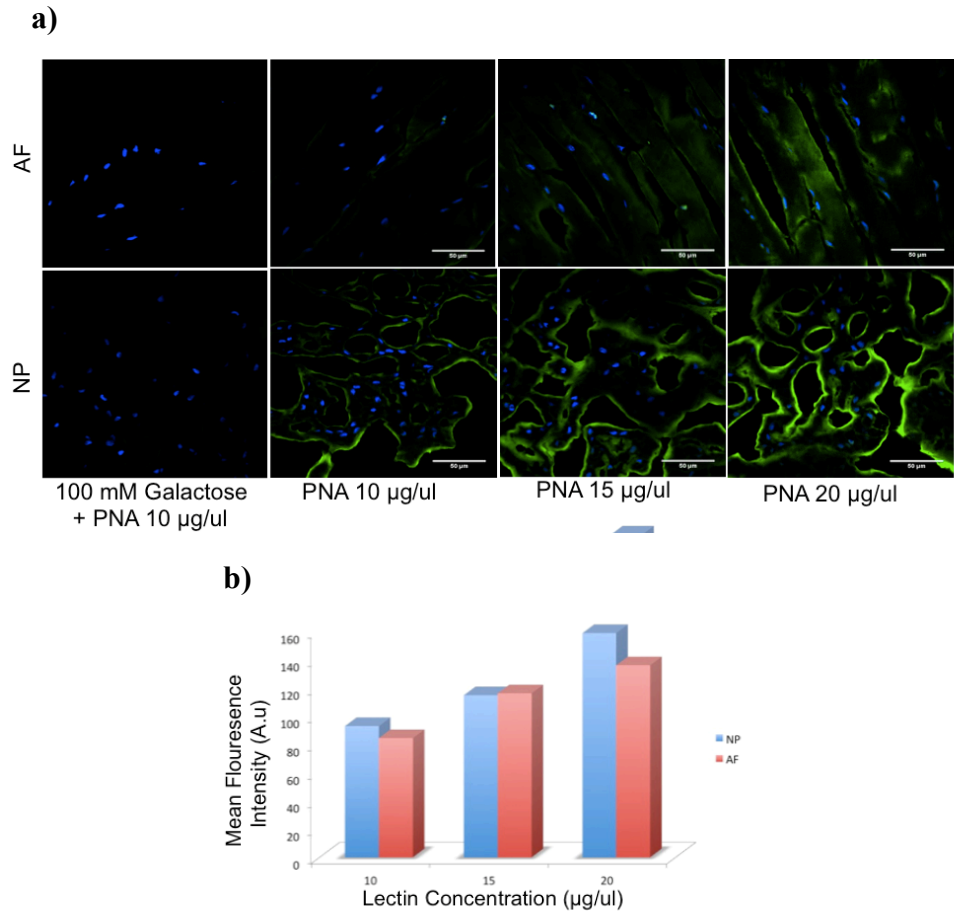

Figure Y.5 Confocal microphotographs showing PNA bond to Gal-β-(1,3)-GalNAc (T-antigen) indicated in green fluorescence and the expression was abolished using inhibitor sugar of galactose. *Significant differences were noted between the different groups (n = 3, one-way ANOVA, $p < 0.05$). Data of mean fluorescence intensity and represented as mean ± S.E.M. Scale bar = 50µm.

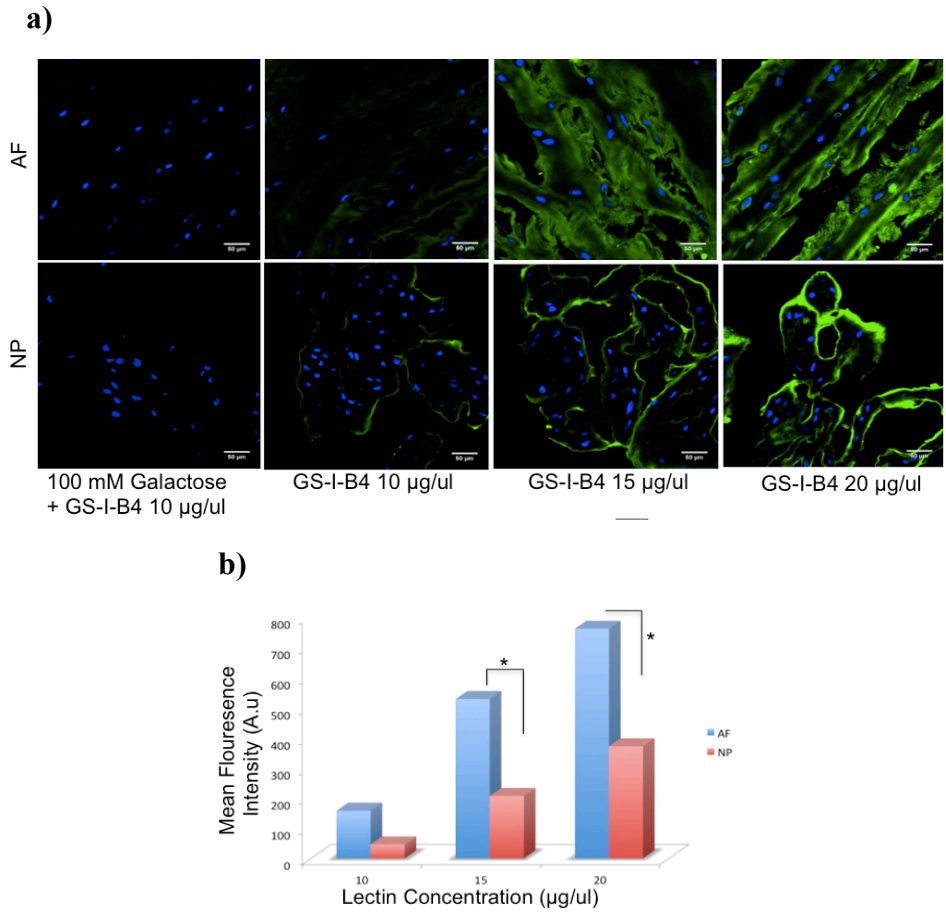

Figure Y.6 GS-I-B4 has binding affinity to terminal α-linked Gal residues which was indicated by confocal analysis (in green fluorescence). The binding was diminished using galactose. *Significant differences were noted between the different groups (n = 3, one-way ANOVA, $p < 0.05$). Data of mean fluorescence intensity and represented as mean ± S.E.M. Scale bar = 50µm.

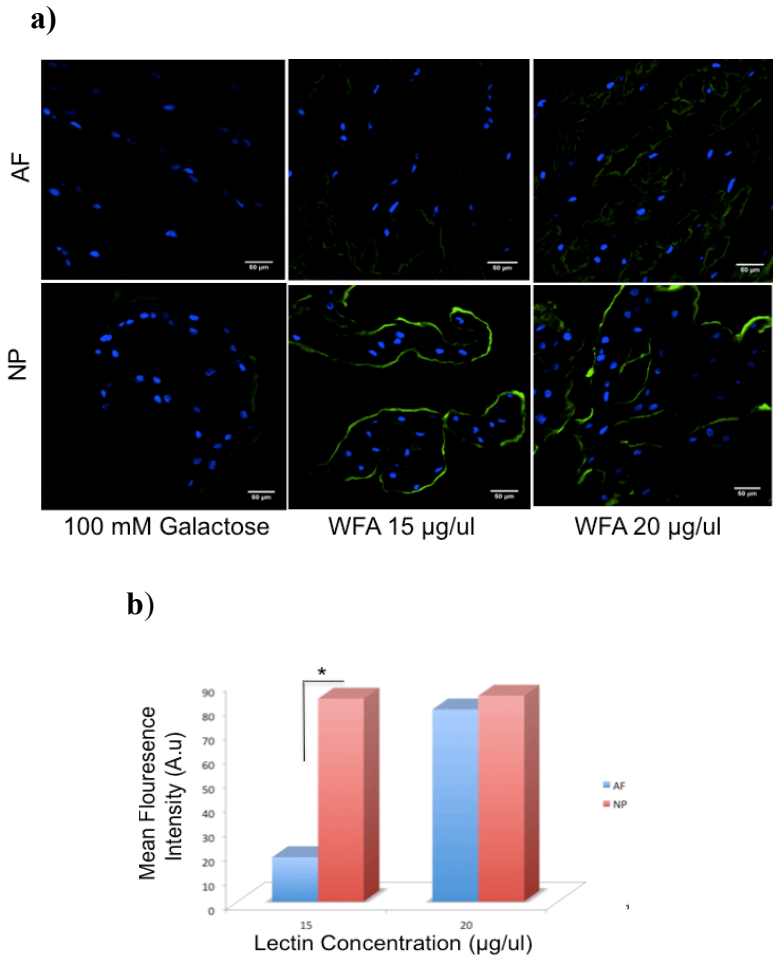

Figure Y.7 WFA stained a or b-linked terminal GalNAc and chondroitin sulfate which was indicated in green fluorescence. This binding was diminished using galactose. *Significant differences were noted between the different groups (n = 3, one-way ANOVA, $p < 0.05$). Data of area fraction was normalised to total area and represented as mean ± S.E.M. Scale bar = 50µm.

LLC, USA), 1:100 mouse monocloncal anti-CGRP antibody (Cat. ab81887, Abcam, UK) was performed in the disc tissue sections. Sections were incubated with secondary antibody donkey anti-rabbit Alexa Fluor® 555 (Cat. ab150074, Abcam, UK), donkey anti-goat Alexa Fluor® 488 (Cat. ab150129, Abcam, UK) and goat anti-mouse Cy®5 (A10524, Thermofisher Scientific, USA) at 1:200 diluted in PBS for two hours and then washed with PBS-T before counterstaining with DAPI (1:1000 in PBS) for five minutes.

For spinal cord tissue, three set of double staining were carried out; the first set used 1:1000 mouse monoclonal anti-acetylated α-tubulin (Cat. T6793, Sigma-Aldrich, Ireland) and 1:100 rabbit polyclonal anti-GAP43 (Cat. ab12274, Abcam, UK) in tissue sections; secondly, 1:200 goat Anti-TRPV1 (AF3066, Novus Biologicals, LLC, USA) and rabbit polyclonal anti-GAP43 (Cat. ab12274, Abcam, UK); lastly, rabbit anti-*cFos* (PC05L) and 1:500 mouse monoclonal anti-acetylated α-tubulin (Cat. T6793, Sigma-Aldrich, Ireland). Sections were then incubated with secondary antibody donkey anti-goat Alexa Fluor® 488 (Cat. Ab150129, Abcam, UK), donkey anti-rabbit Alexa Fluor® 555 (Cat. ab150074, Abcam, UK) and donkey anti-mouse (Cat.A21202, Invitrogen, Ireland). Hoescht® (Life Technology, Ireland) were used to stain nuclei. All stained sections were washed with PBS-T before mounting the coverslip. The slides were cured at 4°C in the dark for one day before imaging with a laser confocal microscope (Olympus Fluoview 1000, USA).

Results

The expression of GAP43 protein was observed in AF of injured disc, which was co-localised with TRPV1 and CGRP stained for nociceptor and neuropeptide respectively. In contrast, no immuno-positive stained for tissue incubated with only secondary antibodies, indicating no cross-reactivity species between secondary antibodies used (Figure Z.1). Spinal cord lesion epicentre (TT171) and the lesion borders (TT114) revealed positive GAP43 protein co-localised with α-tubulin stained for axonal nerve growth for nerve regeneration (Figure Z.2). In addition, TRPV1 and *c-Fos* were observed in injured spinal cord, suggesting activation of sensory nerve (Figure Z.3). Overall, these results indicate that antibodies used in the disc are stained for nerve tissue, which has been confirmed by positive staining in an injured spinal cord tissue.

a)

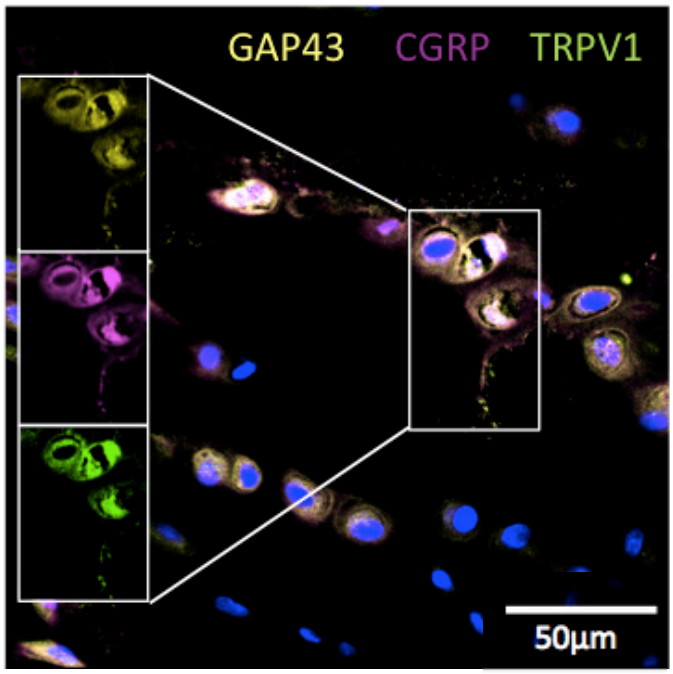

b)

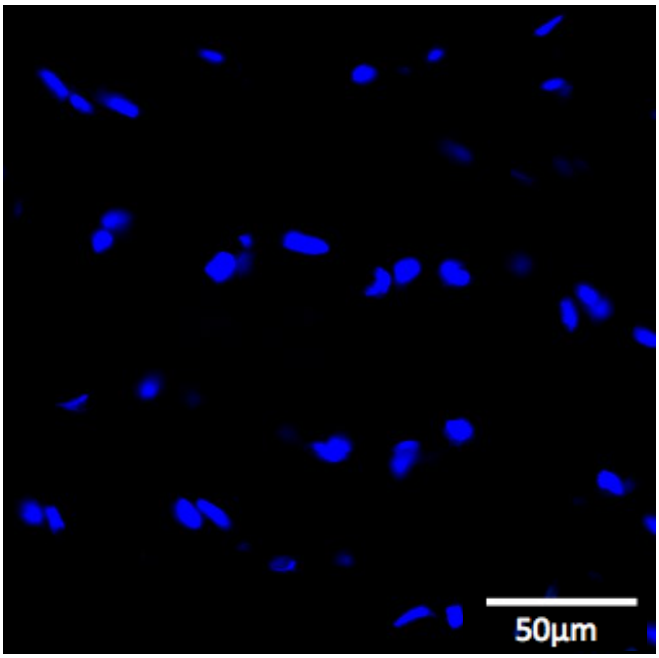

Figure Z.1 Confocal images of positive stained GAP43 protein (yellow), CGRP (magenta) and TRPV1 (green) in AF tissue at post-injury day 29 (a) with negative control (b) Scale bar = 50µm.

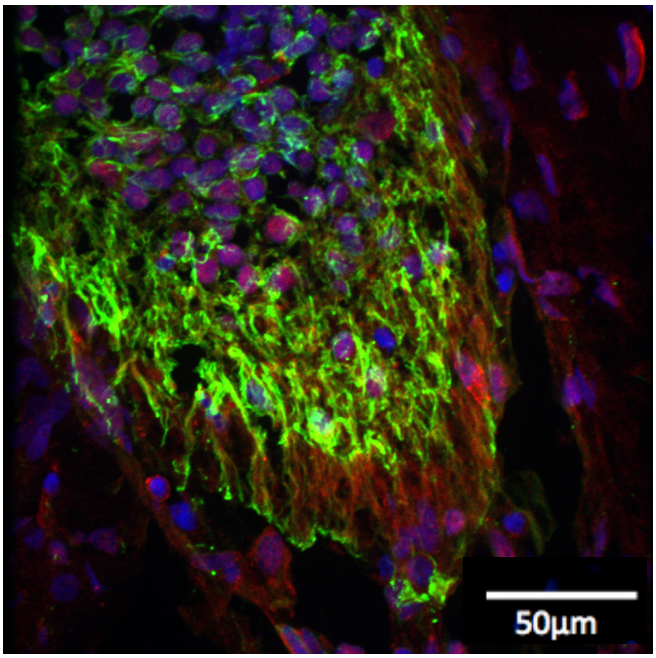

Figure Z.2 Positive control of GAP43 antibody. A Maximum projection of confocal images of positive stained GAP43 protein (red) and acetylated tubulin (green) in injured spinal cord of Xenopus sp. Scale bar = 50µm.

a)

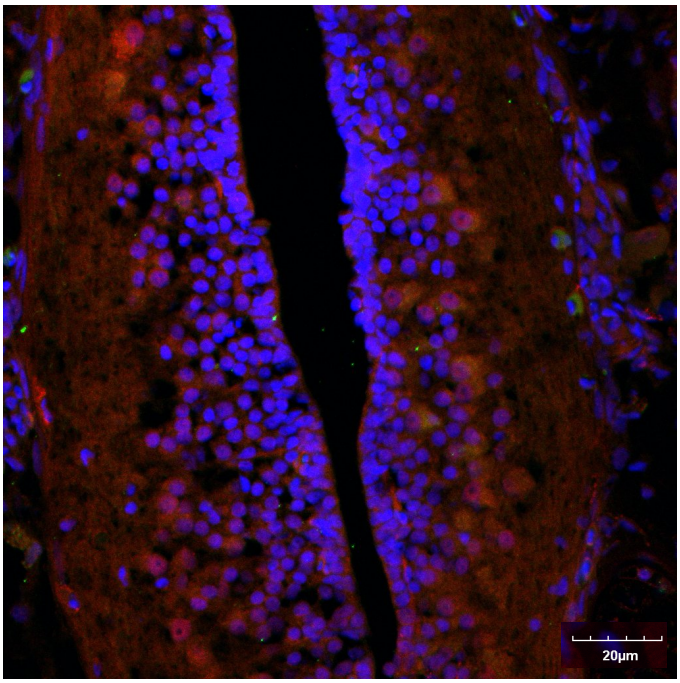

b)

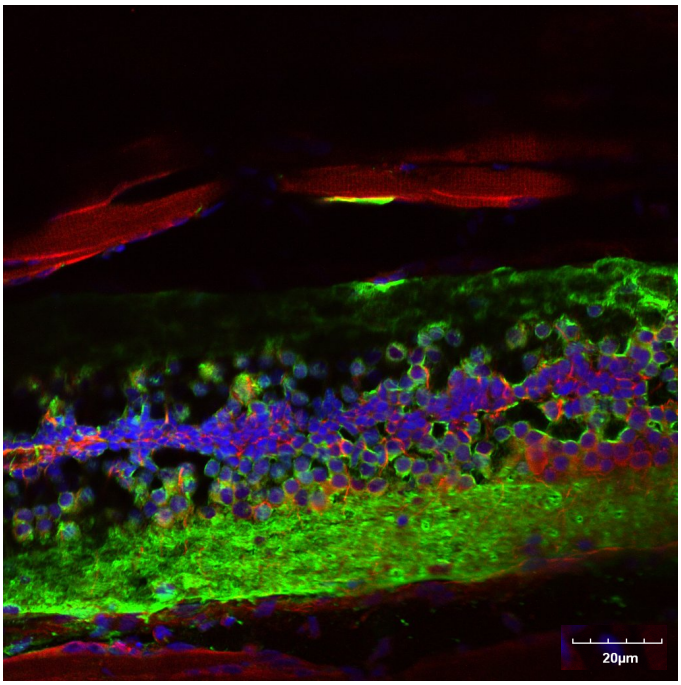

Figure Z.3 Positive control of TRPV1 and *c-Fos* antibodies. A maximum projection of confocal images of positive stained TRPV1 (green) and GAP43 (red) (a) and, *c-Fos* (red) and acetylated tubulin (green) (b) in injured spinal cord of Xenopus sp. Scale bar = 50µm.

AA. Clinical Opinion for the Use of Hyaluronic Acid Hydrogel in Degenerative Disc Disease for the Treatment of Discogenic Pain

Introduction

Hyaluronic acid (HA) is known to have a diverse biological function, not only for extracellular matrix (ECM) deposition, but also for therapeutic efficacy. It has been clinically used in patients with osteoarthritic pain and results in long term functional improvement. However, a trial to test the effectiveness of stem cells with HA injections in patients with back pain due to disc degeneration has only been carried out recently. In this study, HA hydrogel has been tested in a relevant inflammation model and painful disc degeneration *in vivo*, and offers a promising strategy for disc regeneration in treating discogenic pain. Therefore, a next step is planned to further determine the efficacy of HA hydrogel in degenerative disc for the treatment of discogenic pain. Prior to this, an opinion from clinicians who currently involved with the spine surgery is required.

Methods

Briefly, a questionnaire was designed as in Appendix AA.1 using multiple choice questions. The interview sessions were conducted with clinicians including orthopedic surgeons and neurosurgeons in Galway, Ireland, San Diego and New York, USA (Table AA.1).

Table AA.1 Details of individual respondent.

Country	Initial
Ireland	AD
	FB
	DT
	A
Germany	GL
Mexico	M
China	C

Appendix AA.1

Questionnaire - Use of Hyaluronic Acid Hydrogel in Degenerative Disc for the Treatment Back Pain

1. What is your specialty

   Orthopaedic Surgeon □

Neurosurgeon □

Other, please specify _____

2. In what country do you practice? _____
3. What is the incidence (number of patients) with mechanical low back pain possibly related to disc pathology in your country practice annually?

   _____

Question 4-8, please read this summary:

In clinical practice in osteoarthritis, hyaluronic acid (HA) has been used for some time. However a trial to test the effectiveness of stem cells with HA injections in patients with back pain due to disc degeneration has only been carried out recently [1]. In a rat degenerative disc model, HA hydrogel is found to reduce pain by down-regulating peripheral and spinal nociception markers and by inhibiting sensory hyper-innervation in AF and NP tissues. It is also found that the HA hydrogel alters the expression of sugar moieties relative to that in untreated degenerated disc. Additionally, HA hydrogel modulates key inflammatory pathways and protein regulators to respectively reduce inflammation and regulate matrix components [2-3]. In cell studies, HA hydrogel reduces inflammation markers and neurotrophins possibly by binding of the cell surface receptor [4]. Overall, these findings show that pain is modulated by HA hydrogel therapy through its alteration in glycomic and protein regulatory pathways, suggesting the potential therapeutic HA application in disc degeneration for the treatment of back pain.

4. Given that summary above, do you see a therapeutic role for HA hydrogel in disc degeneration and back pain?

   Yes □

   No □

   Other, please specify _____

5. Do you think that disc repair with HA hydrogel has potential to reduce back pain in patients with degenerative disc disease?

   Yes □

   No □

   Other, please specify _____

6. Given that HA has a safety record in clinical trials for other applications, do you think that progression to human clinical trials is reasonable or is there something to be gained by using a larger animal model?

   Progression to clinical trial □

   Larger animal first □

   Other, please specify _____

7. Do you see a role for HA hydrogel in percutaneous minimally invasive modification of the intervertebral disc in the treatment of back pain?

   Yes □

   No □

   Other, please specify _____

8. Based on your practice, can you suggest any other procedures in which it is appropriate to use HA hydrogel in disc degeneration for the treatment of back pain? _____

References for the questionnaire:

1. NCT01290367. Safety and Preliminary Efficacy Study of Mesenchymal Precursor Cells (MPCs) in Subjects With Lumbar Back Pain. https://clinicaltrials.gov/ct2/show/NCT01290367. (9 June 2017).

2. Isa, I. L. M. *et al*. Hyaluronic acid hydrogel alleviates nociceptive behaviour through inhibition of sensory hyper-innervation and nociception markers, attenuates the systemic I inflammatory response and regulates glycomic and proteomic signature in a novel model of pain associated with intervertebral disc degeneration. ORS. (2017).

3. Isa, I. L. M. *et al*. Regulation of inflammation, neurotrophins, glycosylation, sensory nerve innervation and pain in intervertebral disc degeneration using an implantable hyaluronic acid hydrogel. *Front. Bioeng. Biotechnol*. (2016). doi:10.3389/conf.FBIOE.2016.01.01510.

4. Isa, I. L. M. *et al*. Hyaluronic acid based hydrogels attenuate inflammatory receptors and neurotrophins in interleukin-1β induced inflammation model of nucleus pulposus cells. *Biomacromolecules*. 16, 1714–1725 (2015).

Results

Of the seven clinicians, four of them were from Ireland, one from China and one from Germany, who were orthopedic surgeon. Only one neurosurgeon, practically based in Mexico, has been interviewed, (Figure AA.1). The annual incidence of patients who experienced mechanical low back pain rather than neuropathic pain related to disc pathology was estimated at 20–30 %, 30–40 % and 20–40% of adult population in Ireland, Germany and China respectively. Around 60–70 % of the total population that suffered back pain was estimated in Mexico (Figure AA.2).

Based on HA efficacy summary given during the interview (Appendix AA1), six clinicians (85.71%) were of the opinion that HA hydrogel has a therapeutic role in discogenic back pain. Thus, five of them (71.43%) agreed that disc repair with HA hydrogel can reduce back pain in patients with degenerative disc disease (Figure AA.3). This suggests that HA has potential in degenerative disc for the treatment of discogenic pain. Clinicians were then being asked whether human trials should now proceed or if trials in larger animals should take place first. The majority of them (71.43%) thought that HA hydrogel should be tested in a larger animal model before direct translation to the clinic. However, two clinicians recommended that HA hydrogel study should be carried out (directly) in human clinical trial since the different physiological condition between animal and human is to be considered, especially in the biomechanics of spine (Figure AA.4a).

Next, a further question was asked as to what is the appropriate clinical procedure with HA hydrogel in disc degeneration for the treatment of back pain. Five of them (71.43%) agreed that percutaneous minimally invasive modification is the most viable modality such as injectable is currently on demand to delay and/or avoid surgical intervention in patients (Figure AA.4b). Thus, more clinical procedures have been suggested such as in lumbar decompression, after discectomy, intradiscal injection in vertebrae burst fracture and is in conflict between interbody and facet joint (Table AA.2). However, one of the clinicians opinion that the findings of larger animal studies (Figure AA.4b) will determine the clinical use.

a)

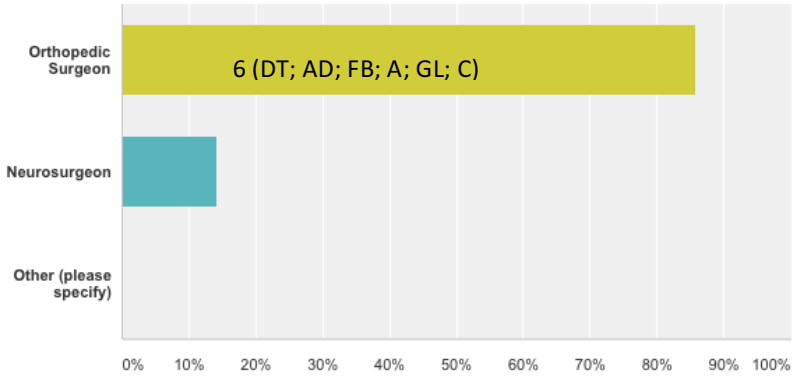

b)

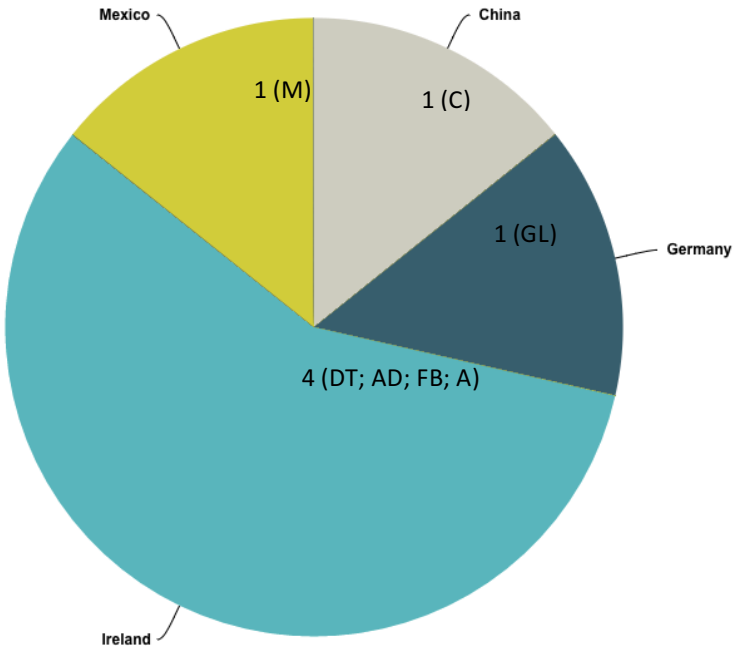

Figure AA.1 Responding demographics. The total number of orthopedic surgeons and neurosurgeons that were interviewed (a) and their country of practice has been noted (b).

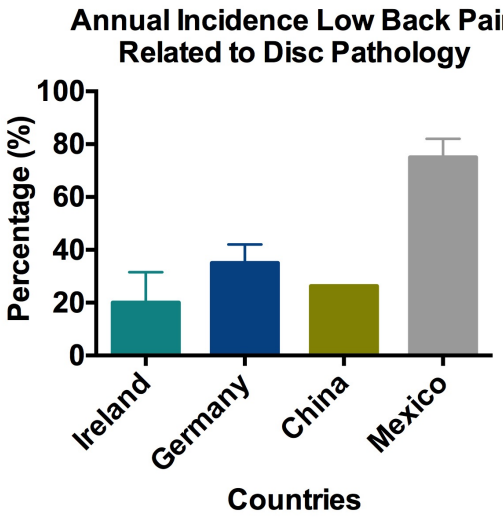

Figure AA.2 Estimated annual incidence low back pain in patients associated with degenerative disc disease corresponds to their countries.

a)

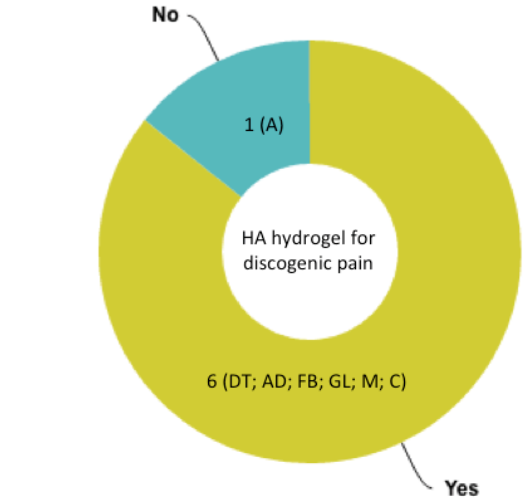

b)

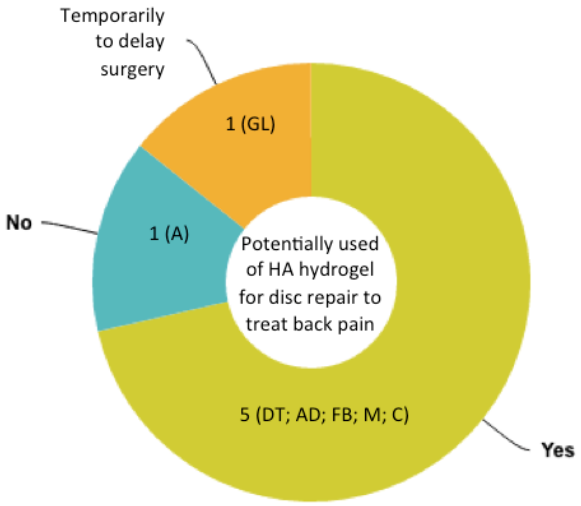

Figure AA.3 Clinical opinion on the therapeutic role for HA hydrogel for discogenic pain (a) and HA hydrogel potentially being used for disc repair in degenerated disc in treating back pain (b).

a)

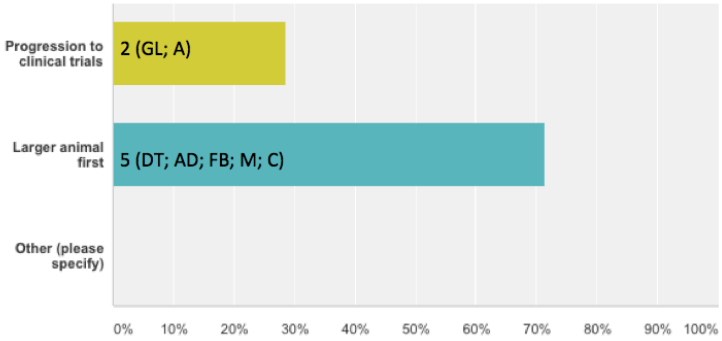

b)

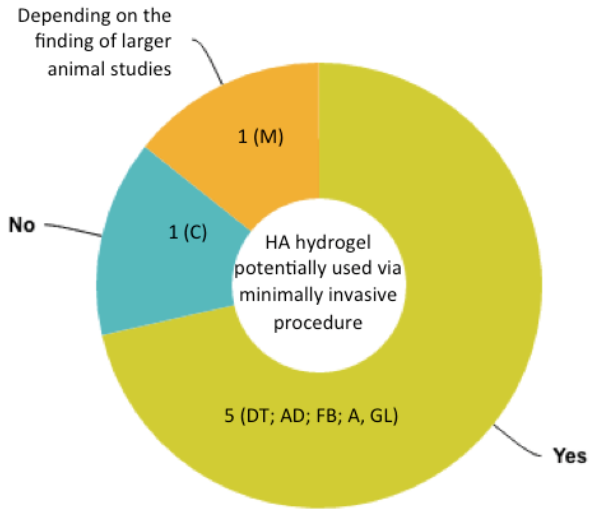

Figure AA.4 (a) Reliable future studies of efficacy of HA hydrogel. (b) Clinical opinion on the use of HA hydrogel through minimally invasive procedure.

Table AA.2 Clinically relevant spine procedures for application of an injectable HA hydrogel.

Suggestions for Other Clinical Procedures
In open lumbar decompression
In treating AF defect after discectomy
In vertebrae burst fracture classification AO A31 intradiscal injection
In reducing the confliction between interbody and facet joint

AB. Patent Submission, Journal Publications and Conference Proceedings

Patent Submitted (1)

1. **Isa, I. L. M.**, Pandit, A. Regeneration of diseased intervertebral disc. 2016

Invention Disclosure Filed (1)

1. **Isa, I. L. M**., Pandit, A. Hyaluronan hydrogel which regulates inflammation, neurotrophic factors and glycosylation profile to reduce sensory nerve innervation and pain in intervertebral disc disease, Tech-2016-029.

Published Manuscripts (2)

1. **Isa I. L. M.,** Srivastava A., Tiernan D., Owens P., Rooney P., Dockery P., and Pandit A. Hyaluronic acid based hydrogels attenuate inflammatory receptors and neurotrophins in interleukin-1β induced inflammation model of nucleus pulposus cells. *Biomacromolecules*. 2015, 16, 1714−1725.
2. Srivastava A., **Isa I. L. M.,** Rooney P., Pandit A. Bioengineered three-dimensional diseased intervertebral disc model revealing inflammatory crosstalk. *Biomaterials*. 2017.

Manuscripts to be Submitted (2)

1. **Isa I. L. M.,** Abbah S. A., Kilcoyne M., Dockery P., Finn D. P., Pandit A. Implantation of hyaluronic acid hydrogel prevents the pain phenotype in a rat model with intervertebral-disc injury.
2. **Isa I. L. M.,** Devitt A., Abbah S. A., Pandit A. Therapeutic biomaterials for intervertebral disc regeneration in the treatment of discogenic pain.

Manuscript Under Submission (1)

1. Larrañaga A., **Isa I. L. M.**, Patil V., Thamboo S., Lomora M., Fernández-Yague M. A., Sarasua J., Palivan C. G., Pandit A. Antioxidant functionalized polymer capsules to prevent oxidative stress. 2017

Published Book Chapter (1)

1. Graceffa, V., Wu, Z., Gaspar, D., Spanoudes, K., **Isa I. L. M**., Biggs, M., Mullen, A. M., Pandit, A. and Zeugolis, D. I. 'Xenogenic tissues and biomaterials for the skeletal system.' *Reference Module in Materials Science and Materials Engineering*. 2017.

Conferences Proceedings (14)

1. **Isa I. L. M.**, Abbah S. A., Kilcoyne M., Carroll O., Wyne K., Srivastava A., Tiernan D., Owens P., Joshi L., Dockery P., Finn D. P., Pandit A. Hyaluronic acid hydrogel alleviates nociceptive behaviour through inhibition of sensory hyper-innervation and nociception markers, attenuates the systemic inflammatory response and regulates glycomic and proteomic signature in a novel model of pain associated with intervertebral disc degeneration. Orthopedic Research Society Meeting, San Diego, USA, 19-22 March 2017. Oral Presentation.
2. **Isa I. L. M.** and Pandit A. Current spine research at CÚRAM. Irish Spine Society Meeting, NUI Galway, 4 Nov 2016. Oral Presentation.
3. **Isa I. L. M.,** Srivastava A., Kilcoyne M., Abbah S. A., Carroll O., Tiernan D., Owens P., Joshi L., Dockery P, Finn D. P., Pandit A. Modulation of inflammation, neurotrophins, glycosylation, sensory nerve innervation and pain in intervertebral disc degeneration using an implantable hyaluronic acid hydrogel. Ireland-Japan Biomaterials and Tissue Engineering, Meyrick Hotel, Galway, Ireland, June 22, 2016. Oral Presentation.
4. **Isa I. L. M.,** Srivastava A., Kilcoyne M., Abbah S. A., Carroll O., Tiernan D., Owens P, Joshi L, Dockery P, Finn D P, Pandit A. Regulation of inflammation, neurotrophins, glycosylation, sensory nerve innervation and pain in intervertebral disc degeneration using an implantable hyaluronic acid hydrogel. *Front. Bioeng. Biotechnol. Conference Abstract: 10th World Biomaterials Congress*. doi: 10.3389/conf.FBIOE.2016.01.01510. May 17-22, 2016. Oral Presentation.

5. Larrañaga A., **Isa I. L. M.,** Sarasua J., Pandit A. Development of anti-oxidant hollow polymer microreactors to prevent oxidative stress in interleukin-Iβ induced inflammation model. World Biomaterials Congress, Canada, May 17-22, 2016.
6. **Isa I. L. M.,** Srivastava A, Abbah S. A., Carroll O., Tiernan D., Owens P., Dockery P., Finn D. P., Pandit A. Modulation of extracellular matrix activity, neurotropic factors and sensory innervation associated pain in intervertebral disc degeneration using a hyaluronic acid hydrogel. Global Spine Journal 06(S01). April 2016. DOI: 10.1055/s-0036-1582591. April 13-16, 2016, Dubai, UAE. Oral Presentation.
7. Srivastava A., **Isa I. L. M.,** Rooney P., Pandit A. Deciphering intervertebral disc molecular crosstalk under IL1-β-induced inflammation in a three dimensional model. BiTERM, India, April 14, 2016.
8. **Isa I. L. M.,** Abbah S. A., Kilcoyne M., Carroll O., Srivastava A., Tiernan D., Owens P., Joshi L., Dockery .P, Finn D. P., Pandit A. Development and characterisation of a novel rat model of pain associated with intervertebral disc injury. Centre for Pain Research Annual Day, March 14, 2016, NUI Galway, Ireland. Oral Presentation.
9. **Isa I. L. M.,** Kilcoyne M., Abbah S. A., Carroll O., Srivastava A., Tiernan D., Owens P., Finn D. P., Dockery .P, Pandit A. Anatomical feature and glycophenotype of coccygeal intervertebral disc in healthy and *in vivo* injury pain model. Orthopedic Research Society Annual Meeting, March 5-8, 2016, Florida, USA. Poster.
10. **Isa I. L. M.,** Srivastava A., Tiernan D., Owens P., Finn D. P., Dockery P., Pandit A. Modulation of extracellular matrix activity, neurotrophin expression and innervation using a hyaluronic acid in response to 3D *in vitro* inflammation and in an *in vivo* intervertebral disc injury model. 3rd International Philadephia Spine Research Symposium, November 9-12, 2015, Philadelphia, USA. Poster.
11. **Isa I. L. M.,** Srivastava A., Tiernan D., Owens P., Rooney P., Dockery P., and Pandit A. Hyaluronic acid based hydrogels attenuate inflammatory receptor and neurotrophins in interleukin-1β induced inflammation model of nucleus pulposus cells through binding cell surface receptor CD44. Oral Presentation at Pain Research Day, 27 January 2015, NUI Galway, Ireland. Oral Presentation.

12. **Isa I. L. M.,** Srivastava A., Tiernan D., Owens P., Rooney P., Dockery P., and Pandit A. Hyaluronic acid based hydrogels attenuate inflammatory receptor and neurotrophins in IL-1β induced inflammation model of nucleus pulposus cell cultures. Matrix Biology Ireland, 21 November 2014, NUI Galway, Ireland. Oral Presentation.
13. **Isa I. L. M.,** Srivastava A., Tiernan D. and Pandit A. Hyaluronic acid based-hydrogels attenuate inflammatory receptor and neurotrophins in IL-1β induced inflammation model of nucleus pulposus cell cultures. 26th Annual Conference European Society for Biomaterials (ESB), Liverpool, UK, 31 August – 3 Sept 2014. Oral Presentation.
14. **Isa I. L. M.,** Srivastava A., Tiernan D., Owens P., Rooney P., Dockery P., and Pandit A. A therapeutic effect of hyaluronic acid based-hydrogels on *in vitro* inflammation model of nucleus pulposus. European Cell Material (eCM), 24-26 June 2014, Davos, Switzerland. Oral Presentation.

AC. References

[1] C. E. Schanté, G. Zuber, C. Herlin, and T. F. Vandamme, "Chemical modifications of hyaluronic acid for the synthesis of derivatives for a broad range of biomedical applications," *Carbohydr. Polym.*, vol. 85, no. 3, pp. 469–489, 2011.

[2] G. Fontana, A. Srivastava, D. Thomas, P. Lalor, P. Dockery, and A. Pandit, "Three-dimensional microgel platform for the production of cell factories tailored for the nucleus pulposus," *Bioconjug. Chem.*, 2014.

[3] J. Cox and M. Mann, "MaxQuant enables high peptide identification rates, individualized p.p.b.-range mass accuracies and proteome-wide protein quantification," *Nat. Biotechnol.*, vol. 26, no. 12, pp. 1367–72, 2008.

[4] S. Tyanova, T. Temu, P. Sinitcyn, A. Carlson, M. Y. Hein, T. Geiger, M. Mann, and J. Cox, "The Perseus computational platform for comprehensive analysis of (prote)omics data," *Nat. Methods*, vol. 13, no. 9, pp. 731–40, 2016.

[5] A. J. Freemont, T. E. Peacock, P. Goupille, J. A. Hoyland, J. O. Brien, and M. I. V Jayson, "Early report nerve ingrowth into diseased intervertebral disc in chronic back pain," *Lancet*, vol. 350, pp. 178–181, 1997.

[6] J. M. Lee, J. Y. Song, M. Baek, H. Y. Jung, H. Kang, I. B. Han, Y. Do Kwon, and D. E. Shin, "Interleukin-1β induces angiogenesis and innervation in human intervertebral disc degeneration," *J. Orthop. Res.*, vol. 29, no. 2, pp. 265–9, Mar. 2011.

[7] A. J. Freemont, A. Watkins, C. LeMaitre, P. Baird, M. Jeziorska, M. T. N. Knight, E. R. S. Ross, J. P. O'Brien, and J. A. Hoyland, "Nerve growth factor expression and innervation of the painful intervertebral disc," *J. Pathol.*, vol. 197, no. 3, pp. 286–92, Jul. 2002.

[8] S. M. Richardson, D. Purmessur, P. Baird, B. Probyn, A. J. Freemont, and J. A Hoyland, "Degenerate human nucleus pulposus cells promote neurite outgrowth in neural cells," *PLoS One*, vol. 7, no. 10, p. e47735, Jan. 2012.